Heat Release Rate in Ventilation-Limited Furniture Fires

by

Bronwyn Forrest

A thesis
presented to the University of Waterloo
in fulfillment of the
thesis requirement for the degree of
Masters of Applied Science
in
Mechanical Engineering

Waterloo, Ontario, Canada, 2020

Examining Committee Membership

The following served on the Examining Committee for this thesis. The decision of the Examining Committee is by majority vote.

Supervisor:	Elizabeth Weckman Professor, Dept. of Mechanical and Mechatronics Engineering University of Waterloo
Internal Member:	Noah Ryder Adjunct Professor, Dept. Mechanical and Mechatronics Engineering University of Waterloo
Internal-External Member:	Christine Moresoli Professor, Dept. of Chemical Engineering University of Waterloo

Author's Declaration

I hereby declare that I am the sole author of this thesis. This is a true copy of the thesis, including any required final revisions, as accepted by my examiners.

I understand that my thesis may be made electronically available to the public.

Abstract

There has always been motivation to investigate and understand fires with hopes of implementing useful changes to fire safety procedures, standards, codes, and education. Due to the unpredictability and destructive nature of fires, the concerns that fires pose to societies are ever changing as communities, cities and populations grow and evolve. As a result, the scientific community strives to continually grow and evolve with the changes, therefore driving a necessity for expanding our wealth of knowledge and understanding of fires.

The purpose of this research is to further expand on our very limited scientific knowledge of the impacts of ventilation-limited environments on the heat release rate of furniture fires, specifically in a modern residential context. For this, data from a series of nine large-scale fires initiated in the living room of a multi-compartment, two-storey burn structure were analyzed and interpreted to determine key characteristics of the environment as it evolved during the fires. The structure was well sealed to mimic the shift in modern home design towards less air leakage and higher energy-efficiency resulting in ventilation-limited fires and setting the current experiments apart from the much-studied well-ventilated compartment fires. Fires were fuelled by three distinct types of sofa, each custom built of a foam and fabric combination that complied with different furniture flammability standards. Ignition at one end of the couch facilitated comparison of fire spread across each sofa. The modern residential context here, then, refers both to the use of modern furniture materials and to newer methods of residential construction as these have an impact on fire growth, development, and spread as well as the chemistry and physics of a compartment fire environment.

One of the most important parameters in fire safety is the heat release rate of the fire. It is such an important measure because it is essentially the power of the fire and can provide valuable information as to how the fire will grow, spread and develop. As such, heat release rate is used as an input into many computational and numerical models which are then used to conduct hazard and risk assessments that impact fire safety decisions such as evacuation. Due to the importance of this input, there has to be assurance that the magnitude of the peak heat released, or the time-resolved heat release rate curve of a material are calculated with confidence and account for specific characteristics of the fuel-source and environmental conditions. One goal of this research is to provide comparisons of existing methods for the calculation of heat release rate of furniture fires. Also included in this work is a newly developed image analysis program that uses the video footage recorded from the tests to compute the height and width of the flames, which are used as inputs into several of the selected numerical models. Information with regards to the physics

that occur in a ventilation-limited fire environment fuelled by upholstered furniture as the primary fuel source and the interactions between the changing environment and the heat release rate are also discussed.

Specific to the enclosure dynamics, some key results were found. First, temperature profiles varied throughout the structure. The environment stratified in areas closest to the fire, whereas areas further away remained more uniform in temperature. Smoke movement throughout the structure, when coupled with gas sensor data, indicated interesting oxygen transport patterns that supported burning of the couches throughout the fires. As such, the stair between floors was an important connection, and the smoke layer also played a key role as it interfered with the fire plume and contributed radiation to the surfaces in the enclosure. With respect to calculated values of heat release rate, there was good agreement across numerical methods; mass loss rate and the predictive cone calorimeter to full-scale couch peak heat release rate method described in this work; however, the Babrauskas methods and Heskestad's flame height correlation did not always produce comparable results. The non-fire-retardant couch consistently had the highest peak heat release rate, followed by the lightly-fire-retardant couch and lowest was the fire-retardant couch.

In summary, this body of work compares values of heat release rate determined using available calculation methods and correlations used by practicing engineers as inputs into models. In doing so, it also provides new information on the characteristics and impacts of ventilation-limited environments on fire growth, development, smoke movement and heat release rate of furniture fires. Based on the results, the need for much better understanding of the effects of a ventilation-limited environment on the overall burning characteristics of furniture and ensuing physics of the fire is highlighted, which in turn, would guide choices for appropriate calculation methods for the heat release rate and other important characteristics of a range of fuel sources across different fire scenarios.

Acknowledgements

There are many people I need to thank, for without the support network I was fortunate to have, this thesis would not have been possible. Thank you to my lab mates; Jennifer, Vusal and Hannah for helping me with various projects, with a special acknowledgment to Jennifer for suffering through the tedious first iterations of the image analysis with me.

Thank you to Jay Walsh and Sean Murray for your excellent work with helping me develop the video processing code, your time and work added so much value to this thesis, my sincerest thank you.

I would also like to thank Noah Ryder for helping with all of the time syncing of the data and debugging the gas sensor data. Another thank you goes to Andy Barber for helping me with small scale testing in a rush towards the end of data crunching.

To my supervisor Beth, words cannot express how grateful I am for this opportunity, and how thankful I am that you took me under your wing. You've taught me so much more than just the contents of this thesis and have helped me grow as a student, leader and overall person. Thank you for always believing in me, encouraging me, and editing my work in pain-staking detail. Thank you for all you do. I look forward to a bright future ahead with you.

Dedication

This is dedicated to my family and friends. Thank you for listening to my complaints and supporting me through each hurdle. Thank you for believing in me and encouraging me to pursue this degree.

To Braden, thank you for being so wonderfully positive over the past two years and for reminding me to make every day fun and inspired.

With love, thank you all.

Table of Contents

List of Figures

List of Tables

Chapter 1

Introduction

Fires can be extremely destructive. The loss of property and financial toll can be felt by entire communities, cities and countries. For example, the forest fires that took place in Fort McMurray in 2016 were determined to be the most expensive natural disaster in Canada, with estimated insured losses of around 3.7 billion dollars [4]. There are not only financial implications of a major fire event, but emotional and mental strain can be devastating to individuals, families and communities. In the Grenfell Tower fire that occurred in the UK in 2017, 72 people were killed. An additional 2,400 survivors and family members were screened for PTSD and 700 adults and children are currently being treated for mental illness as a result of the traumatic event [5]. For reasons like these, researchers and engineers strive to improve the fire safety and resilience of our buildings and communities by acquiring more knowledge and better understanding the growth and development of fires. The focus of this thesis is on the behaviour of residential fires which occur in large numbers despite current research and prevention efforts by a variety of companies, research facilities and government organizations.

In Ontario, there were 5,243 residential fires in 2016 which made up 73 percent of all structure loss fires (total 7,169) that occurred that year [1] [6]. Even a small flame from a seemingly small ignition source, like a cigarette on an upholstered furniture item, has the potential to develop into a large, devastating fire in only a few minutes [7]. In Europe, statistics reflect that upholstered furniture fires are indeed a major cause of fatalities [7]. In Canada, cooking and smoking equipment have been the two highest causes of fires in residential settings from 2005-2014, as these two combined sources are responsible for 6 of 10 fires that occurred in this time frame [8] In Ontario, Manitoba, Alberta and British

[1] loss fire refers to a fire resulting in an injury, fatality or dollar loss

Columbia, there were 1,733 fire related deaths between 2005-2014, with senior citizens making up the largest percentage [8]. In Manitoba, Alberta and British Columbia, 70% of fire deaths are concluded to be from smoke inhalation and 30% from burns [8]. In general, fires are decreasing in frequency; however in the nine-year time-frame from 2005-2014 in Canada, there were 126,773 residential fires out of the total 205,332 structure fires reported, meaning residential fires make up 60% of all structure fires [8]. This prevalence is cause for concern, and motivation for fire safety research.

Depending on the ignition source, a fire on an upholstered furniture item may ignite and start to flame and grow quickly. Alternately it may smolder for a long period of time before a visible flame occurs with subsequent potential to grow to a large fire at a very fast rate. In both instances, the quickly growing fire inhibits occupants' ability to escape [9]. Further concern with residential fires is that their behaviour is constantly changing. Thus, they often present and develop in ways that fire researchers do not fully understand and fire fighters do not fully comprehend how to combat. Changes in fire behaviour can arise due to a large combination of factors, including different construction materials and interior furnishings, as well as changes in overall construction as a result of new energy and building codes and construction practice. In this thesis, outcomes from residential furniture fires are explored. Well controlled test fires were set in a structure configured to mimic an energy-efficient residential building envelope. In particular, this work contributes new data and insight regarding development of residential fires fueled by three distinct types of upholstered couches in low ventilation environments. Results provide information on fires developed on a relatively small, but important subset of the wide variety of furniture types, burning behaviour, fire scenarios and residential configurations that could occur. As such, they fill existing gaps in our overall knowledge of fire development and contribute to the development of more reliable and accurate assessment tools for quantitative evaluation of residential fire hazards.

Materials used to construct upholstered furniture are changing towards more synthetic materials at a fast rate. The result of these changes is significant in terms of fire growth, flame spread and progression to a fully involved compartment fire. This was highlighted in experiments conducted by the UL Firefighter Safety Research Institute [10]. Observed differences in fire growth between the compartments in which furnishings and decor were 'modern' in one, and 'legacy' in the other, were very obvious. Modern furnishings were defined as being comprised of synthetic materials such as polyurethane foam with man-made covering fabrics. Legacy furnishings were constructed of materials of more natural and animal origin, such as cotton and wool. The modern compartment took 3 minutes and 30 seconds to reach flashover, [2] whereas the legacy furniture took 20 minutes and

[2]Flashover is defined as the spontaneous combustion of all ignitable surfaces within a compartment [11]

30 seconds to reach flashover [10]. The comparison speaks volumes to the impacts that materials have on residential fire growth and spread. Modern furniture has taken a turn away from traditional materials like cotton and animal by-products such as wool, towards manufactured plastics and foams. To counteract their inherent flammability, these materials may also contain fire-retardant additives, which are intended to slow the progression and spread of a fire by making the pyrolysis and combustion process less efficient. In turn, pyrolysis products and products of incomplete combustion like carbon monoxide and other material-specific products may be released in the combustion process although the time evolution of these species has not been well studied. In any case, there are indications that modern fires have the potential to pose quite different threats than legacy fires to the occupants of a residence in terms of life safety and ability to egress. Investigating the nature, levels and rates of production of fire gases under differing conditions is a crucial aspect of fire safety and forms a key part of the research conducted in the present work.

At the same time as materials have changed, there has been a shift in building construction or home renovation to emphasize energy-efficiency, in line with world-wide motivation to create more sustainable homes and communities, in light of our changing climate. Energy-efficiency is achieved by constructing or modifying the building envelope to be effectively airtight, through better insulation, weather sealing, installation of double or triple pane windows and heat recovery ventilators. Effectively, this limits the amount of mass and energy transfer from the mechanically controlled interior of a space to the ambient and variable exterior environment. This can provide many societal, financial and environmental benefits, however the concern is that the majority of the changes made to buildings to adhere to this energy-efficient model have been done without thorough investigation into their fire safety implications. There is evidence that these homes may act as sealed boxes with a controlled and limited amount of oxygen available. This can have serious impact in the event of a fire in relation to ventilation pathways between compartments and levels of the structure, fire heat release rate, fire growth, flame spread and overall oxygen transport locally and globally as the fire progresses. Such issues provide further motivation for this work, as investigation into the fire dynamics of more energy efficient building configurations is of paramount importance to public safety over the longer term. In this research, therefore, the fire environment throughout a structure is researched in concert with detailed tracking of the heat release rate of the furniture to explore the numerous interactions and thereby build a stronger foundation of understanding of the physics of fire development in building environments where ventilation is limited.

One of the ways that fires can be characterized is by analysis of the heat release rate of the fire. It is a measure of the overall size of the fire and when considered on a time-resolved basis can be an essential tool for gaining understanding of the progression of a

physical fire environment. For example, four types of fires have been observed in research on burning characteristics of European furniture. These are a) fast developing and high peak heat release rate, b) delayed development and moderate peak heat release rate, c) slow development and low peak heat release rate and d) very limited burning [9]. The limited burning fires were considered safest of the four, whereas the fast developing and high peak heat release rate fires were deemed most dangerous as they progressed to dangerous levels quickly [9]. Thus, time resolved heat release rate curves are very useful in hazard assessment because they provide information on the burning history and ensuing hazards of a fire [9].

There are different ways that heat release rate can be calculated or estimated for a fire. These methods and the ensuing values are used in hazard and risk assessments, which in turn impact decision-making in regards to building design, safety systems and human egress. Based on the specific inputs used, however, heat release rate calculation methods can yield different values. Moreover, as the building, dwelling and/or characteristics of the fuel change, the fire behaviour will mirror the changes. For example, a fire will burn differently in a fully oxygenated ambient environment (well-ventilated condition), compared to one wherein oxygen is being consumed at a fast enough rate that levels decrease below ambient, typically designated as a ventilation-limited environment. Based on the brief discussion above, as our building envelopes change towards being more airtight, the question is raised as to how will the environment impact the fire heat release rate and thus how will the resultant fire behave. As such, it is important to conduct more in-depth analysis of the evolution of fire heat release rate in new scenarios as well as to assess whether the values of heat release rate calculated from widely-used methods remain comparable, accurate and applicable. This will lead to a better representation of the fire environment which, along with characterization of the nature, levels and rates of production of fire gases, is critical to evaluation of fire safety.

The two main objectives of this research, therefore, are to enhance current understanding of the evolution of a fire environment from ventilated into ventilation limited modes of burning, specifically with respect to:

1. time-dependent characterization of fire heat release rate and assessment of the associated heat release rate calculation methods by providing a comprehensive comparison of available techniques when used with input from the experimental results and;

2. impacts of an evolving fire environment, from a well-ventilated into a ventilation-limited mode of burning, on fire development, fire heat release rate, smoke and oxygen movement, and generation of toxic products.

1.1 Motivation

The motivation for the above objectives comes from the desire to provide new and valuable information about heat release rate, gas concentrations and smoke flow through structures due to a ventilation-limited fire environment in one compartment. Results can inform the community on the importance of heat release rate calculation methods appropriate to reflect the behaviour of real fuels in ventilation-limited fire environments, further the development of models for overall fire development with time and in both respects, lead to potentially positive impact on human safety in residential fires.

In support of these objectives, the present thesis is divided into the following Chapters. The literature review in Chapter 2 begins with an overview of the importance of heat release rate in characterization of fires, theoretical ways to calculate heat release rate based on chemistry and physics, followed by additional background on fluid mechanics as it pertains to overall fire behaviour. Well-ventilated and ventilation-limited fires at various scales are also discussed. Following this is a more in-depth look at the evolution, strengths and weaknesses of current heat release rate models and experimental measurements, in context of experimental work and methods related to furniture fires. Building on the overview of what has been done to date, Chapter 3 presents the experimental methods utilized in the present study, including a description of the fuel and fire burn structure, instrumentation and data analysis methodologies applied. In Chapter 4, representative results of the experiments and analyses are presented with discussion of their import and implications on fire safety. Finally, key conclusions and recommendations from the research are summarized in Chapter 5. Results of repeat tests are included in Appendix A, details on data acquisition and corrections can be found in Appendix B and the image processing code can be found in Appendix C.

Chapter 2

Literature Review

2.1 Fire Behaviour and Heat Release Rate

In support of the objectives and motivation outlined in the Introduction, this chapter begins with a general summary of the importance of heat release rate in characterization of fire behaviour, followed by topics related to the theory behind calculating and measuring heat release rate. In this context, bench-scale cone calorimetry and correlations for flame geometry and heat transfer will also be discussed. These theories build the basis for the heat release rate calculation and measurement methods chosen and utilized in this work.

Heat release rate is considered to be the most important parameter in fire hazard and risk assessment as it provides a measure of the overall power of the fire [12] as well as critical information regarding fire behaviour. It is also a key input into correlations used to determine time for occupant egress and in design for fire detection, suppression or control (i.e. sprinklers) [13]. The ability to predict the progression of a fire, which is often based on estimation of heat release rate calculated on a per unit area basis over time [14], is also the first step in performance based design [15]. In addition to the heat release rate, defining the time-resolved progression of other variables such as temperatures, gaseous species and smoke transfer are crucial when attempting to assess the development and behaviour of fires [15]. Within a compartment, the evolution of the fire is dependent on the combustion process and the enclosure configuration and materials [15]. The resultant environment then determines the interactions between various factors such as the building and combustion processes and their impacts on human egress, structural integrity and necessary protection and countermeasures (detection and suppression) [15]. Up-to-date, reliable and useful data pertaining to the evolution of realistic fires has long been sought after by the fire safety

engineering and research communities to drive informed decisions, particularly in regards to human safety [15].

One of the many challenges in achieving the above goal is that heat release rate is not an inherent property of a material, unlike thermophysical properties such as thermal conductivity for a metal for example. Rather, the heat release rate from even a well defined fuel source depends on the conditions under which the material is burning [13] such as availability of oxygen and heat feedback to the fuel surface to support combustion. There are many ways to calculate the heat release rate, which can be grouped into three broad categories: combined theoretical-analytical methods, experimental-analytical methods and experimental-correlational methods. Theoretical-analytical techniques for estimation of heat release rate are based on an understanding of physical and chemical parameters which are used to develop theoretical expressions. These types of equations have to be verified with actual experimentally obtained inputs in order to ensure the equations produce representative and accurate predictions across a range of fire conditions. Experimental-analytical techniques analyze data collected during experiments to develop predictive equations or models for heat release rate based on combined quantitative/qualitative evidence, using analysis supported by the expected physical and chemical theory for fire behaviour. Finally, experimental-correlational methods base equations or models for heat release rate on trends seen over a large number of experiments conducted. Depending on the experimental configurations upon which they are based, these methods can incorporate a wide range of parameters from material combustion chemistry to the physical shape of the fuel load [16] but are limited in application to the range of parameters included in the data upon which they are determined.

An example of how heat release rate can be calculated using an analytical-theoretical relation is the 'mass loss rate method' which is formulated on the basis the heat release rate equals the product of the heat of combustion (kJ/kg) and the mass burning rate of a material involved in the fire [13].

$$\dot{Q}_{theoretical}(kW) = \dot{m}\Delta H_{complete} \tag{2.1}$$

While the theoretical or complete heat of combustion is entirely dependent on the energy stored in the bonds of the molecules, in reality, the effective heat of combustion obtained during a fire will change depending on the details of how the bonds in the material break and undergo oxidation during combustion. Therefore, it will also change based on the specific conditions of the fire scenario. In a fire situation, this effective heat of combustion is used to calculate the total heat release, and the ratio between the total fire heat release and theoretical heat release is the combustion efficiency [17]. Due to heat transfer in a fire, changes in the heat of combustion are also coupled to changes in the mass burning rate so

in the context of fires, heat release rate is not a material property, but can be calculated in a fashion similar to the theoretical relationship using the product of an effective heat of combustion and a mass loss rate per unit area of burning material, along with a rate of fire growth, via change in fire size, in a given scenario. The mass burning rate and heat of combustion are two variables that can be obtained easily, and for a subsection of fuels there are documented values of these variables, therefore this 'mass loss rate method' is widely used in a variety of applications, and is also one of the methods selected for this work.

2.1.1 Power-Law Fire Growth

Another simplistic model of the heat release rate, much like the mass loss rate method described above is the power-law fire growth curve, or the t^2 fire growth curve. After ignition, the heat release rate during the growth phase of fire development can be characterized as increasing proportionally to the power of 2, from time after ignition, t and incubation time t_o, and the constant of proportionality is governed by the α, or the growth factor in kW/sec^2 shown in the Equation 2.2 below [18, 19].

$$\dot{Q} = \alpha(t - t_o)^2 \tag{2.2}$$

The values of growth rate, α, have been calculated by measuring how long it took the heat release rate of the fire to reach 1055kW after ignition [19]. The rate of growth of fires were then classified as slow, medium, fast and ultra-fast and the respective α values were determined for each classification, shown in Table 2.1 below [19].

Type	α (kW/sec^2)	Growth Time
slow	0.00293	600s
medium	0.01172	300s
fast	0.0469	150s
ultra-fast	0.1876	75s

Table 2.1: t^2 Growth Rate α Values

Many different commodities were tested to group various common materials/items into general groups which could then be used to conduct design and hazard calculations. Over time, there have been numerous additional calculation methods developed for the prediction of the heat release rate, which raises two important questions:

- which method is most appropriate for prediction of heat release rate for a given fuel source and fire environment, and
- out of the available methods which incorporate different input parameters, which input parameters are most important to most accurately represent the physics and chemistry present in a given fire environment?

It is important to state that there is no generic 'one-size fits all' method for calculating the heat release rate in a given fire scenario. No one parameter appears to be universally more important than another. Realistically, the more variables present in an equation(s) to account for as many of the interacting physical and chemical processes as possible, the more accurate should be the prediction of heat release rate. Added complexities to predicting the heat release rate, or calculating the heat release rate from experimental data are the effects of the changing environment on the physics of the fire and difficulties in accurate collection of data in the severe environments characteristic in fire situations. For example, a lack of oxygen will change the fire chemistry and heat transfer processes, which together lead to a decrease in the effective heat of combustion and mass loss rate of a material as there is less oxygen and less, or different fuel vapour, available for combustion, effectively decreasing the heat release rate of the material. As the environment changes, the heat release rate then clearly changes as well, which highlights another important insight: time-resolved measurements and models for heat release rate provide much more information and guidance compared to methods that provide only a single peak or steady-state value.

Before a more detailed look at the evolution of compartment fires with respect to physics and fluid mechanics as they pertain to behaviour of both well-ventilated and ventilation-limited fires, the next sections review fundamental elements related to determination of fire heat release rate. One of the first and most important standardized, bench-scale methods to directly measure the effective heat release rate of a material, the cone calorimeter, is presented in the next section. This fire performance test is designed to experimentally estimate effective heat of combustion and mass loss rates of small, representative samples of a material. The method is significant in that it based on the theory of oxygen consumption, and while it is only briefly introduced here, specific data obtained from the method will be discussed in further detail in the context of determining the heat release rate of furniture materials later in the Chapter. Following this, fundamental relationships linking heat release rate to fire growth or fire size, through determination of flame geometry and heat transfer, are addressed. Together these present a basis for the set of calculation methods, concepts and other experimental techniques presented later in this chapter.

2.2 Principles of Oxygen Consumption Calorimetry

The cone, or oxygen depletion, calorimeter is one of the most widely used methods to estimate the thermal response and heat release rate of materials in well-ventilated conditions. It is based on the theoretical-analytical principle of oxygen consumption during burning. The method was born in 1917, when Thornton discovered that organic liquids and gases release an approximately constant net value of heat per unit mass of oxygen consumed during complete combustion [20]. This was subsequently found to be true for organic solids as well, leading to determination of a constant average value of 13.1 MJ energy released/kg of oxygen consumed for a wide range of hydrocarbon materials [21]. The basic principle of oxygen calorimetry, then, recognizes that there is a predictable relationship between the amount of oxygen consumed and net heat released in an oxidation reaction, due to the fact that combustion requires oxygen to drive the reaction process [22]. With this discovery, the earliest test method for measuring heat release rate of a fuel was developed by Thompson and Cousins at Factory Mutual Research Laboratories in 1959 [23]. Since that first medium-sized apparatus, there were many iterations made towards an apparatus that could be used to determine the heat release rate of a material using principles of oxygen consumption. These eventually led to the present day cone calorimeter, developed in the 1980s by Vytenis Babrauskas at NIST [24]. With the addition of gas analyzers to measure oxygen, carbon monoxide and carbon dioxide, commercial cone calorimeters have become the most widely used bench-scale apparatus for determination of heat release rate of materials [22].

Testing in a cone calorimeter may also demonstrate interesting burning characteristics of a material or provide qualitative data to explain abnormalities in behaviour of a material when tested at larger-scale, though it is not without certain limitations as well. For example, one important caveat in using calorimetry data in prediction of behaviour of real fires is that if a building configuration and/or fuel load in a fire promotes a transition from open-air burning to a ventilation-limited combustion environment, data obtained from open-air calorimeter experiments does not apply to the whole fire scenario. Thus, as ventilation-limited fires become more prevalent with recent changes in building configurations and fuel, extreme care must be taken in applying results from standard calorimetry methods to estimation of materials behaviour under these conditions. Unfortunately, however, there is not a consistent and reliable small-scale experimental technique available to study fire performance of materials under ventilation-limited conditions either.

Even when conditions are appropriate, the cone calorimeter test can at best only provide preliminary insight as to how a material may act in a full-scale fire environment. It is extremely difficult to use it as a predictive test in determining actual heat release rate

in real fire scenarios since there are too many parameters specific to the small-scale test method that do not directly scale to a full-scale fire, and similarly too many parameters in a real, full-scale fire scenario that are not represented in the smaller scale cone calorimeter test.

The above limitations gave rise to the development of large-scale test apparatus, based on the same principles of operation, that was designed to explore the heat release rates and burning characteristics of different materials in closer to a full-scale fire environment. Scaling between cone calorimeter data, and the large-scale counterparts, also led to different methods by which to use bench-scale data to develop predictive tools for fire behaviour and heat release rate in realistic situations. All of these will be discussed in the context of the present work later in this Chapter. First, similar to the initial studies on oxygen consumption forming the basis for development of the cone calorimeter method for determination of effective heat release rate of small samples of material, work done to understand the physics and relationships between fire size, flame geometry, radiation and entrainment in simplified fire experiments, most often pool fires in large enclosures, led to the correlations for heat release rate of early stage fires in open-burning configurations widely used by engineers today. Due to their importance and use in the present work, these are briefly reviewed in the next section.

2.3 Correlations for Flame Geometry

Determining the flame height of a fire is not only useful information from a scientific perspective, but also from the perspective of engineering application. Understanding how large the flaming zone in a fire plume will be for a particular fuel source, diameter and environmental conditions are important for hazard and risk assessments. Fire plume behaviour, including flame height, is integral to assessing radiation heat transfer from a fire and determining proper suppression mechanisms. In terms of the visible flame, the luminous zone closest to the fire source, where most of the combustion reactions originate, appears to stay steady, whereas regions above that appear intermittent due to presence of vortex structures linked to flame 'puffing' [25, 17]. The cyclical, intermittent flaming pattern generated as a result of turbulent motions has been seen to produce less distinct visible flame tips at the furthest downstream points of the flaming zones in fire plumes. Variations in flame height as a result of undulations, eddies and billows of the tip therefore make it difficult to judge the instantaneous flame height by eye, leading to the concept that flame height in a fire should be determined based on where the tip of the flames appeared most frequently [26]. In this light, a variety of models for estimating flame height of fire plumes were developed

over the 1970s and 1980s for a wide range of fires; from buoyancy-driven pool fires with low Froude numbers (defined in Equation 2.3 below), in which the flame height to diameter ratio ranged from 0.1-10 [27, 28, 29, 30], to high Froude number, jet flames [26] and high momentum jets, in which the flame height no longer varies with the fuel flow rate and is several hundred times greater that the diameter of the fire source. In the context of this work, a brief overview of the correlations for flame height in buoyancy-driven pool fire regimes will be presented.

$$Q* = \frac{\dot{Q}}{\rho_\infty c_\rho T_\infty Z^2 \sqrt{gZ}} \tag{2.3}$$

Where Q* is a dimensionless parameter, $\dot{Q}$ is the total heat release rate (mass loss rate and effective heat of combustion), Z is burner diameter, and ρ_∞, c_ρ and T_∞ are the density, specific heat and temperature of ambient air.

Steward [28] predicted flame height based on the amount of excess air entrained in turbulent buoyant diffusion flames (pool fires) under conditions of stoichiometric mixing. He proposed flame height to be a function of the amount of heat released and the physical properties of the fire and fuel, by which he showed that flame height correlated to the point at which 400% excess air is entrained on the centreline of the fire plume [28]. In the prediction, he developed a dimensionless combustion number, N_{CO}, which was derived from consideration of the conservation equations in the burning zone using various parameters such as the stoichiometric air/fuel ratio, density of air and the radius of the pool of liquid fuel [28]. The chemical properties of the fuel were not explicitly included in the expression, but rather inferred through the stoichiometric ratio since flame height was specified as a function of the combustion number.

Towards the higher Froude number pool fires and jet flame burning regime, Becker et al. [26] developed an entrainment model and universal model for determining the flame length of vertical free turbulent diffusion flames established over fuels burning in unconfined environments. It was determined that the visible flame length was a function of the mass fraction of air in a stoichiometric fuel-air mixture, density, effective jet diameter, gravity, entrainment and momentum growth of the plume (as defined using Reynolds and Richardson numbers). The entrainment model accounted for aerodynamic characteristics of the fire, whereas the universal model was meant to be more general. It was determined that turbulent flame lengths were longer than laminar ones due to the impacts that turbulence had on the structure of the fire plume [26], and this led to work on understanding the role that air entrainment plays on plume structure and combustion, as carried out by Zukoski et al [30]. It was proposed that the vortices observed in the plume were primarily

responsible for entraining air. In the experiments, it was observed that vortices form near the base of the fire, and as the fuel within them is consumed, they move upward through the plume and eventually vanish, an effect which then lowers the top of the visible flames to the next forming vortex [30]. The Figure 2.1 below visually demonstrates the three boundaries of a 60kW methane diffusion flame in a 0.2m porous-bed burner which are; the top of the luminous flame Z_j and the two symmetric indentations formed by the vortical ring structures at Z_{j+1} and Z_{j+2}, thought to be primary sources of entrainment [30].

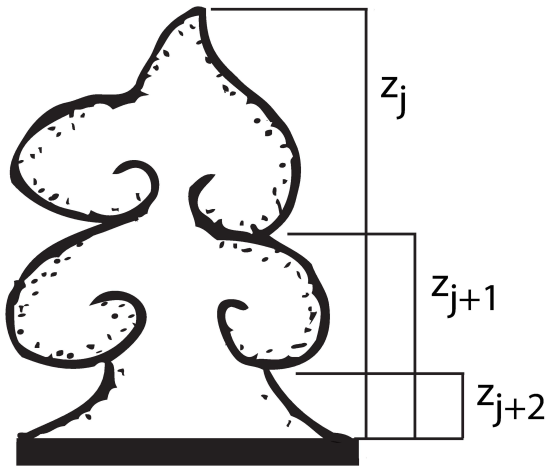

Figure 2.1: Vortical Structure of Fire Plume

This cyclical 'puffing' is repeatable enough that it can be used to determine an average flame height over time, leading Becker and Liang [26], amongst others, to analyze video footage of fire plumes to determine where the flame tip was for 10%, 50% and 90% of the time. In most studies at this time, however, the need for more precise measurement tools was highlighted, as judgement of flame presence by the human eye was found to be subject to an array of potential errors. This difficulty has led researchers to develop image processing tools specifically for determination of fire geometry. Some of these are discussed towards the end of the Chapter as they form the basis for development of an image processing tool for determination of flame geometry from recorded videos that formed a critical element of this work.

Pool fire experiments provided a strong physical basis for more experimental-analytical work to develop correlations related to buoyant diffusion flames in pool fires. In this light, Heskestad developed a correlation relating flame height, L, pool diameter, D, and his own version of combustion number, N, across a range of sizes of liquid pool fires, other horizontal

surface fires and jet flames [29, 31, 17]. The correlation was first presented in the following form and verified for fires in the range of N between 10^-5 - 10^5 [29]:

$$L/D = -1.02 + 15.6N^{\frac{1}{5}} \tag{2.4}$$

where L is the flame height, D is the diameter of the fire source, (or effective diameter for non-circular fire sources found by an equivalent area method as shown by this expression: $\frac{\pi D^2}{4}$), and N is a non-dimensional parameter, defined by:

$$N = \left[\frac{c_\rho T_\infty}{g\rho_\infty^2(\frac{H_c}{r})^3}\right]\frac{\dot{Q}^2}{D^5} \tag{2.5}$$

where c_ρ is the specific heat of air, g is acceleration due to gravity, ρ is the density of air, H_c is the actual lower heat of combustion (effective heat of combustion), and r is the actual mass stoichiometric ratio of air to volatiles. This correlation was developed for fires burning in standard atmospheric conditions (T=298K, 760mmHg or 101.3kPa). When tests were conducted at varying ambient temperatures, the flame height was found to increase, and the N parameter was found to appropriately account for this proportional relationship as well [31]. After its derivation, the equation was also found to be representative of flame heights observed for large, deep fuel loads, for example wood pallets stacked 3.3m high [17]. To obtain better predictions in this case, or if the diameter of the fire was not a circle, it was necessary to determine an effective diameter for the surface area of fuel burning as shown above [29]. Algebraically, a dimensional form of Equation 2.4 can be developed, first by defining a coefficient A [17]:

$$A = 15.6\left[\frac{c_\rho T_\infty}{g\rho_\infty^2(\frac{H_c}{r})^3}\right]^{\frac{1}{5}} \tag{2.6}$$

and simplifying to

$$L = -1.02D + A\dot{Q}^{\frac{2}{5}} \tag{2.7}$$

The coefficient, A, lies in the narrow range of 0.226 to 0.240, with a typical value taken as 0.235, due to the fact that the $\frac{H_c}{r}$ which is the term representing the heat released per unit of air entering the combustion process by mass, does not vary greatly over a large range of gaseous or liquid hydrocarbon fuels and has been found to remain between the range of 2900-3200 kJ/kg [17]. Therefore, assuming normal atmospheric conditions and A = 0.235 which is typical of fuels (excluding acetylene, hydrogen and gasoline which all

deviate significantly from the aforementioned range), the correlation is presented in the well-known form:

$$L = -1.02D + 0.235\dot{Q}^{\frac{2}{5}} \tag{2.8}$$

Where L and D are flame height and fire source diameter respectively, in meters, and $\dot{Q}$ is fire heat release rate in kW, found by taking the product of the mass loss rate and an effective heat of combustion. This equation has been found to be approximately valid over a range of fire characteristics of $7 < \frac{\dot{Q}^{\frac{2}{5}}}{D} < 700\frac{kW^{\frac{2}{5}}}{m}$; however, it should be noted that the flame height relations have not been tested outside of this range [32].

Heskestad's correlation is one of the most versatile and widely used methods for estimation of heat release rate in fires. Therefore it was selected to the calculate the heat release rate of the furniture fires in this research [33]; however, since it was developed based on small pool fire plumes burning in large well-ventilated enclosures, for the present application it is also necessary to investigate whether, or how, the correlation can appropriately be applied to fuel sources such as furniture and also to those fires in the limited-ventilation conditions observed in the present experiments.

2.4 Heat Release Rate and Heat Transfer

Heat transfer occurring as a result of the total heat release rate of a fire is comprised of three main portions. One portion radiates back to the fuel surface, another is lost by radiation to the surroundings and a convective portion encompasses the fraction of heat which is carried on the convective fire plume. Understanding these contributions as they relate to heat release in fires is important for the successful prediction of overall fire behaviour [31, 30] and also in estimating full-scale fire behaviour from small-scale flammability tests such as the cone calorimeter discussed in Section 2.2 [34]. Consideration of radiation is particularly true for full-scale fires since radiation has been proven theoretically and experimentally to be the dominating form of heat transfer at large scale and is thus of direct significance in determining the relationship between fire size and heat release rate. The effective heat release rate from a fire is inherently linked to variations in radiative heat flux to the fuel surface via a positive feedback loop between heat flux incident on the fuel surface driving further evaporation and thus fuel mass burning rate which is then directly linked back to the heat release rate in large fires [35, 36]. Calculation methods for radiation heat transfer are based on determination of the emissive power of the radiating body. This is the relationship between the properties of the emitting (radiating) body ϵ, temperature

of that body to the fourth power and the Stefan-Boltzman constant, 5.67×10^{-8} W/m^{2}K^4, σ, and is represented by Equation 2.9 below [37].

$$E(kW/m^2) = \epsilon\sigma T^4 \tag{2.9}$$

To calculate the intensity of radiant energy from the emitting body that would be received at a target, a configuration factor ϕ is added to the above equation. There are many configuration factors that have been mathematically derived for various configurations [38] as it depends on the shape of the emitting body, the shape of the target, and the geometrical positions of these two bodies in space [37]. Here, the value of epsilon (emitting body) was assumed to be equal to 1, as fires have previously been successfully characterized as black body emitters [37].

Radiation is directly coupled with soot formation [35, 36] as well as to radiative heat flux to the surroundings [34]. In reality, 80% or more of the radiation from a luminous turbulent flame to its surroundings is emitted by the soot, while the remaining 20% comes from the gases (oxygen, carbon dioxide, unburnt hydrocarbons) so it was thought that the radiative fraction from turbulent flames will increase with an increase of soot volume fraction [35]. For fuels with a high sooting propensity (like propylene or isobutene), fire radiative fractions are around 0.4-0.43 [39], compared to only half of that for fuels like alcohols with lower soot production [40]. Based on a variety of fuels tested in 4.6cm, 7.1cm and 30cm diameter pans, it was found that methanol in a 30cm pan had a radiative fraction of 0.17, whereas MMA (methyl methacrylate) in an even smaller 4.6cm pan had a radiative fraction of double the value, 0.34 [40]. Interestingly, within a spectrum of luminous fuels, the radiative fraction ranged between 0.27 and 0.34 with no apparent trend between radiation and measured sooting propensity of a material [40]. These findings are consistent with other studies in which 7.6 to 125cm diameter benzene pools [41] and 25 to 1000cm diameter heptane pools [42] were burned with measured radiative fractions between 34%-36% and 30%-36% respectively, even though benzene has a higher tendency to produce soot than heptane. Such results arise because pool diameter and therefore availability of air and fire size, has an impact on the radiative fraction for certain fuels. When short-chain silicone liquids were tested, values of radiative fraction increased from 0.3 to 0.45 as burner diameter increased from 0.1m to 0.6m, but for long-chain silicone liquids and alcohols, the radiative fraction stayed nearly constant with burner diameter, consistent with the fact that there were less particulates in those fire plumes [43]. Given the inherent coupling between combustion processes, soot formation, radiation and heat release rate, the overall fire environment also has an impact on radiation from a fire; however, sometimes the links are not straightforward to interpret. For instance, in ventilation-limited or vitiated environments, measurements

have indicated that the radiative fraction from flames over 30cm diameter PMMA pool fires actually reduced from 0.36 to 0.25 when oxygen decreased from ambient to 18% during burning, perhaps because any anticipated increase in soot production due to decreased availability of oxygen was outweighed by a reduction in soot production at the lower overall fire temperatures [44].

Such results show that radiation is important when determining the heat release rate during compartment fires, and may be particularly difficult to account for in fires which transition from conditions of well-ventilated to limited-ventilation burning. One possible method by which to assess the relationship is to couple estimations of fire heat release rate to determinations of radiation heat flux through point source radiation calculation methods. These are derived from the assumption that, when considering radiation to a target far away from a fire, the fire can be modelled as a point source of radiation located at the geometric centre of the fire plume. Heat is radiated outwards from this point in hemispheres [38]. This concept, represented in Equation 2.10 below, relates the heat flux per unit area, at a distance R from the fire center, by the inverse square law of distance between the fire and target [38].

$$\dot{q}''(kW/m^2) = \frac{\dot{Q}\chi_{rad}}{4\pi R^2} \tag{2.10}$$

where $\dot{Q}$ is the heat release rate, calculated using the product of the mass loss rate and heat of combustion Equation 2.1 previously discussed, and χ_{rad} is the radiative fraction, or the fraction of total heat produced from the combustion process which is radiated outwards throughout the space. To apply this equation in a given fire situation, however, knowledge of the radiative fraction of the fire is of key import.

Typically, the radiative fraction for a pool fire under steady state burning conditions is assumed to be 0.3 [37], but as already indicated above that value is subject to change based on the fuel, sooting propensity, and diameter of the fire [39, 40, 42]. If the fuel is producing increased amounts of soot and/or due to changing oxygen availability as a fire grows, this will also tend toward increasing radiative fraction from the fire. In the Sections above, the discussion has focused on results from literature which largely pertained to materials burning in large, open-air, well-ventilated situations so these at best provide only benchmark values to what might happen in a real fire. Instead, in a real fire, key characteristics such as radiative fraction are very difficult to estimate a priori since radiation heat transfer both into the compartment and also to the vaporizing fuel surface depends on many factors, which in turn, very much depend on the specifics of the environment in which the fuel is burning. Thus, it is now necessary to turn our attention to discussion

of overall fire dynamics, and consequently fire heat release rates, in 'real' fire situations, since those are of most concern here. The following sections therefore, outline important concepts related to overall fire development and key characteristics of compartment fires.

2.5 Compartment Fire Dynamics

Due to the inherent coupling between heat release rate and the compartment fire environment, background relating to fire behaviour and fluid mechanics as it pertains to compartment fires is presented. Literature corresponding to ventilation-limited fires is summarized following preliminary general sections, as ventilation-limited fires are the specific fire environments that form the focus of this work. The discussion builds on the background provided above, further elucidating the impact of the overall compartment on fire behaviour and heat release rate.

2.5.1 Fires and Ventilation

The life-cycle of every compartment fire can be schematically represented, or when values are known can be defined, using fire heat release rate as a function of time, as illustrated in the generalized plot in Figure 2.2 [45]. As the fuel is heated toward ignition, the air and fuel are separated, so pyrolysis gases and air must diffuse from areas of high concentration to areas of low concentration and mix, assisted by turbulent mixing, with the surrounding air to within a flammable concentration. When ignition of the flammable mixture occurs, a sustained diffusion flame is established [46] which becomes the fire. The fire proceeds first through a growth phase, then transitions into a steady burning period or fully developed stage and finally burns out via a period of decay. The total heat energy released from the fuels consumed in the fire is the integrated area under the fire heat release rate-time curve. The temperature and certain combustion products generated within a fire compartment follow curves very similar to those characterizing the heat release rate of the fire. When oxygen is depleted during combustion, the oxygen levels follow the inverse of this curve.

After ignition, and during the growth phase, there is usually sufficient oxygen available for combustion, the fire is considered fuel-controlled and the growth and progression of the fire are entirely dependent on the quantity of fuel available to the combustion zone at any time [11]. During this stage, flames will establish on the surface of the fuel, and as the material continues to pyrolyze due to heat feedback from the flaming regions, the resulting flames will grow. It is at this stage, where the area involved in burning is still quite

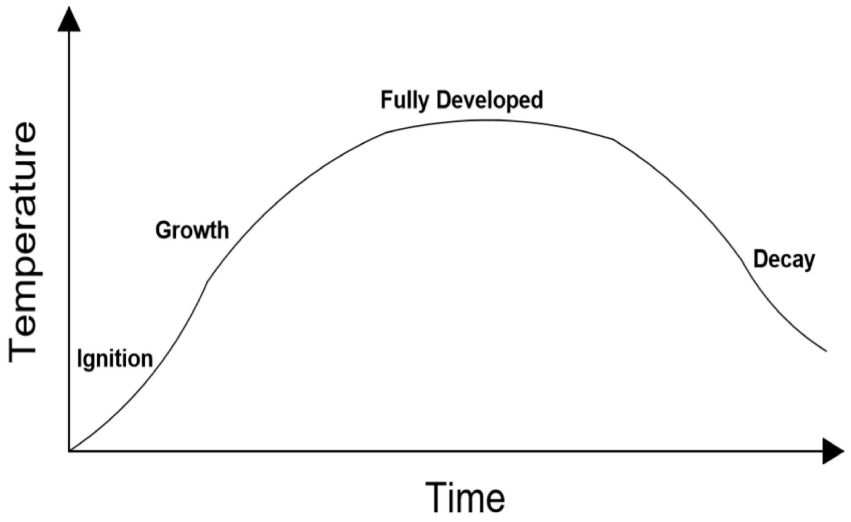

Figure 2.2: Typical Fire Growth Curve

small and localized, that the fire can be described by the pool fire correlations discussed in Section 2.3 above. As burning continues, both complete and incomplete products of combustion will be generated in the form of hot gases and smoke [11]. The less dense hot gases will rise due to buoyancy; the resulting flow, including the flames, is referred to as the fire plume [11]. The main mode of heat transfer to the surroundings during the initial growth phase of a fire is via convection from this hot plume [11]. As more heated combustion products and fire gases are generated, the temperature of the surrounding air in the compartment will increase, combining with increased radiation to the fuel surface, to create a positive feedback loop between the fire plume, vaporizing fuel surface and the hot smoke layer, resulting in a faster rate of fuel pyrolysis and larger fire plume. Therefore, the heat release follows an increasing parabolic trend as the fire grows, and there are proportional relationships between the temperatures in the compartment, the fire size, flame spread and the amount of smoke produced. Understanding the interactions between the various physical parameters is important for the determination of the heat release rate. Further, understanding how the compartment geometry, oxygen levels, mass and energy transfer between fire and fuel, as well as between vents and levels of a structure, impact the heat release rate is crucial for development of comprehensive correlations and models of fire development under the range of conditions possible across different scenarios.

It is known that the heat release rate is dependent on the air supply, such that when the available ventilation into a room increases, the heat release rate also increases [47]. The

duration of the fire can also increase when the same fire load is placed in a larger room in which more air is available, and thus the fire is supplied with sufficient air for more complete combustion, for a longer time; however, the intensity (magnitude of heat release rate) does not necessarily increase with the size of the room [47]. Ratios of compartment size, opening size and fire load ratio do govern the overall development and subsequent behaviour of a fire.

As the fire grows in size and energy, it will transition to the fully-developed stage where heat release rate is usually modelled as being at a constant, steady state value for a period of time. In this fully-developed stage, radiation is the governing mode of heat transfer to areas surrounding the fire [11]. During the fully-developed stage, the fire will continue to burn as long as the triangle of combustion is present and balanced; sufficient oxygen, heat and fuel. Once one of these crucial components begins to disappear, the combustion will begin to decay and eventually cease [11]. This can occur in different manners under different conditions. Typically when the fire environment remains rich in oxygen, then as the majority of the fuel is consumed, the temperatures in the compartment and overall energy released diminish, and the decay phase begins [11]. Alternately, in other environments oxygen levels can become depleted during the growth or fully-developed stages and the fire can progress to being ventilation-controlled. In this case, the fire can still decay due to consumption of fuel if there is sufficient oxygen to support combustion or, the fire can decay and self-extinguish due to the limited levels of oxygen [11].

In the transition between the growth and fully-developed stages, an interesting phenomenon called flashover can occur. Flashover has been experimentally observed in some enclosure fires when temperatures within the upper regions of the compartment are at least 600°C and/or levels of heat flux to the floor reach 20kW/m^2 [11]. It is thought that these conditions result in significant heat build-up and feedback to other combustibles present within the enclosure. As such, flashover is often defined as a rapid transition of a growth phase fire to a fully-developed fire characterized by rapid ignition of all available combustibles within the compartment [11]. Flashover requires sufficient quantities of incoming fresh air to support burning of all the available fuel within a compartment, so requires that doors and windows are open, or other openings are available. When this is not the case, and oxygen levels within the compartment start to deplete below ambient levels, combustion of fuel becomes dependent on the amount of oxygen that can be entrained by the fire, and the compartment fire environment is referred to as ventilation-limited [11].

2.5.2 Compartment and Fire Flows

As previously described, buoyancy is a governing fluid dynamic force in fires. As such, fires and fire plumes are modelled as buoyancy-controlled or buoyancy-dominated flows, such that the rate at which fuel is entering the pyrolysis zone is slow, and the upward velocity of the flaming area, plume of hot gases and consequent entrainment of air back toward the combustion regions, are largely governed by buoyancy forces [46]. Due to these same characteristics, while the flow of fuel to the pyrolysis zone is generally considered to be laminar, the developing flow in the fire plume undergoes a transition to turbulent flow with height above the fuel. The fire plume itself can be separated into three main zones as shown in Figure 2.3 [48]. Recall, near the base is the 'persistent flame zone' where combustion takes place, and the tip of the flaming area occurs above this, in the 'intermittent flame zone'. It is this zone that is most closely aligned with the visible flame height of a fire, as described by correlations of Becker and Liang [26], Zukoski [30, 25], Steward [28] and Heskestad [29, 31] above. In the intermittent zone, hot combustion gases continue to interact with the surrounding ambient air, resulting in complex fluid flows, including fluctuations and oscillations in the height of the visible flaming area within the plume. Often, the tip of the flame will separate away from the main flaming body as a result of the instability between the upward flow of the fire plume and the surrounding air making it difficult to determine time resolved values of flame height. As a result, in addition to studies to determine average flame height in a fire, there has been work done to characterize the frequency of fire oscillations and develop relations between these, heat release rate, flame height and fire diameter [26, 30].

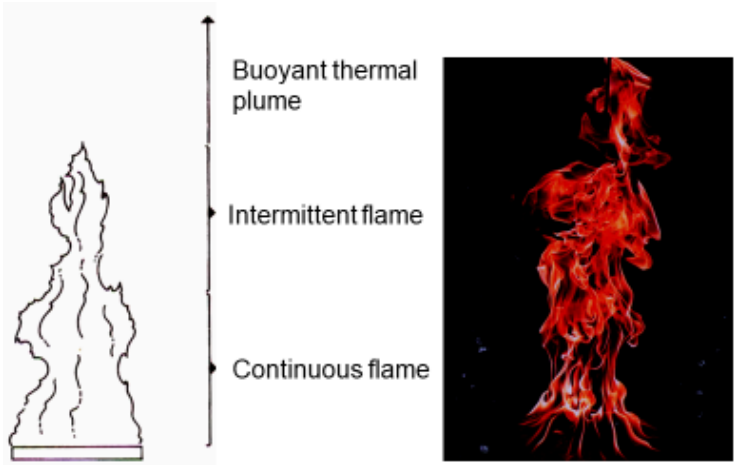

Figure 2.3: Fire Plume Diagram

Above the intermittent flame zone, is the buoyant plume comprised of hot fire gases and combustion products. During the time that the fire grows in a compartment, the plume gases rise and start to accumulate at the ceiling and then spread throughout the space as a momentum-driven jet, referred to as the ceiling jet [11]. The process of the fire plume feeding energy and mass to the ceiling jet and the formation of the smoke layer at the ceiling while incoming ambient air is drawn in through the lower region, results in two distinct layers within a fire compartment; the hot upper layer and cool lower layer [1]. As the fire progresses with time, the primary exchange of fluids within the fire compartment depends on a balance in which the rate of gas expansion and buoyant flows in the fire plume lead to pressure differences sufficient to drive entrainment to the flaming zones [1, 49].

The presence of a compartment around a growing fire plume impacts fire development and heat release rate as the walls and other surfaces can absorb heat from the flames and radiate heat back to other combustible surfaces. They also impact overall flow patterns of smoke and hot gases and directly affect the rate of entrainment when walls or corners create physical barriers to free air flow into the fire plume. As the hot smoke layer develops, there is radiative feedback from that layer to the fire and to other surfaces in the compartment, which can result in a positive feedback loop and increase the rate of fire development. Due to the impacts of the compartment on the fire growth, factors to account for the presence of walls and ceilings have been correlated and are used in equations to calculate ceiling jet temperatures and velocities, but these are largely applicable only in well-ventilated fire situations [50].

When the fire is in a compartment, the only supply of fresh air is through openings in the compartment boundaries. If all vents within a compartment are closed, the smoke layer thickens and descends lower within the space over time. Even in a less well-sealed compartment, air in-flow may be insufficient to keep up with the rate of oxygen consumption of the combustion reactions, and air outflow may not be sufficient to exhaust the building plume gases, also causing the hot gas layer to descend and oxygen levels in the lower layer to decrease. In these situations, the hot layer can impinge on the top of the fire plume which may then impact the overall burning characteristics of the fuel. Also, it can lead to contamination of the incoming air with smoke, and the fire burns in ventilation-limited conditions [51]. As shown in Figure 2.4 below, as the smoke layer descends, mixing can occur due to secondary flows such as [1]:

- exchange of descending cold fluid from the upper to the lower layer,
- shear mixing along interfaces between hot gases and incoming flows, and
- wall flows.

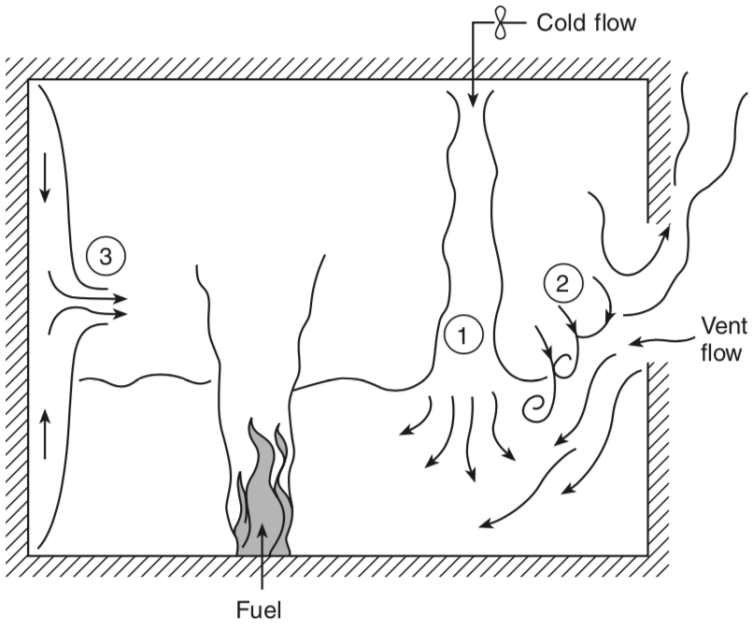

Figure 2.4: Reproduced with Permission from [1] Vent Flows in a Compartment

In a multiple compartment, and/or a multiple storey structure with open vents connecting the spaces, hot gases and smoke still accumulate in the fire compartment, but as they reach vents, they also migrate to, and start to accumulate in, areas other than the room of fire origin. The exchange of hot fire gases and smoke through different vents and compartments, as well as the incoming flow of 'fresh' air to each compartment is important for sustaining the fire in the fire compartment and also governs when, where, and how the fire pulls oxygen from adjacent compartments to support burning. Investigation of the hot gas and air flow patterns as they evolve during fires then, provides important insight into how and why the behaviour, and thus heat release rate, of a fire changes as the compartment environment changes. Despite the importance of these physical phenomena that occur, these aspects have not been well studied.

Some aspects of compartment fire dynamics have been well studied. Correlations for compartment temperatures, fire plume and ceiling jet characteristics and flashover criteria been derived based on experimental investigation of well-ventilated, early stage and steady-state fires and independently for post-flashover fires, though the latter are not outlined here [11, 1]. However, it is clear from Figure 2.4 that fire flows, and thus heat release histories, are much more complex than can be described by simplified steady state correlations between parameters. In addition to correlations of heat release rate with fire plume and

ceiling jet flows, other aspects of fluid mechanics are also pertinent to understanding of smoke movement and plume dynamics. For example, in a scenario in which a smoke layer flows along a solid boundary, like a ceiling, the principles of boundary layer flow will apply and there will have to be a slowing of the flowing smoke so it is eventually zero at the surface of the ceiling since the smoke layer cannot pass through the solid ceiling [52]. Similarly, flow velocity gradients present between the turbulent hot smoke and relatively quiescent cool ambient layers result in the formation of shear layers [52] between the hot gases and cooler air which then lead to mixing and contamination of the 'fresh air' in the cooler layer with smoke particulates [51], as illustrated in Figures 2.4 and 2.5. Opposing flows of different densities and turbulence levels can also lead to the formation of vortical flow patterns visualized as rotational 'swirls' within the fluid [52].

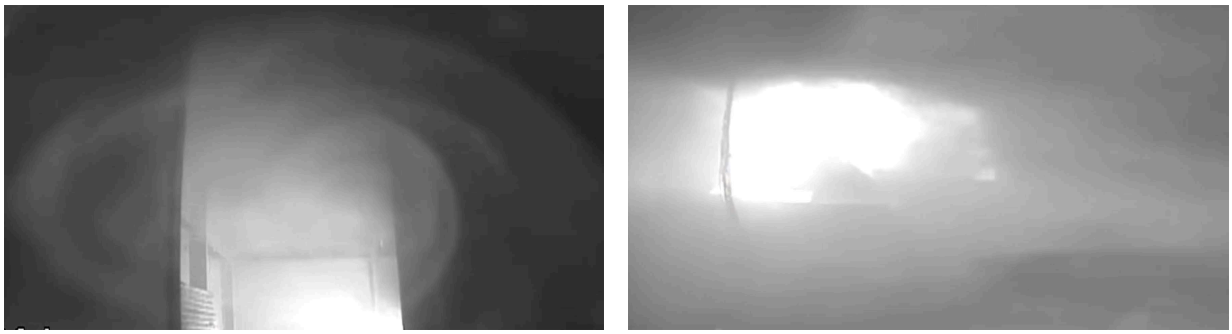

(a) Vortical Flow Second Floor Compartment (b) Smoke Layer Impingement on Fire Plume

Figure 2.5: Smoke Flow Examples During Compartment Couch Fire

All of these flow conditions have been observed in fires as shown in Figure 2.5 and thus should be considered and accounted for in development of more comprehensive models and methods for understanding the evolution of a fire environment from well-ventilated into ventilation-limited modes of burning. Thus, they are also necessary to consider in order to gain insight into fire development, fire heat release rate, smoke and oxygen movement, and generation of toxic products during real fires. To date, however, there has been little detailed research into many of these time-dependent aspects of fire behaviour and smoke development during real fires, and even less into aspects of time-dependent fire behaviour associated with ventilation-limited fires [1], because as discussed in Section 2.3 above, many of the fundamental elements of fire behaviour have been investigated using the experimental model of a small fire plume in a large enclosure. This will have similar burning characteristics as a fire burning outside in an open-air configuration with no wind. Since there is plenty of oxygen available for combustion in both situations, they present excellent starting points for study of the key physical processes and interactions that determine the

overall dynamics, geometry and heat transfer characteristics of a simple fire plume early in the fire growth phase but are less useful in extrapolating to fully developed fire behaviour or heat release rate and fire development under limited ventilation conditions [11, 1].

Other considerations specific to compartment fires involve understanding the impacts of an occlusion on the physics of a fire plume and how that might translate into any changes in the overall fire structure as well. It has been found that there is an impact on the entrainment rate when studies were conducted with 0.5m methane porous-bed diffusion flames with a heat release of 55kW [30]. A 1.22m wide wall was placed to block half of the burner, forming a semi-circle fuel bed, and as a result, entrainment was reduced to 0.57 (43% of the original value), close to the theoretical value of 0.63, and the average plume temperature increased by a factor of 1.75 [30] with consequent impact of fire radiation for example. Similar to the above configuration, when a fire is situated in a corner, theoretically, the entrainment rate would decrease by a factor of 0.4 and the temperature would increase by a factor of 2.5 [30] based on the theory that the rate of entrainment into a plume is proportional to the cube root of the heat release rate [30]. In experiments, walls and corners have been found to impact ceiling jet velocity and temperatures and factors have been developed to adjust the convective fraction of the heat release rate to provide more accurate predictions of ceiling jet velocities and temperatures as well [50].

With the above general introduction to key concepts around heat release rate, fire development and fluid mechanics of fire plumes and compartment fires, the following sections delve into more detail of experiments and characterization of these parameters for materials burning in ventilation-limited fire situations.

2.6 Ventilation-Limited Fires

In comparison with well-ventilated fires, there has been less research and investigation into compartment-fire interactions and their impacts on fire development during ventilation-limited fires, which are themselves typically characterized by lower temperatures, lower levels of oxygen and more smoke production. Thus, for ventilation-limited fires, some studies have been undertaken to better understand the impacts that the fire, radiation and compartment interactions have on various physical parameters, such as the heat release rate and smoke movement. The following sections outline key results from existing literature related to fire progression in ventilation limited fire situations, beginning with small-scale investigations and progressing to larger-scale studies.

2.6.1 Small-Scale Ventilation-Limited Experiments

Beginning at small-scale, it is first noted that there is not a reliable, consistent and generally accepted bench-scale test equivalent to the cone calorimeter (discussed above for testing in well-ventilated conditions) available by which to investigate the heat release rate from small, representative samples of a given material under prescribed ventilation-limited environments. Instead, small-scale experiments into the burning characteristics of simple fire models, again often pool fires, under limited ventilation conditions commenced with small enclosure fires. From these, specific burning and extinction regimes related to ventilation-limited fires have been found. In this context, small-scale experiments are considered to be tests conducted in small compartment sizes less than $1m^3$. In studies into the behaviour of heptane pool fires of varying diameters (6.5-19cm) using $40cm^3$ compartments with ceiling and floor vents of varying sizes ($0.02\text{-}0.24m^2$), four regimes of burning were identified [53]. Regime 1 occurs when the vent size is too small for the size of the fire and is defined as extinction of the fire due to smoke filling the compartment [53]. In this case, not enough air is supplied to the fire through the small vent to sustain burning of the fuel [53]. Regime 2 also involves extinction of the flames, but this time as a result of the flames blowing-off the fuel source due to inflow of air from a lower vent [53]. Regime 3 is marked by steady oscillating flames, which cycle in size from small to original before extinction. Here, extinction does not occur until burnout (all fuel consumed) [53]. As well as oscillating flames, ghosting flames or flames that periodically lift off the fuel surface are seen in this regime before the flame is extinguished [53]. Finally, Regime 4 is marked by sufficient air inflow to sustain steady burning of the fire until all the fuel is exhausted [53]. In the case of regimes 2 and 3, burning was seen at the vent, suggesting that all of the oxygen in the incoming air is completely burned to sustain combustion. This occurs as a result of the ventilation-limited mode of burning inside the compartment [53]. In these small compartments, concentrations of oxygen before extinction were measured at between 10% and 14% for regimes 1 and 2, and oxygen decreased as low as 6% near the fuel pan during regime 3 [53]. It is clear then that the fuel-to-air ratio within a fire compartment greatly impacts the development and burning characteristics of a fire.

Similar regimes of burning to the above have also been seen in other small-scale experiments of methanol pan fires in cubic compartments ranging from $0.15m^3$ - $0.7m^3$ [54]. Depending on the vent size, $A\sqrt{H}$, differences in fuel burning rate and flame behaviour were observed [54]. Critical values of vent size for each compartment size were generated based on the size of vent required to maintain steady burning in that compartment [54]. When the vent size was too small for the compartment, or fuel supply was too large for the amount of incoming air, there were oscillating flames, extinction of flames and decreased

burning rates [54, 53]. In other words, if the fuel-to-air ratio in a given fire situation is not optimal, as a result of compartment size, geometry, vent size, ventilation rate and/or amount of fuel, the fire cannot reach a quasi steady-state and oscillation and ghosting flames are seen; this is particularly true when ventilation becomes significantly limited [55]. In a 0.75m^3 compartment with a small ceiling vent, the mole fraction of oxygen at the time the fire extinguished was about 9% lower than in compartments with large ceiling vents [55]. Further, if the heat release rate is large relative to the size of the compartment, lower levels of oxygen were measured within the compartment [55] as more oxygen was required to sustain combustion of the fuel.

These small-scale experiments demonstrate the relationship between vent size, oxygen levels measured at different positions in the enclosure and fire behaviour, as mirrored in differing values of heat release rate and the types of flames observed. They also set the foundation for larger-scale experiments through which temperatures, smoke and oxygen distribution profiles within a compartment can be examined. Such investigations are important for characterization of the physics that occur in compartment fires burning in limited ventilation conditions. The next two sections on intermediate-scale, followed by large-scale, studies discuss the impacts that the compartment size, vent size, mechanical ventilation and fuel source have on various physical parameters, as well as the overall fire behaviour and heat release rate for limited ventilation fires. Intermediate-scale tests are defined as compartment sizes larger than 1m^3, and less than a standard ISO 9705 single compartment, which is 3.6m long x 2.4m wide x 2.4m high and roughly 21m^3 [56]. Large-scale experiments are therefore single compartment rooms greater than or equal the cubic area of the ISO 9705 standard room, through to multi-compartment configurations.

2.6.2 Intermediate-Scale Ventilation-Limited Experiments

At intermediate-scale, the inherent connection between oxygen concentration and heat release rate within a 1.9m^3 compartment has been further demonstrated in experiments in which ventilation rate was varied to directly study the effects of different air supply rates on heat release rate, oxygen levels and combustion products of liquid pool fires [57]. As ventilation rate or vent size decreased, the heat release rate also decreased. In some cases when there was no external air supply, the fire self-extinguished when only 20 percent of the fuel load had burned [57]. During their initial growth, comparable fires followed very similar trends in heat release rate, as there was enough air available in the compartment for combustion of that specific fuel. As the oxygen was consumed, differences that depended on the amount of incoming air were seen in the heat release rate of the pool fires [57], consistent with what was also seen at small-scale [55].

Studies conducted in intermediate-scale compartments have explored the influences of vent size and configuration on the resulting fire behaviour, temperatures in the compartment, smoke flow patterns, heat release rate and concentrations of oxygen and combustion products. 30cm diameter heptane pool fire tests in a 1m x 1m x 1.5m compartment with a door vent (0.45m x 0.25m) and roof vents of varying diameters (0.15m - 0.4m) demonstrate a few key aspects of the dynamics of limited ventilation compartment fires [58]. In each test, a thick smoke layer developed as the fuel was consumed. As the smoke layer accumulated and descended close to the floor, smoke exited out the door and roof vents, and a neutral plane consistently developed in the door vent [58]. As the roof vent size increased, there was an increased amount of smoke and flames flowing from the roof vent, and decreased flow of smoke out the door vent, resulting in a rise in the height of the neutral plane and more incoming air [58]. As the roof vent decreased in diameter, there was more smoke flow out of the door vent and in turn a decrease in the incoming air through the door vent and therefore a decrease in the height of the neutral plane [58]. These results showed an important relationship between the vent sizes; when the roof vent decreases in size, the more efficient pathway for the hot gases is impeded therefore forcing the buoyant gases to flow out of the door vent. Because a smaller percentage of hot gases can flow out of a smaller ceiling vent, there is more accumulation of smoke within the compartment, more flow and therefore a thicker layer of smoke out the door (lower neutral plane height). In terms of temperatures in the compartment, it was also found that the larger roof opening resulted in higher temperatures, as high as 1200°C in the upper layer, as it allowed more incoming fresh air and resulted in more efficient combustion [58].

As a result of smoke filling within a compartment, oxygen levels within the compartment are impacted and changes occur in the mass burning rate of the fuel. These were measured in tests conducted in a $1.6m^3$ compartment (with a ceiling height of 1.5m with 1.5m diameter chimney vent and a door vent). In this work, 4.6kg pine wood cribs were burned with mechanical ventilation of the compartment [59]. The lowest ventilation rates were designed to represent air-starved fires, and the upper ventilation rates were designed to represent well-ventilated fires [59]. Gas samples were taken from the chimney vent, temperatures in the compartment and mass loss of the cribs were measured [59]. The heat release rate was calculated using principles of oxygen depletion with the measured mass loss rate of the cribs and oxygen, carbon dioxide and carbon monoxide concentrations in the smoke flow out of the chimney vent. The latter were assumed to reflect the mean composition of these gases in smoke layer [59]. When the ventilation rate was 11 air changes per hour (ACH), the average upper layer temperature was 500°C at the peak, minimum oxygen measured at the chimney vent was about 5%, peak CO was about 4% and CO_2 was 13% [59]. When the ventilation rate was lower than 11 ACH, the cribs only

partially burned, and at a rate of 3 ACH the crib fire self-extinguished about 5 minutes after ignition as there was not enough oxygen to sustain burning [59]. Interestingly, when the air exchange rate was 5 ACH, smoldering combustion was responsible for the mass burned. Under these conditions, upper layer temperatures were about 300°C and measured oxygen concentration were about 12%. Conversely, when the ventilation rate was high, at 37 ACH, peak upper layer temperatures measured around 600°C, and oxygen concentration was about 4% [59]. The results highlight differences between smoldering and flaming combustion; smoldering combustion does not involve as much fuel and does not generate nearly as much heat or smoke, so hot layer temperatures are lower, there is more mixing in the compartment and higher levels of oxygen are measured at the chimney vent. When open flames were established, the mass loss rate, upper layer temperature and heat release rate increased as ventilation rate increased [59]. In terms of heat release rate, there was discrepancy between values calculated based on mass loss rate and effective heat of combustion versus those based on oxygen consumption principles. Once a factor to represent combustion efficiency was determined (45% combustion efficiency) and applied to the mass loss rate calculation, the resultant heat release rates between the methods were comparable [59].

As these results show, increased ventilation rates support higher fuel consumption rates and more complete combustion, thus higher overall heat release rates. In addition to its impact on concentrations of incomplete combustion products, ventilation can also impact radiative fraction of total heat released and, through this, radiant heat transfer to the fire and its surroundings [44]. In another $8m^3$ compartment, the effects of heat feedback to the fuel surface from the enclosure were studied revealing interesting trends with respect to the radiative and convective fractions in pool fires [60]. Heptane pool fires (0.26m and 0.3m in diameter) were placed 0.38m above the floor in the compartment and ventilation was varied [60]. Molar concentrations of O_2, CO and CO_2 were measured near the edge of the fuel pan and Gardon-gauge radiometers were used to measure the radiation from the flames [60]. For the 0.26m heptane pool fires, when the ventilation rate was decreased from 4 ACH - 0.5 ACH, oxygen concentrations decreased by 29%, from 18% to 13% and the radiant heat from the fire to the surrounding compartment decreased by 56% from 2.5 to $1.1kW/m^2$ [60]. For the 0.3m heptane fires, when the ventilation rate was changed from 4 ACH to 0.5 ACH, oxygen decreased 26%, from 10.5%-7.8% and the radiant heat decreased by 60% from 4 to $1.6kW/m^2$ [60]. Trends from these tests show that a slight increase in pan diameter resulted in an increased radiative fraction from the flame, and that radiative fraction decreases when oxygen decreases.

Predicated by the above discussions linking fire behaviour to overall concentrations of oxygen in a compartment, the concept of the plume equivalence ratio, PER, and

global equivalence ratio, GER, have been introduced when discussing the characteristics of ventilation-limited fires. The concepts of the PER and GER arise through the question of potential correlations between oxygen availability, heat release rate, CO and smoke production during these fires [61].

2.6.3 Global Equivalence Ratio

The PER is defined as the fuel-mass flow divided by the air-mass entrainment rate into the fire plume normalized by the stoichiometric ratio of fuel to air for the fuel being burned [62]. The GER similarly, is the ratio of the mass fuel-air flow ratio in the upper layer (fuel mass divided by air mass) normalized by the stoichiometric ratio [62]. In other words, it is the ratio between the actual fuel-mass flow to air-mass flow in a compartment fire divided by the respective ratio under stoichiometric conditions [61]. Experiments conducted by Beyler with gas, liquid and solid fuels (such as PMMA and pine wood) under a cylindrical hood allowed for detailed measurements of species concentrations in the upper layer and therefore it was possible to derive the ratio of combustion products from the fuel to the mass of entrained air and calculate the GER [62]. It should be noted here that the experiments were designed for steady-state burning conditions in which no air or fuel entered the upper layer except the contributions of the fire plume, and as such, PER is equal to GER in these experiments [62, 61]. A GER>1 represents a ventilation-limited fire environment, and a GER<1 represents a well-ventilated environment [62, 63]. In these hood tests, key findings were that major flame species production, including CO can be correlated in terms of the GER and relatively constant concentrations of CO are generated at both low and high values of GER. When the fuel supply and entrainment rates, and therefore the GER, in diffusion flames were varied, species generation was not sensitive to the flame structure but instead was related to the actual fuel-to-air ratio of the plume in steady-state conditions. As anticipated, generation of CO was much greater in fuel-rich conditions compared to fuel-lean conditions [62]. This experimental design by Beyler is not representative of a 'real' compartment fire or multi-compartment fire scenario, as in reality, ambient air and smoke in a fire are transferred throughout the space(s) via the complex flows described in Section 2.5.2, leading to varying GER at various locations. Nonetheless, the study did allow for a physically based understanding of some of the under-ventilated fire phenomena.

Other studies have examined the relationship between the flammability of the smoke and GER in a 2.2m^3 compartment with an inlet vent through a lower opening and an upper exhaust vent ranging in size from 0.25m-0.51m wide by 0.16m-0.32m high [64]. All air entrained by the fire entered from the inlet air duct and all the combustion products exhausted through the upper exhaust vent [64]. This allowed for direct measurement of

the fuel-to-air ratio, obtained by measuring the mass loss rate of fuel using a load cell and the flow rate of entrained air using a velocity probe positioned at the lower inlet duct [64]. Outside of the compartment a hood collected all combustion products so CO and CO_2 measurements could be determined as well [64]. The fires were fuelled by hexane pool fires burning in 0.15m, 0.23m and 0.28m pans. Two different combustion phenomena were observed in the smoke exiting through the exhaust vent. These were referred to as external burning with one characterized by external jet flames and the other by non-momentum driven flames burning in the fuel-rich exhaust smoke [64]. Generally, an increase in GER in the fire compartment was related to the mode of external burning. For example, when the initial flashes of external burning were observed, measured values of GER were 1.3, and as external burning progressed to a sustained state, the GER had increased to 1.8 [64]. There also appeared to be a clear relationship between vent size and GER at the onset of external burning. For smaller openings ($40m^2$), the GER was higher when external burning occurred, while for the same GER and smaller openings, relatively smaller external jets were observed [64]. In these experiments, as GER increased, there was an increase in the CO yields measured from both the upper layer in the compartment and the 'downstream' exhaust duct [64]. The increase in upper layer CO yields reached a plateau of around 0.23g/g when the GER was 1.7; however, also at a value of GER of 1.7, the CO yields measured at the downstream point decreased [64]. This decrease in CO yield downstream in the exhaust duct is supported by the observation of sustained external burning of the exiting smoke at this point too [64].

In other studies, it has been suggested that GER can also be estimated by the ratio between the 'theoretical' heat release rate (product of mass loss rate and effective heat of combustion) and the maximum heat release rate determined under ventilation-controlled burning [65]. The latter value is derived based on the product of the ventilation controlled mass flow of air into the compartment and the energy released per kilogram of air completely consumed (3000kJ/kg) [65]. In one study, tests were conducted in a corridor configuration, 3m long, 0.5m wide and 0.5m high, constructed from six cubic boxes, with controlled and varied inflow air [66]. A fire with low heat release rate was established on a propane burner, flush with the floor, in the center of the last compartment at the far end of the corridor and therefore furthest away from the opening [66]. Fire size was controlled between 15 and 60kW and air inflow was controlled by the size of the door opening (0.075m-0.25m wide by 0.1m-0.3m high) [66]. The tests were designed to reach ventilation-limited conditions by choosing a heat release rate that was greater than the calculated ventilation-controlled heat release rate such that GER>1 [66]. It was found that critical ventilation occurred for the largest opening for a fire heat release rate of 26.85kW, with a clear link between ventilation and fire size. In terms of gas concentration

measurements, CO measured at the ceiling roughly 1.5m down the corridor from the pool fire and closer to the opening, ranged between 3% vol with the 0.20m x 0.2m vent and 4.5% vol withe the 0.075m x 0.3m vent during the 50kW fire tests [66]. Consistent with expectations, it was found that when the GER was higher, the measured CO in the upper layer was also higher [66]. For example in the 0.1m x 0.25m opening tests, when the heat release rate was 25kW the GER was 1.3 and CO levels were roughly 2.5% vol in the upper layer of the corridor, and when the heat release rate was 60kW the GER was 3.2 and CO levels were roughly 4% vol in the upper layer of the corridor [66]. Oxygen concentration measured in the bottom layer of the corridor, about 1.5m away from the pool fire and therefore roughly halfway through the corridor, was 5-6% vol during these tests as well [66].

Further building upon the findings that increasing GER is related to increasing amounts of incomplete combustion products, large scale tests conducted in an ISO 9705 room with a wide range of liquid fuels burning in pans ranging from $0.5m^2$ to $1.4m^2$ in size and with varying door vent size demonstrated that the yields of CO, TUHC (total unburnt hydrocarbons) and HCN all increased, and consequently heat release rate decreased, as the GER increased over 1.0 and the fire progressed to ventilation-limited burning [67]. It was found that the nature and quantity of combustion products depended on the GER. As the environment shifted from well-ventilated to ventilation-limited, there was a shift in the yield of products containing nitrogen from NO_x to NH_3 and HCN [67]. Furthering the understanding of the relationship between the fire heat release rate, oxygen levels, smoke production and amounts of incomplete combustion products is key to making informed decisions around fire hazard assessments and egress. Therefore, having a parameter such as the GER against which to correlate key parameters of fire behaviour, might make characterizing large scale fire environments easier, in turn potentially allowing for design of structures with better account taken of critical ventilation parameters across compartments.

To conclude, the GER is one way to define a ventilation-limited fire environment. Relationships between CO concentrations, vent size, external burning and GER have been explored. While such results appear to facilitate definition of relationships between GER and overall fire development, it must be recognized that in real fires, a GER greater than 1 may not be simultaneously met locally and globally, as ventilation may become quite limited local to the combustion zone, with consequent impact on fire behaviour and heat release rate [67] at a different rate than oxygen is consumed within the entire compartment. This points to a weakness in applying the concept of GER in compartment fires, and even further underlines the importance of distinguishing between global and local ventilation conditions, and thus the global (compartment) and local (fire combustion zones)

equivalence ratios as well.

2.6.4 Large-Scale Ventilation-Limited Experiments

In 1978, Warren Fitzgerald made the first attempt to develop a technique for measuring heat release rate in full-scale enclosure fires [68]. A 2.7m x 2.7m x 2.7m test enclosure was instrumented with thermocouples and a load cell, and had a forced air supply of $0.19 m^3/s$ through a small supply duct. Another duct was used to exhaust the combustion products, which also had a port for extracting gas samples [68]. This test method was designed for the measurement of free-standing and relatively small fuel loads; mainly pool fires of polymers [69]. Interestingly, it was found that in this enclosure, when a 0.9m diameter pool fire of PMMA was tested, the burning rate was much lower than for a smaller fire and did not follow trends which had been previously observed, suggesting that the room was becoming vitiated, or ventilation-limited. It was supposed that the air available for combustion was contaminated with re-circulating combustion products, so the oxygen level in the enclosure had dropped well below the usual 21% in ambient air and not enough oxygen was available in the air around the fire to support complete combustion of the evaporating PMMA fuel [69].

While these results are now much better understood for a variety of fuels, in reality very limited numbers of large experiments have been conducted to investigate the development and progression of compartment fires to under ventilation limited conditions. Some were focused toward determination of a critical vent size, the required size of opening to promote a well-ventilated environment for a given fire size. Others sought insight into the amounts of incomplete combustion products found in a smoke layer as the ventilation, and thus parameters such as global equivalence ratio discussed above, changed. In all, attempts were made to further understanding and develop new correlations for important aspects of fire behaviour, such as heat release rate, and ventilation-limited compartment fire dynamics.

Outside of using GER as a threshold technique to determine if an environment has progressed to ventilation-limited, low oxygen levels have also been used as a marker of ventilation-limited environments in compartment fires. Low levels of oxygen result in incomplete combustion of the fuel vapour so they not only result in increased smoke production and increased quantities of incomplete products, but also impact the mass loss rate and, therefore, heat release rate of the fire. Key information in a fire safety assessment is the mass burning rate of the fuel. In most enclosure or confined configurations, the burning rate of the fuel is dependent on the environmental conditions, in particular the air around the fire, and the amount of radiative energy feedback from the hot surrounding

gases and flames to the vaporizing fuel surface [70]. Investigations into the impacts of ventilation changes and configurations on mass loss rate (synonymous with mass burning rates), heat release rate, oxygen levels, temperature and pressure distributions are focused in the next several paragraphs. These present the characteristics of the low oxygen, ventilation limited environment, and contrast some of the physics introduced for the well-ventilated compartment fire explained in the beginning of the chapter.

Wood pallet fires were run in a large-scale multi-compartment layout [71]. The wood pallets were placed in a fire room sized 2.44m x 6.1m x 2.6m, which connected to two other compartments of the same dimensions, with connecting doors that allowed smoke from the fire compartment to fill the attached secondary compartments. Ventilation decreased as smoke filled the fire room, as reflected in low measured oxygen levels of around 4% at the door between the rooms [71]. As ventilation decreased, mass loss of the fuel also decreased [71]. Other studies comparing mass burning rates between free burning and enclosed $0.2m^2$ and $0.4m^2$ TPH pool fires further indicated these trends. The pool fires were situated 0.4m above the ground in a large-scale enclosure with inlet and exhaust ducts installed near the ceiling and gas concentrations were measured continuously near the pool fire, near the floor and at the ceiling [72]. In the first 120 seconds of burning, the mass burning rate profiles between the compartment fire with a ventilation rate of 4.7/h and the open-burning fire were quite similar [72]. This first phase was subdivided into three parts which included a flame propagation phase, followed by an increase in mass loss to a primary peak, and then a slight decrease in the mass loss corresponding to when lower levels of oxygen were measured in the lower regions of the enclosure [72]. The second phase of burning was different between the compartment fire and the open-burning situation. At this point, the mass loss in the compartment test is lower than that measured in open-burning, but this is followed by a period in which the mass loss increases to peak values greater than for the open-burning fire which seem to begin when when oxygen concentration was 18% vol near the pool [72]. Fourier Transform Analysis of variations in pixel intensity with time from video footage supported the trends seen in mass loss [72]. During the first stage, puffing frequencies of the two fires were about the same at 1.5Hz. During the second phase in the compartment fire, however the frequency decreased to 1.2Hz which suggests a larger fire (higher mass burning rate) potentially due to differing fire plume and air flow in the compartment [72]. The evidence is consistent since the increase in mass loss corresponds with rapid decrease (consumption) of oxygen in the lower region of the compartment [72]. In the third phase of burning, the mass loss is steady, but much lower for the compartment fire (4g/s) compared to the open-burning fire (14g/s), until the fire is extinguished [72]. In the upper layer of the compartment, oxygen levels decreased to 13% volume, in the lower layer to 14% volume and, near the base of the pool, they were also 14% volume [72]. When

the ventilation rate was changed within the enclosure, the magnitude and time to reach peak mass burning rate was the same; however in the steady burning phase, the mass burning rate decreased as ventilation into the compartment decreased [72]. Additionally, the $0.2m^2$ pool fire had a mass burning rate similar to the same size fire in the free-burning scenario for a longer duration compared to that for the larger $0.4m^2$ fire. This again supports that the mass burning rate is governed by fire diameter in combination with the quantity oxygen available to sustain burning, and also the rate of generation of gases in fire plume and therefore the rate at which hot plume gases fill the compartment [72].

Similar trends to those recorded above were seen in a comparison study of the behaviour of liquid pool fires in open-air, 1-room and 2-room test configurations [70] with mechanical ventilation. The rooms were each 5m x 6m x 4m high interconnected by a 0.7m x 2.1m door but closed to the exterior [70]. The heat release rate of the pool fires tested ranged between 150kW-900kW. Oxygen was measured inside the fire room near the pool burner, in the upper layer and in the lower layer of the fire compartment [70]. Four regimes of mass loss rate were observed. These consisted of an initial burning period, a transition phase, stationary burning and finally extinction [70]. The initial stage involves the initial rise in mass loss rate towards the primary peak value. For each test at varying ventilation rates, this behaviour was extremely comparable to that seen in the open-burning case [70], consistent with the findings described above [72]. The transition phase was noted to have two sub-phases. The first was identified to have a mass loss rate similar to that of the open-burning profile for the same pool fire, and the second was characterized by a peak in burning rate as a result of the flow of air around the flame, followed by a decrease in mass loss rate to the value characteristic of the stationary phase of steady burning [70]. The observed behaviour is a result of changes in the ambient properties in the room, namely the accumulation of smoke, transport of smoke throughout the spaces and oxygen depletion in the available air [70, 72]. In the stationary phase, the mass burning rates of the compartment pool fires are lower when compared to the open air tests, and depending on the scenario, extinction occurred due to lack of oxygen or lack of fuel [70]. Further, patterns were observed in the consumption of oxygen. Initially, the oxygen in the upper regions of the compartment was consumed, followed by consumption of oxygen from air in the lower regions of the compartment and the regions closest to the flames and the surface of the pool. By the end of test, the upper regions of the compartment appeared to have the lowest amount of oxygen present, which was slightly lower than levels of oxygen measured in lower regions and near the flames [70, 72]. Similar to the TPH fires described above [72], the mass burning rate varied in proportional to the ventilation rate, and the main effect of changing the ventilation within the compartment was seen in the value of mass burning rate during the steady-burning or stationary phase [70]. In other large-scale experiments

involving pool fires, decreases in the fuel mass loss rates were also seen when inlet or exhausts were closed, and extinction of the fire occurred when molar oxygen concentration in those compartments was at 15% volume. [73].

In a 3.4m x 3.3m x 3.05m high compartment, effects of both natural and forced ventilation on the resulting fire environments were examined for different fuel sources such as liquids, wood and polyurethane slabs [74]. In the natural ventilation tests, the door and window vents were utilized in configurations of either open door, 1/4 opened door, or open window [74]. In the forced ventilation tests, ducts were installed and the rate of ventilation was either 0.29kg/s, 0.45kg/s or 0.74kg/s [74]. There was an exhaust vent for combustion products (0.28m x 0.28m). Temperatures, flow rates and oxygen levels were measured throughout the compartment [74]. In the forced ventilation tests, fuel burning rates increased with ventilation rate. The thermal environment showed two-layer characteristics, however oxygen measurements pointed towards a well-mixed environment; in the case of a polyurethane slab fire with 0.74kg/s forced ventilation, the minimum oxygen concentration was 14% at all heights [74]. In the natural ventilation tests, both the temperature and oxygen data show distributions consistent with a two-layer compartment, with hot upper layer and cooler lower layer characteristic of the well-ventilated case. However, when the window or the 1/4 opened door provided inlet ventilation, more mixing occurred and the two-layer oxygen distribution was less defined and temperature distributions indicated either one or two-layer environments [74]. These temperature profiles were similar to other experiments conducted in 4m x 6m x 4.5m compartments with both low and high air inlets [75]. In these tests, with methane gas fires ranging from 100-400kW, high rates of air inflow at positions low in the compartment and low rates of inlet air at positions high in the compartment were both found to result in two-layered thermal environments, whereas, low rate of inlet air at low positions, and high rates of inlet air at high positions led to one-layer, well-mixed thermal environments [75]. The natural ventilation tests demonstrated the relationship between geometry of the vent and compartment environment. As the size of the vent decreased, the quantity of incoming air decreased and impacted the fire and the compartment environment [74]. Consistent with other tests, lower levels of oxygen led to a reduction of burning rate, regardless of fuel type [74]. In the test with the door vent open only 1/4 and a polyurethane slab as fuel, oxygen concentration decreased to about 12% throughout the compartment [74]. Investigation into differences in the mass burning rate with decreased oxygen at the base of the flame suggested that under conditions of depleted oxygen, the fuel burning rates could dip to values as low as 1/3 of the burning rate in a free burning/ambient environment [74].

As described previously, the typical representation of a compartment fire includes a hot upper layer of smoke and gases, and a cooler lower layer of ambient air. However,

this two-zone model does not always hold, and as seen in the experiments conducted above [74], the ventilation, fuel size and configuration of the enclosure [75] can lead to species concentration and thermal profiles which are not always the same [74, 75]. Within a compartment, the temperature profiles are not always uniform, depending on the fuel placement and ventilation parameters. For example, a 2-seat foam and leather sofa tested in a ISO 9705 room under normal conditions produced a peak heat release rate of 1000kW [76]. Temperature profiles varied throughout the space, with a two-layer profile in the opening to the room and in the middle of the room, a stratified profile similar to a two-zone distribution in the corner near the opening in the wall, and stratified profiles near the rear wall corner, near the middle of the rear wall, and in the upper layers of the compartment [76].

In addition to understanding temperature distributions throughout a compartment, insights into the relationship between pressure in a compartment and ventilation rate can provide valuable information as to how smoke and other hot buoyant gases will flow between compartments in multi-compartment configurations [77]. Fire affects smoke flow in several ways. It generates hot gases which flow upward due to buoyancy and increase temperatures in the room. Fire induced flows characterized by buoyancy and expansion of gases, are low speed and can cover large spatial regions [78]. This can lead to changes in static pressure with magnitude related to the physical dimensions of the compartment and size of fire. Before ignition, mechanical ventilation may cause a drop in pressure between rooms, however once ignition occurs, the expanding combustion gases generate pressure and, depending on the heat release rate, the small build-up in pressure due to the fire may reverse the drop in the static pressure on the upstream side relative to the downstream side. Studying these physical interactions are therefore important to understanding flow patterns of smoke [77]. To investigate the coupling between pressure and smoke flow, tests were conducted in a three-room configuration with controlled ventilation. Each room was 5m x 6m x 4m high and connected to the adjacent room by a door vent. The fire heat release rate was controlled by a propane gas burner in the center room, to study the impacts of smoke flow into the upstream and downstream compartments under different conditions [77]. Heat release rates were varied from 100 to 400kW, and ventilation rates ranged from 500 to 3100 m^3/ hr. The compartment connected by the upstream doorway had the inlet duct and the compartment connected by the downstream doorway had the exhaust duct [77]. As the heat release rate increased, the velocity of flow measured in the doorway between compartments (when ventilation is kept constant) increased, the height of the neutral plane decreased and the velocity profiles between the two doorways were asymmetric [77]. At a constant heat release rate with varying ventilation rates, an increase in ventilation rate resulted in increased rates of incoming air and increased heights of the

neutral plane at the upstream doorway [77]. At the downstream doorway, the increased ventilation rate reduced the rate of incoming air and decreased the height of the neutral plane [77].

As a fire grows larger, there is more oxygen needed for combustion, and this is reflected in the rate of flow of the incoming fresh air. For example, in an ISO 9705 room with a gas burner, when the burner heat release rate was set to 34kW, the velocity of the flow into the room, measured at the door vent by both particle image velocimetry (PIV) analysis and bidirectional probes, was about 0.5m/s, while velocity of the smoke out was about 0.25m/s and the height of the neutral plane was approximately 1.1m [78]. When the heat release rate was increased to 511kW, the velocity of incoming air increased to 2m/s, outgoing flow rate of smoke also increased to about 2m/s, and the height of the neutral plane decreased to about 0.9m [78].

Many aspects of pressure build-up in a compartment and smoke flow out of a compartment will be similar for well-ventilated and ventilation-limited cases. However, many of the existing studies have been constrained to well-ventilated fires in single adjoining compartments and the history of pressure changes, and thus smoke flow, will be different for limited ventilation fires and in multi-compartment scenarios. Further understanding is needed into how smoke flows throughout not only multi-compartment, but also multi-storey structures. Thus, links between fire development, heat release rate and trends in smoke flow will be further investigated using the results of the experiments analyzed for this work. Exploration of full-scale trends in fire behaviour and ensuing physics have been discussed in the previous section. To conclude this section on ventilation-limited fires, the concepts of scaling fires is presented as scaling can potentially be used to study fires at small-scale in order to better characterize fires in ventilation-limited environments.

Large-scale compartments and structures are difficult to procure for full-scale investigation of fire behaviour and instrumentation and conduct of repeated large scale fire experiments is extremely expensive. As a result, scaling methods and models have been developed by many researchers as invaluable tools by which to extend existing results to more realistic fire scenarios. Adding to this, real fuel sources are much more complex than those normally utilized for controlled studies. In this regard, not only testing the fire performance and properties of these fuels, but also modelling the combustion process becomes more difficult. In the following sections, the concept of scaling of enclosure fires is first provided, which leads into scaling work done for furniture, and then discussion of heat release rate characteristics of the complex fuel source that was used in the experimental work presented in this thesis.

2.6.5 Scaling of Fire Enclosure Size

Large-scale experiments are expensive to conduct and it is certainly not always feasible for researchers to utilize these for investigations of the fire performance of different material combinations and furniture configurations. Even building an ISO standard room or procuring spaces of similar dimensions to those described in Section 2.6.4 above in order to run test burns can be challenging. As a result, there have been attempts to use smaller-scale enclosures to model fires in larger enclosures as a way to allow flexibility in testing and therefore to better develop fire scaling and predictive techniques. For example, experiments conducted by Parker and Lee in 1975 used a 0.76m x 0.76m x 0.61m enclosure to model fires that took place in a 3m x 3m x 2.4m enclosure. They recognized that for successful correlation between scales, major fire phenomena that took place in the large-scale enclosure had to be mirrored in the small-scale model. Since flashover was observed to occur in the large-scale experiments when temperatures in the hot layer reached 700°C, it was determined that the hot layer temperature could be indicative of the fire building to a size where there was potential for rapid fire growth within the room [79]. Predictive equations for upper layer temperatures were then developed using principles of heat transfer, based on fire heat release rate, thermophysical properties of the room materials and the following assumptions [79]:

- two temperature regions form in the compartment (a hot upper layer that is exhausted through any room openings, and a cool lower layer of inlet ventilation air),
- mass flow rate and heat capacity of the combustion products are equal to those of the incoming ambient air and therefore the convective losses through the opening are assumed to be a product of the density, heat capacity and volumetric flow rate of incoming air,
- radiation can be neglected because radiative heat transfer from the upper layer air to the enclosure is low and is therefore confined to the upper regions of the walls and ceiling, and
- the heat flux back to the boundary surfaces is approximately proportional to the temperature rise in the hot layer.

An equation to predict an oxygen depletion fraction was also developed based on the relationship between the heat release into a space, a characteristic temperature rise, oxygen consumption, heat release per unit area of material burning (acquired in a cone calorimeter test), area of material involved in the fire (information from flame spread test), a ratio of

involved area to floor area, and a ventilation parameter which is the volumetric flow of the inlet air divided by the floor area [79]. The last two parameters, the ratio of burning fuel surface area relative to the floor area and the ratio of inlet air supply relative to the floor area, as well as the thickness of any wall materials, were deemed important to preserve when scaling in order to account for proper air flow and heat transfer characteristics [79]. In the small-scale tests, a variety of measurements were collected, including temperatures in the upper layer and oxygen concentration in the outgoing air, as well as mass burning rate. From the small-scale data, the predictive equations were used to calculate upper layer temperatures in the full-scale enclosure [79] and compared against measurements from actual fires conducted at full-scale [79]. Agreement for upper layer temperatures and oxygen depletion were reasonably good for most tests, which highlighted that scaling and predictive measures could be useful given knowledge of how to scale compartments to be proportional in terms of geometry, volume and oxygen content [79]. On the other hand, the model did not predict more complex tests very well. These were tests with a combination of air supply fully off or doors closed/partially closed, and in one case there was ventilation, but there was an opening to another area of the enclosure that was closed off for some but not other tests [79]. Inconsistencies in the prediction of upper layer temperature and oxygen depletion for enclosures with limited ventilation and/or configurations which open to more sub-compartments and allow for transport of combustion products away from the main fire area, pointed to the fact that there was still work needed in terms of fully scaling ventilation-limited fires and extension to multi-compartment fires.

In other tests, heptane and dodecane were burnt in an $8m^3$ compartment, which was scaled down from from a $100m^3$ compartment using a Froude scaling technique, taking care to maintain a Reynolds number large enough to maintain turbulence [80]. The fire heat release rate was scaled to under 130kW (from 1MW in the full sized compartments). A mechanical duct 0.2m x 0.2m in size, located 0.3m from the floor supplied air at rates ranging from 24 to $40m^3/h$, and exhaust was ducted through the ceiling [80]. A load cell was used to measure mass loss of the fuel, and heat release rate was calculated as the product of the mass loss rate and heat of combustion [80]. Gas sampling and chromatography were used to measure oxygen, CO, CO_2, and total unburnt hydrocarbon (TUHC) concentrations at the extraction duct [80]. For the 0.3m heptane fires, at a ventilation rate of 3 ACH, oxygen was measured to decrease to roughly 6% vol, and CO/TUHC were measured to be roughly 1.0-1.5% vol[80]. For a higher ventilation rate of 5 ACH, measured oxygen concentrations were still low, roughly 6-8% vol, indicating a ventilation-limited environment, and CO/TUHC were measured around 0.1-0.5% vol [80]. Similarly, for the 0.4m dodecane pool fires at a ventilation rate of 3 ACH, oxygen measured was between 5-10% vol, and CO/TUHC were measured around 0-1.6% vol [80]. At the high ventilation

rate of 5 ACH, oxygen was measured between 8-5% vol and the CO/TUHC were 0.1-2.4% vol [80]. While reported concentrations may not match values obtained in full-scale fires, they again clearly point to the link between level of ventilation, air fuel ratio at the fire and final composition of upper layer gases in a fire compartment.

Similarly, in a smoke density scaling study it was concluded that there is no simple relationship to scale from a small to large scale test. Predictive techniques had better agreement when CO was included as one of the correlating parameters [81]. In fact, the best predictive model found was a logistic linear multiple regression model which included CO production, time to reach peak heat release rate after ignition and a variable determined to be 0 for wood and 1 for all plastic materials [81]. Although this model provided more agreeable comparisons across test scales, results were only accurate for full-scale smoke production up to fire sizes of 400kW for materials that transition to flashover in 10 minutes [81]. Although there were limitations, this study did show that it was possible to create a simple predictive technique for smoke production in terms of relatively simple measures [81]. For example, it was possible to predict whether the smoke to heat production ratio of items in a full-scale environment was likely to be above or below a given threshold based on the corresponding bench scale smoke data [81]. Importantly for the present research, it highlighted that it is very important to interpret the combustion conditions appropriately in a given fire environment in order to find relationships between small and large-scale test results since the production of fire effluents, and hence heat release rate and other critical parameters, are directly influenced by the local combustion conditions [81]. This last point is very important for the use of any predictive model in various fire environments, since in reality no two fire environments will be the same. Very importantly as well, combustion can be difficult to represent appropriately, especially when the fuels get very complex. This is particularly the case for furniture which formed the fuel in the present research, wherein there are two or more materials, each with their own combustion mechanisms. These considerations form the focus of the next several sections.

2.7 Nature of Complex Fuels: Furniture

The heat release rate of a furniture fire is a result of combustion and thermal processes which are dependent on the combinations of materials involved and are also connected in three-dimensional space [82]. The burning process is quite complex and is considered to have three reactions which develop concurrently; 1) endothermic pyrolysis of the material undergoing combustion, 2) flaming combustion of some fraction, or all, of the gaseous products, and 3) oxidation of the char layer that forms on the surface of the material,

often referred to as smoldering combustion [82]. The heat necessary to drive pyrolysis can come from the flaming region of a fire plume, from the oxidizing char, or, as in the case of a controlled incident heat flux for cone calorimeter or other testing purposes, from an external source [82]. While a cone heater provides radiation heat flux to the fuel surface, heat transfer from the flames to the unburnt fuel surface primarily comes from radiative and convective heat transfer, whereas heat transfer from an oxidizing char surface to other unburnt fuel surface is via conduction [82]. This underlines the physical complexity of detailing the fuel heating processes, prompting development of methods to understand the phenomena using more global measures as well. To shed further light on these, this section will first cover some properties of furniture materials, specifically polyurethane foam and fabrics similar to those making up the fuel in the present research. Following this are sections summarizing key elements of small-scale testing of furniture composites through to large-scale compartment furniture fire tests.

2.7.1 Polyurethane Foam

Polyurethanes (PU) are a large class of polymers used in a variety of industries, such as building construction, automotive and furnishings, for a multitude of purposes. They come in many different forms from rigid and flexible foams to rubbers, coatings or adhesives [83]. Polyurethane is made by reacting diisocyanates or polyisocyanates with diols or polyols. The proportion of reagents, and specific catalysts used, can result in the different products [83]. Details of the specific bonds and cross-linking in a given product have an impact on the thermal and decomposition properties of polyurethane [83], with the weakest links (allophanate and biuret cross-links in the case of flexible foams) dissociating at temperatures as low as 110-170°C [83]. This would therefore be characteristic of polyurethane foams that might be used for cushions in upholstered furniture construction. Knowing that flexible polyurethane foams are thermally weak, there have been efforts to add fire retardant additives, referred to herein as FR, to the foam to make it thermally more robust. As a result, work has been done to understand the combustion process, thermal degradation process and combustion products when these FR additives are present as well [84, 85, 86, 87].

Without FR, the flammability of polyurethane foams depend on the structure of the polyols and amount of isocyanurate present in the network [83]. The density of the foam also impacts flammability as highly porous and lightweight foams can support faster flame spread mechanisms [88]. In general, the combustion of flexible polyurethane foam can be described as a two step process. Initially, a layer may tend to melt and leave behind a black, char-like material which can propagate along the surface or drill down into the foam [83]. This initial phase is then followed by combustion of the molten material and tar [89].

In terms of combustion products, some concerns have been voiced about certain harmful effluents produced by polyurethane foam during combustion, with FR additives potentially contributing additional amounts and kinds of products as well. Since there is nitrogen present in the chemical structure of the foam, when pyrolysis occurs, a certain amount of hydrogen cyanide, or HCN, may be produced [90] and nitrogen oxides may be formed depending on details of the combustion process [83]. However, literature on comparative combustion gases from other nitrogen containing materials, such as wood, is scant and the effects of FR additives on the toxicity of the gases produced from polyurethane foam combustion are contradictory [83] which supports the premise of this work that more data and investigation into combustion products produced in small-scale and full-scale fire environments, under differing ventilation conditions, fuelled by both non-FR, herein referred to as NFR, and FR foams is important with regards to informing the community about the impacts of these materials on various aspects of risk in different fire scenarios.

2.7.2 Fabrics

There are many types of fabric coupled to the foam elements in upholstered furniture. These include nylon, olefin, polyester, cotton/wool, and leather, each used for different comfort and aesthetic appeal. Similar to polyurethane, there are questions as to how these fabrics act in a fire scenario and by extension, how these materials interact with the underlying polyurethane foam to alter burning characteristics and combustion chemistry of the fabric foam assembly. Also similar to polyurethane foam, the fabric materials may contain fire retardant additives, resulting in the need to study different NFR and FR fabric and foam combinations.

Fabrics, like other polymers, can be broken into two categories: thermosetting and thermoplastic. In a fire, thermosetting materials will typically not melt and instead char, whereas thermoplastic materials will melt and promote pool type burning. In the context of furniture used in this research, polyester would be a thermoplastic fabric which tends to melt and pool during combustion, whereas cotton, being cellulose-based, has thermosetting characteristics and will char when burned. Such differences in behaviour have led to the concept of barrier fabrics used for their ability to prevent a fire from involving the underlying polyurethane foam and thus aiding the fire to self-extinguish. Even if a barrier fabric is not used, it has been noted by many researchers that foam flammability and burning characteristics are altered when fabric is involved in the combustion process [91, 92, 93, 94, 95, 96]. For example, less smoke production has been recorded when the fabric in a furniture combination is excluded in a cone calorimeter test sample [97] and melting fabrics have been seen to decrease time to ignition [96], while charring fabrics can

delay ignition time [96]. Varying the fabric tested in composite samples with a consistent polyurethane foam can lead to changes in the magnitude of the peak heat release rate as well [96]. These findings clearly suggest that fabrics play a large role in the nature of the burning behaviour of the composite materials assemblies found in furniture, prompting researchers to develop different test methods and models specifically for use in evaluation of furniture fires. Key research findings related to characterization of heat release rate of furniture materials via small-scaling testing in the cone calorimeter are discussed in the following section.

2.7.3 Cone Calorimeter Testing of Foam and Fabric

As mentioned in Section 2.2, the cone calorimeter is a widely used tool for examination of the heat release of materials and material combinations under well-ventilated burning conditions. The test provides a wide variety of data and is versatile, as many different kinds and combinations of materials can be tested. Today, there are two common test standards applied for the testing of materials in the cone calorimeter; ISO 5660 [98] and ASTM E1354 [99]. In short, a 100mm x 100mm x 25mm piece of a material is placed in a sample holder which sits horizontally [99, 98] on a load cell and is subjected to a known value of radiant heat flux from the cone heater situated directly above. The standard test is run in open air, with or without external pilot ignition by a spark igniter, and a given sample may or may not ignite. Pyrolysis and/or combustion gases are collected through an exhaust running at nearly constant volume flow rate and passed through a gas analyzer system. The time resolved species concentration and mass loss rate data is collected and later processed to estimate a variety of output parameters, such as the time to ignition, heat release rate, mass loss rate, effective heat of combustion and rate of smoke production to name a few. The cone heater can subject a sample to a surface radiant heat flux up to 100kW/m^2, though it is much more common to use lower flux levels such as 35 or 50kW/m^2. Due to the size of the samples, this test method is considered to be bench-scale. Data provides valuable information for researchers and industry since it can be used to conduct a relative comparison of materials in terms of their ignitability and/or heat release rate. Therefore, it has been widely used to test polyurethane foams and combinations of polyurethane foams and fabrics used in furniture construction both as a screening tool for new materials for flammability and other fire related properties, and also an important step in the process of developing new materials [100]. Further, since the cone calorimeter was deemed an appropriate tool for discerning the fire behaviour of different polyurethane foams [101], cone calorimeter test data has been used as a basis on which to develop models for scaling small-scale test results to estimate behaviour of full furniture items [102, 9, 103, 104].

At a fundamental scale, the cone calorimeter has been used to determine how polyurethane foam degrades and burns when heated. Typically these foams exhibit a characteristic double peaked heat release rate curves where the first peak is due to the complete breakdown on the cellular polyurethane structure leading to the viscous char-like brown/black tar, and the second is due to the combustion of that tar product [89]. The magnitude and time to the first peak strongly depends on the density and thus degree of open cells present in the foam [89]. Other studies have probed differences in fire performance of foams as differing amounts of reagents, such as isocyanurate rings, are added in the polyurethane composition. These are theoretically added to make the foam more stable [83] and consistent with this, when a sample of foam with a high percentage of isocyanurate rings is tested 20% of the starting mass was lost, compared to an original foam that had a relatively lower percentage that lost 60% of the original mass [101].

Both the importance of testing, as well as some of the challenges in testing even at bench-scale, came to light as the cone calorimeter was applied to test composite foam and fabric combinations found in furniture, and further again as fire-retardant additives were added to the foam and fabric. Due to success in using the test in understanding new formulations of foam, it was applied to compare, characterize and understand the fire performance of the newer fire-retardant (FR) materials versus non fire-retardant (NFR) materials as well. Under the cone calorimeter, some FR materials, as anticipated, were found to take about twice as long to ignite and lost a smaller fraction of their starting mass when compared to their NFR counterparts [97]. Other consistent characteristics of FR polyurethane foams were decreased values of peak heat release rate and longer times to ignition and peak heat release rate when compared to their NFR counterparts [101, 89]. In general also, was an observed increase in CO production [97] and overall smoke production when certain additives, like halogenated FRs, were present [101, 89].

In comparative experiments between FR and NFR furniture combination samples, peak heat release rates and calculated heats of combustion of the FR samples were found to be lower at 290 kW/m^2 and between 15-18 MJ/kg respectively, less by 40% and 35% relative to comparable NFR combinations which indicated peak heat release rate values of $470kW/m^2$ and heat of combustion around 27 MJ/kg [97]. On the other hand, it was found that some foams, when tested alone without a fabric counterpart, behaved differently compared to composite furniture materials tested in-situ [97]. For example, in the cone calorimeter, tests conducted on a NFR foam alone indicated peak heat release rate values of $540kW/m^2$, unexpectedly higher than for a combination of the same NFR foam with fabric for which the peak HRR was only $470kW/m^2$. The opposite was seen for the FR materials. The FR foam tested alone had a peak HRR of $180kW/m^2$, lower than the combination foam and fabric which was $290kW/m^2$. In other testing, foam without the

corresponding fabric was quicker to ignite compared to foam and fabric combinations for both NFR and FR foam and fabric combinations [97]. Further, time to ignition was seen to take longer with charring fabrics and foam composites compared to foam only samples [96]. During examination of other fire performance parameters, both FR and NFR foam and fabric combinations were observed to produce relatively the same amount of smoke, though FR combinations produced higher yields of CO and HCN [97]. Some foam and fabric combinations were also seen to produce slightly less CO_2/CO relative to foam only tests, but this was not consistent across all combinations of materials [97]. Inconsistencies across different studies highlight the importance of understanding the specificity of the particular furniture combination being examined, as well as limitations in the test methods being employed.

Testing furniture foam and fabric combinations in the cone calorimeter can be challenging, in part due to the flow rate of the exhaust. When the flow is set at the designated 24 L/s, the fabric, when cut to the 100mm x 100mm specifications [98], is very thin and often so light that it typically does not stay under the edge frame and in the sample holder. To avoid this, some researchers will secure the fabric by wiring it to the holder [93] or cut extra length of fabric so it covers the sides of the foam [92], but each of these brings with it different heat transfer pathways between the heater, fabric and sample holder. There are also conflicting experimental requirements with respect to the thickness of the foam tested in the cone calorimeter. The cone calorimeter test, as per the ISO specifications restricts the sample to a total of 25mm thick [98], so some researchers comply when testing foam and fabric mock-up combinations [91]. However, when considering the configuration of a couch cushion; there is a thick piece of foam (much more than 25mm) and a relatively thin layer of fabric. Thereby it can be argued that the ISO specifications do not directly allow for an accurate foam to fabric ratio, and as such some researchers follow another set of furniture testing guidelines, CBUF, which will be explained in further detail in the next section [105]. In this instance, they opt to cut the foam samples to be 50mm thick when testing foam and fabric [92, 93, 106] or foam only [89] as a better representation of a furniture item. In addition to the 50mm foam thickness, the CBUF guidelines do not require the edge frame piece of the sample holder to be used [105]. This may be to maintain an appropriate amount of spacing between the foam, barriers, glues and/or fabric materials present in the furniture mock-up configuration, and therefore not alter heat transfer mechanisms between the layers. Another challenge with testing foam in the cone calorimeter relates to the test apparatus which was designed to subject the sample to a constant radiant flux, achieved by maintaining the 25 mm spacing between the radiant cone heater and the surface of the specimen [98] for the duration of a test. However, in the case of foams which melt, this spacing cannot be maintained and therefore the intensity of

the radiant flux changes, as the actual heat incident on, and thus absorbed by, the sample from the cone heater decreases from start to end of a test [107].

It is clear that the composition of each material, the details of the fabric interactions with the foam and the test method itself greatly impact the burning behaviour and measured results for composite upholstered furniture samples studied in the cone calorimeter. During development of design and hazard assessments, therefore, this leads to a real danger of over-generalizing the behaviour of furniture in a full-scale fire based on data obtained only through small-scale testing.

The following section therefore introduces larger-scale experimental techniques for estimating the heat release rate of furniture items under well-ventilated fire conditions. This includes large scale standard test methods and experiments, as well as correlations and predictive methods that have been developed for the calculation of heat release rate of furniture fires. The final section of this discussion includes a summary of full-scale, furniture fire experiments that have been conducted to the same end as well.

2.8 Furniture: Correlations, Scaling and Modelling

Attempts at scaling enclosure fires, and at times the variance in results for different fuels, sizes and configurations of compartments [69], demonstrated that there was a need for a standardized test method for the measurement of heat release rate in large-scale enclosure fires. It was deemed that this should be based on the well understood and documented principles of oxygen consumption calorimetry with hope to facilitate scaling between small-scale and larger-scale tests as well as be designed for versatility so a wide range of materials used in construction (floor/ceiling coverings and wall linings) that were not necessarily free-standing like pool-fires or furniture could be tested [108]. This led to the development of the standard NORDTEST/ISO fire room test, which utilized a 2.4m x 3.6m x 2.4m room, with a 0.8m x 2.0m doorway opening [56]. The exhaust system could be adjusted within the range of 0.5kg/s to 4.0kg/s, and a collection hood and gas sampling was incorporated similar to the cone calorimeter, so the heat release rate measurements and computations were done according to the standard oxygen consumption calorimetry principles [108]. Around the same time that the large-scale room fire test standards for heat release rate measurement were being developed [69], there were efforts being made to create a test standard and apparatus for large-scale open-air calorimetry to complement the bench-scale cone calorimeter as well [108].

2.8.1 Furniture Calorimeter

As discussed previously in Section 2.5.1, a very small fire in a large room has very similar burning characteristics as the same fire burning outside with no wind and plenty of oxygen available for combustion. At the same time, for larger fires in enclosures, the environment at times transitioned to a ventilation-limited state, as was seen in the PMMA test described above [69] and was discussed in much more detail in Section 2.6. This highlighted the need to study the dynamics and burning characteristics of large items in well-ventilated conditions, in which oxygen levels would not alter or impact the combustion and fire development over the fuel [108]. Two apparatus were developed for the purpose. One was from the National Bureau of Standards (NBS) and the other from Factory Mutual Research Corporation (FMRC). Their name, furniture calorimeter, was coined because the earliest application of the apparatus was for testing upholstered furniture; however, they have since been used to test many other items as well [108]. The furniture calorimeter is based on the principle of oxygen consumption calorimetry and is similar to the bench-scale cone calorimeter in terms of main instrumentation which includes a load cell, oxygen, gas and flow rate instrumentation in the exhaust stack (located over the load cell), a smoke photometer also located in the exhaust stack and a radiometer [108]. The addition of the furniture calorimeter and standard room calorimeter test experiments to the repertoire of oxygen depletion based calorimeter tests allowed researchers to test a wide variety of furniture items across a range of different test configurations, and carry-out comparative studies across different scales. Through these experiments, it was found that the various tests could be applied to determine differences in heat release and other important burning characteristics between furniture material types and combinations, but that, depending on test method, there were also differences in performance seen between the individual materials and material combinations making up upholstered chairs and other furniture as well.

In extension of some of the cone calorimeter results from Section 2.7.3 to larger scale using the furniture calorimeter, it was found that less CO and more CO_2 was produced in full furniture tests in comparison to comparable material combinations studied in the cone calorimeter [97]. Such comparisons provided useful information with respect to some of the differences in foam and fabric behaviour based on composition as well as across test scales but are not particularly pertinent here since by necessity, they used a limited number of the possible foam and fabric combinations that were available at the time. Instead, new methods by which to extend the tests to other foam and fabric combinations were investigated, as well as techniques to assess fire performance of furniture available in different markets globally. There was still need to conduct extensive tests at large-scale;

however, testing furniture at large-scale can be difficult and costly, so researchers turned to different methods by which to scale results from bench-scale to large-scale in attempts to determine fire performance for a broader subset of materials and material combinations found in real, commercially available furnishings. In particular, as series of predictive techniques were developed for the purpose of using a bench-scale input, which is relatively easier to obtain, to predict full-scale furniture fire behaviour. These various techniques are the subject of the next section.

2.8.2 Furniture Models and Predictive Techniques

Correlation of outputs, like heat release rate, oxygen depletion, smoke production and amount of combustion products, from bench scale testing to full-scale furniture experiments for the purpose of generating predictive equations for hazard and risk assessment parameters is of paramount interest to the fire safety community. The approaches taken can be broadly sorted into four main areas including:

1. use of cone calorimeter data and material properties to predict peak heat release rate of furniture items [103, 104, 109],
2. comparative studies of bench-scale to large-scale furniture test data to build predictive heat release rate models of varying complexity [110, 97, 111, 9],
3. computer modelling to predict heat release rate and time to peak heat release rate during furniture fires [82] and,
4. use of furniture calorimeter data to predict how a furniture item will burn in an enclosure considering flame spread and radiative feedback mechanisms of the large scale item and compartment [112].

Many would argue that understanding the fire performance of material combinations at small-scale with extension of results to what would happen in real scale fires fuelled by furniture constructed of the same materials is one of the only practical ways to study and compare the multitude of scenarios that can present during a fire. Predictive tools that enable accurate prediction of the environment, and/or heat release rate, of large-scale furniture fires from bench-scale input data are therefore extremely useful and valuable. Having these, enable an engineer or researcher to predict important parameters such as fire spread, smoke and toxic gas production, and determine fire hazards and their impact

with reliable accuracy for a variety of different realistic furniture fire scenarios [82]. In the context of this thesis, the first three items listed will be the focus of this section.

To start, one predictive technique, chosen as one of the methods to calculate a value of peak heat release rate of the large scale furniture fires included in this thesis, utilizes two material properties: the heat of gasification and the effective heat of combustion, both found from examination of cone calorimeter data from a representative sample of material [113, 109, 104]. The measured mass loss rate per unit area is plotted over a range of incident heat fluxes as determined through cone calorimeter tests of representative samples. From this relatively linear relationship, the reciprocal of the slope is used to find a measure of the heat of gasification [113, 109] in a manner to parallel to taking the mean heat flux to surface of a liquid fuel and dividing by the heat of vaporization to determine the mass burning rate of the fuel [114]. When using a cone calorimeter, the net heat flux from the cone, actually consists of the external heat flux radiating from the cone heater to the surface of the fuel, as well as the heat radiating from the flaming area back to the vaporizing fuel surface, minus any heat losses from the surface to the exterior environment as shown in Equation 2.11. Thus an estimate of the losses can be found by taking the x-intercept of the mass loss rate per unit area versus heat flux plot as well.

$$\dot{m}''_{eff} = \frac{q''_e + q''_f - q''_l}{\Delta h_g} \tag{2.11}$$

Where q''_e is the external flux from the cone heater to the surface of the fuel, q''_f is the heat flux from the flaming area back to the surface of the fuel, q''_l are the losses from the surface of the material and Δh_g is the heat of gasification. In the absence of the cone heater but in a similar fashion, the net heat flux from the flame to a larger fuel surface divided by this value of effective heat of gasification would result in a value of the effective mass loss rate at full-scale, which can then be used in conjunction with the effective heat of combustion and area of the fuel bed to predict the peak heat release rate of a full-scale fire. This equation is extremely difficult to apply to a real fire, however, since it is challenging to determine the appropriate input for the net heat flux from the flame to the surface of the fuel. This value is dependent on the amount of radiation from the flaming zone to the surface of the vaporizing fuel which varies depending on fuel type, air availability and fire size. In work done by Mudan with 1m diameter kerosene pool fires, it was estimated that the luminous zone of the flaming body covered 20% of the surface of the flame, and that these luminous areas had emissive powers ranging between 110-130 kW/m2, whereas cooler areas had much lower emissive powers of approximately 20kW/m^2 [115]. In comparison, gasoline fires burning in 10m diameter pools have been

found to have emissive powers of 220 kW/m^2 [115], while other research indicated that the emissive power of 'hot spots', or luminous flaming zones, ranged between 33-430kW/m^2 and the cooler, sooty regions ranged between 6-50kW/m^2 [116]. Since such values are generally characteristic of radiation from the flames to exterior surroundings, however, it is much less clear what an equivalent value would be for radiative transfer back to the fuel surface within the fire plume. As described in Section 2.4, what portion of the flame radiation reaches the fuel surface is compounded by the fact that radiation increases with pool diameter, and in the case of large pool fires, it has further been shown that there is a certain transition point wherein the radiation decreases due to 'shielding' effects by soot layers which are cooler [117]. In attempts to separate and correlate the heat flux to the sample surface and the heat losses using cone calorimeter data, mass loss rate data was measured over a range of oxygen concentrations and irradiance levels and a linear relationship between oxygen concentration and flame radiation was found [104], although the results again become difficult to apply in predictions of full-scale fire behaviour.

Another way to predict full scale heat release rate is not by consideration of the material properties and radiative heat transfer within the fire, but rather using correlated correction factors derived from a large number of experiments conducted on various types of furniture. In early work by Babrauskas [97, 102], representative samples of common household furniture of the time (between 1982-1984) were tested in the furniture calorimeter using a 50kW gas burner to simulate an ignition source similar to a wastebasket fire [110]. The chairs had either wooden or plastic frames and were constructed with cotton, FR cotton, polyurethane and FR polyurethane for padding with cotton or polyolefin fabric coverings [110]. In the furniture calorimeter, peak heat release rate values ranged from 370kW-1900kW for a chair, and up to 3120kW for a three-cushion couch [110]. Representative samples of the fabric and padding from the chairs (excluding frame materials) were also tested in the cone calorimeter [110]. Afterwards, a complementary set of experiments were conducted in the furniture calorimeter with mock-ups constructed on a steel frame, using polyurethane foam (both FR and NFR) or neoprene foam, with polyolefin or cotton fabric coverings [110]. The following correlation, shown by Equation 2.12, for peak heat release rate of the furniture items was developed based on the results.

$$\dot{Q}(kW) = 0.63\dot{q}''_{bs}[frame factor][mass factor][style factor] \tag{2.12}$$

Where $\dot{q}_{fs}$ is the predicted full-scale peak heat release rate in kW; $\dot{q}''_{bs}$ is the bench scale heat release rate of representative sample of the furniture item as measured in the cone calorimeter 180s after ignition when subjected to a irradiance of 25kW/m^2; mass factor is the total combustible mass of each item of furniture; and frame and style factors are related to the material of the frame and shape of the furniture respectively [110]. In the

above equation, the frame factor reflected the contribution that a specific frame material made to the overall severity of the fire during the time of peak burning [110]. The style factor was based on observations of qualitative differences amongst burning characteristics of ornate versus rectilinear shaped furniture and the fact that some chairs with more ornate designs had higher values of peak heat release rate [110]. Therefore, although a detailed investigation into different flame spread mechanisms across different styles of furniture was not made, incorporation of this factor was deemed important to the final correlation [110].

The above predictive correlation was found to be successful for furniture that exhibited peak heat release rate values over a range between 400kW to over 3000kW [110]. Interestingly, mock-ups constructed with neoprene foams exhibited a very low heat release rate of 120kW, and promoted very little flame spread were excluded in determining the final equation. Furniture material combinations with high measured values of heat release rate at the bench scale, $\dot{q}''_{bs}$, were considered to support propagating fires and for these, peak values of heat release rate for the full-scale furniture items were proportional to the product of the variables described above [110]. Furniture material combinations with low values of heat release at bench scale, on the other hand, related to non-propagating fires on the full-scale items and in these, the mass, style and frame factors did not have an effect on the values of peak heat release rate because the fire did not grow large enough to burn a significant portion of the foam, fabric and frame [110]. This was demonstrated when the equation described above was used to predict the peak heat release rates for NFR and FR chairs [97]. While the correlation predicted a value of peak heat release rate of 1800kW for the NFR chair, it unexpectedly suggested a higher value of peak heat release rate of 2100kW for the FR chairs. When these chairs were tested in the furniture calorimeter, the measured value of peak heat release rate was 1200kW for the NFR chair, while that for the FR chair, as expected, was much lower at about 75kW [97]. In subsequent work related to predicting the heat release rates expected from institutional furniture, similar issues were encountered because that furniture was designed to limit flame spread and therefore was generally more fire-retardant [110]. Again, this highlighted the need for a different correlation for non-propagating fires, since in the above correlation the combustible mass is an important parameter, so when furniture is designed to limit flame spread and therefore only a very small fraction of the combustible mass is consumed, the correlation breaks down [110]. Further investigation into the data obtained from the cone calorimeter tests of representative furniture material combinations, revealed that bench scale testing at the specified value of irradiance of 25kW/m^2 was not suitable to determine $\dot{q}''_{bs}$ for highly FR furniture materials. Instead, for institutional furniture or more FR domestic furniture, testing at 35kW/m^2 appeared to be much more appropriate [110].

Furthering this correlational work, a way to simplify the above relationship even further

was determined to be to remove the cone calorimeter or bench-scale input data from the equation all together. Instead, this was replaced by more generic padding and mass factors based on specific furniture items of interest as shown in the Equation 2.13 below [111]:

$$\dot{Q}(kW) = 210[fabricfactor][paddingfactor][massfactor][stylefactor] \tag{2.13}$$

Due to their simplicity and ease of application to a variety of different furniture types, both of these correlations have been selected for use in estimating values of the peak heat release rate of the furniture fires included in this study. This is in part to compare how these correlations predict peak values of heat release rate compared to the other methods selected, but also to see if heat release rates of modern furniture can be accurately predicted using these correlations that were based on studies related to fire performance of the materials of the time.

To build upon existing methods for scaling, it is also necessary to broaden our general understanding of burning characteristics of furniture items in order to identify consistent indicators for the anticipated trends in fire development over time. So while many of these initial test results, data and predictive tools were very useful, significantly more information was required due to the variability and sheer quantity of furnishings available. This meant that there was still need for relatively inexpensive and more universal methods by which to predict fire performance of full furniture items. One such method was development of a computer model as described in the next section.

The furniture fire model (FFM) was formulated by Dietenberger [82] to help address the challenge of scaling measurements of heat release rate in furniture fires from bench-scale to large-scale as well as adding a fire (combustion) model into the multi-compartment Fire and Smoke Transport Model (FAST) which was being developed by NIST at that time [118]. The FAST model requires that mass loss rate, heat of combustion and species yields be collected through furniture or cone calorimeter testing of each item to be used as the 'fire' input in a given simulation [118]. In the case of furniture, which burns via more detailed combustion processes than other items due to the multiple materials burning, the FFM provides dynamic, quasi-three dimensional predictions of the growth and burnout of furniture fires in a room, while the smoke transport sub-models in FAST predict the spread of fire gases, smoke and fire into adjacent compartments [82]. In FFM, the furniture is modelled as connected panels and multiple flame volumes can attach to the polygonal bases and sides of the panels. This is done via critical temperature determinations in the model. As a given panel reaches a critical temperature, it begins to pyrolyze and then partake in the subsequent fire. Hot upper layers and cool lower layers that form in several rooms are considered and radiation and heat exchange between flames, objects and gases is taken into

account [82]. The dynamic model allows consideration of changes in the temperature of various surfaces throughout the space, which allows account of flame spread in any direction and scaling of the burning history of surface elements with time and space, for changing rates of production of heat, fuel and combustion products, and account for the growth of, and heat transfer from, the gas layer as the fire grows [82]. Although predictions for many parameters related to fire development are considered (surface temperature, ignition and flame spread properties, combustion products and soot, local burn history, local convective heat flux and pyrolysis rate) [82], for the purpose of this thesis, the methods used for scaling the heat release and mass loss rates in the model are deemed most important and discussed further here. In short, for successful scaling of heat release and mass loss rates, it was found that the key was to determine variables that related to effective values of heat of combustion (in contrast to using the theoretical value for heat of combustion) and heat of pyrolysis as functions of the scaled burn time of the material [82]. Results from the FFM, using cone calorimeter data as input, compared well to experimental results on furniture mock-ups conducted in the furniture calorimeter [82]. Predicted peak burning rates were in very good agreement with furniture calorimeter data at corresponding times after ignition, however due to burning on the outside surfaces of the mock-up furniture (behaviour not accounted for in the model), the modelled behaviour did not follow the shape recorded in the decay phase of furniture calorimeter results [82]. The model also slightly under-predicted the mass loss rate of the fuel when compared to furniture calorimeter data but overall, did well in predicting full-scale furniture burning behaviour using inputs from bench scale data [82].

In other work that merged experimental and modelling approaches, the Combustion Behaviour of Upholstered Furniture (CBUF) project was created to develop appropriate tools for hazard assessment of furniture fires [9]. The CBUF project included over 1500 experiments to test fire performance of furniture items and materials using existing methods, including cone calorimeter, ISO 9705 room, furniture calorimeter and Lateral Ignition and Flame Spread Test (LIFT). The main goals of the project were to: 1) address the hazards associated with a furniture fire after ignition and understand the burning behaviour and fire phenomena, 2) develop predictive mathematical models and correlations for fire performance of furniture and 3) provide "quality assured test protocols suitable and robust enough for routine testing of upholstered furniture". From the results, a database was established pertaining to heat release rate, temperature, heat flux, smoke density and a selection of toxic gas species (measured using FTIR) from each of the furniture material combinations and full scale items tested [9]. In general, data collected from the ISO 5660 cone calorimeter tests of the composites (fabrics, linings and padding) was used to predict results of testing a particular furniture item constructed of those materials in the Furniture

Calorimeter (to the NT FIRE 032 standard [119]), and further to predict phenomena that occurred in the ISO 9705 standard test room as a result of ignition of a furniture item based on the furniture calorimeter results [9].

Experimentally, the CBUF project consisted of two test series: the first series involved study of the burning characteristics of real furniture items from the European market, and the second tests involved investigation of fires fuelled by custom-made furniture which were designed and configured specifically to study the impacts of materials, construction, ventilation conditions and other parameters on the fire environment so as to provide new data for use in the mathematical modelling of furniture fire scenarios [9]. In these latter tests, furniture fires were run at larger scale in three configurations of fire compartment to develop better understanding of how ventilation conditions impact the fire environment as well. These consisted of a) rooms with ventilation openings, b) closed-off large rooms, and c) closed-off small rooms [9].

To complement the first set of experimental data, three mathematical models were developed to estimate full-scale furniture behaviour with cone calorimeter data as input. These built on previous work, relying on physics established for burning of building materials, with specific application to furniture, and particularly with development of novel models to treat composite furniture materials [9]. In brief, the first model is a factor-based model, which is based on a series of statistically correlated factors related to the overall burning behaviour of furniture as determined through experimental testing. The second model is based on an area-convolution technique which incorporates empirically justified expressions for the measured change in burning area as a function of time for various types of furniture. More specifically, the second model uses a convolution technique, integrating the burning area over time based on the assumption that during combustion, each element per unit area involved in a fire on a full-scale furniture item contributes approximately equally, and to the same extent as in a cone calorimeter test [120]. In addition, the model includes expressions to account for flame spread phenomena such as underside burning and pool burning of melted foam/fabric should that be appropriate in a particular situation [120]. The third model is based on an extension of thermal fire spread theory which allows prediction of the burning behaviour of a full-scale composite item by predicting the behaviour of each of the individual components (fabric, padding, liners etc) [9]. Since these models and correlations rely heavily on the basic test input data in the CBUF database, it was noted that care should be taken when using the models for furniture products that differed greatly from the types tested as part of the CBUF project [9]. This limitation has led to follow up research and testing of the CBUF models with more recent furniture materials and designs [120, 96] as well as comparing results of the same furniture items tested in furniture calorimeter and ISO room [121] results of which will be elaborated later

in this section.

Experiments in the second series of CBUF tests consisted of furniture items burning a standard ISO 9705 room. Data indicated that a typical two-zone type of compartment environment developed in the experiments, where the hot upper layer contained the smoke and fire gases. The lower layer consisted mostly of incoming fresh air entering from the compartment openings, and the interface between the two layers remained quite distinct. As the fire progressed, the upper layer gases underwent mixing with entrained air, effectively lowering their temperature and the overall concentration of toxic species in the upper reaches of the compartment [9]. It was further found that the upper layer contained several toxic gases; the height of the interface could be predicted from the heat release rate and could be used as one measure of tenability; and in a room that was closed, even a small amount of fuel lost (a few hundred grams) could be sufficient to create untenable levels [9].

To extend the CBUF results into professional practice, design and testing procedures were included in the final CBUF documentation [105]. These explained how data was collected from the test methods (often cone calorimeter or furniture calorimeter tests), how certain furniture was then modelled, and how correlations could be applied to determine if that specific furniture item met certain fire safety requirements [9]. Safety requirements were selected by those responsible for regulation, accounting for the level of performance required, harmonization and cost benefit analysis [9]. The necessary level of performance was based on acceptable tenability limits for a furniture fire in a room scenario [9]. Hazard analyses based on the test results revealed that predicting the time history of heat release rate for a furniture item was required, but full-scale testing was not needed to do this to an acceptable level [9]. Instead three useful testing procedures were proposed. It was suggested that to determine the fire risk associated with a furniture item, one could either 1) test the furniture item in the furniture calorimeter, or 2) test the composite materials from the furniture item in the cone calorimeter, or 3) test the material components separately in the cone calorimeter. Options two and three then require the use of one of the three different furniture prediction models described above for estimation of full-scale burning behaviour of the furniture item under test [9].

It is important to validate any correlations and predictive models across a wide-range of furniture types, to explore the limitations in the models and provide recommendations on how to create a more robust methodology. As a result, there has been follow on work done in New Zealand that compared the results of the CBUF models to newer upholstered furniture tested in the furniture and cone calorimeters [96, 120] as well as compared results of identical sets of chairs in both the furniture calorimeter and ISO room [121]. The furniture items were made of polyurethane foam, fabric coverings were polyester, nylon and cotton and two styles of armchair and one sofa design (as defined by the CBUF guidelines

[105]) were tested [96, 120]. With the specific NZ furniture used, it was concluded that the factor-based CBUF model was a poor predictor of the burning behaviour of the NZ furniture with respect to peak heat release rate, total heat released and time to peak heat release rate [96, 120]. Similarly, it did not accurately predict the full-scale burning of the more modern modified and high-resilience foams used in the NZ furniture [96]. It was suspected that the reason that this model significantly under-predicted peak heat release rate and time to peak heat release rate was due to an over-dependence of the correlations on the total mass of combustible material in the furniture, rather than a more detailed approach that appropriately accounted for the composition of specific materials and in particular, the role that fabrics might play in the combustion process [96, 120]. As noted in other work with material combinations studied with the cone calorimeter [97], the interaction between the fabric and foam is important. It was concluded that the second CBUF model, based on area convolution principles, did better at predicting outcomes compared to the first model, but still demonstrated variability in agreement depending on furniture type. Again, fabric was concluded to play a large role in the combustion process and lack of full account for this affected the integrity of key input parameters, and thus outputs, such as the area burning with time [120]. Moreover, there are contrasting results of identical chairs constructed with polyurethane foam and varying fabrics, some of which were FR-treated, tested in the furniture calorimeter and in the ISO room test [121]. The peak heat release rate measured in the ISO room tests were higher than the measured peak heat release rates in the furniture calorimeter [121]. This difference was attributed to the radiative feedback from the walls and smoke layer in the ISO compartment fire tests that would not have been present to the same degree in the the furniture calorimeter, or open-burning configuration [121]. It was also found that the relative ranking of peak heat release rate in terms of magnitude between the chairs in the ISO room differed from the relative ranking of the chairs tested under the furniture calorimeter [121]. This result suggested that due to the nature of the foams used in the construction, some of the chairs had better fire performance in the open-burning configuration compared to the enclosed compartment test, but this was not investigated further [121]. The time to peak heat release rate also differed between the ISO room test and the furniture calorimeter for a given set of identical chairs, typically time to peak heat release rate was faster under the furniture calorimeter, but again, this was not consistent for every type of chair set tested [121]. In terms of the mole fraction of CO/CO_2 measured, the ISO room tests consistently measured higher values compared to the furniture calorimeter [121].

At large-scale, the types of foam and fabric can have a significant impact on fire development in furniture fires and therefore the time varying burn history of the item [96, 121]. Due to these noted limitations in the CBUF calculations when tried against furniture from

a different country, those methods were not selected as part of this study. These limitations point to the true complexity associated with finding universal expressions with which to predict burning behaviour of furniture [121]. Inconsistencies between types of furniture, model selection and method of testing highlight the need for additional work to generate a larger database containing more results for a wider variety of furniture. In future, to expand knowledge of the strengths and/or limitations of the correlations, however, it would be of interest to run the furniture used in this body of work as an additional comparison case.

The discussion above has focused on fairly foundational studies related to compartment fire development in well-ventilated and limited ventilation situations, as well as small- through larger-scale methods to test furnishing materials and furniture items. The following section integrates the two elements, focusing on experimental investigations of enclosure fires fuelled by full furniture items, or studies into fire development in mock-ups of various residential and building room configurations the situation most comparable to the full residential furniture fire tests under study in this research.

2.9 Compartment Furniture Fire Tests

In research most directly related to the present thesis, large-scale fire experiments have also been conducted in a 3.6m x 3.6m x 2.44m compartment with a single door connected to a hallway, and window opening, with typical furnishings (bed, armchair, dresser, waste-basket, end table and carpet) [122]. In these, temperature profiles within the compartment changed in various locations as the environment evolved. In the middle of the compartment, temperature was linearly stratified until the fire reached its peak heat release rate, then compartment temperatures became uniform. Near the window and at the door of the compartment, the profile was two-layered until the peak heat release, then again became uniform. Outside of the compartment, in the hallway, the temperature profile remained stratified through the test [122]. At peak heat release rate, upper layer temperatures ranged from 650°C to 700°C by the window, to 900°C in the middle of the room and 850°C at the door. In general, oxygen concentrations in the upper layer were 6% volume [122]. These results are consistent with other work conducted in the same size compartment with similar sizes and configuration of vents as well as furnishings [123]. In [123] as well, oxygen concentration was comparable, measured to be 5% volume in the hot layer while CO concentrations, not reported in [122], were 4.8% volume [123].

To explore the development of fires in furnished rooms, full-scale tests were conducted in 3.7m x 5.5m rooms, furnished to be mock-ups of a hotel room [124]. Intermittent sampling

of various gases such as CO, CO_2, O_2, NO_x and HCN_2 was done. An upholstered chair was ignited and the fire was left to burn unperturbed. As the fire established on the chair, it had generated enough radiative energy to spread to the sofa after roughly 3.5 minutes [124]. The sofa had a nylon/polyester blend fabric, and once the sofa was involved, it took 6 minutes to reach flashover within the compartment [124]. Gas concentrations measured from sampling lines located 1.7m above the floor provided interesting data around the time of flashover. Maximum CO, CO_2 and HCN concentrations were about 70,000ppm, 14.2% and 1160ppm respectively, and minimum oxygen concentration was extremely low, measured as 0.2% [124]. In these tests, the ionization smoke detector activated 21 seconds after ignition and the fast-response sprinkler mounted on the wall activated when oxygen levels were still very close to ambient (roughly 19%), CO was about 200ppm, and the temperature in the room was 60°C, therefore well before flashover [124]. It was determined that once the smoke detector activated, escape from the room was quite possible and the sprinklers activated when conditions were still relatively tenable [124]. If there was an issue with the sprinklers and/or the smoke detector, there was a 2-3 minute time lapse before flashover in which the oxygen rapidly decreased in the burn room [124]. To limit potential progression to flashover, it was found that automated venting strategies could be used to vent smoke out of the compartment and therefore hinder the build-up of the hot smoke layer in the compartment [125]. Without venting, other studies have found that even a waste paper basket ignition source can lead a positive feedback loop of heat transfer within a compartment fire resulting in hot layer temperatures of over 800°C before firefighter interventions and thus flashover in a compartment in about 2 minutes [125]. Clearly strategies to interfere with the potential for such positive feedback to occur can be crucial as fire safety interventions.

To compare the differences between toxic species generation and flashover potential of different types of materials, given the variation of furniture items on the market, two experiments were conducted in 3.6m x 4.5m x 2.5m high compartments which led to a hallway [126]. In one test, the compartment was furnished with organic, cellulose-based, and wood materials, and in the other test, the compartment was furnished with polyester, polyurethane foams and wood products where about 27% of the combustible mass was synthetic [126]. A 0.5m x 0.5m cotton cushion was used as an ignition source and was inserted between another cushion and blanket on the floor, with an additional layer of bedding on top [126]. Gas samples were taken at specific times at two locations. One was just below the ceiling in the hallway, and the other just below the ceiling in the burn room [126]. In the test with the organic materials, smoldering combustion was initially the most prolific mode of burning. When flaming did occur (about 30 minutes after ignition), gas concentrations in the compartments started to change [126]. During flaming ignition,

oxygen levels in the burn room decreased to around 18%, CO_2 increased to 3%, and CO increased to 0.3%, however once flashover occurred, oxygen concentrations in the burn room further decreased to 2.8%, CO_2 increased to 16%, CO increased to 5%. Other gases such as HCN and acrolein were measured in relatively smaller amounts, 530ppm and 16ppm, respectively [126]. In the experiment with synthetic materials, flaming combustion and the increase in upper layer temperatures to the onset of flashover was achieved much more quickly [126]. The concentrations of some gases were close to the same in this experiment compared to the tests with the organic materials after flashover. Just after flashover in the synthetic tests, oxygen concentrations in the upper layer decreased to about 3%, CO_2 increased to 13%, and CO to 6.5%. HCN concentrations were higher, at 2500ppm, with concentrations of HCl of 800ppm and acrolein of 150ppm [126]. In a similar experimental set up in terms of compartment size and material selection and distribution, the effect of vent openings on the fire environment were studied [127]. In this experiment, the fires were conducted in a two-storey structure, the burn room had a floor area of $9.7m^2$ and two openings each 1.95m x 0.8m, one to the hallway and one to outside [127]. The area of the opening to the outside ranged from $0.39m^2$ to $2.34m^2$. Above the opening was a large hood to collect smoke and gas exiting the burn room [127]. In addition to the hood, there were also gas sampling probes installed at 0.1m below the ceiling in the burn room center as well as at several other locations. The tubes were sent for later analysis [127]. For both of these experimental series with the different materials (series 1 had all natural polymers, and series 2 had synthetic and natural polymers), temperatures in the upper layer by the doorway were roughly 800-900°C and oxygen decreased in the upper layer to below 5-6% regardless of the size of the opening [127]. The difference between the two series appeared in the concentrations of CO and HCN, which were both measured at higher concentrations in the upper layer in the experiments with the combination of natural and synthetic polymers [127]. When the opening to the room was smaller restricting air to the fire, higher amounts of CO were measured in the burn room and high concentrations of CO and HCN were measured in areas further away from the fire [127].

It is known that ventilation is a major factor related to the progression of the fire environment, and in the cases of natural ventilation, it is governed by the degree of an open, or closed, door. In bedroom mock-up configurations, some with the door to the hallway closed, and others with the door to the hallway open, differences in oxygen, CO and CO_2 were measured with FTIR, NDIR (CO/CO_2) and paramagnetic (O_2) sensors [128]. Sampling probes for measuring the gases were positioned at 1.5m to simulate nose-height, and at 0.6m to simulate the height of a person's head while sleeping [128]. During the test with the door closed, it appeared that the fire extinguished due to lack of available oxygen for combustion [128]. Under these conditions, CO was measured by the FTIR to

be about 2000-4000uL/L in the middle of the room at 1m and 2m, HCN was 50uL/L, and oxygen was 16% volume in the middle of the room at both 1m and 2m [128]. In tests with the door open, the concentrations of CO and CO_2 were lower, but oxygen concentrations were measured to be around 13% in the middle of the bedroom at 2m and 18% in the hallway [128].

With the rise of FR materials, similar to the comparison between organics and synthetics, comparisons between full-scale enclosure fires fuelled by FR and NFR furniture materials have been conducted. A study was conducted to compare the toxic yields from on-the-market mattresses in the UK [129]. Representative samples of material from four mattresses with coverings (used as sofa-beds) were tested in the calorimeter (25mm thick and 35kW/m^2) and full-scale tests of the mattresses were conducted in a shipping container of dimensions 3.4m x 2.25m x 2.4m with an inlet (0.32m x 0.32m) and an outlet (1.04m x 0.2m) [129]. One of the mattresses, referred to as UK-FR, was comprised of combustion modified flexible PU foam, a polyester layer, and FR fabric which was tested and found to contain Cl and Br FR additives. Another was sourced from China with the same materials as the UK-FR and was found to have P and Cl FR additives, referred to as Ch-FR [129]. Another mattress, referred to as EU-Mat, was made of flexible PU foam, a polyester layer, and NFR fabric, and the last mattress, made in the UK, referred to as FR-free, was made of a poly-cotton pad, a woollen layer, and a cotton-wool blend fabric cover [129]. In the cone calorimeter, the UK-FR and Ch-FR took the longest to ignite and generated the highest amounts of CO and HCN, which was sampled from the cone and measured separately using bubblers. Consistent with findings by Babrauskas, the NFR materials had higher heat release rates compared to the FR counterparts [129, 97]. Interestingly, the FR-free mattress, made of primarily organic materials, had a heat release rate around 175kW/m^2, similar to the FR mattresses [129]. At large scale, the NFR EU-Mat ignited the fastest, and produced the highest temperatures in the compartment, followed by the UK-FR and Ch-FR mattresses, and finally the FR-free mattress which ignited and then smoldered for the duration of the test, resulting in very low compartment temperatures [129]. In terms of CO concentrations, the EU-Mat generated the highest levels at about 25000ppm, followed by the UK-FR, Ch-FR and FR-free which were 11,000ppm, 7500ppm, and 2000ppm respectively [129]. The authors ranked the mattresses from low to high in terms of both the toxic and flammability hazards based on both bench scale and large scale test data [129]. Based on the cone calorimeter results, the flammability hazard (from low to high) ranks as UK-FR, Ch-FR, FR-free, and EU-Mat, while the toxic hazard (from low to high) ranks as FR-free, EU-Mat, UK-FR and Ch-FR [129]. Based on the large scale data, the flammability hazard (low to high) ranking is different, running as FR-free, Ch-FR, UK-FR, and EU-Mat. Similarly, rankings of the toxic hazard (from low to high) also differ, fol-

lowing FR-free, EU-Mat, Ch-FR and UK-FR [129]. The discrepancies between the hazard rankings between small scale and large scale test data, as well as between rankings based on toxic versus flammability hazards clearly demonstrate the difficulty when it comes to characterizing the hazards associated with furniture in fires. In the first instance, is the trade-off between dangers associated with flammability versus toxic exposures. To further complicate the assessment, the quantities of toxic gases produced are largely dependent on the materials chosen, configuration and ventilation in the structure, as well as location and types of sensor employed.

In other comparative experiments with furniture from different areas of the world, ISO 9705 standard rooms were furnished with a coffee table, end table and chair, flat screen TV, 12kg of books and a 3-seat sofa from 3 different locations [130]. The couches came from IKEA in France, the UK and the US [130]. Samples of the couches were tested for specific elemental FR additives and the couch from France contained, chlorine, Cl, in the foam and antimony, Sb, in the loose filling; the couch from the UK contained phosphorous, P, in the foam and Cl in the loose filling; and the couch from the US contained Cl in the loose filling [130]. On average, the room fire tests fuelled by the French couch reached average peak heat release rates of 3032kW after 6.5min, with flashover occurring at 5min after ignition. The British couch had an average peak heat release rate of 2670kW, reached after 21min, with flashover occurring at 20min after ignition. In the case of the US couch, the average peak HRR was 2874kW, reached after 7min, with flashover again occurring at 5min after ignition [130]. Carbon monoxide concentrations measured using FTIR at a position 0.457m above the floor in the center of the room ranged from 18,000ppm for the UK couch to 31,000ppm for the French couch to 60,000ppm for the US couch [130]. CO_2 concentrations measured in the same locations were 13,300ppm for the UK couch, 12,500ppm for the French couch and 14,700ppm for the US couch and oxygen was not measured [130]. As with the testing above, it is clear that the hazard ranking across the three furniture types were different depending on which parameter was employed in the assessment.

Large scale furniture tests which highlight the differences in the environment when the ventilation into the room changes were conducted by Wolfe et al. [131] in a four-room apartment-style layout, totalling 41.8m^2 in floor area. There were four different rooms within this space (living room, kitchen, bedroom, and dining room) connected by 0.91m x 2.03m doors [131]. The living room was the 'burn room' and was open to the dining room through the door vent [131]. Sofas were tested under three different burning regimes: smoldering, non-accelerated flaming, and accelerated flaming conditions [131]. The sofas were made from polyurethane foam padding and a 100% cotton fabric covering that met the

requirements of the California Bureau of Home Furnishings Technical Bulletin 117 [1] [131]. The smoldering tests had no ventilation, and the flaming tests had either a fully closed window, a window half open ($0.12m^2$) or fully open ($0.24m^2$) [131]. Overall development of the fires followed trends described earlier. Smoldering fires did not have significant mass loss, oxygen levels stayed around ambient and maximum CO measured was 0.075%, whereas flaming ignition sofa fires with minimal to no ventilation (window half open or fully closed) became vitiated and extinguished when there was still a significant portion of sofa remaining [131]. Sofa fires with enough ventilation via the fully opened window, followed a normal course of development, illustrated in Figure 2.2 in Section 2.5.1, though the fire was manually suppressed before reaching flashover [131]. A critical vent size could be determined for the particular sofa burned, which for these tests was around the size of a full open window or $0.24m^2$ [131]. In a sofa test with the window closed and ignited with a small flaming source, peak measured temperatures were only 286°C, the couch lost only 12% of its initial mass and only sections of the seat/back approximately 0.91m wide actually burned. Calculated peak heat release rate was 353kW, oxygen concentration dropped to 13.6% in the upper layer of the burn room (2.41m), peak CO_2 concentration was 4.5% and peak CO was 0.4% [131]. When the sofa was tested with a half open window and a small flaming ignition source, peak temperature was 630°C, the couch lost 14% of the initial mass, the calculated peak HRR was 862kW, oxygen concentrations dropped to 3.4% in the upper layer of the room, peak CO_2 was 14.3% and peak CO was 5.5% [131]. For the sofa tested with a fully open window and a small flaming ignition source, the peak temperature before suppression was 638°C, the couch lost about 11% of its initial mass, the calculated peak HRR was 1.03MW (which occurred just before suppression), oxygen concentration dropped to 4.8% in the upper layer of the burn room (2.41m), peak CO_2 was 12.9% and peak CO was 3.7% [131]. In an accelerated sofa test involving use of a larger ignition source used to simulate an arson scenario, with a half open window, peak temperature was 345°C, about 8% of the initial mass of the sofa burned, the calculated peak HRR was 300kW, oxygen levels dropped to 16.3% in the upper layer of the burn room (2.41m), peak CO_2 was 3.7% and peak CO was 0.3% [131]. To summarize, it is again clear that ventilation into a full scale fire room impacts the size of the fire, the rate at which it grows and the total burn time. Moreover, the amount of ventilation needed to maintain burning is dependent on the type of fuel as well as the specifics of the space and fire scenarios.

As shown in the results discussed in the previous sections, there are specific charac-

[1] This California Bureau of Home Furnishings Technical Bulletin 117 was updated in 2013 to a new smolder standard Technical Bulletin 117-2013 [132] to make the testing of materials more rigorous therefore making materials more fire-safe.

teristics of furniture fires, ventilation-limited fires and multi-compartment configurations that have been explored, but there is still room for furthering our scientific understanding of these complex scenarios. For example, a common way to calculate the heat release rate of a material is by calculating the product of the mass loss rate and heat of combustion. However, there are other methods that involve other fire parameters, such as flame heights and diameters. In addition there is a wealth of untapped information and insight into overall burning characteristics and fire behaviour that can be gleaned from analysis of videos taken during fire experiments at full scale. As such, there has been work done in recent years to develop image processing tools for determination of flame height and fire spread across burning fuel items. A few of these tools and their limitations are presented in the next section since they form one key element of the final fire development and heat release rate analyses conducted in this research.

2.10 Video Processing and Analysis

In response to what was identified in the early pool fire work in terms of difficulty in determination of flame height by the human eye, as presented in Section 2.3, there has been some work done to develop image processing tools for the analysis of furniture fire footage. Image processing, in addition to being applied to measure flame heights, can provide insight into fire growth and flame spread rates as well as burning characteristics and smoke development within the fire compartment and throughout a structure. It also provides visual data to support and explain trends seen in other data. The majority of existing algorithms for fire image processing are based on determination of the temporal changes of one or several parameters unique to a fire, such as colour, motion, and/or flickering, essentially related to spatial changes in radiative emission from the visible flame plume [133]. Considering motion as the parameter, programming for motion can allow for the elimination of non-fire objects which are stationary and therefore detect the motion of the fire [133]. With focus on colour, a spatial difference analysis can be developed that involves identifying variations in pixel colours, or RGB values, to distinguish flames and flame-like objects, such as reflections on a smooth surface, from one another as well as from the image background [133]. Other tools are histogram-based, segmenting bright objects within each frame using a threshold system [134]. Then, to enhance flame features, pixel saturation is maximized and boxes containing the flames are defined. 3D flames are then created through 'blob' matching, and fire growth is predicted due to the inherent relationship between the area of the fire, flame size and rate of burning [134]. Data captured using a multi-modal long wavelength infrared-visual flame detector, merged with thermal

data collected from a sofa fire test in the ISO 9705 room, was used to develop input for CFD model predictions and correct predictions related to fire size and smoke interface height [135]. In this kind of analysis, Heskestad's flame height correlation [17] can be used to calculate the heat release rate of the fire using the flame height as captured from the program [135], or flame height outputs from a program can be validated by comparing them to the calculated flame heights [136] from Heskestad's flame height correlation [17]. Other programs use the technique of progressive scanning (scanning across all lines of the image), then convert the scanned image to grey-scale with the maximum amount of contrast between the foreground (fire) and background, which essentially generates a binary or black-and-white image of flaming and non-flaming regions [136]. A problem identified with application of this last image analysis program to investigate fire characteristic during chair fires, was that the position of the base of the flame changed as the fire burned down through the cushion [136]. This issue was not addressed in the reported image processing tool, and therefore there is a fairly large error margin in calculated flame heights due to the portion of the fire not taken into account. In short, no existing image analysis programs were identified that could be applied directly in the present research. Therefore a new tool was developed for this purpose, taking into account known issues such as that noted above.

2.11 Impetus for Research

To close, it has been identified that using the heat release rate calculated as the product of the mass loss rate and heat of combustion, or alternately using the very commonly applied alpha t^2 [18] analysis for heat release rate are not always appropriate for ventilation-limited fire scenarios as these calculation methods were derived based on well-ventilated fire situations [71]. There have been attempts to correct such heat release rate values for use in computational fluid dynamics (CFD) computations that are often used to predict upper layer temperatures and smoke evolution during compartment fires [71]. Alternately, attempts have been made to develop corrections to heat release rate calculated as the product of the mass loss rate and heat of combustion based on combustion efficiency factors to furnish values more comparable to values of heat release rate determined using oxygen consumption principles [59]. Such corrections to values of heat release rate may have been appropriate, but it is important to consider that due to inherent assumptions and inaccuracies in CFD models, adjustment of a key input parameter such as heat release rate to predict measured temperature distributions may well result in misrepresenting the physics that actually occurred. Moreover, it is also important to rely no solely on temperature data for comparison of real fire situations to output from a computer model [74]. Further,

when using furniture calorimeter data as input into fire models, it is very important to give consideration to most probable oxygen concentrations at the flame base in a particular situation, since assuming well-ventilated burning may lead to over-estimations of upper layer temperatures and therefore errors in hazard analysis for key fire developments, such as potential for flashover in the compartment [74]. Due to such severe limitations, it is important to conduct work that carefully characterizes different fire environments so modellers have detailed data by which to verify models. Numerous ways for calculating heat release rate from complex fuels such as furniture should also be investigated, to explore appropriate ways of calculating that parameter for a variety of fire scenarios.

In the literature, there have not been many comparisons between heat release rate values calculated using several different methods based on input data from the same test, so there is no evidence, and thus concern, as to whether a given method is appropriate for use in a particular fire scenario. At the same time, the situation is too complex to determine a single best method for calculation, since every furniture fire is different. Burning behaviour and the yields of toxic products are dependent on the material composition, temperature and oxygen concentration [129]. Flame retardants further affect fire safety through changes in ignitability, changes in rate of fire growth, and changes in toxicity of the combustion products and smoke [129]. Thus, material choice and combinations of materials are essential for the design of safe furniture. Finally, oxygen calorimetry is not always available and is largely applicable only to well-ventilated situations, yet it is also known the environment impacts physical parameters used as input into heat release rate models such as mass loss rate. It is very important therefore to explore and compare a range of different ways to calculate heat release rate from different types of experimentally obtained results. These needs and gaps in knowledge form the impetus for the research conducted and presented in this research.

With the knowledge formed from this Chapter on calculation methods of heat release rate, compartment fires, ventilation-limited fires and the complexity of furniture fires, Chapter 3 presents the experimental methods utilized in the present study, including a description of the fuel and fire burn structure, instrumentation and data analysis methodologies applied. In Chapter 4, the representative results of the experiments and analyses of the heat release rate methods selected are presented with discussion of their import and implications on fire safety. Finally, key conclusions and recommendations from the research are summarized in Chapter 5. Results of repeat tests are included in Appendix A, details on data acquisition and corrections can be found in Appendix B and the image processing code can be found in Appendix C.

Chapter 3

Methods

This chapter commences with a review of the objectives of the present research, which informed the selection of methods to be used, and consequently the type of data and model inputs that had to be obtained from the existing experimental data. These objectives are:

- to enhance current understanding of the evolution of a fire environment from ventilated into ventilation limited modes of burning,
- perform a time dependent characterization of fire heat release rate throughout the modes of burning, and
- assess the associated heat release rate calculation methods by providing a comprehensive comparison of available techniques using input derived from the experimental results.

Together, these objectives will shed light on the impacts of an evolving fire environment, from well ventilated into ventilation-limited modes of burning, on fire development, fire heat release rate, smoke and oxygen movement, and generation of toxic products in a two-storey, multi-compartment burn structure.

The experimental data used in this analysis was collected from a series of fire tests that were conducted in 2015 in the burn structure at the University of Waterloo Live Fire Research Facility. These generated a rich body of quantitative and qualitative data for studies of the transition of furniture fires from well-ventilated to limited-ventilation modes of burning. This data, combined with information from the literature, was used to investigate use of different heat release rate calculation methods for fires fuelled by three distinct

furniture types, as well as explore the impacts of the changing compartment environment on these values of heat release rate, smoke and oxygen movement and generation of base toxic products.

In this Chapter, the experimental methods and instrumentation used in the 2015 studies are described, followed by a summary of the existing heat release rate calculation methods chosen for this study with summary of their key input parameters and justification for their use. The methods and analysis used to determine each of the inputs required for the various calculation methods are then outlined, highlighting development of a new image analysis technique designed to process video images and deduce time varying values of flame height and diameter for use in the calculations. The chapter will end with an explanation of an analysis performed to deduce the radiative contributions of the fire and smoke layer, and to thereby estimate the radiative fraction of the fires under investigation.

3.1 Experimentation

Nine large-scale furniture tests were conducted at the University of Waterloo Live Fire Research Facility in the summer of 2015. Three types of custom-built furniture adhering to three different furniture standards were tested in triplicate. The data used in this analysis comes from these repeatable furniture tests which are described in further detail below [137].

3.1.1 The Structure and Instrumentation

The tests took place in the two-storey burn structure located at the University of Waterloo Fire Research Facility shown in Figure 3.1a below. This multi-compartment structure had a steel outer frame and steel studs. It had 116.2m^2 total floor area and 287.6m^3 total volume. The overall area of each floor is 8.3m by 7.0m with ceiling height of 2.35m on the main floor and 2.6m on the second floor. The top floor of the structure was left with steel studs exposed and all of the window openings were closed and sealed with spray foam. The main floor was furred with steel studs then insulated with 15.9mm thick type X gypsum board throughout. In the fire compartment, also referred to as the living (burn) room, for added resistance the walls were further reinforced with a layer of 15.9mm thick concrete board. The ceiling was insulated with non-combustible fibre insulation, then clad with a single layer of type X gypsum further reinforced with a single layer of concrete board. Seams throughout the main floor were sealed with fire rated caulking as seen in the image

of the fire compartment in Figure 3.1b below. The dimensions of the burn room itself were 4.32m x 3.2m. This room opened to a hallway on one side and an adjacent compartment (main floor SW room) of 4.5m x 4.32m on the other. A door vent connected the burn room to the adjacent room on the first floor (1.8m x 0.85m) and an open stair connected the two floors of the structure through an opening that is 1.1m wide x 2.4m high. To mimic window placement in a living room type configuration, two 0.6m x 0.9m double pane (Jeld-Wen Low-E Vinyl-clad) slider windows were installed in the burn room, one behind the couch and one behind the chair. Another window of the same type was installed in the adjacent main floor compartment as well. A schematic of the full floor layout of the structure is shown in Figure 3.2 below.

(a) Outside View of Structure

(b) Fire Compartment

Figure 3.1: Testing Facility at the University of Waterloo Research Facility

Opening and cracks to the exterior of the structure were sealed and all windows and exterior doors were kept closed throughout the duration of each test in order to achieve a ventilation-limited mode of burning. The stair and other interior doorways were kept open and free of obstructions to allow for transport of gases freely out of the burn room, between the storeys and compartments of the structure. The house was considered effectively air-tight, except for some small leakage observed out of the functional openings (main doors) as the sealant expanded due to heat exposure.

Before each test, a matched set of one couch, a chair, coffee and end table were positioned in the burn room. The couch was then ignited using a wooden crib and isopropanol wick in accordance with the BS 5852 standard [138]. The ignition location was the middle and back of the far right cushion (cushion closest to door 1 in Figure 3.2 below). Once ignition of the crib and subsequently the couch was achieved, the fire was left unperturbed

to burn until decay, at which time the fire service entered the structure to put out any remaining flames with as little water as possible.

The instrumentation for the nine tests was as follows, with different components positioned as shown in Figure 3.2 below.

- To record the mass loss, the couches were placed on four MARS MSB60 weigh scales;
- A water-cooled Gardon heat flux meter was located on the wall adjacent to the couch approximately 1m above the floor, and 3m away from the couch. It was aligned roughly with the centre of the second cushion on the couch to collect data with respect to the radiant heat flux, denoted as HF1;
- Type K ceramic fibre and Inconel sheathed 24-gauge thermocouples were installed singly and in vertical rakes throughout the structure to measure the thermal development of the environment. Key to the present research were nine vertical thermocouple rakes, each with three to eight thermocouples, denoted by Tx in the figure;
- Eight 19mm diameter, bidirectional velocity probes each connected to a differential pressure transducer and corresponding thermocouple were installed at the opening of the staircase on the first floor to measure the velocity of the flows up and down the staircase. These are denoted by P1 at the entrance of the staircase;
- Four Lorex CVC7572, 720x480 pixel combined colour-night vision security cameras, each with 3.6mm wide-angle lens to capture a 78 degree field of view were placed throughout the structure to record the smoke development and fire spread from multiple angles. These are denoted by Vx in the layout and
- Electrochemical sensors for measuring oxygen and carbon monoxide, in conjunction with relative humidity and light sensors, were mounted in boxes positioned 0.6m above the floor in the burn room, adjacent main floor compartment (main floor SW room) and second floor compartment (second floor SW room). These are denoted by the O_2 and CO labels.

3.1.2 The Fuel

Three distinct types of custom built couches and chairs were burned in this test series. The furniture was constructed on identical wooden frames, and the polyurethane foam

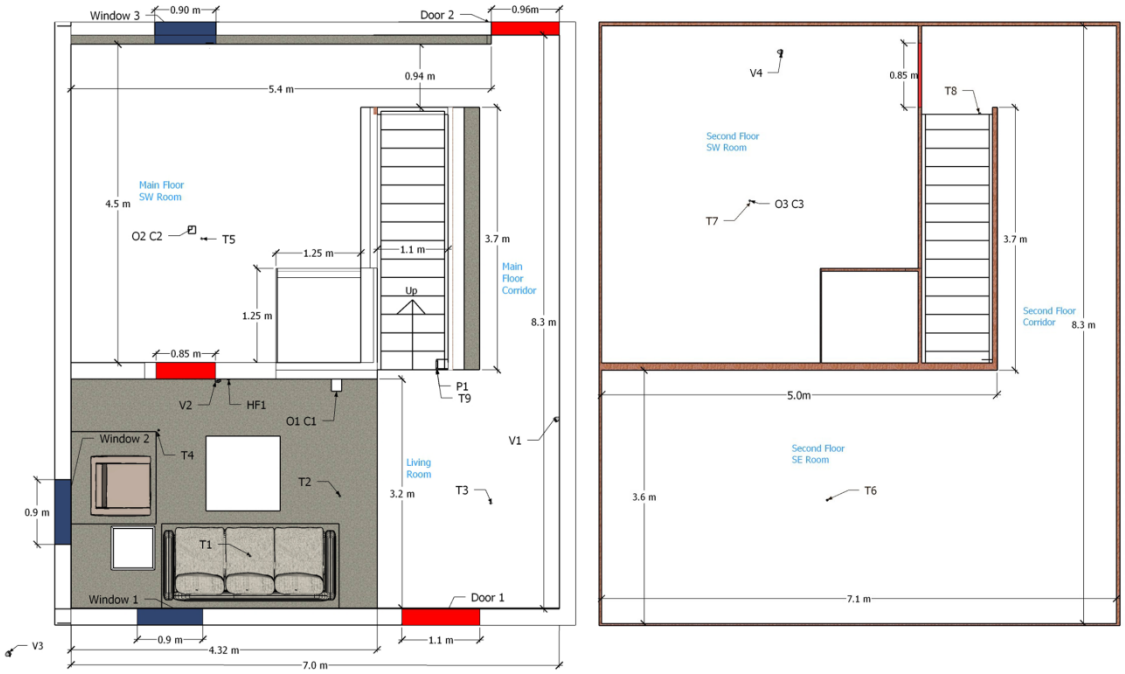

Figure 3.2: Floor Plan, borrowed with permission from [2]

and fabrics used were selected to comply with three different furniture standards from around the world; here designated as Netherlands, Manchester and Tennessee. Each of the three types was constructed with similar amounts of foam and fabric, so the initial masses of each item were very similar, as shown in Table 3.1 below. Differences between the initial masses are largely due to the difference in foam density.

One of the main distinguishing features between the couches in the context of this work, was that some couches were constructed of NFR and others of FR materials. Since the details of the compositions were proprietary, to distinguish between NFR and FR here, the chlorine (Cl) and bromine (Br) content is considered, as these two halogens are commonly used as FR additives. The Netherlands couches, referred to as NFR couch A, were considered to be the non-fire-retardant couches as they were built with polyurethane foam and polyester fabric that contained only 0.44% wt Cl and 0.17% wt Cl respectively. The Manchester couches, referred to as FR couch B, were considered to be the fire-retardant couches as they were built with 3.0% wt Cl polyurethane foam and a combination of bromine and chlorine (5.2% and 3.6% wt respectively) in the polyester fabric. The Tennessee couches, referred to as LFR couch C, were considered to be lightly fire-retardant, and were built with 0.9% wt Cl polyurethane foam and 0.11% wt Cl cotton fabric.

Test Furniture Type	Foam (kg)	Fabric (kg)	Frame Materials (kg)	Initial Mass (kg)	Final Mass (kg)
2 NFR A	10.48	7.48	42.08	60.04	39.41
3 LFR C	8.36	5.70	38.48	52.54	33.88
4 FR B	10.22	9.16	41.82	61.20	38.58
5 NFR A	10.44	7.72	41.94	60.10	38.82
6 LFR C	8.52	5.70	41.96	56.18	34.85
7 FR B	10.10	9.18	41.3	60.58	46.30
8 NFR A	10.60	7.68	38.2	56.48	35.45
9 LFR C	8.36	5.70	38.34	52.40	32.07

Table 3.1: Summary of Furniture Information for Each Test

3.1.3 Data Acquisition

There were multiple acquisition systems used to collect data during these large experiments. The weigh scales, heat flux gauge, thermocouples and bidirectional differential pressure transducers were all hardwired into modules and connected to backplanes of a National Instruments (NI) distributed data acquisition (DAQ) system configured using FieldPoint. Data was logged using custom LabView software. The modules and backplanes were located in an interior shaft of the burn structure, which was sealed for the tests. Signals were digitally transmitted back to the main computer system via 100 Mbps Ethernet connection. The security cameras were individually connected to a DVR and the electrochemical sensors, in conjunction with the relative humidity and light sensors, were locally connected to Arduino boards with signals transmitted via wireless to a dedicated computer. The NI DAQ sampled at a rate of 1.1 sample per second, the arduinos at a rate of 1 sample/5 seconds and the security cameras had a frame rate of 30 frames/ second.

Both the NI DAQ and the DVR have internal clocks, but because the NI DAQ was not connected to the internet during the tests, the clocks were not synchronized to one another or to a GPS timestamp. Additionally, many of the ardunios did not have a synchronized timestamp either, so ignition time had to be calculated for each system using a combination of the main stopwatch times, as recorded on the master test sheets, timestamped photographs of the tests and watching the video footage to locate images capturing ignition and recording the GPS timestamp on that image from the camera data. Once those times were aligned, the corresponding data point and time of occurrence was backed out individually for each system. Details on how this was done can be found in

Appendix B.

3.1.4 Raw Signal Analysis

The couches were placed on a drywall platform of dimensions 457.2mm x 457.2mm, supported at each corner by four MARS MSB60 weigh scales. Each scale had a maximum capacity of 40kg, and a +/- 0.01kg resolution. The output voltage was converted to kilograms using a linear calibration curve generated before the start of each test.

The Vatell TG1000-1 thin foil circular Gardon heat flux gauge, with a +/- 3% manufacturer specified accuracy, had a linear calibration curve generated by the manufacturer. This was used to convert the output voltage to radiant heat flux per unit area (kW/m^2).

The type-K ceramic fibre and Inconel sheathed 24 gauge thermocouples, with +/-2.2°C manufacturer specified accuracy, also generated a voltage signal which is converted to temperature in Kelvin by the data logger, with no correction for radiation applied in the post-processing (with the exception of one case which will be explained in the radiative contributions section).

The eight 19mm-diameter bidirectional velocity probes each with a corresponding type-K ceramic fibre and Inconel sheathed 24 gauge thermocouple, were installed on a vertical rake in the bottom of the staircase doorway, 0.15m from the right side of the stairwell opening and spaced 0.2m apart. Each bidirectional velocity probe was connected to an individually manufacturer calibrated Setra 267 differential pressure transducer with a range of +/-25 kPa and a 0.5% FS accuracy. The output voltage of the pressure transducers were converted to differential pressure values via a manufacturer supplied calibration curve. This was then used in conjunction with the temperature measured at the probe to calculate velocity at the probe using Bernoulli's equation, as will be further explained in the subsequent velocity conversion section.

The oxygen sensor was a ME2-O2-ϕ20 amperometric sensor with a range of 0-25% volume and <15 second response time [139]. The electrochemical carbon monoxide sensor was a MQ-7 electrocatalytic sensor with an operating range of 20-2000ppm and a 30 second response time [139]. Both of these sensors were manufactured by Winsen Electronic Technology Ltd already paired with a customized PCB board. The sensors were calibrated in the UW Fire Lab using a Limiting Oxygen Index (LOI) test system modified for that purpose [139]. Linear calibration curves were generated for each sensor and then used to convert the mV output recorded by the on-board Arduino to gas concentrations in parts per million for carbon monoxide and percent volume for oxygen respectively.

Calibration curves for the weigh scales, heat flux gauge, oxygen and carbon monoxide sensors can be found in Appendix B.

3.1.5 Velocity Conversion

In order to calculate velocity from bidirectional velocity probes situated on the vertical rake positioned at the bottom of the staircase, further conversion of the temperature and differential pressure data is required. The velocity of flow up and down the staircase was calculated using Equation 3.1 below:

$$V = \frac{1}{k} \times \sqrt{2 \times \frac{P - P_{static}}{\left(\frac{P_{ambient}}{RT}\right)}} \tag{3.1}$$

where V is velocity in m/s, k is a calibration coefficient to correct for geometrical design of the bidirectional probe, $P - P_{static}$ is the measured differential pressure in Pa, $P_{ambient}$ is the ambient pressure as measured and recorded by the local weather station at the time of the test, R is the universal gas constant (287.05 J/kg K) and T is the temperature in K measured locally at the probe. Once the raw data were converted, the velocities were smoothed using a 30-point moving average, and the smoothed velocities are used to generate the curves and profiles shown in Chapter 4.

Now that the overall experiment has been described and the instrumentation briefly addressed, the next section defines and discusses the methods and correlations selected for the calculation and comparison of heat release rate in the furniture fires in this work. The methods for obtaining any required inputs that did not come directly from the raw test data are also outlined in each part.

3.2 Heat Release Rate Calculation Methods

A variety of methods and correlations were used to compare and contrast differences in calculated and predicted values of heat release rate based on the present large scale furniture fire experiments. Some of these methods are used to predict a peak value of heat release rate, whereas others can be used to generate a time-resolved heat release rate curve.

The methods utilized to calculate heat release rate were chosen for a number of reasons. First, all of the methods are commonly used and referenced in the literature, although many

have not already been comprehensively checked for use in predicting heat release rates from fires fueled by a variety of more modern furniture types. In addition, methods that required a cross-section of input variables were chosen to allow comparison across methods that incorporated different parameters based on chemical or physical theories. Several methods were chosen to represent a selection of those that incorporate variables and use results obtained from either the cone calorimeter or from larger-scale tests. Finally, some correlations found in the literature were determined for certain fuels under very specific conditions. For these, it was of interest to assess their potential versatility for determination of fire heat release rate from different fuels and in different compartment fire environments.

These reasons together provide valuable information to researchers and engineers with respect to which methods are appropriate to use for a given fuel and environmental conditions. Insight should also be gained into what forms of experimental data can be used as inputs into the various methods, as well as into potential limitations of these inputs. Given the above reasons therefore, the following methods are used for calculation of the furniture fire heat release rates in this work:

- Mass Loss Rate Method [13]
- Heskestad Flame Height Correlation [17]
- Babrauskas Correlations [110, 111]
    1. Bench Scale Correlation
    2. Full Furniture Correlation
- Cone Extrapolation Method [104, 109]

All of the inputs needed for these methods are obtained directly and indirectly from a combination of large-scale experimental data obtained during the furniture fires described above and subsequent smaller-scale cone calorimeter testing of samples of all of the furniture materials. The equations for each of the methods, and additional information related to necessary inputs for their use, are explained in the subsequent sections.

3.2.1 Mass Loss Rate Method

The basic calculation for heat release rate as a function of time in a fire is to multiply a representative value of mass loss rate of fuel at a given time during the fire by the

corresponding representative value for the heat of combustion, termed the effective heat of combustion, for that fuel. At a given point in time, fire heat release rate, $\dot{Q}$, can be calculated according to Equation 3.2 below.

$$\dot{Q}(kW) = \Delta H_{c,eff} \dot{m} \tag{3.2}$$

For this calculation, the mass loss rate was calculated as a function of time directly from data recorded from the weigh scales during the experiment. There is less certainty in the appropriate value to use for the effective heat of combustion for each couch combination, which although often specified by only an average value for a given material(s), in reality also varies with time. In this case, it was decided to use an average value and additional sets of experiments were undertaken to determine appropriate average values for the effective heats of combustion for each couch combination tested here. Since these tests are independent of the heat release rate equations in this section, they are discussed in Section 3.3.1, as part of a larger Section dedicated to the methods used to measure other inputs needed for the heat release rate calculations.

3.2.2 Heskestad Flame Height Correlation

As discussed in the literature review, a second common method by which to estimate heat release rate is through use of the correlation by Heskestad [31] which was originally derived as a relation between steady state fire heat release rate, flame height and diameter according to Equation 3.3. The equation can be rearranged to solve for total heat release rate, $\dot{Q}$ as shown in Equation 3.4 [17].

$$l = 0.23 \dot{Q}_{tot}^{2/5} - 1.02D \tag{3.3}$$

$$\dot{Q}_{tot} = \left(\frac{l + 1.02D}{0.23} \right)^{5/2} \tag{3.4}$$

To apply this method in a time-resolved fashion for the current work, it was necessary to find a series of discrete values for flame height and width as a function of time for each of the fires. Geometric dimensions for the fires were not immediately available in the initial data from the 2015 burns, so a new image processing methodology was developed and applied to time sequences of individual images from the fire videos to estimate the flame height and width inputs needed for this correlation. The resulting image processing

program is outlined in more detail in Section 3.3.3 again as one of the additional inputs needed for the heat release rate methods in Section 3.3.

3.2.3 Babrauskas Correlations

Babrauskas [110, 111], as mentioned previously, developed two correlations for the prediction of a value of the peak heat release rate for propagating fires established over a variety of different upholstered furniture types. These are listed as Equations 2.12 for cases where cone calorimetry data for the materials in the furniture are available and 2.13, a simplified method that can be used for estimation of peak heat release rate based on generic material characteristics, thereby avoiding the necessity for cone calorimetry data when such data are not available.

1. Bench Scale Correlation

$$\dot{Q}(kW) = 0.63\dot{q}''_{bs}[frame factor][mass factor][style factor] \tag{3.5}$$

   where $\dot{q}_{bs}$ is the measured value of heat release from cone calorimeter tests of the furniture materials under an incident heat flux of 25kW/m^2, averaged over the first 180s after ignition. For cone calorimeter tests conducted at 35kW/m^2 and 50kW/m^2 instead of 25kW/m^2 (which was the heat flux that this correlation was original derived for), there are correction factors of 0.45 and 0.315, respectively, used in Equation 2.12.

2. Full Furniture Correlation

$$\dot{Q}(kW) = 210[fabric factor][padding factor][mass factor][style factor] \tag{3.6}$$

Across a large number of tests, it was found that certain furniture parameters changed the overall burning characteristics of different furniture items [110, 111]. Based on the trends, numerical values for the various factors emerged, and different combinations of factors were found important in each of the correlations. Values for the factors used in both equations are listed below, with factors in bold font indicating the values that were chosen as input into the above equations for the three present furniture types.

Frame Factor

- 1.66 for non-combustible frames
- 0.18 for charring plastic frames

- **0.3 for wood frames**
- 0.58 melting frames

Style Factor

- **1 for plain, rectilinear shapes**
- 1.5 for ornate, convoluted shapes

Fabric Factor

- **1 for thermoplastic fabrics (melting fabrics like polyester)**
- **0.4 for cellulosic fabrics (cotton)**
- 0.25 for PVC or polyurethane fabrics (faux leather)

Padding Factor

- 0.4 for cotton batting
- 1 for mixed materials
- **1 for polyurethane foam or latex foam**
- 0.4 for neoprene foam

3.2.4 Cone Extrapolation Method

The extrapolation method described in Section 2.8.2 was selected as the fourth and final way to calculate heat release rate of the furniture fires. This method uses two material properties, the effective heat of combustion and the heat of gasification. Determination of both are included in Section 3.3 of this Chapter.

In order to calculate the peak heat release rate of the fire, it was assumed that there was no external heat flux to the surface of the fuel, q''_e, in addition to that coming from the fire plume. Further, losses from the surface, q''_l, were considered to be negligible. Thus, consideration of the smoke layer as a radiating body that applies additional heat flux to the surface of burning fuel, similar to the cone heater in the small-scale experiments,

was not incorporated into this expression, although could be done in future iterations of this estimation. Instead, for each of the fires, the heat flux from the flames back to the fuel surface, q''_f, was estimated to fall within the range of values outlined for the kerosene pool fires discussed in Section 2.8.2 [115]. Therefore, the peak heat release rate of the fire was estimated for each of three values of surface heat flux, q''_f: 110kW/m^2, 120kW/m^2 and 130kW/m^2. These values were chosen since these furniture fires, due to the polyurethane present are somewhat comparable to gasoline and kerosene fires as all produce sooty, relatively low temperature flames [115, 116]. The effective mass loss rate, denoted as $\dot{m}''_{eff}$ was found via Equation 2.11 using the heat of gasification of the furniture materials and the three values of net heat flux from the fire back to the surface of the burning couch. Peak heat release rates for each of the couch fires were then predicted using Equation 3.7

$$HRR_{extrapolated}(kW) = \dot{m}''_{eff} \times \Delta H_{c,eff} \times Area_{peak} \tag{3.7}$$

Where, $\Delta H_{c,eff}$ is the effective heat of combustion calculated for each furniture type based on cone calorimeter data. The area of the fire is estimated to be 1.58m^2 at the time of peak heat release rate, assuming that all of the combustible surfaces - the sitting cushions, back cushions and both arm rests - were fully involved in the fire as supported by the video footage and observed rates of flame spread.

This extrapolation method is premised on the assumption that, as the couch burns, the flaming area can be thought of as discretized into an array of square burning areas, each of similar dimension and each burning in a fashion similar to a single cone calorimeter sample of the same material. By extrapolating the mass loss rate measured in the cone sample test, up to the mass loss rate of the full-scale couch, by way of Equation 2.11, the full scale heat release rate remains a function of the mass loss rate and heat of combustion [13] normalized with respect to the area of fuel burning at any given time.

While only the peak values are estimated in the present research, time-dependent values of fire heat release rate could be determined based on estimates of the effective heats of combustion and gasification for each furniture material or combination of materials coupled with time-resolved estimates of fire heat release rate, and hence heat flux back to the burning surface, as well as simultaneously determined values for the heights and widths of the fire. Since these parameters are critical for input to several of the estimation procedures discussed above, the methods used for determining the effective heats of combustion and gasification of the couch materials are outlined in more detail in the next section, followed by a description of the image processing program used to determine flame geometry.

3.3 Other Inputs for Heat Release Rate Calculations

3.3.1 Effective Heat of Combustion

The furniture used in this research was comprised mainly of polyurethane foam, polyester and cotton fabrics; however, the exact composition of the materials was proprietary and therefore not available to the researchers. To determine representative values for the effective heats of combustion of the materials, two approaches are possible. In the first, a value could be taken from the literature for a similar material. Alternately, the value could be measured based on small samples of the materials used in construction of the items burned. Significant uncertainty surrounds the first option because there are many documented values for the heat of combustion for polyurethane foam. For example, predetermined values from the literature for polyurethane foam vary between 17MJ/kg and 20MJ/kg [140]. It is known, however, that the heat of combustion is strongly related to the nature of the chemical bonds, thus detailed composition, of the foam that was burned. Without knowing the exact chemical make-up of the polyurethane foam documented in the literature relative to that in the present tests, it was decided to experimentally determine effective values for the heat of combustion for each furniture type to provide some level of confidence for this input in the calculation methods.

A further issue arises in using even an experimentally determined value for the heat of combustion which is based on testing a sample of material. This is that the conditions of the tests, and thus values for heat of combustion, may not be representative of those encountered in the fire scenario [13]. For example, the theoretical or ideal heat of combustion would be determined using the adiabatic bomb calorimeter, a test method that is carefully designed such that there are no energy losses during the measurement process. More realistically in a fire, the energy derived from a burning material is lower than this. It might be determined as the sum of a radiative and a convective fraction of energy released, but each of these will also always be lower in magnitude than a theoretical value [13]. Further , if the value is found under very good burning conditions with a constant supply of oxygen and relatively complete combustion of the material, it will not be suitable for use in calculating the heat release rate for a fire scenario in which levels of oxygen are changing and decreasing below ambient. Thus, even when using a measured value for the effective heat of combustion, the method of measurement becomes important.

This entire picture is further complicated in the present research by evidence found previously that polyurethane foams can exhibit differing flammability characteristics when covered with fabrics [91]. Therefore, for the present research it was concluded that it was important to determine effective values for the heat of combustion for the complex fuel loads

representing each type of furniture. This was accomplished through independent testing of the foam and fabric materials, alone and together as a composite sample, in an Fire Testing Technology (FTT) cone calorimeter system available at University of Waterloo. Values for effective heats of combustion were calculated from the results for each specific material combination. In 2018, the first set of composite tests were run on 25mm thick foam samples with one piece of fabric placed on top. The fabric was cut with enough length to partially cover part of the unexposed sides of the foam when the sample holder edge piece was placed on top. This was to keep the fabric secured over the foam such that the exhaust flow of the test instrument would not pull the fabric off the surface of the foam over the duration of the test. In 2020, a second set of tests were run on composite foam and fabric samples, adapted slightly in terms of the ASTM E 1354 material specifications [99]. Composite samples were comprised of 50mm thick foam pieces, again with a piece of fabric overlaid (as previously described). This ratio of foam to fabric was considered more appropriate as it is closer to the ratio of foam and fabric of a cushion in the real piece of furniture [92]. The value of Total Heat Released, or THR, in MJ/m^2,calculated by the ConeCalc5 software [141] was used with the surface area of the sample (0.00884m^2) and the mass of the sample consumed (in kg) to estimate a value of effective heat of combustion for that specific material combination by Equation 3.8 below:

$$\Delta H_{c,eff}(kJ/kg) = \frac{THR(kJ/m^2) \times 0.00884m^2}{m_{consumed}(kg)} \tag{3.8}$$

The final measured values for the heats of combustion for all furniture foam and composites are included in the first Section of the Results and Discussion Chapter, titled Effective Heat of Combustion.

3.3.2 Heat of Gasification

The heats of gasification for representative samples of each furniture material were determined based on values of mass loss rate measured using the cone calorimeter under several levels of incident heat flux as described in Section 2.8.2. Measured values of mass loss rate per unit area for both NFR A and FR B couch materials were determined from cone calorimeter tests of foam samples conducted at incident heat flux values of 20kW/m^2, 30kW/m^2 and 35kW/m^2, with an additional value from a test at 50kW/m^2 for a foam and fabric combination for each couch. In the case of LFR couch C, mass loss rates per area were taken from tests on foam at incident heat flux levels of 20kW/m^2 and 30kW/m^2 with an additional value at 35kW/m^2 from the foam and fabric combination test. Due

to variation in mass loss rate over the duration of a cone calorimeter test, mass loss rate values were chosen as those at or around the peak values output by the ConeCalc5 software [141]. The heat of gasification was taken as the reciprocal slope of the linear trend-line fit to a scatter plot of mass loss rate per cone area (kg/ s m^2) versus heat flux (kW/m^2). The final values and several limitations in these determinations will be discussed further in Chapter 4.

The next section explains the geometrical inputs required for calculation methods as well as the methods used to determine them.

3.3.3 Fire Geometry: Flame Heights and Widths, Burning Area and Effective Diameter

There were several fire geometry inputs required for the various calculations performed as part of this study: 1) flame height and width were required for Heskestad's flame height correlation to calculate the heat release rate as shown in Equation 3.4, 2) to calculate the flame heights using Heskestad's correlation, Equation 3.3, and compare the estimates to measured flame heights from the image analysis program, fire heat release rate was calculated using the mass loss rate relationship and measured flame widths were needed, 3) fuel bed area measurements were required for the cone extrapolation method, Equation 3.7, and 4) flaming area, specifically flame heights and widths, were required to determine shape factors for the emissive power calculations. As a result, an image analysis program was developed to approximate the flame heights and widths as a function of time in such a manner that the outputs from the program could be used as inputs into these correlations and area calculations. The next section explains the image processing program used to measure time resolved values of flame height and width in the furniture fires. Measurements were based on footage and individual images captured using the hybrid colour-night vision security cameras, and more in depth analysis of the video footage was also used with these values to estimate fuel bed areas.

Image Processing Program: Flame Heights and Widths

Flame heights and widths were determined using frames from the eight videos (one from each test) captured using the Lorex colour-night vision security camera that was positioned to look directly at the fire on the couch, labelled as V2 in Figure 3.2 above. After analyzing several commercially available image analysis processing options, the Fiji software program which uses ImageJ code [142] was chosen as a platform for development of a new image

analysis methodology by which to determine flame height and width as functions of time. The outputs from the code are used to determine the flame areas used in the Heskestad correlation [17].

In the first step, the original 30fps video footage was spliced, using a VLC movie player [143], into individual images and down-sampled via equal time increments, to represent the fire growth rate at 5 images per second. The usable cut footage was started after ignition at a point when the couch was visibly burning and stopped when smoke in the compartment obscured the fire by flowing heavily over the camera face, blocking any view of the flaming regions.

The spliced frames are read into Fiji and for computational ease, the colours on all frames are inverted so that the fire is dark, and dark areas in the original image are light, as shown below in Figures 3.3. The code then finds a consistent reference point that relates to the base of the fire. Other work [136] identified difficulties with determining flame heights in the later stages of fires due to changing reference locations as the fire burns down through the sitting cushion. If the baseline of the fire is then set to be at the constant height aligned with the top of the sitting cushion, a percentage of the flame height is not accounted for. To try to correct for this, the reference line for flame width here was set along the top surface of a table in each frame, and the algorithm searched and corrected for the instantaneous base of the flame below that line. That way, as the fire burns down through the sitting cushion, the entire flaming area is accounted for. The unfortunate trade-off to this occurs in the earliest stages of the fire, since the program cannot distinguish whether the portion of flame it 'sees' as being below the top of the cushion is a result of burn through which should be accounted for in determining flame height or is simply an artefact in the image because of the view angle as the fire spreads from front to back of the couch, resulting in the same apparent effect. While outside the scope of the present work, this could potentially be accounted for by inserting additional features into future iterations of the image processing program.

The code next identifies the location of 'fire' along the reference line based on analysis of the colour values within each pixel. After some trial and error, the green and blue content of each pixel were used to set the threshold because there is more variability in green-blue than with red values when analyzing an inverted image. Specifically, if a pixel is found to have an average green-blue value of less than 10, that pixel is considered to be 'flaming'.

Once pixels were identified as potential flames in a frame, the software searched for edges of the 'flames' by checking a square of 8 px x 8 px in size to both the right and left of the identified flame pixel. On the right hand side of the fire, if the colour content

(a) Original Camera Footage (b) After Image Processing

Figure 3.3: Couch Fire Example Before and After Image Processing

in less than 35% of the pixels in the square to the right of the identified 'flaming' pixel indicate flame, and at the same time if the colour content in more than 65% of the pixels in the square to the left of the 'flaming' pixel indicate flame, then the 'flaming' pixel is identified as aligning with a flame edge, and is stored as x_2. The code then proceeds to the left to find x_1, by checking each square until it identifies a 'flaming' pixel where greater than 65% of the colour content in the square to the right and less than 35% of the content in the square to the left indicate flame. Both of these conditions must be true simultaneously on a given side of the flaming region for that pixel to be identified as a flame edge. To determine the height of the flaming area in the image, the vertical extent of 'flaming' pixels is determined for each column across the span of width (between x_1 and x_2) by moving vertically and checking for pixels with average green-blue values of less than 10, and comparing these values of height to the height determined along the center column, located at a position halfway between x_1 and x_2. The comparison between heights in each column and the center-line height allows the code to account for tilted fire plumes and/or the unsteady flaming regions that are characteristic of real fires. Similar to the verification for the widths, once a 'flaming' edge pixel is detected during the flame height determinations, the code checks with rectangles above and below that pixel position to ensure all the pixels with 'flames' are included in the height output. The final code can be found in Appendix C.

There are several sources of known uncertainty in the measurement of flame height using the current methodology. First, there is parallax in the video camera that cannot be corrected out, as the video camera was not originally set up to be perfectly square to the couch, but was also moved from its original location long before attempts were made to

apply image processing to the video data. This parallax impacts the width measurements creating an approximately 5% error margin as the field of view of the camera was not accounted for. With respect to the impact of the camera field of view on determining flame heights, there may be as much as a 20% error margin since roughly 17.5" (0.4445m) of visible cushion could be seen at the centre back of the couch; however, in the corner there was roughly 22.25" (0.5715m) of back cushion seen in the camera image. A single scaling factor, based on the visible height of the back centre point was chosen to convert pixel values of flame heights, as output from the image processing program, to visible height. As a result, measured flame heights reported in Chapter 4 may be on the order of 20% systematically too low due to this bias. Additionally, as noted above, as the fire initially grows and moves towards the front of the couch, there are over-predictions of flame height as the fire gets closer to the camera. In the later stages of the fire, as the compartment starts to fill with smoke that flows over the top of the flaming region of the fire and the lens of the video camera, the total height and width of the fire are not discernible from the images due to obscuration of various sections of the camera image by smoke. In the couch A and B fires there was significant smoke production, so after a certain point, reliable measurements from the video footage were not available. Furthermore, the 8px x 8px box that was chosen to check for flaming regions was selected because as the box became larger, computation time increased drastically. In the current form, computational time with this code ranged from roughly 2 hours, when videos were about 5 minutes long, to over 5 hours, when videos were over 15 minutes long. While image processing proved to be a powerful tool in this research, the above limitations led to use of some significant suppositions, pointing to the need for extremely careful camera placement and improved image processing tools for use in future full-scale fire tests.

Burning Areas and Effective Diameters

Direct observation of the flame videos, coupled with the image processing for variations in flame heights and widths with time, pointed to the fact that there were different shapes and areas of burning fuel during a test, particularly as different sections of the couch became involved in the fire. Two main stages are shown in Figure 3.4 below. In the early stages of the fire, the fire was primarily burning on the sitting and back cushions, and as it grew and more surfaces became involved, including the arm rest, the effective area of the fuel bed changed as well.

Due to the shape of the couch with a sitting cushion, back cushion and arm rest connected perpendicularly, it was determined that as the fire progressed to involve the different surfaces, an effective area of all the burning surfaces was required to calculate an

(a) Early-Stage

(b) Late-Stage

Figure 3.4: Differences in Fuel Bed Areas

effective diameter of the fire that more accurately represented the full area of the couch that was burning. This effective diameter could then be used as input into the Heskestad correlation and the effective areas of the fuel bed at peak used as the area parameter input into the cone extrapolation method. In the early stages of the fire, when the fire was spreading across the sitting cushion and up the back cushion, as shown in Figure 3.4a, the area of the flame was estimated using Equation 3.9:

$$Area_{effective} = (2 \times height_{flame}) \times width_{flame} \tag{3.9}$$

to accounted for the observable spread across the sitting cushion, as well as up the back and outward towards the front of the sitting cushion. In the analysis, the outward spread of the flame across the cushion was assumed to equal the height of the flame spreading up the back cushion since the processing of any side camera angles, such as those shown in Figure 3.4, was not within the scope of the present work.

Once the flame height was equal to the height of the back cushion, it was assumed that the height of the cushion was representative of the fuel involved in the burning on the back of the couch, so the above Equation was adjusted so that the $height_{flame}$ in Equation 3.9 was fixed as the height of the centre back cushion provides(0.4445m) to be consistent with the scaling factor used in the image processing program. For simplicity, the height of the couch back was also taken to represent the full depth of the sitting cushion (outward spread), though this may underestimate the true area of the fuel burning, and hence effective diameter of the fire, by approximately 13% and 10% respectively. Only the

width of the fire then continued to change as the fire spread horizontally across the sitting cushions of the couch.

When the arm rests became involved at various points in time, Equation 3.10 was used to calculate the effective area of the fuel bed:

$$Area_{effective} = (width \times 0.4445m) + ((0.1524m + width) \times 0.4445m) \tag{3.10}$$

This effectively flattens out the couch so that all three surfaces - the back cushion, sitting cushion and arm rest - are no longer perpendicular but connected on the same plane. The 0.1524m was the height of the arm rest, which was added to the time varying measurement of fire width. The equations can be visualized in the diagram below (Figure 3.5).

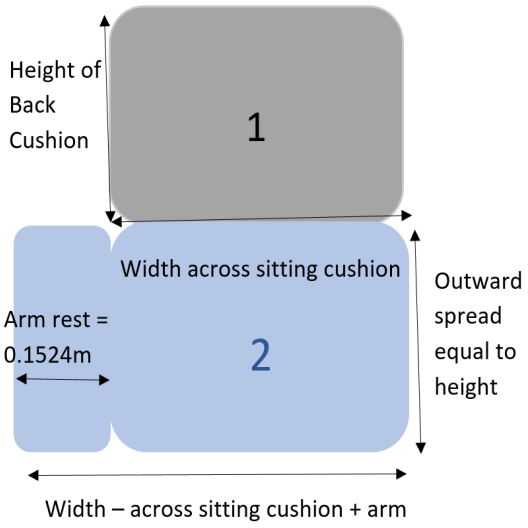

Figure 3.5: Effective Area Diagram

Once these areas were determined for each of the couches over the course of the three stages of burning, the effective diameter was calculated using Heskestad's corrective equation based on an equivalent area of the fire (used for example when determining the equivalent diameter of a fire established on wood cribs), shown in the Correlations for Flame Geometry section of Chapter 2, and re-arranged as follows:

$$D_{effective} = \sqrt{\frac{Area \times 4}{\pi}} \tag{3.11}$$

Finally, with respect to the radiation calculations, the flame area, or the radiating body, was considered to be rectangular in shape and was therefore determined on a time-resolved basis as the product of the height by the width of the fire as output by the image processing program as a function of time. These calculations are discussed further in the section below.

3.4 Potential Methods to Cross-Correlate Heat Release Rate Input Parameters and Calculations

In a final stage of this research, estimates of heat release rate determined using the mass loss method were combined with flame geometry and flame emissive power estimates in radiation calculations. Results were compared to measured values of heat flux determined by the gauge, HF1, located at a 3-meter distance from the fire on the adjacent wall. This allowed exploration of potential radiative heat transfer contributions from both the hot smoke layer and the fire to a point on the adjacent wall of the compartment, as well as further assessment and substantiation of the relationships between measured raw data, derived input data and calculated values with respect to some of the coupled heat transfer effects in these compartment fire environments. The methods used to determine the radiative contributions of both the fire and smoke layer are explained in the next section.

3.4.1 Point Source and Emissive Power Radiation Calculations

The heat flux gauge measured the total heat flux from the fire compartment to the gauge face. This is comprised of convective and radiative contributions from both the fire and the smoke layer. It is of interest here to compare measured heat flux values to those calculated using the point source radiation estimates with input data from independently measured experimental fire parameters. The first check is done via equation 2.10 for point source radiation presented in Section 2.4 of Chapter 2. This equation can be re-arranged as Equation 3.12 to solve for the heat flux from the fire, estimated as a point source of radiation assumed to be in the center of the flaming area, to the heat flux gauge modelled as a target at some distance, R, away from the fire. The distance from the fire to the gauge was estimated to be constant at 3m which represents a point from the centre of the cushion horizontally directly to the gauge. This will result in some error since in reality it should be the time varying distance from the center of the fire to the gauge which will

migrate across the cushion horizontally and increase in height vertically to correspond with the midpoint of the growing fire plume.

$$\dot{q}''_{fire}(kW/m^2) = \frac{\chi_{rad}\Delta H_c \dot{m}}{4\pi R^2} \tag{3.12}$$

As shown in Equation 3.12, the radiative portion of the total heat release, χ_{rad}, is used for this calculation with the remainder of the fire heat release rate going to heat the convective plume of hot product gases. Although the radiative fraction is often assumed to be 30% of the total heat release [37], it was of interest to directly estimate the radiative fraction for these furniture fires due to the complex nature and unknown sooting propensity of the fuel and the changing ventilation conditions during the fire. Therefore, as a final step in analysis above, the radiative fraction from the fire was calculated on a time-resolved basis by dividing the measured heat flux from the gauge, by that estimated based on a point source analysis of heat flux from the fire, via Equation 3.13 below.

$$\chi_{rad} = \frac{\dot{q}''_{measured}}{\dot{Q}4\pi R^2} \tag{3.13}$$

Through the analysis, estimated values of radiative fraction during the early stages of the fire, when the oxygen levels were still at or only slightly under ambient levels and before the smoke layer developed, could be compared to values estimated at later stages in fire development to determine any differences over the course of fire growth and development.

As a second assessment, the radiative energy from the fire compartment to the heat flux gauge can also be calculated using the principles of emissive power. In the case of these fires, it was of interest to try to examine the importance of radiative contributions to the heat flux gauge from not only the flaming fire plume, but also from the hot smoke layer. This was especially the case as the smoke layer became thick and descended down from the ceiling of the compartment. Using the equation for emissive power, shown by Equation 2.9 below, the radiative contributions for both the fire and the smoke layer were therefore calculated, each based on their own representative temperature and specific shape factor, or ϕ.

$$\dot{q}''(kW/m^2) = \phi\sigma\epsilon T^4 \tag{3.14}$$

The shape factor for the fire is shown in the Figure 3.6 below, and is represented by Equation 3.15 for radiation from a rectangular surface to the centre of a parallel infinitesimal element a certain distance away from one corner of the radiating surface [144].

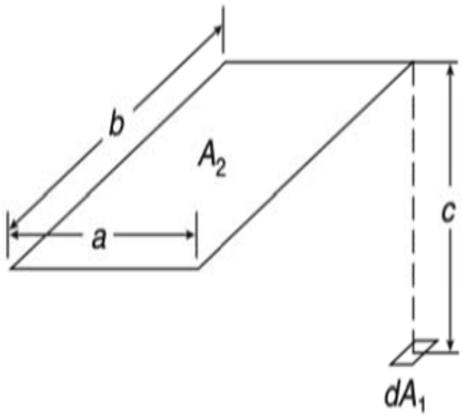

Figure 3.6: Reproduced with permission from [3] ϕ to a perpendicular definite rectangle

$$\phi_{d1-2} = \frac{1}{2\pi}\left[\frac{X}{\sqrt{1+X^2}}\tan^{-1}\left(\frac{Y}{\sqrt{1+X^2}}\right) + \frac{Y}{\sqrt{1+Y^2}}\tan^{-1}\left(\frac{X}{\sqrt{1+Y^2}}\right)\right] \tag{3.15}$$

where X=a/c and Y=b/c, for which a is the height of the rectangular fire area, b is the width of the rectangular fire area and c is the distance from the fire to the heat flux gauge [144].

Similarly, the ceiling shape factor is shown by Figure 3.7 below, and represented by Equation 3.16, from a rectangular surface to an perpendicular infinitesimal element, connected from the corner of the radiating surface [144].

$$\phi_{d1-2} = \frac{1}{2\pi}\left[\tan^{-1}\left(\frac{1}{Y}\right) - \frac{Y}{\sqrt{X^2+Y^2}}\tan^{-1}\left(\frac{1}{\sqrt{X^2+Y^2}}\right)\right] \tag{3.16}$$

Where X=c/b and Y=a/b, for which a is half the length of the ceiling, b is the width of the ceiling, and c is the distance between the bottom of the ceiling and the gauge [144]. At the beginning of the fire, the distance c would extend from the gauge to the ceiling height, while as the fire progresses and the compartment begins to fill with smoke, the distance would became the distance between the bottom of the hot smoke layer and the gauge instead.

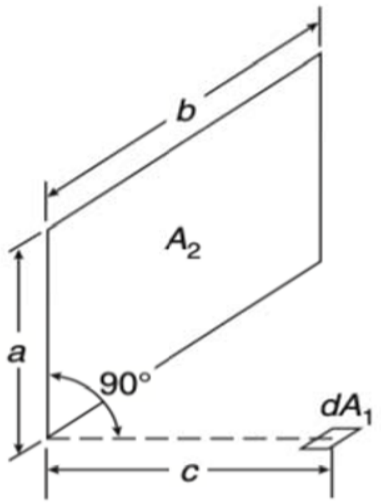

Figure 3.7: Reproduced with permission from [3] ϕ to a parallel definite rectangle

The fire temperatures used were based on thermocouple data measured as near to the flaming area as possible and were assumed to be isotropic throughout the entire visible flaming region of the fire. A 50K correction was applied to the measured fire temperatures to account for radiation and soot deposition on the thermocouples [145]. The area of the fire was assumed to be rectangular in shape, and was therefore taken as the product of the time varying height and width as output from the image analysis program.

For the temperature input to the smoke layer calculations, temperatures were taken as the values measured by the thermocouple on the rake in the middle of the living (burn) room, T2 in Figure 3.2 in Section 3.1.1 above, and located as close to the descending boundary of the smoke layer as possible. Due to the difficulty in tracking the boundary of the smoke layer continuously with time, values of ceiling layer radiation were interpolated based on the slopes of the respective relationships determined for temperature and distance from smoke layer to heat flux gauge fit using values taken at three discrete points in time. The times corresponded to the time when the smoke layer covered the ceiling so that no seams in the concrete board were visible (assumed to be 1cm thick), to when the smoke layer descended to the top of the window, and to when the smoke layer descended to the bottom of the window. With the depth of the smoke layer estimated at these times, and the known height from the heat flux gauge to the ceiling, the necessary input into the shape factor for height could be determined over time. Calculating the slope of a smoke layer depth versus time curve, and assuming a relatively constant smoke filling, the slope

was used to estimate the rate of smoke filling and therefore change in height from the smoke layer to the gauge over time. To mimic a time-resolved temperature curve for the smoke layer as it descended into the compartment, temperatures were linearly interpolated between the three discrete points in time as well.

Based on the experimental data available and the methods for calculation of fire heat release rate outlined here, it is clear that before undertaking a full comparison of results from the different heat release rate calculation methods, an overall knowledge of the fire progression was necessary. In addition, several ancillary experiments and analyses had to be conducted to determine key input parameters that were not collected as part of the original data from the large 2015 house fire experiments. The next Chapter, then, opens with presentation and discussion of results from the cone calorimeter tests for all furniture materials, including calculated values for effective heats of combustion for each furniture type. This leads into a description of the overall fire behaviour, flame geometry and compartment characteristics, including the oxygen and carbon monoxide levels, velocity profiles at the staircase, temperatures in the compartment, and heat flux measurements. The Chapter ends with a presentation, comparison and discussion of the results from the four heat release rate calculation methods chosen for this research. Based on the results obtained, conclusions and recommendations are then outlined in the final chapter of the thesis.

Chapter 4

Results and Discussion

This chapter will start with a discussion of the heats of combustion of the materials determined for each furniture type and used as inputs into the mass loss rate and cone extrapolation methods. Following this, the overall fire behaviour will be discussed for one of each representative furniture type, supplemented with picture chronologies of these tests. Results and discussion of the ensuing fire environments will be presented, including thermal and gaseous species evolution from the perspectives of smoke and air movement, as well as radiative contributions and heat flux. Once the environmental conditions and overall behaviour of the fires are well understood, the second part of the chapter delves into results from the various methods employed for calculation of heat release rate. Those sections compare and contrast the results of each method and provide a discussion on the strengths, weaknesses and appropriateness of each method in each particular fire scenario.

In the full set of nine fire tests, there were three furniture types tested in triplicate; however, the first test, an FR B couch test, was exempted from the analysis due to errors in the load cell data. Therefore, only eight of the nine tests were analyzed. For the most part through this Chapter, results from three representative tests were selected for presentation and discussion of the data. In the early sections of the chapter, the overall description and characterization of the fire environments in terms of oxygen levels, carbon monoxide concentrations, temperatures, radiative contributions and velocity profiles are presented for tests 4, 5 and 6, as representative FR B, NFR A and LFR C furniture fires respectively. The ancillary test data for overall fire development and environmental characterization for tests 2 (NFR A), 3 (LFR C), 7 (FR B), 8 (NFR A) and 9 (LFR C), can be found in Appendix A.

In the second part of the Chapter, heat release rate results are shown for all eight

tests in sections discussing the t^2 fire growth curve and Babrauskas correlations, while only representative tests 4 (FR B), 5 (NFR A) and 6 (LFR C) are included in the main body for discussions of results from the mass loss rate, cone extrapolation and Heskestad flame height correlations. For the ancillary tests, heat release rate results for these correlations can also be found in Appendix A.

Finally, it should also be noted that gaseous data was not collected during test 6 (LFR C test); however due to the consistency in the heat release rate curves, and thus overall fire progression, between tests 3 and 6, the data from test 3 was used for the oxygen and carbon monoxide curves, which was over-plotted with the heat release rate curves for both tests 3 and 6 (Ci and Cii) in that part of the discussion.

4.1 Cone Calorimeter Material Characterization

4.1.1 Effective Heat of Combustion

To start, representative samples of materials used in construction of the furniture were tested in the cone calorimeter. The heats of combustion were calculated via the calculation method described in Section 3.3.1, using the total heat release as output from the ConeCalc5 software [141], the exposed surface area and the mass of the sample consumed during a test. The heats of combustion were calculated based on data collected during testing of samples of foam only and furniture composite samples conducted in both 2018 and 2020. Results are summarized in Table 4.1. Samples listed as foam only were all 25mm thick pieces, and the 2018 composite samples were also comprised of 25mm thick pieces of foam with one layer of fabric. In 2020, the composite samples were constructed with 50mm of foam with one layer of fabric. The percent differences included for the composite tests in the Table are the differences between the average heat of combustion determined using data from all composites tests of that furniture type and the heat of combustion for a particular composite configuration. Averages for all of the composite tests conducted (with ignition) are 21.1MJ/kg, 17.0MJ/kg and 17.2MJ/kg for NFR A, FR B and LFR C materials respectively.

Referring to the summary Table 4.1, there is a small change in value from 19.6MJ/kg to 21.2MJ/kg, for a difference of 1.6MJ/kg (7.8%), in the heat of combustion for the foam only samples between 2018 and 2020 for couch A and from 20.5MJ/kg to 23MJ/kg, or a 2.5MJ/kg (11.5%) difference for couch C foams. There is even less difference from 13.4MJ/kg to 14.0MJ/kg, or only 0.6MJ/kg (4.4%), between results for Couch B foams

Furniture Type	2018 25mm Foam (MJ/kg)	2020 25mm Foam (MJ/kg)	2018 Composite (MJ/kg)	2020 Composite (MJ/kg)
NFR A	19.6	21.2	17.5 (19%)	22.9 (8%)
FR B	13.4	14.0	12.0 (35%)	19.5 (14%)
LFR C	20.5	23.0	16.5 (4%)	17.5 (2%)

Table 4.1: Calculated Effective Heats of Combustion of Foam and Furniture Composites

over that same time period. These differences all lie within the bounds of the embedded uncertainties in indirect calculation of the heat release rate by the cone calorimeter [146]. Despite this, the consistent differences across all three foam only samples of the materials as tested in 2018 and 2020 highlights that further investigation into the aging of foam and fabrics may also be essential to understanding potential changes in heat release rate, and therefore fire risk, over the life-cycle of composite furniture products.

In terms of the composite tests, in 2020 the NFR A and FR B composites of 50mm thick foam with one layer of fabric did not ignite under an incident heat flux of 35kW/m^2 and instead new samples were tested with an incident flux of 50kW/m^2 to achieve ignition. This is contradictory to not only the first round of composite tests with 25mm of foam and one layer of fabric in which all the samples did ignite, but also to other work in which 35kW/m^2 was sufficient for ignition of foams [110, 147]. In contrast, the LFR couch C composite materials with the thicker foam piece did ignite when exposed to a heat flux of 35kW/m^2. At first, it was thought that the change in incident heat flux needed for ignition was due to changes in the structure of the foam or change in fire retardants with aging. The former was thought to be very unlikely, although chlorine is a heavy compound, and depending on the way the FR couch B foam was manufactured, it may have stabilized the molecular structure over long periods of time than for the other couch foams. The latter could be an issue, since subsequent tests of 25mm thick foam only samples for both NFR couch A and FR couch B foams were conducted and ignition occurred with an incident flux of 35kW/m^2. In addition, 2020 values of heat of combustion are higher than those measured in 2018 for 25mm thick foam only samples which might be consistent with changes in the foam additives due to aging. In all cases, there may have been changes in heat transfer through the fabric and into the sample as a result of the thicker sample as well. These results highlight the need for more thorough investigations into possible insulating effects that thicker foam samples have on the ignitability of composite specimens, as well as into aging of furniture foams and possible changes in thermal or fire retardant properties with time.

Another hypothesis that might explain why the composites of the NFR couch A and FR couch B materials did not ignite in 2020 is that the polyester fabric may have aged, perhaps making it more susceptible to forming a tarry-char layer over the sample surface as it degraded at lower levels of incident heat flux. This is different from how it previously appeared to melt onto and into the surface of the foam and therefore would change the overall burning characteristics of the composite. In contrast, when ignited under the higher heat flux of 50kW/m^2 shown in the Table, the effective heat of combustion of the composite material is clearly much higher than in 2018, due to a combination of the higher incident flux and potential changes in the surface material as well. In future, more work will be conducted to investigate and shed light on these kinds of changes in behaviour over time as part of an independent study on the impact of aging on the fire performance of furniture materials.

Interestingly, as seen in Table 4.1, the heats of combustion for the LFR couch C composite materials are more consistent than for the other couches, even though there was an apparently large increase in the heat of combustion of the foam from 2018-2020. Although not feasible to investigate further due to inherent variability in testing fabrics alone in the cone calorimeter, this might suggest that the cotton properties are key in governing the burning behaviour of these composites, and that they stayed more consistent over the years. Textiles such as cotton and polyester are subject to degradation over time and one of the ways that these materials can become damaged is through light exposure [148]. There is a spectrum of resistance to light deterioration over a range of textiles, and it has been found that cotton is more resistant to light exposure than polyester materials [148]. Over the two years, the extra fabric used in the construction of the furniture items was stored in clear plastic bags in various rooms of the lab that would have subjected the fabrics to a high degree of light exposure. Relatively more light damage to the polyester fabric may be a contributing factor to the change in the cone calorimeter results seen above as well.

Based on the results outlined above, it was concluded that the original heats of combustion calculated from the 2018 composite tests would be used as input into the calculations conducted during this research. The values used for each furniture type are therefore **17.5MJ/kg** (NFR couch A), **12.0MJ/kg** (FR couch B) and **16.5MJ/kg** (LFR couch C).

These values fall well within the wide range of values reported in the literature for similar upholstered furniture items. In one set of large scale experiments with furnishings where the heats of combustion were calculated in a similar fashion, reported values for heats of combustion ranged between 11-22MJ/kg [149]. In other work, the assumed value for the heat of combustion for a polyurethane foam and polyester-cotton fabric upholstered couch was much higher 24.4MJ/kg [150], while other calculated values for the heat of

combustion of furniture made from polyurethane foam and cotton in adherence with the California Bureau of Home Furnishings Technical Bulletin 117, were listed as ranging from 13.1-14.8MJ/kg [131], lower than the most comparable Couch C in this work.

4.1.2 Heat of Gasification

Results of the cone calorimeter testing of representative samples of materials used in construction of the furniture were also used to determine the effective heat of gasification of each of the couch materials according to the methods outlined in Section 3.3.2.

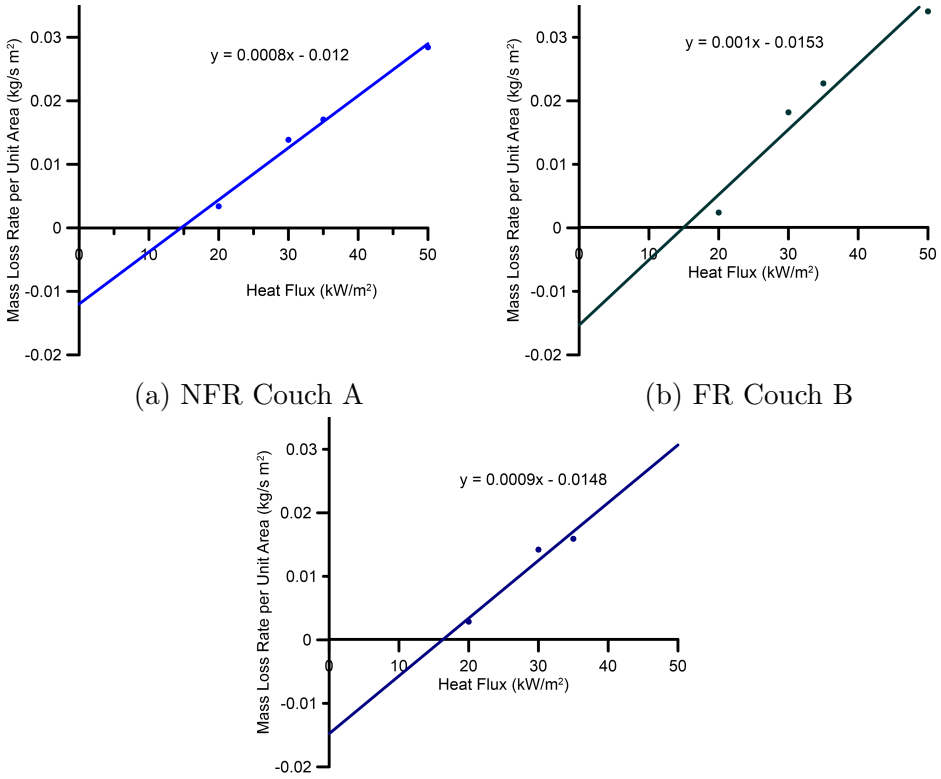

(a) NFR Couch A

(b) FR Couch B

(c) LFR Couch C

Figure 4.1: Mass Loss Rate per Unit Area and Heat Flux Plots for Each Representative Furniture Type

Plotted in the Figures 4.1 are representative values of measured mass loss rate per unit area versus incident heat flux used in the corresponding test. The heats of gasification

calculated for NFR A, FR B and LFR C couches respectively are 1250kJ/kg, 1000kJ/kg and 1111kJ/kg. These values fall within the range of values reported elsewhere for heats of gasification for flexible polyurethane foams of 1.16kJ/kg-1.22kJ/kg [104], and are slightly higher than that of 900kJ/kg of foam with melamine additives [86]. These heats of gasification are used in conjunction with the three values of q''_f outlined in Section 3.2.4 to calculate the effective mass loss rate which is then used to predict the peak heat release rate of the fire based on the area of the couch burning and the effective heat of combustion described above as per Equation 3.7.

4.2 Overall Fire Behaviour

This section will start with an exploration of the results from three representative full-scale tests, one of each furniture type; NFR couch A (Test 5), FR couch B (Test 4) and LFR couch C (Test 6). Results for fires established on each furniture type will be presented to compare and contrast the resultant smoke development and movement throughout the space, in conjunction with CO and O_2 data and the development of the thermal environments, to provide insight into environmental characteristics of ventilation-limited multi-storey and multi-compartment furniture fires. Ancillary test results are compiled into Appendix A.

4.2.1 Overall Consumption of Fuel

A representative picture of a couch before and after a test is shown in Figures 4.2 below. Across all the furniture types tested, 14kg to 23kg of the 56 to 62kg initial mass of the couches was consumed in the fires. This included all of the combustible foam and fabric as well as relatively smaller portions of the wood frames, 3kg to 8kg of the initial 38kg to 42kg wood frame and spring mass. The wood frames charred but were left largely intact after each test. Table 3.1 in Chapter 3 contains details on the relative masses of each furniture item tested.

4.2.2 Chronology of Fire Events

Chronologies of the key fire events and picture timelines of these events for the representative tests of each furniture type are shown for NFR couch A in Table 4.2 and Figure 4.3, for FR couch B in Table 4.3, and Figure 4.4 and for LFR couch C in Table 4.4 and Figure

(a) Before Test (b) After Test

Figure 4.2: Representative Couch Before and After Test

4.5. These demonstrate certain similarities and differences in the progression of each of the furniture fires. The images are taken from video footage recorded by the camera facing the couch and positioned on the adjacent wall, labelled as V2 in the floor plan Figure 3.2 in the previous Chapter.

The alphabetical captions in the pictorial timelines correspond with the events presented in the same order as the corresponding chronologies. Captions a) - g) are for the following events respectively: 1st cushion fully involved (defined as the time when the full sitting cushion, back cushion and arm rest are all fully involved), the observed time when the smoke descends to the top of the window behind the couch, the time for the heat release rate to reach approximately 500kW (calculated by the mass loss rate method), the time for the fire to reach peak heat release rate (calculated by the mass loss rate method), the time when minimum oxygen concentrations are measured in the living (burn) room, the time when minimum oxygen concentrations are measured in the adjacent main floor SW compartment and the time when minimum oxygen concentrations are measured on the second floor. Some of the tests do not have corresponding images at a particular event due to the smoke obscuration over the camera. From the chronologies for the NFR couch A, Figure 4.3, FR couch B, Figure 4.4 and LFR couch C, Figure 4.5 tests, some key qualitative differences can be seen in fire development across the three representative couch fires. These link to the resulting thermal, chemical and physical trends seen in the evolution of the living (burn) room environment for these furniture fires as well. Couch A supported the most rapid fire growth, as seen in the time it took for the first cushion to be fully involved in the fire, as well as the time it took the fire to reach both 500kW and peak heat release rate. This is consistent with expectations, since this couch was made of NFR polyester fabric and foam, so was anticipated to have the fastest growth rate as well as the highest magnitude of peak heat release rate of the three furniture types. NFR couch A also produced significant amounts of smoke fairly quickly, as marked by the smoke layer

descending to the top of the window in the second fastest length of time.

1st cushion fully involved (a)	Smoke at top of window (b)	Approx. time to 500kW (c)	Peak HRR (d)	Minimum Oxygen in BR (e) 1F (f), 2F (g)
252s 345kW	285s 1080kW	265s	332s 3345kW	16% at 286s 5% at 346s 9% at 371s

Table 4.2: Chronology of Events for NFR Couch A

(a) (b) (c) (d) (e) (f)

Figure 4.3: Picture Timeline of Events for NFR Couch A

The FR couch B fire had the lowest overall peak heat release rate, again as was expected due to the FR materials used in the construction of the couch, however somewhat surprisingly, the time it took the first cushion to become fully involved, as well as the times to reach 500kW and peak heat release rate were the second fastest out of the three furniture types. In terms of smoke production, the time for the smoke to reach the top of the window in the living (burn) room was shortest for FR couch B. The high quantity of smoke production from this furniture is further demonstrated through the video traces. It was not possible to discern anything in the images from the living (burn) room camera at the time that the minimum oxygen concentrations were measured in the main floor SW compartment or on the second floor due to the amount smoke that filled the living (burn) room and completely obscured the camera. This is again consistent with the materials in the furniture, since they contained the highest amount of chlorine-bromine based FR additives and would be expected to produce more smoke since the presence of these specific FR additives generally leads to overall inefficient combustion of any available fuel.

Somewhat unexpectedly, the LFR couch C fire took the longest time to reach all the markers in the timeline and it had the second highest peak heat release rate, very close in magnitude to that for FR couch B. The fabric on the this couch was cotton and therefore charred instead of melting like the polyester fabric on couches NFR A and FR B. The surface char seemed to create a barrier between the vaporizing fuel surface and the more

1st cushion fully involved (a)	Smoke at top of window (b)	Approx. time to 500kW (c)	Peak HRR (d)	Minimum Oxygen in BR (e) 1F (f), 2F (g)
362s 450kW	233s 50kW	370s	443s 1557kW	9% at 436s 9% at 481 11% at 857s

Table 4.3: Chronology of Events for FR Couch B

(a) (b) (c) (d) (e)

Figure 4.4: Picture Timeline of Events for FR Couch B

1st cushion fully involved (a)	Smoke at top of window (b)	Approx. time to 500kW (c)	Peak HRR (d)	Minimum Oxygen in BR (e) 1F (f), 2F (g)
423s 180kW	563s 750kW	535s	659s 1660kW	3% at 612s 6% at 682s 12% at 722s

Table 4.4: Chronology of Events for LFR Couch C

(a) (b) (c) (d) (e) (f) (g)

Figure 4.5: Picture Timeline of Events for LFR Couch C

flammable foam underneath, delaying involvement of the foam in the fire and therefore slowing fire growth and smoke production. Given that the calculated heat of combustion for Couch C materials was much higher than the FR couch B materials, 16.5MJ/kg compared to the 12.0MJ/kg, the decrease in mass burning rate apparently as a result of the charring behaviour of the fabric layer was a governing factor in the rate of growth.

The role of the fabric in the burning behaviour of LFR couch C can also be seen in the different flame spread patterns observed for this couch in comparison to the other couches, evident in the last image, figure (g) in the picture timeline, Figure 4.5, for this couch. In this image, the fire is visibly burning lower on the first seat cushion compared to the middle. In general for the LFR couch C fires, once the fire was established on a cushion and the foam was involved, the fire drilled down through the cushion, burning down at a faster rate than it spread across the surface of the couch. This is a result of the cotton fabric delaying the surface spread. In contrast, in the progressions of both A and B couch fires, Figure 4.3 and Figure 4.4 respectively, it is seen that the fire spreads across the surface of the couch cushions as the polyester fabric melts and creates an accessible vaporizing fuel surface to quickly propagate the flame horizontally. Such differences clearly highlight the impact of the fabric covering materials used in furniture construction in either accelerating, or potentially delaying, the rate of fire growth.

To further understand the overall progression of the fire, time-resolved heat release rate curves for each of the different couch fires, tests 4, 5 and 6 (FR B, NFR A and LFR C), were generated using the mass loss rate method outlined in Section 3.2.1 and are plotted in Figure 4.6. Two heat release rate curves, from tests 3 and 6, are included for the LFR couch C, referred to as LFR Ci and LFR Cii respectively in the plot legend, to demonstrate the repeatability across all tests, as discussed in Senez et al. [137]. The differences in the rates of progression of the furniture fires discussed in the above section are clearly reflected in these curves.

In agreement with what was seen qualitatively in the chronologies and corresponding images above, it can be clearly seen from Figure 4.6 that NFR couch A takes the shortest time to reach peak heat release rate, followed by couch B and then LFR couches Ci and Cii. NFR couch A has the highest peak heat release rate of around 3300kW, followed by LFR couch C at around 1660kW and FR couch B at around 1550kW. Although couch B contained more FR additives than couch C, the heat release rate for couch B grew much more quickly and reached a peak value in less time relative to LFR couch C again supporting possible melting of the polyester fabric and fairly rapid surface flame spread with consequent faster involvement of the underlying foam in the couch B fire. It is also interesting to note that both couches NFR A and FR B have similar shapes in their heat release rate curves. After a peak heat release rate is reached, there is a shoulder as the heat release rate starts to decrease, followed by secondary peaks at around 400s and 700s after ignition for NFR couch A and secondary peaks around 500s, and subsequently at 650s and 800s, after ignition for FR couch B. The reason for these secondary peaks will be further explored in Section 4.4.1.

All in all, the timelines and representative heat release rate curves presented in this

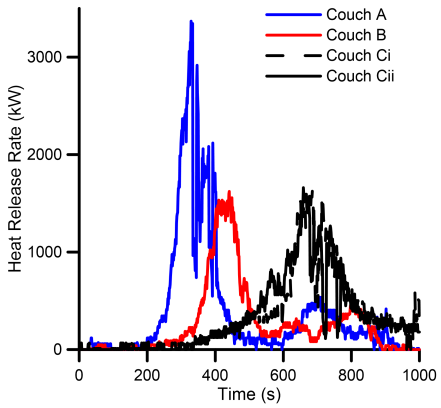

Figure 4.6: Representative Heat Release Rate Curves, borrowed with permission from [2]

section demonstrate some key differences in the growth and development of the furniture fires, which was also found to be reflected in other aspects of the fire geometry and the progression of the environment, as discussed in the next sections.

4.3 Fire Geometry

Presented in this section, in a time-resolved fashion, are measured values of fire width and height as output from the image analysis program, as well as calculated values of effective fuel bed diameter, determined by the methods explained in Section 3.3.2. For clarity, measured values of flame height, flame width and effective diameter of the fire were smoothed with a 10-point moving average before they were plotted against time. Time varying values of estimated flame height, calculated using Heskestad's flame height correlation (recall Equation 3.3) [31], are also provided for each of the three couch fires discussed in the previous Section. The sizes of all three fires fall within the range between $7 < \frac{\dot{Q}^{\frac{2}{5}}}{D} < 700\frac{kW^{\frac{2}{5}}}{m}$ reported as valid for use of this correlation; at the time of peak heat release rate for NFR couch A, the heat release rate is 3345kW and fire diameter is D=1.28m, for FR couch B these are 1557kW and D=0.76m and for LFR couch C, 1660kW and D=1.34m. In all cases, the fires fell towards the low end of the range of validity for the correlation with values of $\frac{\dot{Q}^{\frac{2}{5}}}{D}$ of $20kW^{\frac{2}{5}}/m$, $25kW^{\frac{2}{5}}/m$, $15kW^{\frac{2}{5}}/m$ respectively.

As seen in the images contained in the above Section, the furniture fires burn in a manner that results in complex areas of fuel being involved in the fire during various stages of growth. This is in part, due to the perpendicular positioning of the front and back

cushions and arm rests relative to one another, as well as the specific material combinations in each couch. To start the discussion, the measured widths of the fire as determined using the image analysis program are plotted against time and overlaid with the corresponding calculated values of effective fire diameter. For reference, vertical solid and dashed lines have been added to the plots to represent, respectively, the times at which the first cushion was fully involved, (a) in the chronologies above, and the time when peak heat release rate was reached (labelled as PHRR) and corresponding to time (d) in the chronologies above.

In all cases, measured values of fire width and calculated effective fire diameter follow the expected trends; as the heat release rate increased, the physical size of the fire increased in terms of fire width and area (effective diameter). This is most clearly seen in the measured widths for the couch C fire which mirrored the heat release rate curve above. The fire width initially remained fairly static[1] and then started to increase significantly towards a peak measured width at 400s after ignition, which corresponded to when the heat release rate also started to increase significantly towards peak values for this fire.

After the first cushion was fully involved in both the NFR A and LFR C fires, there was a general upward trend in the width of the fire, as it spread across the couch further and grew towards peak heat release rate. However, in the FR couch B fire, measured values of fire width plateau for a period of time then appear to steeply dip before growing again towards peak values. As highlighted in the FR couch B chronology above, however, these are not 'real' effects but can instead be attributed to the significant smoke production during this fire. As peak heat release rate was reached, the full width of the fire was likely not seen by the video camera since it was most probably obscured by smoke. Nonetheless, where the measurements are valid, it is interesting to note differences in the measured width and effective diameter between NFR couch A and FR couch B as well. The slope of the plot for measured width versus time is initially much steeper in the case of the NFR A fire. Consistent with video observations, one possible cause is that, as a result of the FR additives, the fire on FR couch B took longer to establish and when it did spread, it did not spread horizontally nearly as quickly as for the NFR couch A fire.

In reality, at some time after ignition fires on each of the three representative couches burned across the total 1.64m width of the seating area of the couch taken corner to corner along the horizontal surface of sitting cushions. In comparison, the maximum measured flame widths discernible by the image processing program are smaller than this. When analyzed on a frame by frame basis, the maximum fire widths measured horizontally across

[1]Until roughly 335s seconds after ignition, there were flame wisps in the charring regions on the back and seat cushions in the couch C fire located away from the main flaming body. These led to erroneous identification of the presence of a large fire in the very early stages as is reflected in the figure.

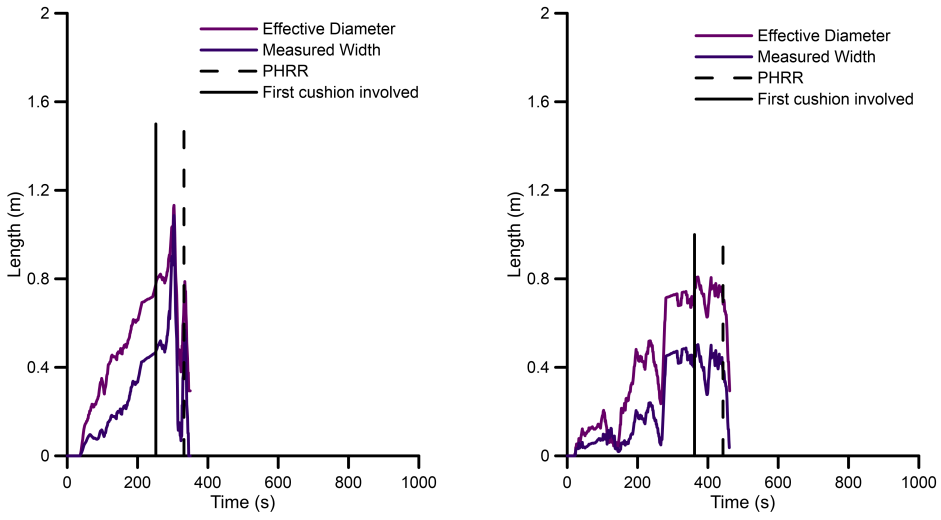

(a) NFR Couch A

(b) FR Couch B

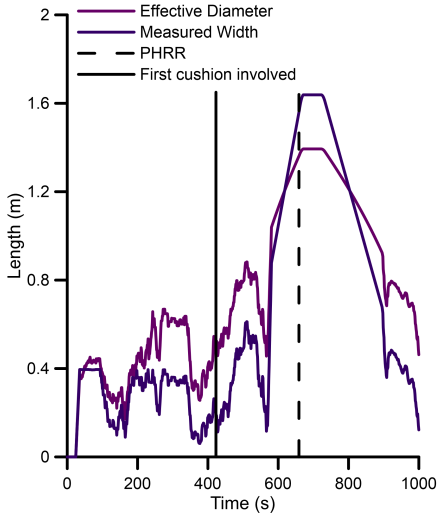

(c) LFR Couch C

Figure 4.7: Measured Flame Widths and Calculated Effective Diameters

the surface of the sitting cushions in the images, were 1.4m, 0.6m and 1.6m for fires on couches NFR A, FR B and LFR C respectively[2]. As demonstrated in the above pictorial timelines for NFR couch A and FR couch B, the true width of the visible flaming fire plume

[2]These maxima are not evident in the figures due to the ten point averaging adopted to clarify overall trends in the time resolved figures.

could not be followed because of the dynamics of fire behaviour and consequent smoke obscuration of the video images as the fire grew in size. Clearly, the above measured values do not reflect the true maximum width of those fires. For LFR couch C on the other hand, it can be seen in the chronology that the descent of the smoke layer did not impact visibility in the living (burn) room before the fire spread across the full width of the couch, so the largest measured width for couch C should be consistent with all three sitting cushions being involved in the fire. The discrepancy between the actual couch width of 1.64m and the measured maximum width, 1.6m, in this case can be attributed to parallax in the image as well as errors introduced by not having sufficient information to incorporate corrections for the camera field of view during analysis.

An alternate measure of fire width was determined by calculating an effective diameter of the fires based on modeling the area of fuel burning as a circular area of equal size to the actual surface area of couch materials engaged in the fire at any given time. The estimated values of effective diameter were calculated at times corresponding to those for the widths discussed above using the image processing program. The respective maximum values of calculated fire area and effective diameter were $1.4m^2$ and 1.3m; $0.6m^2$ and 0.8m; and $1.5m^2$ and 1.4m for the fires on couches NFR A, FR B and LFR C. Values of fire area calculated in this fashion are larger than those that would be determined by simply taking the product of width of the flame as measured by the image analysis program by the depth of the seating cushion on the couch, since these estimates take into account any flame progression onto the back and arms of the couch as well. While values for NFR couch A and FR couch B still do not reflect the fire spread across the full width of couch, the calculated fuel bed area and effective diameter for the fire on the LFR couch C are consistent since the fire has spread across the full length of the couch with little impact of the smoke layer on the visibility of the fire in the videos.

Time-resolved curves of flame height as measured by the image processing program are presented as bright green lines in the Figures 4.8a, 4.8b and 4.8c and shown with representative images at times when measured and correlated values for flame height began to systematically diverge, for the fires established on couches NFR A, FR B and LFR C respectively. Vertical lines are included to indicate major fire events: the first cushion fully involved (solid) and the smoke layer at the top of the window (short dashed), labelled as (a) and (b) in the chronologies above. As a check on the applicability of the flame height measurements in a broader engineering context, it was of interest to investigate use of an existing correlation to estimate the flame height with time. For this it was decided to use Heskestad's correlation for open burning pool fires previously presented as Equation 3.3 [31] because for certain periods of time, the visual appearance of the fire plumes on the couch cushions resembled those that develop over liquid pool and wood crib fires.

Therefore, plotted in Figures 4.8a, 4.8b and 4.8c are time- varying estimates of effective flame height determined with the correlation using the total heat release rate of the fire calculated using the mass loss rate method (product of the mass loss rate and heat of combustion). Two different inputs were tried for the value of fire diameter. As a simplified preliminary case, the measured widths from the image processing program were employed. Resulting values are plotted as the dark green curve labelled as 'original flame height' in the figures. In the second case, values of effective fire diameter derived from the fire area estimations were used as input. These estimates are plotted as the lighter green curve labelled as 'adjusted flame height' in the figures. Also included in the figures are vertical black lines with corresponding images which represent the time at which the Heskestad correlation ceases to predict accurate flame heights and diverts from the measured values output by the image processing program [3] to demonstrate limitations in the use of this correlation in this fire context.

Overall trends in the values of measured flame height from the image analysis program track well with fire heat release rate throughout the early stages of fire growth, when the smoke layer has not yet developed, the fire is centered on the 1st cushion and the heat release rate is under 1MW. Examination of Figure 4.8c for the LFR C fires, points to some notable exceptions however. In this fire, the values of flame height measured by the image processing program in the very early stages of the fire are high relative to the flame heights actually observed and subsequently appear low as fire reaches its peak value of heat release rate even though there is little smoke obscuration in these fires. These are artifacts of the image processing program brought about by the nature of fire development on this couch. Very early in the fire, the fire was characterized by formation of small but visible flamelets on the surface of the char layer that formed on the back cushion of the couch well above the main flaming zone as it established itself on the sitting cushion. The different areas of 'flame' could not be distinguished by the image analysis software, leading to significant over estimates of flame height at these times. The low measured flame heights in the later stages of the fire are consistent with what would be expected around the time of peak heat release rate for this fire because the smoke layer was thick and descended down over top of the fire plume. Due to smoke obscuration of the flaming regions of the fire in the camera images, the image analysis program could not resolve the true flame height under these conditions. Thus, the times at which maximum values of flame height were measured by the image analysis program did not correspond with the time of peak heat release rate but instead occurred when the smoke layer in the compartment was less dense. Consideration of the interactions between the flaming fire plume and the smoke layer are

[3] Similar to the widths discussed above, these measured flame heights have been smoothed with the ten point moving average, so instantaneous values of maximum measured height are not necessarily represented.

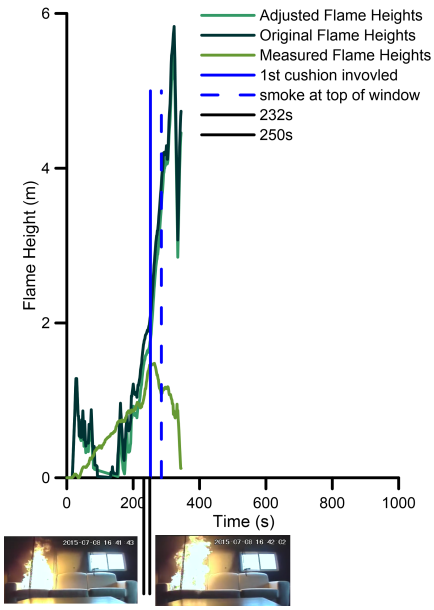

(a) NFR Couch A

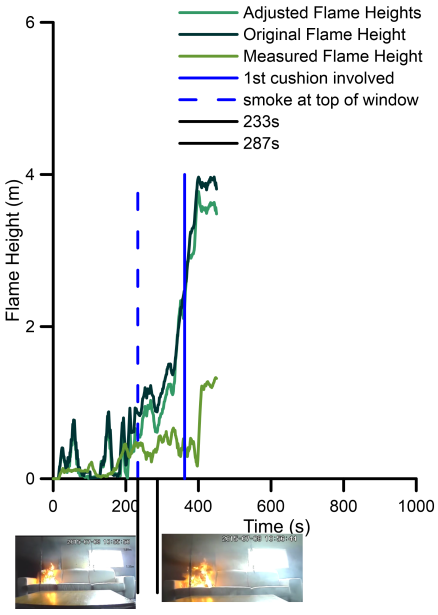

(b) FR Couch B

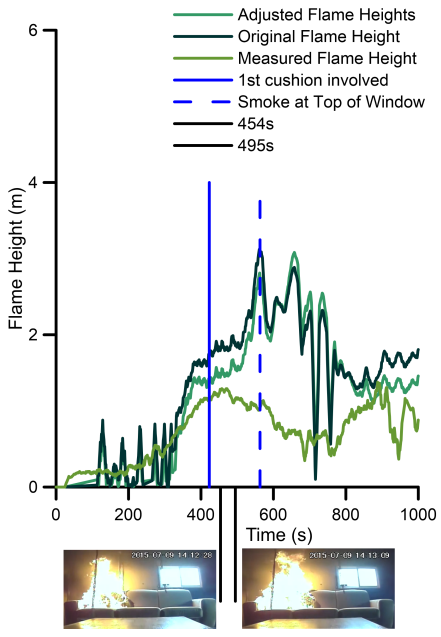

(c) LFR Couch C

Figure 4.8: Calculated and Measured Flame Heights

extremely important when resolving flame heights within a compartment fire and relating these to fire development, as the maximum visible or 'measure-able' flame height does not necessarily correspond with, or provide a good indicator of the peak heat release rate of the fire.

Maximum measured flame heights as determined using the image processing program were 1.6m at 266s, 1.4m at 455s and 1.7m at 462s for couches NFR A, FR B and LFR C respectively. These occur at approximately the same time as the maximum measured fire width (430s) and peak heat release rate (440s) for the fire on FR couch B, but occur markedly before the times when the fires on NFR couch A and LFR couch C reach peak width (312s and 660s respectively) and peak heat release rate (330s and 660s respectively). In all cases, these flame heights appear to be consistent with direct visual measurement of the height from a computer screen for the same images. The ignition location on the sitting cushion was positioned roughly 1m above the floor and the floor to ceiling height of the living (burn) room is 2.35m, with the thickness of the cushion another 0.15m, leaving 1.5m of clear vertical flame height in the compartment. At the same time, the image processing program could not resolve any flames that were under the table. Considering these two factors then, maximum flame heights output by the image processing program may be in error by 0.1 to 0.2m (approximately 10-15%) due to parallax created by the field of view and angle of the camera relative to the couch. It is anticipated that this uncertainty will be lower during the period in which the fire was growing in height since the parallax error will be maximum at distances furthest from the centre-line of the camera lens.

As eluded to above, values of flame height taken from camera images do not include several key three-dimensional, physical phenomena that take place during the fires. Detailed visual examination of the video footage indicates that in reality the flames grew to impinge on, and spread across, the ceiling during the fire, a phenomenon which could not easily be discerned in the planar images from the camera. Added to this, combustion of the foam resulted in downward flame spread through the thickness of the sitting cushion which again could not always be fully be resolved through analysis of images taken with the current camera arrangement. Finally, the polyurethane couch cushions also melted as they burned and the 'burn-through' resulted in 'puddles' of melted foam that fell under the furniture item and burned as additional pool fires underneath the couch. Upon examination of the side-view camera for the couch fires, V1 in Figure 3.2, this burn-through is seen for each representative test included here. An example is shown in Figure 4.9. In all tests, the melted foam landed on top of the load cell, and as a result, contributed to the mass loss rate measured by the weigh scales so, while not accounted for in consideration of fire geometry, is included in the calculated heat release rate for the fire. Again, the extent of this phenomena was not captured by the current image processing program, nor was it

recorded sufficiently in the present tests to determine its effect on the overall geometric characteristics of the fire.

Figure 4.9: Burn-Through

Taken together, the above information does provide evidence that maximum flame heights within a range of roughly 1.4m-1.7m may be appropriate for these fires. Despite any uncertainties in the current image processing tool, these flame heights were close to those measured with video processing tools for similar fires on couches as reported in other work [134, 136].

In all cases, estimated values of effective flame height calculated using Heskestad's correlation follow the trends in fire heat release rate with time, progressing toward their maximum values as peak heat release rate is reached. This is anticipated since generally the input value of heat release rate is weighted more heavily than fire diameter in this correlation. Clear differences were seen between estimates determined using the two input values for fire diameter. In the first instance the total heat release rate of the fire calculated using the mass loss rate method was used with the measured fire width directly output from the image analysis program. This assumed that the only fuel contributing to the 'pool' fire was the sitting cushion of a couch. Use of these inputs resulted in the values plotted as the dark green curves labelled as 'original flame height' in Figures 4.8. As can be seen in the figure, the calculated values of flame height appeared to follow measured values reasonably well for a period of time after ignition but then began to increasingly overestimate the flame height for all three couches as the fire progressed further. Images of the flames taken for each of the fires at the corresponding times are included in the figures

and are discussed further below. As might be anticipated, values of peak flame height were not well predicted for any of the fires. This is in part due to previously discussed limitations in values of measured fire width and height due to camera placement, image processing and difficulty in resolving representative values of these parameters as smoke built in the compartment. More importantly though, as the fire grows toward its maximum height, it will be affected both by the ceiling clearance and the fact that, in these limited ventilation fires, the oxygen levels are decreasing, reaching 5-9% measured 0.6m above the floor or approximately the height of the base of the fire. These conditions are clearly not representative of the open-burning fire scenario for which this flame height correlation was originally derived.

Despite the limitations, it is still of engineering interest to determine if the correlation is able to provide estimates of the time dependent values of fire geometry before the fires impinges on the ceiling or becomes significantly affected by availability of air. Based on analysis of a subset of images taken from other camera views, it was observed that there were discrepancies in assuming that the fire widths, as output by the image processing program, were truly reflective of the actual area of fuel involved in the fire, even in the fairly early stages of the fire. This suggested that more refined inputs for fire diameter should be used in the flame height correlation to account for the more complex burning patterns of the furniture fires under study. As such, the diameter input to the correlation was changed to the effective diameter calculated as described above. Adjusted values are plotted as as the lighter green curve labelled as 'adjusted flame height' in Figures 4.8. Use of this adjustment resulted in better prediction of flame heights, though in general the values of height still became considerably over-predicted at a fairly early stage of fire development. Even with this correction, the correlations cannot account for the fact that the growth of these fires is significantly affected by combined impacts of the complex fuel geometry, presence of the ceiling, restrictions on availability and entrainment of air and, as the fire grows, also by the descending smoke layer in the room, all interactions which were not included in development of the correlation. While there is promise that the correlation could still be useful in the early stages of the fires, these issues confirm the extreme caution that should be used in applying such correlations for even preliminary estimations of fire height in situations with complex fuel geometry and fire environments like those in the present furniture fires.

In order to answer the question of how long an open burning correlation might apply in the present furniture fires, the adjusted values of flame height were examined in further detail. In all cases, values track well with measured values of flame height when the smoke layer has not yet developed (and thus when both measured and estimated values of flame height are most accurate) and the fire is centered on the 1st sitting cushion of a couch.

Times at which the correlation is suspected to start breaking down are indicated for each test by the black vertical lines on Figures 4.8 and supplemented with images below the x-axis. For the NFR couch A fire, Heskestad's correlation ceases to predict accurate effective flame heights between 232s, which is when the smoke is at the height of the top of window and the fire heat release rate is around 238kW and 250s when the fire has grown to 345kW for NFR couch A. For the FR couch B fire this point occurs at a time between 233s and 287s when the fire heat release rate is only 48kW and the fire is not growing. For the LFR couch C fire, which does not produce nearly as much smoke as the other two fires, the correlation seems to hold until the fire heat release rate reaches similar values to those for the NFR couch A fires, times between 454s after ignition, when the fire heat release rate is 258kW and 495s when the fire has grown to 381kW.

In the NFR couch A fire, measured flame heights and adjusted effective flame heights at the times that the correlation appears to break down are between roughly 1.16m and 1.24, and 1.38m and 1.7m respectively. After this, the adjusted effective flame height increases very quickly to a value of 3.25m at the time when the smoke hits the top of the window and the measured HRR is 1297kW. Instantaneous values of measured flame height do increase to the full ceiling height of 1.5m when the measured fire HRR grows to 750kW before decreasing again to roughly 1.3m as the smoke layer descends over the top of the plume and obscures the camera. These combined observations suggest that at least to this point in in growth the fire is still increasing in height in a fashion similar to that predicted using an open-burning flame height correlation such as the one chosen here.

In the FR couch B fire, adjusted effective flame heights are significantly lower, 0.32m and 0.35m than original effective flame heights, 0.6m and 0.73m, during the time when the correlation appears to break down. The adjusted values are also much closer to measured flame heights output from the image processing program. After this time, however, measured flame heights remain approximately constant until significantly later in the fire. In contrast, although the adjusted effective flame height remains notably lower than the original effective flame height, it increases to a value of roughly 3m at 398s when the fire has grown to around 1216kW. For comparison, measured flame heights are only about 0.5m when the fire is 1MW in size on account of the soot laden smoke produced by the fire. This is evident also in the relatively lower pixel saturation (flames appearing more orange-yellow, than white) of images from these flames, often indicative of more incomplete combustion and lower flame temperatures often connected with FR materials.

Lastly, in the LFR couch C fire measured flame heights and adjusted effective flame heights are similar with values of 1.24m and 1.36m and 1.23m and 1.71m respectively at the times when the correlation begins to break down, after which the adjusted effective flame height values increase to over 2m and finally 2.7m at 646s after ignition (roughly

100s after the smoke hits the top of the window) when fire heat release rate is 1223kW. At this stage in the fire, again due to the presence of smoke in the images, measured flame heights decrease to below 1m for a period of time.

It appears from analysis of the earlier stages in all of these fires, that the values of flame height estimated using this correlation deviate from measured values of flame height for several reasons. The first relates to the nature of smoke layer descent in the various fires. The fires have generally grown to ceiling height when the smoke layer starts to descend to the top of the window causing the smoke layer to interacts with the fire plume while also obscuring the view of the full fire height in the image. This effect is particularly seen for the case of the FR couch B fire. As well, and notable in the LFR couch A fire, when the fire starts to spread horizontally across the couch, it transitions from square to rectangular in shape, and significant material on the back of the couch is burning, making estimation of an effective area, and hence representative diameter, of the fire plume very difficult to estimate. Added to the physical effects occurring in the fire compartment, there are inherent inaccuracies in the measured flame heights as a result of the image processing program and fixed camera position. These are especially evident in the later stages of the fire, making direct comparison of measured flame height and effective flame height difficult. Considering the compartment, fuel source, changing flame spread mechanisms and overall dynamic fire environment, however, it can be concluded that the Heskestad flame height correlation could be appropriately applied up to a certain point in fire development, namely, when the fuel bed and environment most closely resemble the open burning configuration by which this correlation was originally derived. Further to this point as well, care should be taken to account for the full area of fuel involved in the fire as it progresses over time.

A final consideration is explored in the case of the NFR couch A and LFR couch C fires in which the high measured values of peak heat release rate result in calculated values of adjusted effective flame height which quickly become significantly higher than any flame height measured from the video images of the fire even accounting for material that melts, drops and burns on the load cell platform. Given the dimensions of the compartment, however, it should also be noted that the estimates of adjusted effective flame height have reached values that suggest the onset of flame extension along the ceiling near the time that estimated and measured values of flame height begin to deviate. An image taken during the NFR A couch A fire at 46 seconds before peak heat release rate (263s after ignition) and shown in 4.10 illustrates that these apparently high effective adjusted values of flame height may not be entirely in error since there is clearly impingement and flame extension along the ceiling. While outside the scope of the present work, this might suggest that existing flame height correlations could be used for prediction of flame geometry for longer times into fire development, for example if the correlation used here was combined

with use of a correction factor or additional correlation which could account for ceiling spread as well. Further experiments and improved analysis would be required, however, to determine whether such an approach was appropriate.

Figure 4.10: Ceiling Interference with Fire Plume

Even if use of existing correlations could be extended to later times after ignition, new methods by which to holistically estimate the geometrical characteristics of fire plumes such as these should also be developed. These should account for the significant impacts of the descending smoke layer on overall fire development, as well as the important interactions taking place in the fire environment as it transitions from well ventilated to ventilation limited conditions.

Now that a foundation has been established in terms of the overall fire behaviour shown through pictorial fire timelines, chronologies and fire geometry, the next Section of this Chapter delves into more specifics of the gaseous and thermal environments developed in the living (burn) room during the three representative furniture fires.

4.4 Characteristics of the Environment

This section will start with a discussion of the concentrations of oxygen and carbon monoxide measured in specific locations within the burn structure. This will then lead into dis-

cussion of the thermal development of the environment in various parts of the structure, presented in terms of time-resolved temperature curves from the thermocouple rakes positioned in the different compartments, as well as a measurements from the heat flux gauge in the living (burn) room. This is followed with an examination of smoke movement and transport between storeys through use of time-resolved velocity curves and velocity profiles at the staircase. This section aims to build a foundation of understanding of the specific conditions and complex interactions that these ventilation-limited fires create to demonstrate the various difficulties encountered when determining a heat release rate of the fires, before moving on to a comparison of the different heat release rate calculation methods presented in the final part of the Chapter.

4.4.1 Gaseous Environment and Heat Release Rate

Measured oxygen concentrations are plotted with heat release rate (as calculated by the mass loss rate method) as functions of time in Figures 4.11a for the fire on NFR couch A, 4.11b for FR couch B and 4.11c for LFR couch C (heat release rate curves from tests 3 and 6 for Ci and Cii respectively, recall gas data from test 3). Gas sensors were located 0.6m above the floor near the staircase in the living (burn) room, 0.6m above the floor and in the center of the main floor SW room, and 0.6m above the floor in the middle of the second floor SW room. It should be remembered that these are local measurements taken at a single measuring location, so are not likely to be entirely indicative of concentrations at all locations within any given space. In all cases, oxygen levels measured throughout the structure depleted to minimum values of between 3% and 12%, however, so the global environment progressed to ventilation-limited during each of the fires. Interestingly, oxygen levels in the living (burn) room for the LFR couch C fire decreased to the lowest values of 3% vol, which is significantly lower than those measured for FR couch B at 9% vol oxygen in the living (burn) room. The apparently higher levels in the living (burn) room for couch A are discussed below. Minimum oxygen concentrations measured in the main floor SW compartment are similar at around 5% vol during the NFR couch A and LFR couch C fires, while they are again slightly higher at 9% vol for couch B. The NFR couch A fire led to the lowest oxygen concentration measured on the second floor at about 9%, followed by the FR couch B fire at about 10% and LFR couch C fire at 12%.

In the NFR couch A fire, the window behind the couch broke at about 314s seconds into the test due to heat from the fire and hot smoke descending in the living (burn) room compartment. This resulted in an influx of oxygen into the burn room, which is the suspected reason why the oxygen there did not decrease below 10% vol like it did in all of the other tests. It is interesting however, that regardless of the window breakage, oxygen

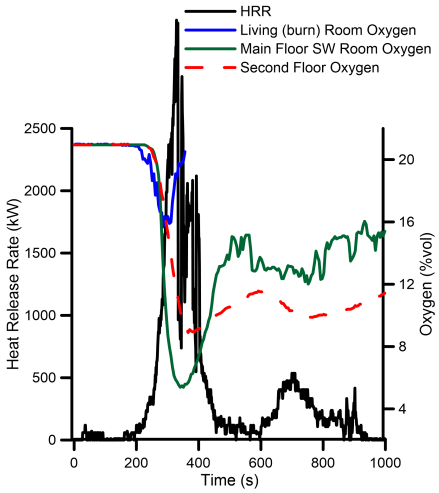

(a) O_2 and HRR, NFR Couch A

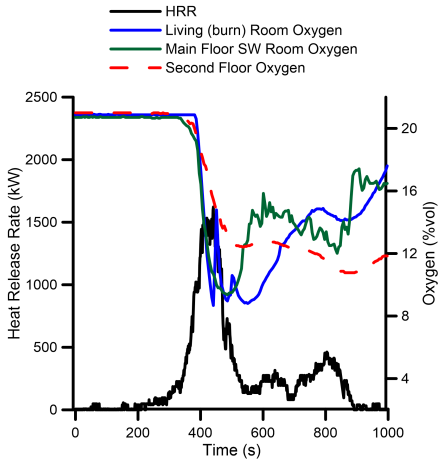

(b) O_2 and HRR, FR Couch B

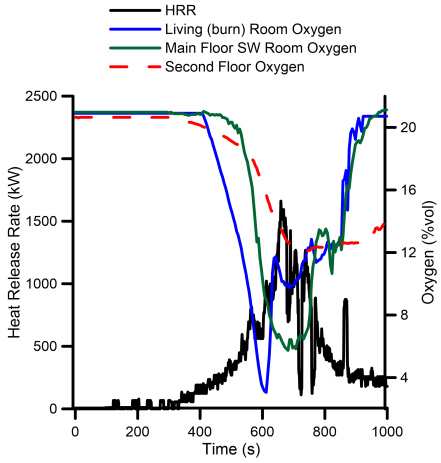

(c) O_2 and HRR, LFR Couch C

Figure 4.11: Oxygen Levels Throughout Structure For Representative Furniture Tests, borrowed by permission from [2]

in the rest of the structure during this test decreased below 10% indicating that there was still not enough fresh ambient air entering the house through the window to make a large impact on the environment outside of the living (burn) room, and the fire still progressed to a ventilation-limited mode of burning and self-extinguished as the fabric and foam on the couch were consumed.

As seen in the chronologies provided in the Section above, there are differences in the time after ignition at which minimum values of oxygen concentration are reached in the various parts of the structure for each test. This is further detailed in the Figures 4.11a, 4.11b, and 4.11c for the fires on each furniture type. Generally, there appears to be a sequence in which oxygen becomes depleted in the various parts of the structure. First, and perhaps as expected, the oxygen in living (burn) room is depleted. This is followed by oxygen in the main floor SW compartment and then the second floor compartment. This trend is most clearly seen in Figure 4.11c for the case of the LFR couch C fire. As the heat release rate starts to increase, oxygen within the living (burn) room is readily consumed, and the fire has to pull oxygen from the next readily available space, which is the main floor SW compartment. Depending on the rate of increase of heat release rate, the fire may draw from both the living (burn) room and the main floor SW compartment almost simultaneously, as suggested by Figures 4.11a and 4.11b for the other two fires. Once a large portion of the oxygen is consumed in the main floor compartments, it appears that oxygen is then pulled from the second floor. The three delays in oxygen consumption in the different areas of the structure are not as obvious in the curves for couch NFR A and FR B fires, but the sequence is consistent as highlighted also in the times to minimum oxygen recorded in the chronologies above. In the case of the NFR couch A and FR couch B fires, the secondary peaks in the heat release rate previously described, and seen in the Figures above (400s and 700s for NFR A, 500s, 650s and 800s for FR B) appear to correspond to times that oxygen concentrations on the second floor decrease, providing further evidence that the fire pulls oxygen from different areas of the structure to support burning as oxygen is depleted from the readily available compartments on the main floor. The fresh air from the second floor that is used in the combustion process may be 'contaminated' as it mixed with smoke in the staircase. This could be a contributing factor as to why the peaks occurring soon after peak heat release rate were not as high as those from the initial burning period. The oxygen and smoke movement through the structure and the mixing processes that ensued, are explained in more detail in Section 4.4.4.

The differing burning characteristics of the fire established on LFR couch C are again reflected in Figure 4.11c. The oxygen at the living (burn) room measurement point is depleted about 100s before the peak HRR of the fire is reached, unlike the other couch fires, in which the peak heat release rate corresponds more closely with time for minimum

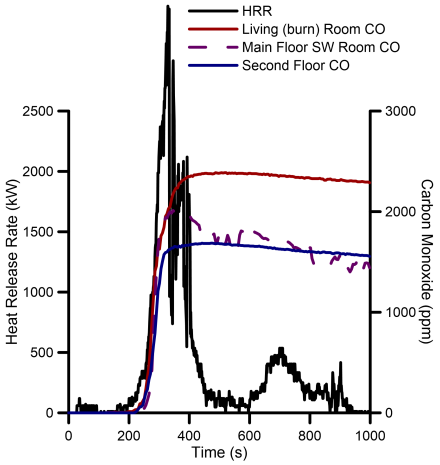

(a) Carbon Monoxide Levels and HRR, NFR Couch A

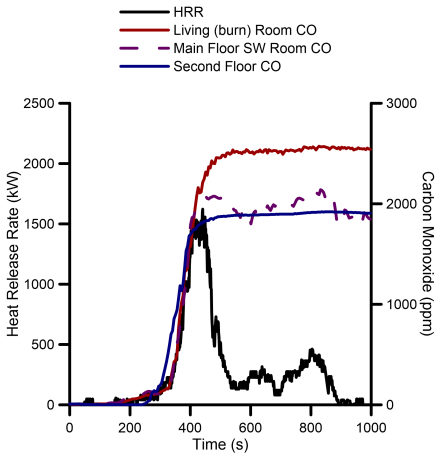

(b) Carbon Monoxide Levels and HRR, FR Couch B

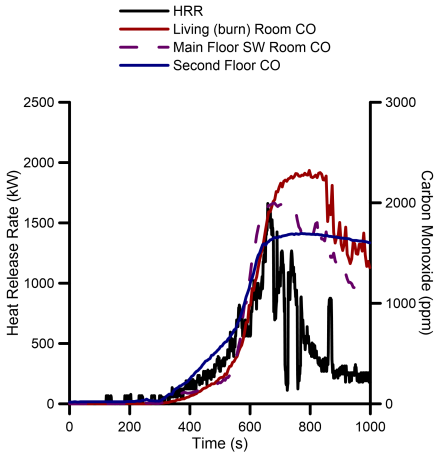

(c) Carbon Monoxide Levels and HRR, LFR Couch C

Figure 4.12: Carbon Monoxide Levels Throughout Structure For Representative Furniture Tests, borrowed by permission from [2]

oxygen concentration to be registered in the main floor SW compartment. In contrast, fires on couches NFR A and FR B both show late secondary peaks in heat release rate which are clearly mirrored in secondary decreases in oxygen levels measured on the second floor, demonstrating again the relationship between pulling oxygen from other areas of the structure to support burning during the later stages of the fire development.

Time-dependent plots of carbon monoxide concentration and heat release rate (mass loss rate method) at various locations throughout the structure are shown in Figures 4.12a, 4.12b and 4.12c for the fires involving couches NFR A, FR B and LFR C respectively. As expected, the trends in carbon monoxide production follow the increasing trends in rate of heat release, and inversely follow those for oxygen concentration. As heat release rate increases towards peak, the carbon monoxide measured in all three areas of the structure increases as well. The carbon monoxide concentrations measured in the living (burn) room are consistently the highest, with peak measured levels around 2300ppm, 2500ppm and 2400ppm for fire fuelled by couches NFR A, FR B and LFR C respectively [4]. Measured carbon monoxide concentrations in the main floor SW compartment are the second highest, again reaching roughly 2000ppm in all tests. Finally, peak CO concentrations measured on the second floor were around 1600ppm for the fires on couches NFR A and LFR C, and closer to 1900ppm for the FR couch B fire. This is consistent with expectations that the fire on FR couch B would lead to the highest concentrations of measured CO throughout the structure as a result of the fire-retardant additives. It is also interesting to note the steeper slope of the CO concentration curves relative to the heat release rate curves in the FR couch B fires, indicating that combustion of this couch produced larger quantities of CO, consistent with the notion that oxygen was not being consumed at as fast a rate as in fires where there was more complete oxidation to CO_2.

With the overall fire development of the couches and the gaseous environments explored, the next step in characterization of the compartment fire environment is an examination of the thermal environment in terms of temperature distributions throughout different areas of the structure and radiative contributions from the fire and smoke layer to heat flux in the living (burn) room compartment.

[4]It should be noted here that the CO sensors saturated at values of concentration at or slightly above 2000ppm, so reported values of 2000ppm and above should be interpreted as indicative of CO concentrations of at least that value

4.4.2 Thermal Development

Measurements of temperature over time after crib ignition for the three representative tests (tests 4/FR B, 5/NFR A and 6/LFR C) in all areas of the structure are provided in Figures 4.13 through 4.18 respectively with thermal stratification profiles in 4.19. The distances included in the legends on each plot in Figures 4.13 through 4.18 correspond to the heights of the thermocouples above the floor. Temperatures on the main floor and second floor for NFR couch A fires are shown by Figures 4.13 and 4.14; for FR couch B fires by Figures 4.15 and 4.16; and for LFR couch C fires by 4.17 and 4.18. As anticipated, the highest measured temperatures were recorded in areas closest to the fire, including at the living (burn) room centre, the corridor side of the living (burn) room, the living (burn) room SW corner and the bottom of the staircase, locations represented by T2, T3, T4 and T9 in the building schematic 3.2 shown in the previous Chapter. For all of the furniture fires, the thermal environment stratified in the areas closest to the fire, whereas less stratification and/or higher degrees of mixing were evident through the more uniform temperature distributions measured in areas that were further away from the fire compartment. This included the the SW compartment on the main floor, the top of the stairs and the second floor compartments.

Also as expected, trends in the plots of temperature versus time follow those seen in the representative heat release rate curves presented in Figure 4.6 in Section 4.2.2. The fire on NFR couch A resulted in the highest temperatures measured globally, followed by that on FR couch B then on LFR couch C. Interestingly, because the magnitudes of the heat release rate were fairly close for the fires on couches FR B and LFR C, it might be expected that the measured temperatures would also be very similar, especially in the living (burn) room, but with temperatures in the LFR couch C fire perhaps being slightly higher than in that on FR couch B. However, peak temperatures measured in the upper layer during the LFR couch C fire were about 300K lower than those measured in the upper layer during the FR couch B fire. Additionally for the fire on LFR couch C, temperatures of around 800K were measured closest to the ceiling throughout the living (burn) room area, in contrast to the relatively lower temperatures measured in some areas in other fire tests. The more uniform ceiling temperature distribution throughout the living (burn) room in this fire suggests that the slower fire growth allowed for increased distribution and mixing of the hot gases across all of the upper regions of the compartment. The temperature distributions in the living (burn) room during the NFR couch A and FR couch B fires, which were faster growing fires, were instead characterized by a zone of hot gases very close to the fire, but much larger decreases in temperature measured at relatively short distances away. For example, in the NFR couch A fire, a temperature of 1200K was measured in the

upper layer in the center of the burn room (effectively right in front of the fire), with a peak temperature of only 1000K recorded a very short distance away on the corridor side of the burn room. Similar differences in upper layer temperature at these two positions are also seen in the FR couch B fire, if not a bit more marked, with about 1100K measured in the center of the burn room and only 800K on the corridor side.

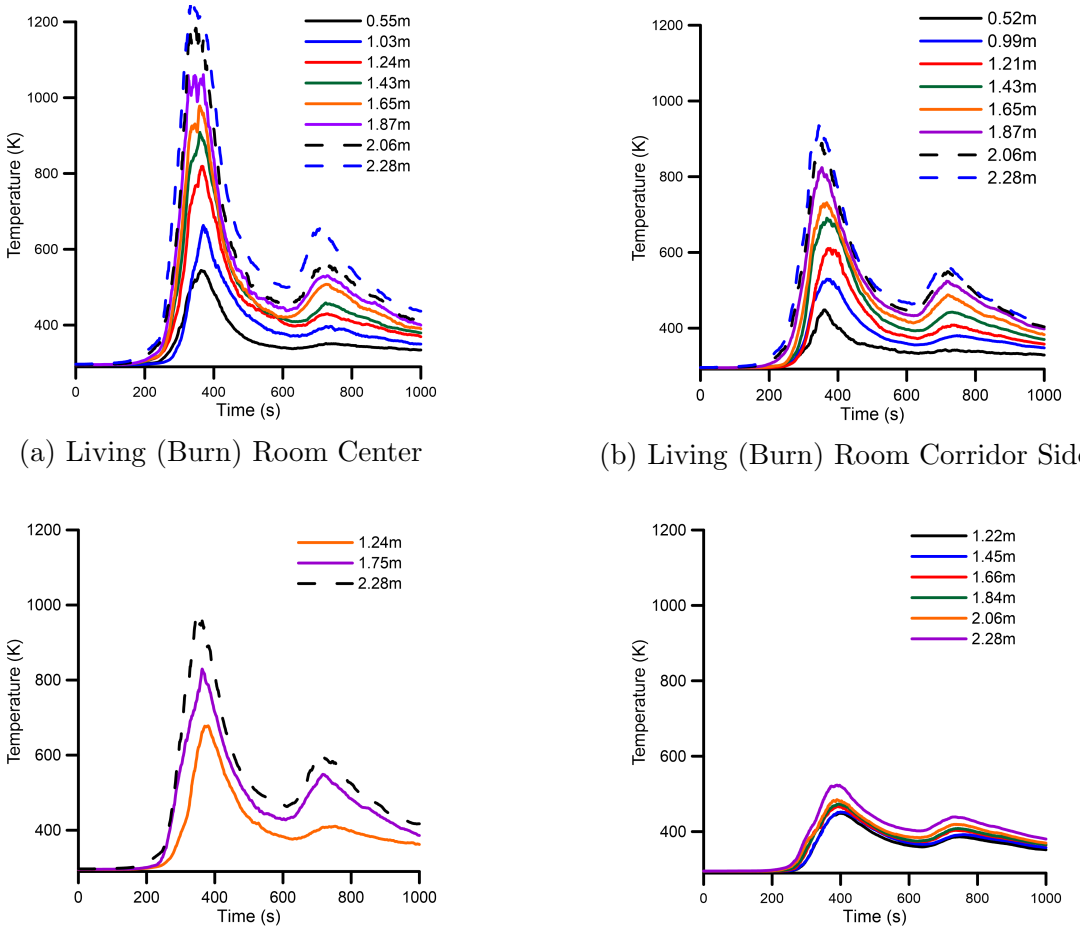

(a) Living (Burn) Room Center

(b) Living (Burn) Room Corridor Side

(c) Living (Burn) Room SW Corner

(d) Main Floor SW Room

Figure 4.13: NFR Couch A Main Floor Temperatures

Figures 4.13a, 4.13b, 4.13c and 4.14a demonstrate the thermal stratification present during the NFR couch A fire test in the living (burn) room center, living (burn) room corridor side, living (burn) room SW corner and at the bottom of the stairs, respectively. Similar profiles were recorded in the same regions for the FR couch B and LFR couch C

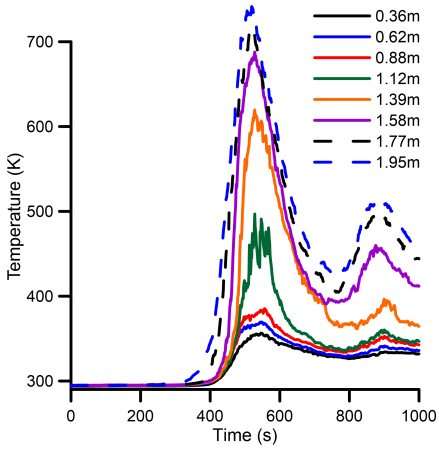

(a) Bottom of Staircase

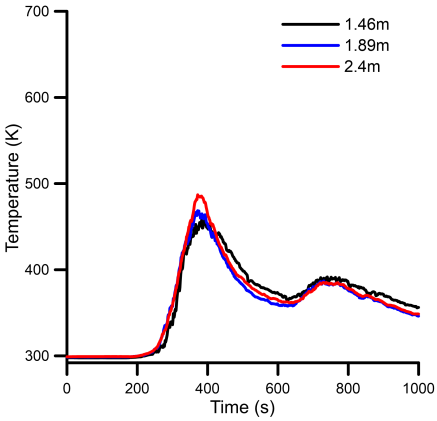

(b) Top of Staircase

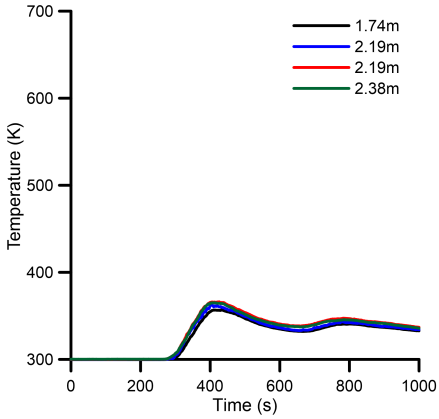

(c) Second Floor SE Room

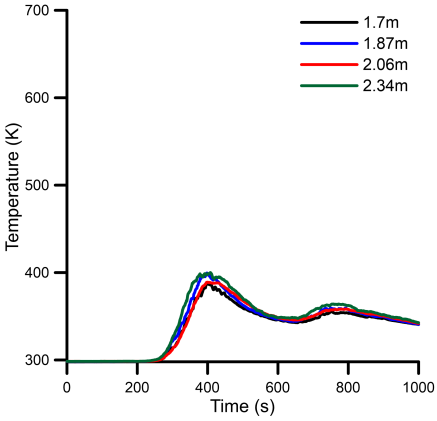

(d) Second Floor SW Room

Figure 4.14: NFR Couch A Staircase and Second Floor Temperatures

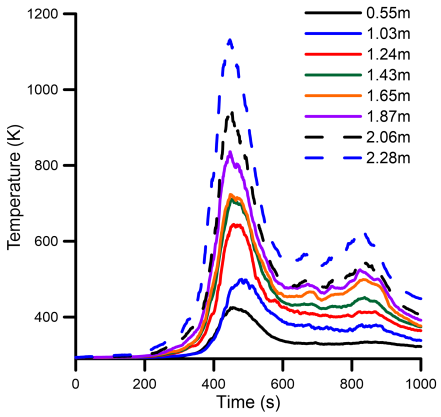

(a) Living (Burn) Room Center

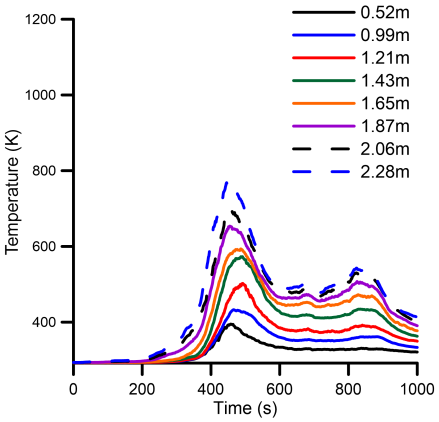

(b) Living (Burn) Room Corridor Side

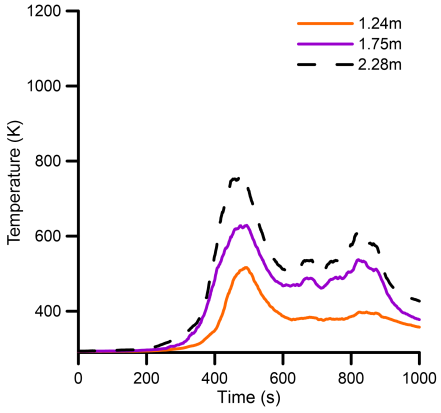

(c) Living (Burn) Room SW Corner

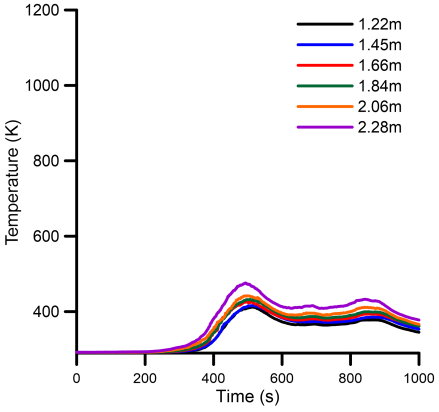

(d) Main Floor SW Room

Figure 4.15: FR Couch B Main Floor Temperatures

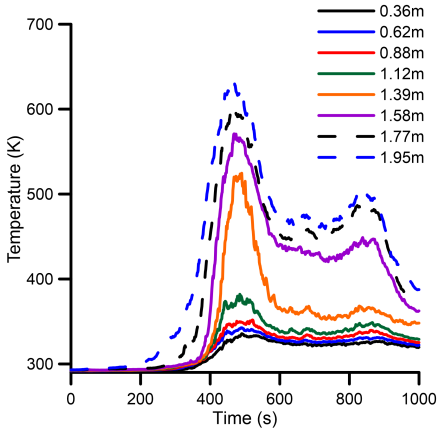

(a) Bottom of Staircase

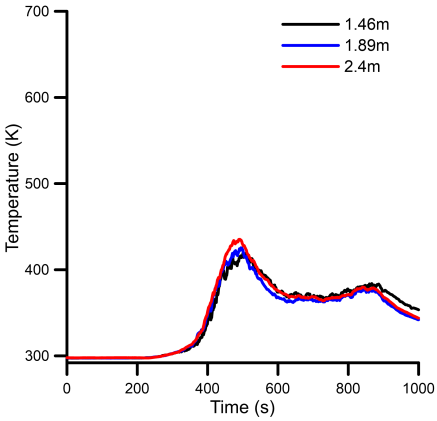

(b) Top of Staircase

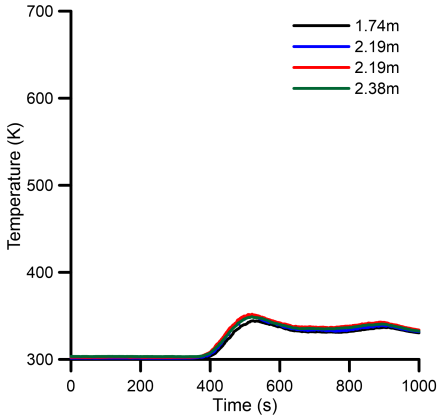

(c) Second Floor SE Room

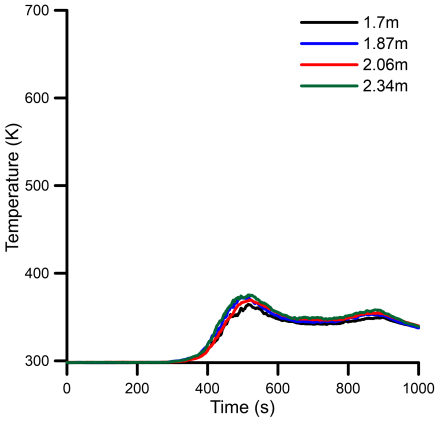

(d) Second Floor SW Room

Figure 4.16: FR Couch B Staircase and Second Floor Temperatures

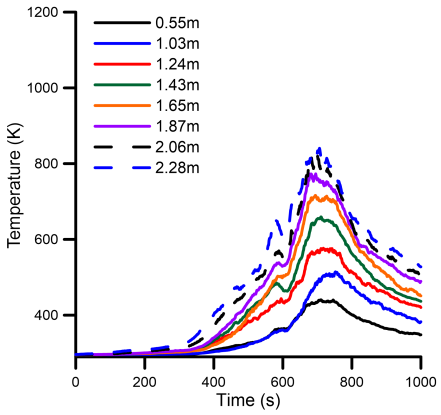

(a) Living (Burn) Room Center

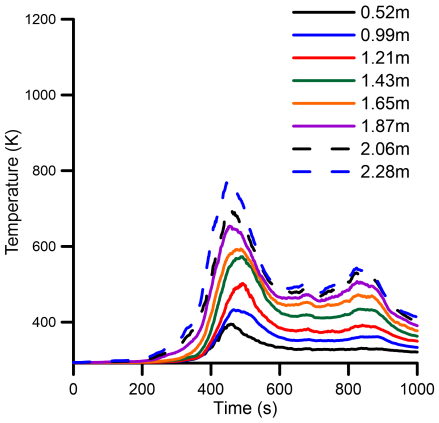

(b) Living (Burn) Room Corridor Side

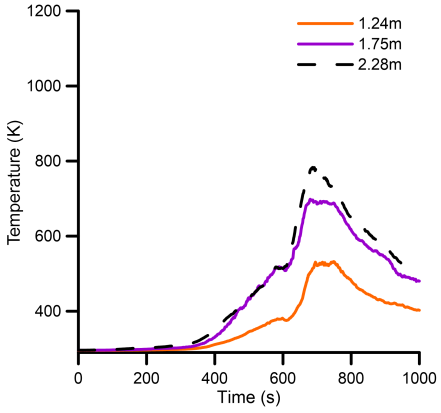

(c) Living (Burn) Room SW Corner

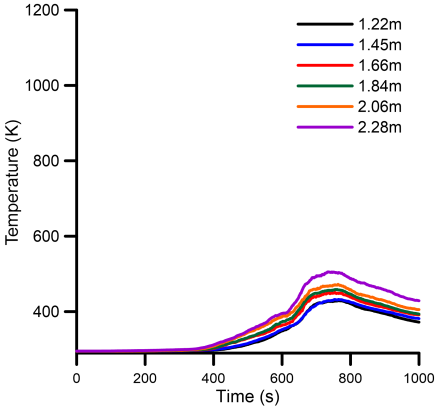

(d) Main Floor SW Room

Figure 4.17: LFR Couch C Main Floor Temperatures

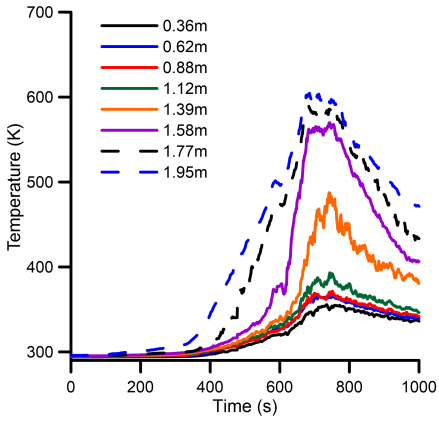

(a) Bottom of Staircase

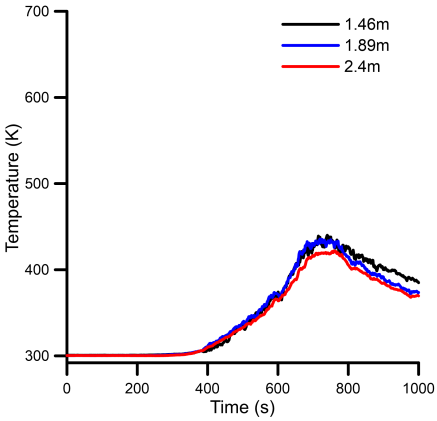

(b) Top of Staircase

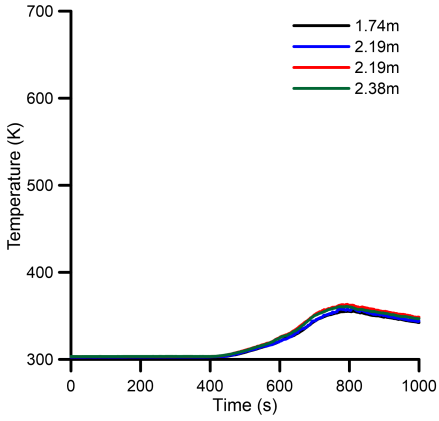

(c) Second Floor SE Room

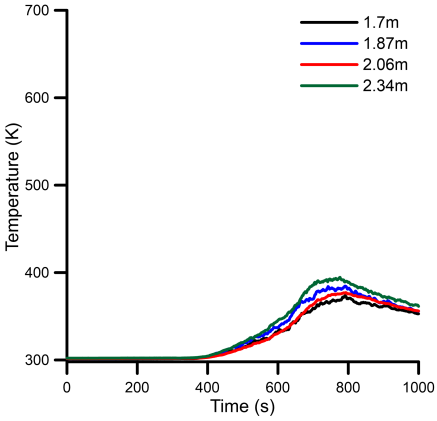

(d) Second Floor SW Room

Figure 4.18: LFR Couch C Staircase and Second Floor Temperatures

fire tests in the subsequent figures as well. There is clear thermal stratification through all stages of the fire development and through the transition of the fire from well-ventilated to ventilation-limited burning. There is evidence of stratification in the main floor SW compartment for all three fire tests as well, seen in Figure 4.13d for example, although to a lesser extent than in the previous Figures which were for locations in the direct vicinity and in the same room as the fire. Since there were openings between the the main living (burn) room into the SW compartment through a door immediately across from the fire, as well as around and down the corridor, smoke could flow freely into the SW compartment. The smoke would mix with the lower air layer along the corridor, as well as with cooler ambient air in the SW compartment leading to less well marked temperature stratification, at least from 1.22m above the floor to the ceiling. With no added natural or forced ventilation into or out of the compartment, the smoke gradually pooled in the upper regions of the compartment potentially leading to the more homogeneous upper hot layer than in other compartments.

The staircase appears to be a crucial element of how the hot gases distribute throughout the structure during these fires. There is a significant change in the thermal profile from floor to ceiling when comparing the top and bottom of the stairs, for example Figures 4.14b and 4.14a respectively from the NFR couch A fire. The thermal profile at the bottom of the staircase is clearly stratified, with a marked difference in temperature between the hot upper and cool lower layers, with a middle region between the two. In the case of NFR couch A, temperatures measured in the upper layer at the bottom of the stairs were greater than 700K, and temperatures in the lower layer were around 350K. Interestingly, at 1.12m above the living (burn) room floor measured temperatures fluctuate between 500 and 550K, a much larger degree of fluctuation than observed at other positions. During the time of peak heat release rate of the fire, the height of 1.12m above the floor could have been close to the height of the neutral plane, at the interface between the cooler fresh air being pulled down the stairs from the second floor onto the main floor and the hot fire gases flowing up the stair. Temperatures measured in the upper regions at the top of the stair, as seen in Figure 4.14b, are roughly 200K lower than temperatures measured in the upper regions at the bottom of the stair as seen in Figure 4.14a. This is because hot gases reaching the top of the stair flow freely into the upper storey compartments, coupled with continued entrainment and mixing of smoke and hot fire gases with cooler ambient air as they travel further away from the fire. This is especially seen on the second floor where temperatures measured in the upper regions of the SE compartment (Figure 4.14c) and the SW compartment (Figure 4.14d) are around 400K, which is 800K lower than the peak temperature measured in the living (burn) room immediately adjacent to the couch A fire, Figure 4.13a.

To further characterize the vertical thermal stratification, particularly in the living (burn) room (at rake T2), vertical profiles of measured temperature with height above the floor are plotted in Figures 4.19a, 4.19b and 4.19c for the NFR couch A, FR couch B and LFR couch C fires respectively, at the time of two different events. The first is when the smoke reaches the top of the window and the second is when the minimum oxygen concentration is reached in the main floor SW compartment. Times at which each of these take place differ from fire to fire, as indicated in the chronologies in Section 4.2 of this Chapter. The vertical temperature profiles measured 30 seconds before and 30 seconds after the time of each event at each position are also included to provide insight into the thermal progression of the environment over time as each of the two events took place. For reference, the height from the floor to the bottom and top of the window are 1.19m and 1.74m respectively. The transitioning slopes of the profiles plotted in Figure 4.19 demonstrate the relatively linear stratification in the compartment, initially in the upper reaches and through more of the compartment over time. This is in marked contrast to the normal 'zone' model concept of a period in which there are two well demarcated uniform temperature layers, normally referred to as the hot upper layer and cooler layer layers. In one instance, for the case of the fire on FR couch B, when the smoke hits the top of the window (233s) the temperature is very uniform from floor to ceiling, with only a slight increase in temperature very near the ceiling. In stark contrast is the stratified temperature profile in the upper regions of the compartment only a very short time later (roughly 200s) when minimum oxygen concentrations are measured in the main floor SW compartment (which is also close to the time at which the peak heat release rate occurs). Vertical profiles of temperature with height for the NFR couch A and LFR couch C fires demonstrate clear temperature stratification through the upper layer, from about 1.0 m above the floor to the ceiling, below which there appears to be a cooler lower layer with relatively uniform temperature. This is consistent with the temperatures measured at the bottom of the staircase mentioned above, where it was postulated that the thermocouple located at the 1.12m height might be sitting in the middle of a mixing region between the hot upper and cooler lower level gases, thus near the height of the neutral plane. The relationship between temperature, mixing regions and neutral plane heights will be further explored in Section 4.3.4, as measured velocity profiles in the entrance to the stair, as well as smoke movement and transport are examined.

To complete the discussion on the thermal development and environment within the living (burn) room, the next section presents information related to the compartment radiation as measured by the heat flux gauge, in comparison to estimates of radiation determined by emissive power and point source calculations for both fire and the smoke layer.

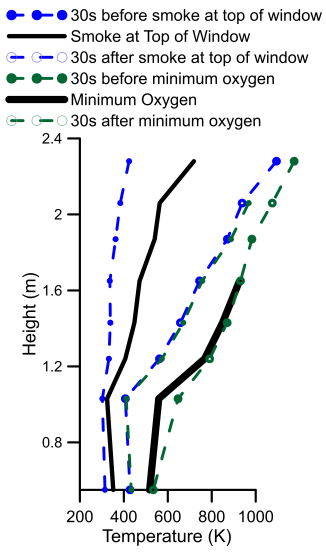

(a) NFR Couch A

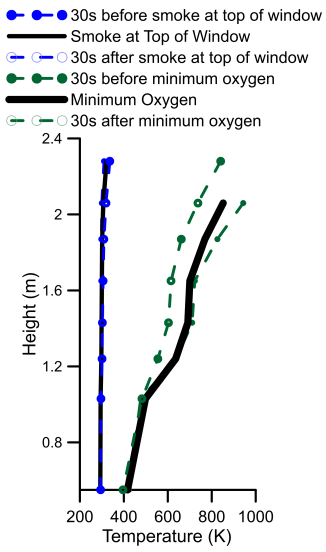

(b) FR Couch B

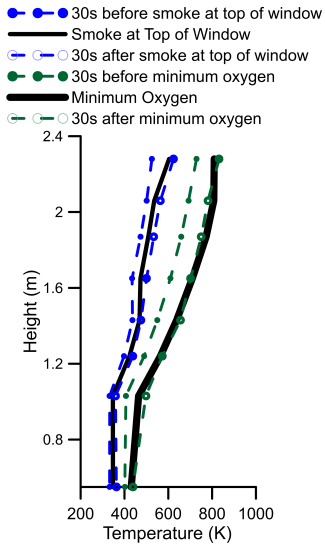

(c) LFR Couch C

Figure 4.19: Temperature Stratification Profiles Living (Burn) Room Center

4.4.3 Heat Flux and Radiative Contributions

Table 4.5 contains a summary of peak heat flux values for the three representative tests as measured by the water cooled Gardon gauge, HF1, placed 3m from the fire on the adjacent wall of the living (burn) room, facing the couch. Also listed are peak measured flame temperatures extracted from the thermocouple rake placed near the second section of the couch (T1 in Figure 3.2 in Chapter 3), with a 50K correction applied to the measured temperature to account for radiation [145].

Furniture Type	Maximum $\dot{q}''_{measured}$	Maximum Flame Temperature
NFR Couch A	13.7kW/m^2	1181K
FR Couch B	5.6kW/m^2	1060K
LFR Couch C	9.6kW/m^2	1031K

Table 4.5: Maximum Heat Flux and Flame Temperatures Measured

Values of maximum heat flux follow the same trends with couch type as seen for peak values of heat release rate in the curves shown in Figure 4.6. The highest overall heat flux value of 13.7kW/m^2 was measured for the fire fuelled by NFR couch A, followed by a peak value of 9.6kW/m^2 for the fire on LFR couch C and 5.6kW/m^2 for the FR couch B fire, as listed in Table 4.5. Based on comparison of the values for fire heat release rates, the measured value of peak heat flux from the FR couch B fires seems very low compared to those from LFR couch C fires since the two fires were characterized by very similar heat release rates. One possible reason for this was that the living (burn) room filled with much more smoke in the couch B fire relative to the LFR couch C fire thereby obscuring a large portion of the flaming fire plume from view by the heat flux gauge. In comparison to the NFR couch A fire, both the FR couch B and LFR couch C fires exhibited slightly lower measured fire temperatures, consistent with lower values heat release rate and of measured heat flux in the Table as well. More smoke movement and convection over the gauge, in conjunction with potentially lower flame temperatures due to more incomplete combustion, will result in a lower value of measured heat flux by the gauge.

The measured values of heat flux were further assessed through cross-checking against estimates of radiation from the fire and smoke layers as they progressed during the tests. Radiative contributions from the fire were estimated using the point source radiation method, as well as an emissive power method, which was also used to estimate the radiative contributions from the smoke layer as described in Section 3.5 of Chapter 3. For

reference, smoke layer temperatures measured at the boundary were around 290K during the early stages of the tests, and increased to roughly 350-600K depending on the fire.

Representative plots of the results from the radiation heat flux calculations are shown in Figures 4.20 through 4.22 for fires established on one of each furniture type which again correspond to the same test data used in the previous sections. Consistent with the above sections as well, ancillary test calculations and results can be found in Appendix A. Each figure consists of time resolved plots of heat flux to the gauge determined in three different ways. The first solid black line presents the values of heat flux measured by the gauge during each fire test. Next, the dotted lines show estimated values for radiation heat flux to the gauge calculated via the point source method using total measured heat release rate (product of mass loss rate and heat of combustion) of the fire without consideration of the radiative fraction. The third red lines are values of radiation heat flux calculated via the point source method using an input heat release rate which has been adjusted using an estimate for the radiative fraction, χ, of the fire. In the case of these last 'adjusted point source' plots, the radiative fraction was chosen so that the calculated and measured peaks were roughly equal. This also allowed examination of the approximate magnitudes of radiative fraction that might be appropriate for this set of fires. The radiative fractions determined for NFR A, FR B and LFR C in this way were 0.47, 0.4 and 0.65 respectively. These are higher than estimates of radiative fraction reported for various polymer compounds [39, 40, 42] in Chapter 2; however, this is likely expected since in the present fires the furniture materials burned incompletely as a result of the ventilation-limited environment. Further, these values of radiative fraction are likely to be high since the point source calculations do not take into consideration any possible radiative contributions from the smoke layer as it develops and descends throughout the compartment. To examine this effect further, total radiative heat flux to the gauge was also calculated by estimating total emissive power determined as the sum of the emissive power from the fire and from the smoke layer. Plots of these values are paired with the plots of radiative heat flux calculated using the point source models for each fire. Superimposed on these are estimates of the contributions from the smoke layer alone, referred to in the plots as the ceiling emissive power. Before additional discussion of these plots, it should be noted that the intent is to measure radiation heat flux with the gauge; however, in later stages of the fire, measurements by the gauge are affected by convection from the smoke layer as it flows over the face of the gauge.

From the plotted values of radiative heat flux to HF1 for each fire, it can be seen that the peak heat flux measured by the gauge occurs at the same time as the peak in heat release rate seen for the NFR couch A and LFR couch C tests, and occurs slightly before the peak heat release rate is measured for the FR couch B test. The curves for both measured

and calculated heat flux have very similar shapes to those for fire heat release rate across the duration of each fire. This is as expected since, as the fire grows in size, there is a proportional increase in the radiation measured by the heat flux gauge from the radiating fire plume. Plots of emissive power further indicate that the radiation from the descending smoke in the ceiling layer contributes a higher percentage of the total flux measured by the gauge in the early stages of the fire, then as the flaming fire plume grows in size, the contributions from the fire become the greater portion of the total flux registered by the gauge.

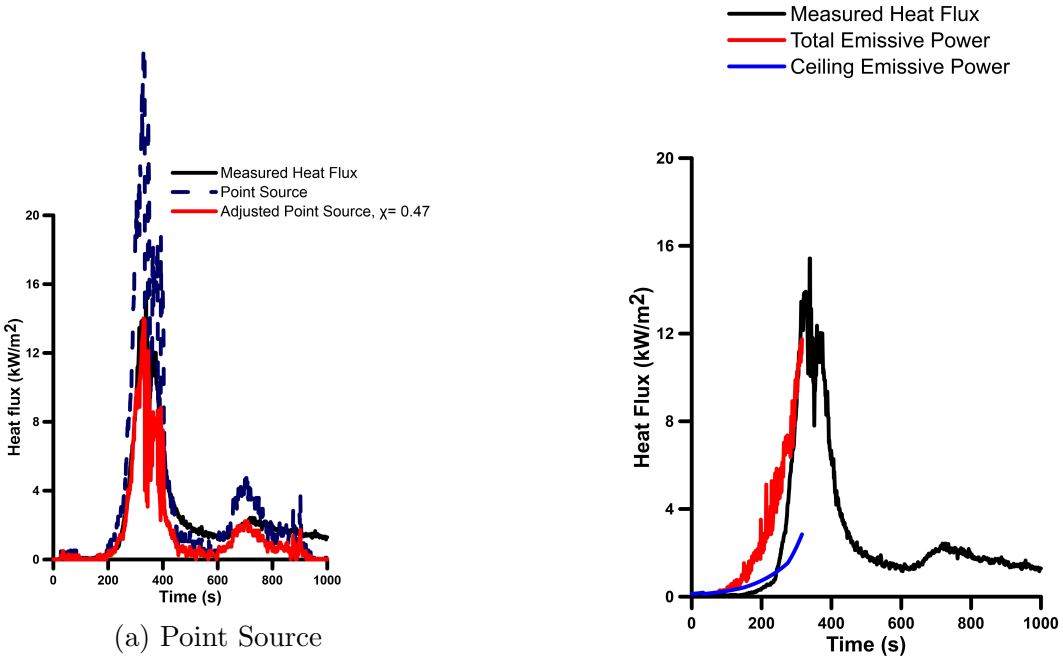

(a) Point Source

(b) Emissive Power

Figure 4.20: Heat Flux Measured by Gauge, Point Source and Emissive Power Radiative Contributions, NFR Couch A

As expected, point source estimations of radiation to HF1, when calculated without consideration of the radiative fraction, greatly over-estimate the heat flux, especially over the relatively short distances between the source and gauge, as was the the case in this compartment. On the other hand, correcting the total fire heat flux based on the constant values of radiative fraction listed above for each fire results in fairly good agreement between measured heat flux and point source estimations of heat flux for all three furniture types through the duration of the burn.

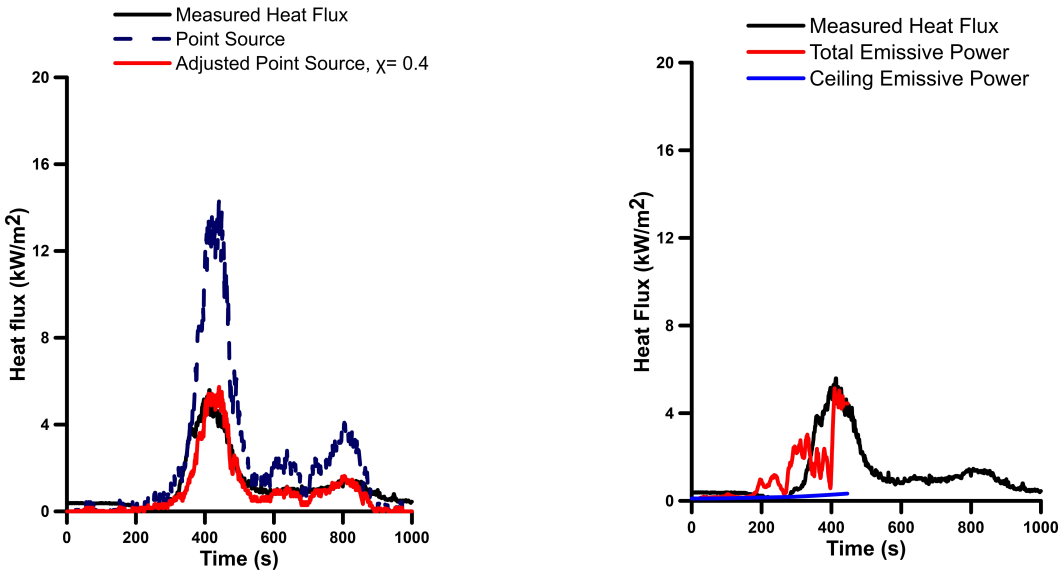

(a) Point Source

(b) Emissive Power

Figure 4.21: Heat Flux Measured by Gauge, Point Source and Emissive Power Radiative Contributions, FR Couch B

The plots of radiation heat flux as estimated using calculations based on the emissive power of the fire and smoke show interesting trends, and also highlight some of the difficulties in acquiring the necessary inputs for flame area in compartment fires with significant smoke production. The heat flux estimations plotted here contain only partial curves due to smoke obscuration over the cameras which impacted determination of complete traces of time-resolved fire width, height and therefore area. Similarly, this impacted the ability to track the smoke layer past a certain point on the video traces. Therefore, all results are plotted only for the early stages of the fire when the compartment environment was relatively clear. Interestingly, for all three fires, plots of total emissive power increase at a faster rate relative to measured values of heat flux in early stages of the fire, especially for fires on the NFR couch A (Figure 4.20b) and LFR couch C (Figure 4.22b). This may result from three possible causes: overestimation of the area of the fire at these times, oversimplification of the true geometric relation between the fire and heat flux gauge by assuming a set distance of 3m, and/or an over-prediction of the flame temperature during the early stages of the fire. In contrast, these calculations predicted the peak heat flux fairly accurately in all cases, both in terms of magnitude and of time to peak values. This suggests that the input parameters were better suited for estimating heat flux to the gauge

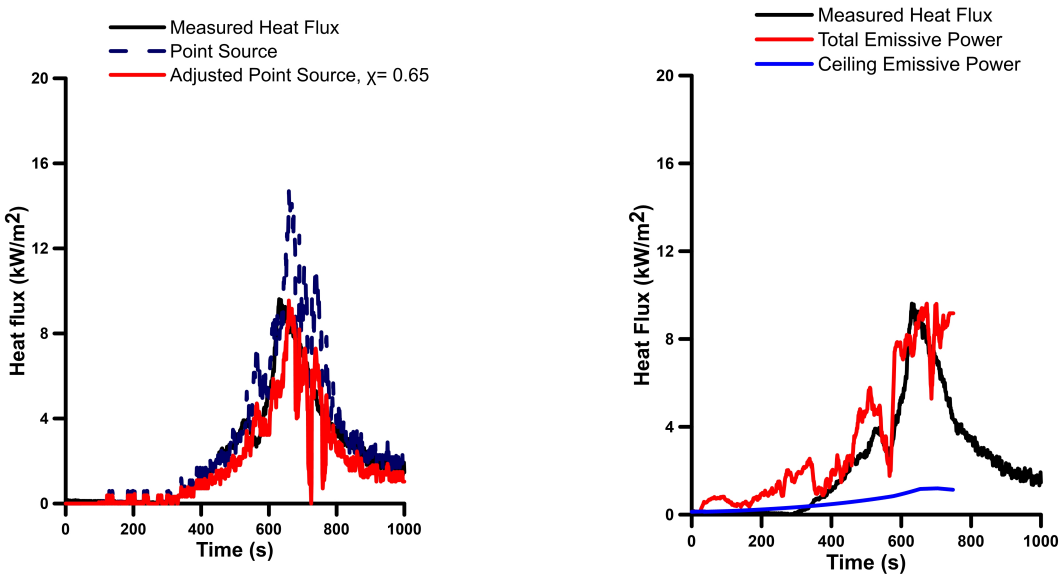

(a) Point Source

(b) Emissive Power

Figure 4.22: Heat Flux Measured by Gauge, Point Source and Emissive Power Radiative Contributions, LFR Couch C

in later stages of fire development, when fire heat release rate was reaching peak, the smoke layer was well established as a radiating body and the fire was centered on the couch and therefore located closer to the set distance of 3m away from the gauge. Figure 4.21b of heat flux values estimated using total emissive power for the FR couch B test shows how the smoke layer impacts the flame area and by extension, leads to under-prediction of the heat flux. In the time leading up to the peak heat release rate, around 400s (peak heat release rate occurs at 440s), a smoke layer is flowing over the fire plume and is quite dense (as seen in the pictorial timeline for FR couch B at the start of the Chapter), so under-prediction in the heat flux over this period of time is expected.

Estimated contributions of radiation from the smoke layer to heat flux in the compartment, as measured by HF1, are also shown in each plot. The smoke layer contribution follows the expected trend with increasing amount of radiation emitted as smoke accumulates in the compartment. The increase in radiative contribution from the smoke layer to measured heat flux at the gauge is least significant for the FR couch B fire, and most significant for the NFR couch A fire. This was somewhat unexpected because the FR couch B fire produced large amounts of smoke that filled the compartment space rather quickly; however, the highest smoke layer temperature taken from the thermocouple rake for the

couch B fire was roughly 350K, which is low compared to measured smoke layer temperatures for the other fires (600K for NFR A and 470K for LFR C respectively). When this low value is used in the emissive power calculation, due to the T^4 dependence, the resulting emissive power is much lower. The relatively lower smoke layer temperature in these tests may be a result of incomplete combustion combined with more mixing of the smoke with cooler gases within the compartment as it was generated. In the case of the NFR A and LFR C fires, when the smoke descended to the top of the window at 285s and 563s after ignition respectively, a change in slope of the curve for smoke layer radiation is seen as it contributes notably to total radiation measured at the gauge. This supports that as a fire compartment fills with smoke and as the smoke layer descends, there can certainly be a higher degree of radiation from the smoke layer that is providing radiative flux back to the surfaces in the compartment, including the combusting fuel bed [11, 121, 70]. Although the total flux from the smoke layer to the gauge for these fires continues to increase, it becomes a smaller overall contributor to the total heat flux during the later stages of the fire as the radiating fire source increases toward peak heat release rate as well.

The above calculations are limited by several considerations that highlight the complexities associated with measuring and predicting radiation within compartment fires. Measurements of heat flux by HF1 are influenced to an unknown degree by convective effects due to smoke and ambient air flowing over the surface of the gauge. Further, the overall estimation of fire contributions to heat flux are limited by estimates of fire size, heat release rate and compartment geometry. The smoke layer contributions to heat flux are limited by the values of temperature used in the calculations and by the fact that the interface between the smoke layer and cooler lower ambient air was difficult to distinguish and that the height of the smoke layer could not be determined after a certain point due to smoke obscuration over the camera. These experimental results and their limitations point to some of the complexities that would be encountered if such contributions were to be accounted for in models of fire behaviour in multi-compartment, multi-storey structures in a broader context. Specifically, accurate methods would be required to represent the overall smoke evolution in the compartment with proper account for fractions of the layer that remained confined with a given compartment versus that which flowed throughout the remainder of the structure. Some of these effects are explored in more detail in the next section; smoke movement and transport.

To complete the discussion on heat flux and radiative contributions, a more in-depth look at how the radiative fraction of the fire evolved over time is presented here. Estimates of radiative fraction were obtained on a time resolved basis by dividing measured values of heat flux by calculated values of heat flux determined using the point source estimation and total heat release rate of the fire. The resulting values of radiative fraction are presented

for the three representative furniture fires in Figures 4.23a, 4.23b and 4.23c for couches NFR A, FR B and LFR C respectively. The axes are truncated horizontally in time to run between 300 and 900s into the fires and vertically such that radiative fraction values run between 0.2 and 1 to better present the interesting distribution of radiative fraction with time in these fires. While a radiative fraction of 1 is not physical and there is thus likely an offset in the magnitudes, the trends in value with time are clearly marked in the plots. Oxygen levels measured in the main floor SW compartment (adjacent to the burn room) and the second floor compartment are superimposed on the plots to highlight possible relationships between heat release rate, ventilation and radiative fraction as well.

In the early stages of fire growth, up to 300s into these tests, values of radiative fraction range between 0.2-0.45 for the fires established on all three couches. The lower end value of 0.2 corresponds to the fire on LFR couch C, which had a relatively smaller fire size and heat release rate during this time, and the higher value of 0.45 corresponding to the estimate of radiative fraction for the fire on NFR couch A which had a relatively larger fire size and heat release rate. From the early-stages towards the time of peak heat release rate, the radiative fractions increased consistently for every furniture fire test, aligned with suggestions in the literature that increasing fire diameter may relate to increasing radiative fraction [43]. The possibility for such a relationship is seen clearly in Figure 4.23c for the LFR couch C fire; despite the marked fluctuations in value, a general trend emerges that as the heat release rate increases and the area of the fuel bed increases, the radiative fraction increases as well.

In all three of the fires, interesting oscillations of the radiative fraction with time are seen. This is especially clear in the plots for the FR couch B fire (Figure 4.23b). These oscillations suggest that the intensity of the fires may have been 'puffing' as a result of limited availability of air in the living (burn) room, interactions between the descending smoke layer and the fire plume and the overall need for the fire to entrain oxygen to support combustion. The radiative fraction decreased with decreasing oxygen concentration, potentially due to oxygen consumption damping combustion in the fire plume during those times. For example in Figure 4.23a, when oxygen reached a minimum in the main SW compartment around 350s into the fire, the radiative fraction dropped to around 0.35-0.4 before increasing above 0.6 as the combustion processes changed. Evidence that the fire is pulling oxygen from different areas of the structure at different times is also seen in these Figures, particularly in the case of the NFR couch A and FR couch B fires. When oxygen levels on the second floor in the FR couch B fire decreased to roughly 11% at 850s, the radiative fraction decreased from above 0.6 at 700s to roughly 0.4, as oxygen from the second floor was consumed by the fire. When less oxygen was available, more soot and incomplete combustion products were generated, flame temperatures decreased and radiative fraction

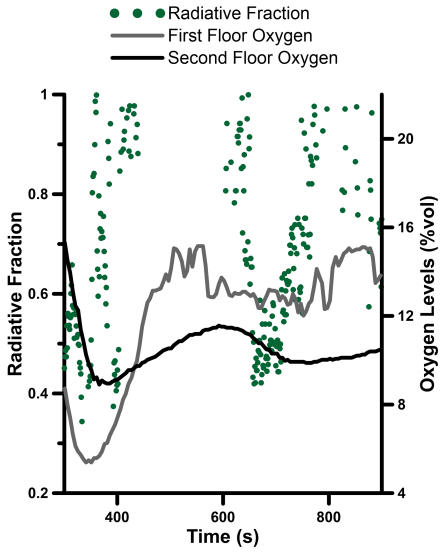

(a) NFR Couch A

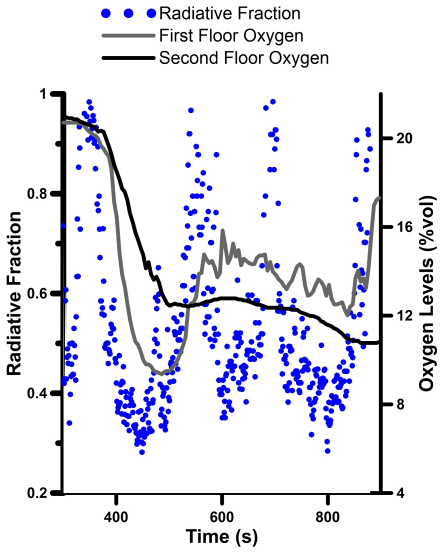

(b) FR Couch B

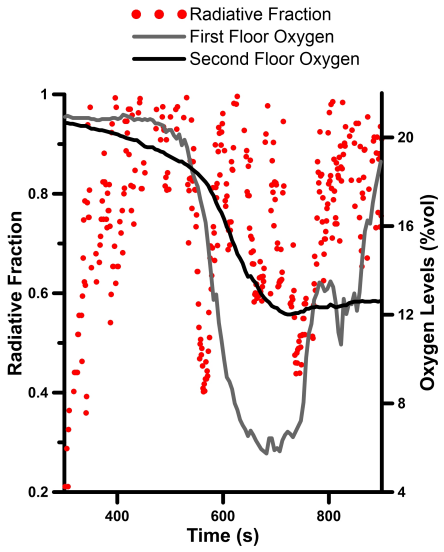

(c) LFR Couch C

Figure 4.23: Radiative Fractions Time-Resolved for Three Representative Tests

decreased as well.

These plots demonstrate the complex interactions between the fire plume, smoke layer, compartment ventilation, fire size and therefore radiative fraction. The significant changes in the radiative fraction observed with time suggest that depending on the type of fire scenario and design calculations required, use of values for radiative fraction outside of the typical magnitude of 0.3 should be used, and particular care should be taken in fires where ventilation may become limited. Finally, these interesting observations merit further investigation via more in depth targeted studies in future as well.

To further examine the relationships between the smoke layer and ventilation, the movement of hot fire gases and smoke out of the living (burn) room and up into the second floor, in conjunction with movement of fresh air downward into the living (burn) room from the second floor, are examined in next section via velocity measurements taken at the bottom of the staircase. Links between smoke movement, heat flux in the fire compartment, and measured values of temperature and oxygen concentration are drawn to paint a holistic picture of the progression of these ventilation-limited furniture fire environments.

4.4.4 Smoke Movement and Transport

The flow of ambient air and smoke between the two floors of the structure are shown in the velocity versus time plots shown in Figures 4.24a, 4.24b and 4.24c below for fire burning on NFR A, FR B and LFR C couches (tests 5, 4 and 6 respectively). The velocity measurements are taken from a series of probes located on the probe rake at the bottom of the stairs, designated as P1 in Figure 3.2, Section 3.1.1 of the previous Chapter. The top velocity probe is positioned 1.95m above the floor, the middle probe 1.39m above the floor and the bottom probe 0.36m above the floor. Positive values of velocity indicate that the flow is coming down the staircase and flowing past the probes into the living (burn) room from the second floor. Negative values indicate the velocity of flow out of the living (burn) room and up the staircase into the second floor. Indicators of the time at which peak temperature and minimum oxygen concentration were recorded for each test is also included on the plots. Time at which peak temperature was reached in the living (burn) room, represented by the short dash line, is taken from the top thermocouple, positioned 2.28m above the floor in the center of the living (burn) room (T2). Times at which minimum oxygen concentrations were measured in the main floor SW compartment and on second floor are represented by the solid and dash-dot lines respectively.

As the fire grows and the hot layer develops, smoke flows up the staircase as indicated by the high negative values of velocity shown in the Figure 4.24. The velocity measured

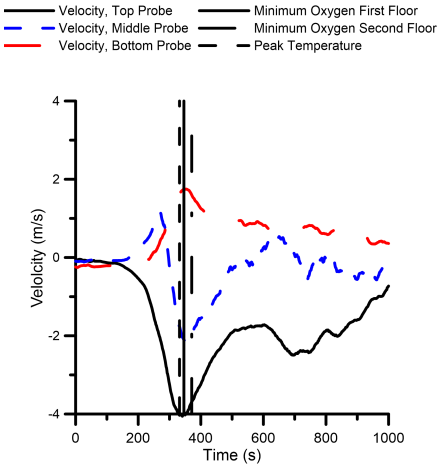

(a) NFR Couch A

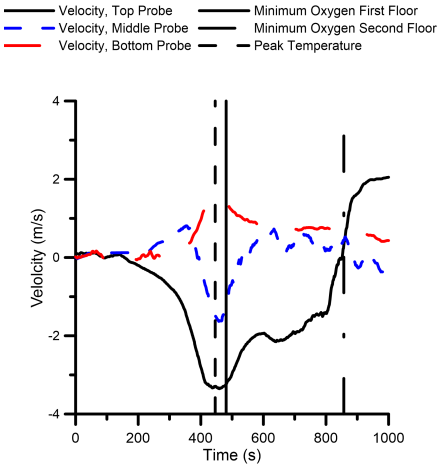

(b) FR Couch B

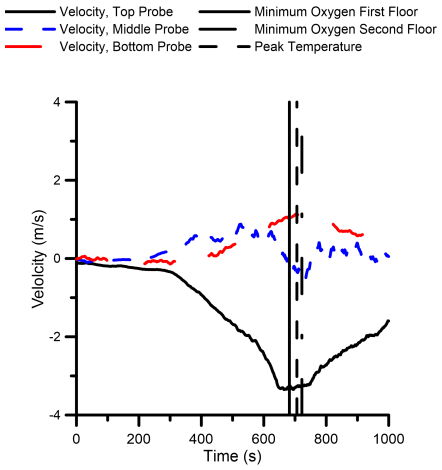

(c) LFR Couch C

Figure 4.24: Velocities at Top, Middle and Bottom of Staircase, with Minimum Oxygen on first and second floors and Peak Temperature Indicated, borrowed by permission from [2]

by the top probe tracks very closely with generation of hot gases from the fire. When examined in conjunction with the heat release rate and temperature curves, it is clear that the velocity up the staircase increases until the times at which minimum oxygen concentrations and peak temperatures are reached, which in turn correspond closely with the time at which the fires burn with peak values of heat release rate as well. This is supported by temperature measurements in the living (burn) room as well. These are reached at times of approximately 330s, 440s and 660s for fires on the NFR A, FR B and LFR C couches respectively, corresponding closely to the highest negative velocity values at the top probe on the rake. After this, the velocity up the staircase decreases, except for short periods in the couch A and couch B fires where the velocity increases again corresponding to the small secondary peaks in heat release rate seen later in those fires. Late in the couch B fire, the velocity flowing up the stairs reverses direction, most likely due to opening of a window or door toward the end of the test. In all tests, as hot gases flow up the staircase, a layer of cooler ambient air flows down the staircase from the second floor into the living (burn) room. This is seen in the positive velocity values shown in the trace from the bottom probe, closest to the floor (0.36m). This probe consistently measures a positive velocity, indicative of a continuous flow of air coming down the staircase from the second level into the living (burn) room. As the fire reaches its peak, sufficient hot gases are being generated in the burn room that the flow up the staircase extends even to, or below, the mid-height of the staircase opening. Velocities measured by the middle probe, which at 1.39m above the floor is thought to be situated close to the neutral plane of the opening, change from positive (flow down the staircase) to negative (flow up the staircase) as the peak heat release rate is reached in each case. That these flows are comprised of hot gases from the descending smoke layer is supported by temperatures measured at this height at the bottom of the stair as well. Peak temperatures measured at the top probe (1.95m above the floor), middle probe (1.39m above the floor) and bottom probe (0.36m above the floor) corresponding to the peak temperature/peak heat release rate for the NFR couch A fire at 330s are 725K, 600K and 450K; for the FR couch B fire at 440s are 625K, 525K and 350K; and for the LFR couch C fire at 660s are 600K, 500K and 350K. The change in direction of flow at the middle probe is consistently seen at near those times as well.

The top and middle bidirectional probes register maximum values of velocity up the staircase at approximately the same time after ignition, a time which roughly corresponds to when the oxygen concentrations on the first floor reach their lowest values suggesting most vigorous combustion of the fire. Consistent with this, peak values of velocity down the staircase are registered by the bottom probe at this time as well. It is interesting to note, however, that this occurs before the lowest values of oxygen concentration of 9%-12%

are measured on the second floor. This supports previous discussions which noted that the fire initially depletes the readily available oxygen in the main floor compartments and only then draws sufficient additional oxygen from the second floor to the burn room to support continued burning and deplete levels on the upper level.

To further explore the progression of smoke development and transfer throughout the structure, vertical profiles of velocity, taken by plotting the velocity as a function of height above the floor in the staircase opening at set times after ignition, are shown for each representative couch fire in Figure 4.25. The three times were chosen to correspond to three key stages of fire development. The time at which the first cushion was fully involved was taken as a marker of early fire development with respect to heat release rate and smoke production, while the time of peak heat release rate is the point of maximum fire development and finally, the time at which minimum oxygen concentrations were measured on the second floor was taken to represent a later stage in the fire event. The vertical slices of velocity in the stairwell opening support the trends seen in the plots above. As the fire grows, there is a significant flow of smoke up the staircase at heights of 1.75m and above, with lower flow velocities measured at heights between 1.25m and 1.75m. Below these heights, there is also a constant counter-flow of fresh air down the staircase from the second floor toward the fire. As expected, the vertical extent of this counter-flow is largest in the early stages of the fire, when there is not yet enough hot gas and smoke production to drive significant flow up the stairs. As the fire reaches peak heat release rate, the velocities at the middle heights in the staircase, near the neutral plane, increase in velocity and change direction to exhaust the increasing quantities of smoke filling the living (burn) room. Relative to the upward velocities of the low density, hot smoke, the counter-flow of denser ambient air is at consistently lower velocity especially in the lowest regions of the staircase. Nonetheless, flows in both directions are significant.

The images in Figure 4.26 below, taken at 265 and 339 seconds after ignition (IGN) respectively, capture some of the interesting elements of flow patterns and air exchange at the top of the staircase, as well as smoke flow between the main and second floors during a FR couch B fire. Images 4.26a and 4.26c were taken from the camera positioned in the second floor SW room facing the landing of the staircase, camera V4 in Figure 3.2 in Chapter 3. Images 2.5b and 4.26d were taken from a camera placed in the corridor of the main floor viewing the living (burn) room from the side, camera V1 in Figure 3.2. This camera was able to capture footage of the fire from a side angle as well as gas and smoke flows between the levels of the structure via the staircase. At 265 seconds after ignition, the heat release rate of the fire is still growing, and there is a clear boundary between the hot upper layer and cooler lower layers of air in the fire compartment and on the upper landing of the staircase. The upper layer of smoke can be seen coming up the staircase and

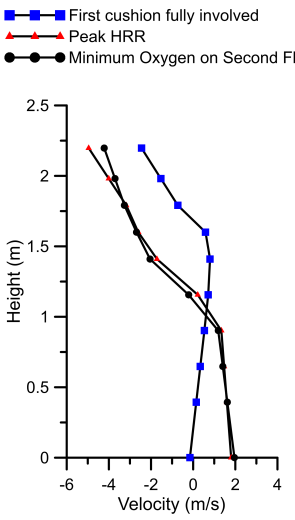

(a) NFR Couch A

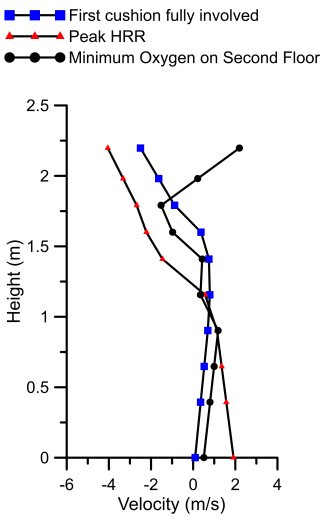

(b) FR Couch B

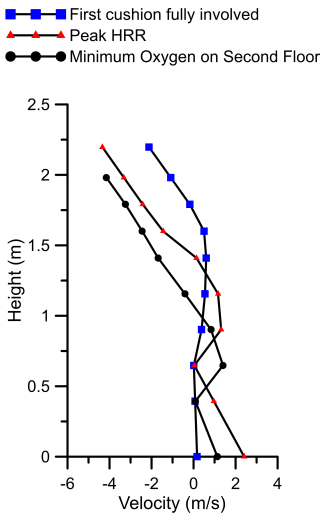

(c) LFR Couch C

Figure 4.25: Velocity Profiles at Bottom of Staircase when First Cushion is fully involved, Peak Heat Release Rate and Minimum Oxygen Measured on the Second Floor, borrowed by permission from [2]

entering the second floor from the living (burn) room, consistent with the layer of smoke that is accumulating in the hot upper layer of the living (burn) room seen in Image 2.5b. At 339 seconds after ignition, Image 4.26c captured the interesting mixing processes that took place when these two opposing flows, the hot less dense fire gases/smoke, and more dense, ambient air, met at an opening. At this point, the velocities of hot smoke flowing up, and cooler air flowing down, the staircase have increased 4.24b. As these two streams meet in the landing on the upper floor, flow interactions and differences in density of the two streams result in the large circular, or vortical flow patterns evident in Image 4.26c. These vortical flows can promote mixing between the smoke and ambient air by disrupting the shear layer and essentially 'sweeping' smoke into the fresh air, thereby drawing smoke laden air back toward the fire on the floor below. As such, these vortical flows may be at least partially responsible for the smoke seen exiting through the bottom regions of the staircase on the main floor in the Image 4.26d.

To integrate the radiative smoke layer contributions with smoke movement during the fire in terms of the velocities measured at the bottom of the staircase and the heat flux measured in the living (burn) room, consideration of smoke filling, and smoke flow out, of the compartment forms an interesting link. In the FR couch B fire, the smoke layer reaches the top of the window at 233s after ignition, before the first cushion is fully involved in the fire (362s). At this point, the smoke layer contributes approximately 20% of the total flux into the compartment, as measured by HF1. As the fire grows from 233s to 362s (smoke at top of the window to first cushion fully involved), the contribution to compartment radiation from the smoke layer decreases to about 8% of the total flux as the velocity up the staircase increases from 0.3m/s to roughly 1.4m/s. As the fire continues to grow towards peak heat release rate, the smoke layer contribution stays roughly the same, at about 7% of the total radiation into the compartment, as the flow up the staircase increases to roughly 3.2m/s. At this time, while the smoke layer has grown deeper, it contributes a relatively smaller percentage of the total radiative flux to heat flux gauge on the wall of the compartment. As the smoke layer gets thicker, a portion of this hot radiating body is lost to the second level as it flows up the staircase, so there is less relative contribution of radiation from the smoke layer as the fire increases in size. At this time, the fire heat release rate is much higher and, due to the balance between the flow of hot smoke up the stairs and cooler air down the stairs, the temperature and depth of the smoke layer has only increased a relatively smaller amount, such that it now contributes a much lower fraction to the total heat flux measured at the gauge on the far wall.

Similar trends are seen in the LFR couch C fire. When the fire is established on the first cushion, the smoke layer is contributing 14% of the total flux to the compartment, and the flow of smoke up the stairs is roughly 1.5m/s. As the fire grows and by extension the

(a) Top of Staircase, 265s after IGN

(b) Living (burn) Room, 265s after IGN

(c) Top of Staircase, 339s after IGN

(d) Living (burn) Room, 339s after IGN

Figure 4.26: Smoke Flows on the Main and Second Floor during a Couch B Fire, borrowed by permission from [2]

smoke layer grows in thickness, when the smoke reaches the top of the window, the smoke layer is contributing 15% of the total compartment flux and the velocity of smoke flow up the stairs has increased slightly to 2m/s. As the heat release rate continues towards the peak at 660s after ignition, peak velocity measured up the stairs is measured to be around 3.2m/s, and the relative contribution of radiation from the smoke layer to heat flux at the compartment wall has decreased to 11%, similar to values seen for the other two fires at this stage as well.

4.4.5 Summary of Environmental Characteristics

Overall oxygen concentrations in the living (burn) room decreased to between 3%-9% depending on the type of couch involved in each fire. Trends in oxygen depletion through the structure were consistent for fires established on the different couch types, as mirrored both through the time resolved measurement of oxygen concentrations in compartments on the main and second storey, but also through examination of the velocity profiles at the opening from the living (burn) room to the staircase, which proved extremely important in terms of exchange and mixing of hot fire gases and cooler ambient air. As anticipated, the velocity of smoke flowing up the upper half of the staircase increased with increasing heat release rate of each fire, and changes in the direction of flow were seen for probes in the middle levels of the staircase as the peak heat release rate was reached, indicating variations in the height of the neutral plane over time. There was a steady counter-flow of air down the staircase in the lower regions, again with increasing velocity over time as minimum oxygen concentrations were registered on the second floor. Carbon monoxide concentrations initially increased according to the increasing slope of the fire heat release rate curves, with highest measured concentrations always evident in the living (burn) room.

Temperatures in the living (burn) room and areas close to the fire exhibit a vertically stratified thermal profile; however, outside of the living (burn) room, particularly on the second floor, temperature stratification is not as marked and more uniform and isotropic temperatures are measured in the upper regions of the spaces due to mixing and entrainment of hot smoke with cooler ambient air as it travels further from the fire. Time-varying temperatures, as well as heat flux measured by the gauge in the living (burn) room, followed the same trends as the fire heat release rate curves. The magnitudes of peak temperatures and peak heat release rate were highest for NFR couch A, with temperatures of 1200K in the living (burn) room and 350K on the second floor and heat release rate of 3345kW. LFR couch C had the second highest peak heat release rate, but the lowest measured peak temperatures on the main floor. Contributions to radiative heat flux from the smoke layer were much smaller relative to the fire; however, as the fire progressed there was an increase in the amount of radiative heat from the smoke layer though it actually contributed a lower percentage of the total radiation into the compartment as the fire grew. As the fire developed, even though there were very low levels of oxygen in the compartment, the radiant energy from the smoke layer positively feedback to the vaporizing fuel surfaces, promoting combustion. The differences in the evolution of many of the key parameters governing the overall progression of the fire highlight the importance of understanding the ventilation and smoke movement pathways in a structure, the specific burning characteristics of the furniture and how those combined characteristics impact the combustion process, in terms

of the local environment as well as the global environment that develops in a structure for a given fire situation.

These test results provide new insight into the interactions between the heat release rate, smoke development, movement and ventilation within a multi-compartment and multi-storey structure. These impact the overall concentrations of oxygen and combustion products throughout the course of the fire. The next section will focus the estimation of fire heat release rate using the selected methods as applied to the three distinct furniture fires outlined above. Similarities, differences, strengths and weaknesses of each of the methods will be discussed, starting with with power law for fire growth, followed by the correlation presented by Heskestad [17], and moving to correlations by Babrauskas [110, 111], ending with the cone extrapolation method developed in the present research. Time-resolved curves of heat release rate calculated using Heskestad's correlation and the cone extrapolation method are compared to the time-resolved estimates of heat release rate obtained via the mass loss rate method and discussed in Section 4.2.2 above. Values of peak heat release rate predicted using the correlation by Babrauskas are compared to the peak values of heat release rate determined using the mass loss rate method as well.

4.5 Heat Release Rate Methods and Comparisons

4.5.1 The Power-Law Fire Growth Curve

Heat release rate versus time plots for each of the eight furniture tests were analyzed to determine estimates of incubation time and time taken for the fire to grow to 1MW in order to calculate values of fire growth rate, α. These included 3 NFR couch A tests, 2 FR couch B tests, and 3 LFR couch C tests. Values for each parameter for all eight tests are tabulated in Table 4.6 to demonstrate the variance in fire growth characteristics within fires burning on the same type of furniture, as well as across furniture types. Below the summary Table 4.6, plots of the heat release rate, calculated using the mass loss rate method are plotted against time with the respective power-law, or t^2 fire growth, curves using the calculated α values for each test. These facilitate comparison of similarities and differences between a potential design calculation for heat release versus values determined directly from the measured mass loss rate for these furniture tests. Values of α are further compared to the design fire values of 0.00293, 0.01172, 0.0469 and 0.1876 in kW/s^2 for slow, medium, fast and ultra-fast fire growth respectively [19].

The values of α for NFR couch A fires, particularly for those on couches Ai and Aii in tests 2 and 5, are $0.1778 kW/sec^2$, very close to the value of 0.1876 kW/sec^2 that is

Furniture Type	Incubation Time (s)	Time to 1MW (s)	Calculated α (kW/sec^2)
T2 NFR couch Ai	200	275	0.1778
T5 NFR couch Aii	200	275	0.1778
T8 NFR couch Aiii	150	200	0.4000
T4 FR couch Bi	290	380	0.1235
T7 FR couch Bii	250	350	0.1000
T3 LFR couch Ci	375	612	0.0178
T6 LFR couch Cii	375	612	0.0178
T9 LFR couch Ciii	300	550	0.0160

Table 4.6: t^2 Fire Growth Curve Inputs

typically used to designate ultra-fast fire growth. The average value of α of 0.1118kW/sec^2 for the FR couch B tests lies between values normally listed for fast and ultra-fast growth fires, but is relatively closer to the value for ultra-fast fire growth as well. The value of α for LFR couch C fires lie between those for medium and fast fire growth, but are relatively closer to medium growth fires, with an average α value of 0.0516kW/sec^2. As seen in the Table 4.6 and Figures 4.27, there are consistent differences in the incubation time between fires on the different types of furniture as well as in time taken for the different fires to reach 1MW in size, as discussed in the first Section of this chapter.

Interestingly as well, there are also notable differences in the incubation period and the time to reach 1MW size for fires within a given type of furniture, in particular NFR couch A. This highlight limitations that occur when fire growth rates for even a single furniture type, and particularly for a range of furniture types, are over-generalized to be represented by one α value. It would appear that a use of upper and lower range values for α values might be more appropriate when conducting a design fire calculation for even a given type of furniture .

The fire growth rates seen in the present results are fairly comparable to other fire growth curves calculated for different furniture types in the 1990s [151]. In this data, the furniture with cotton fabric and treated foam padding had a slow fire growth [151], in comparison to the present LFR couch C which sustained closer to a medium fire growth. The difference may be in the lightly fire-retardant treatment of the foam in the present tests. Also in the 1990 set, furniture that was covered with fabrics that tended to melt and with untreated or lightly treated foam padding sustained fast fire growth [151]. This is comparable to the current data in which both NFR couch A and FR couch B had polyester fabric coverings which tended to melt, as well as untreated and FR treated foam

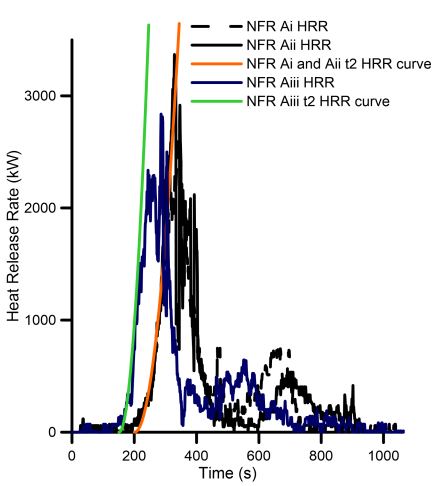

(a) NFR Couch A

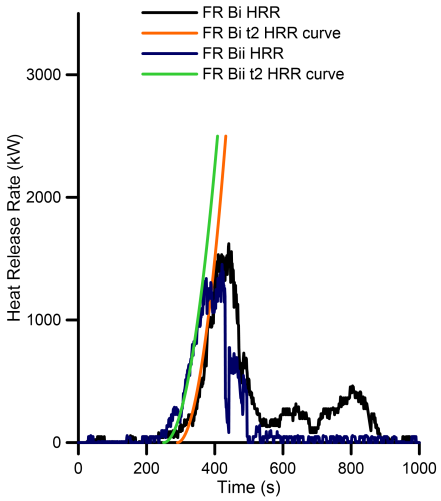

(b) FR Couch B

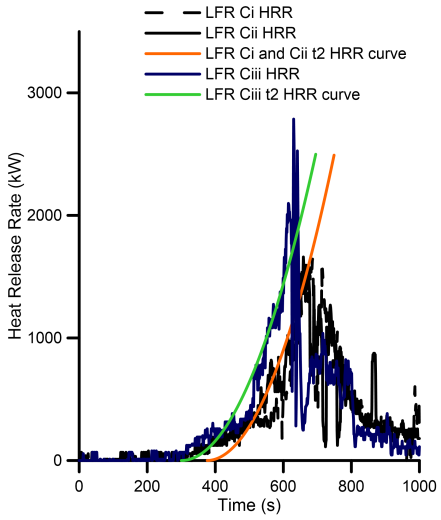

(c) LFR Couch C

Figure 4.27: HRR Calculated from MLR Method and t^2 Fire Growth Curves

respectively. As anticipated, the NFR couch A sustained ultra-fast fire growth, the FR couch B grew more closely according to the fast rate and the fire growth rates for both of these couches were higher relative to the LFR C couches.

4.5.2 Heskestad's Correlation and Mass Loss Rate Methods

A comparison of heat release rates estimated as functions of time using the rearranged form of the Heskestad flame height correlation shown in Equation 3.4 [17] with two different inputs for fire diameter and the mass loss rate method, shown in Equation 3.2 and referred to here as MLR, [13] for each furniture type are shown in the plots in Figures 4.28a, 4.28b and 4.28c for NFR couch A, FR couch B and LFR couch C respectively. In the Figures, the two values of fire diameter, D, input into Heskestad's correlation [17] are labelled 'width-only' and 'effective diameter'. The 'width only' values refer to setting diameter, D, equal to the width of the fire, as measured along the top of the couch sitting cushion, and directly output from the image analysis program. The 'effective diameter' label refers to the diameter, D, calculated by determining the area of fuel burning at a given time and equating that to an equivalent circular source to determine an equivalent diameter [29]. Due to the nature of the burning on the couches, calculation of effective diameter is done in the three parts as described in Section 3.3.2. The heat release rate plots are supplemented with 4 indicators; the time at which the smoke descends to the top of the window (dashed blue line), the time at which the first cushion is fully involved (solid blue line) and two black lines indicating the times corresponding to the images below the axis which represent the times at which the correlation starts to break down as determined in Section 4.3. The values of heat release rate calculated using the mass loss rate method were smoothed with a 10-point moving average to account for noise, and the heat release rate values calculated using the Heskestad correlation were not smoothed [5].

As seen in Figure 4.28, the fire heat release rate of the NFR couch A and FR couch B fires is initially quite well predicted using the Heskestad equation with either the width-only or the effective diameter of the fire as input, though the effective diameter input provided slightly more consistent estimates of fire heat release rate overall. As noted based on earlier discussions of use of this correlation for estimation of flame height, the agreement was best until the time that the fire grew to the size of the first sitting cushion. After this, the fire spread rapidly across the surface of the couch cushions as a result of the melting polyester

[5]For clarity, the x-axis on the NFR A and FR B plots were truncated to 600 seconds to show more detail of fire development over the time before the smoke obscured the camera, whereas the LFR C plot shows the full 1000 seconds of the test

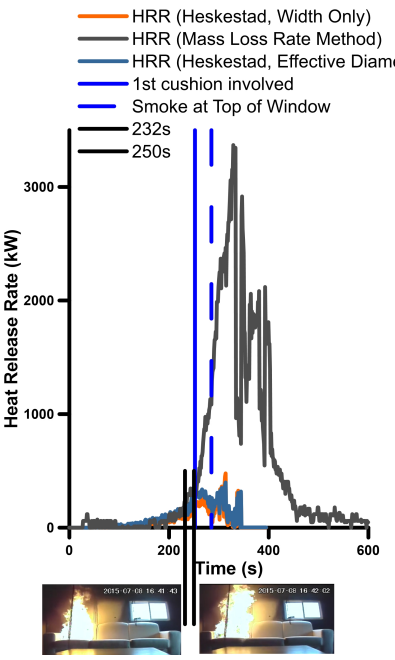

(a) NFR Couch A

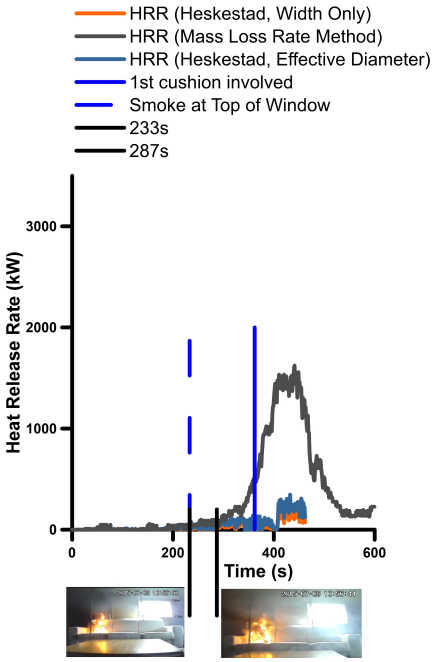

(b) FR Couch B

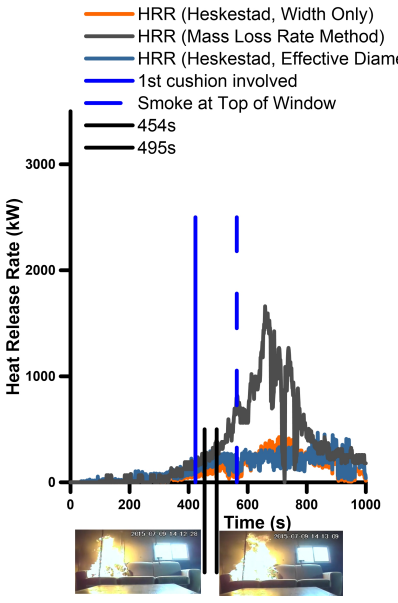

(c) LFR Couch C

Figure 4.28: Heat Release Rates, Heskestad Correlation and MLR Method

fabric and burned less like a circular pool fire, and instead, burned with a rectangular-shaped fuel bed on both planes of the couch surfaces. As anticipated, given the nature of the fire progression across the couch the effective diameter input was more appropriate to use for calculations past this point. As discussed previously with flame height predictions, agreement between the correlation and measured fire heat release rate broke down shortly after this time due to growing interactions between the fire plume, compartment ceiling and descending smoke layer. For the fire on NFR couch A, the point was reached at between 232s and 251s when the fire heat release rate increases in size from about 240kW to 345kW. At this later time, oxygen concentrations measured 0.6m above the floor in the burn room are roughly 16%, which suggests that the environment is no longer that of well-ventilated, open-burning. For FR couch B fires, the predicted heat release rate using Heskestad's correlation ceases to follow the increasing slope of the measured heat release rate curve at between 233s and 287s after ignition, although the fire heat release rate at this time is relatively constant at 50kW. It can be seen clearly in the Figures, that at 287s after ignition and well before the first cushion is fully involved, there was significant smoke production from the fire which built up in the compartment and interacted with the fire plume, rendering the open-burning Heskestad prediction method invalid. In the LFR couch C fire, due to material interactions between the charring cotton fabric and polyurethane foam, the burning behaviour was different than for the other two fires. In this case, the fire appeared to be mostly centered over one section, or a third of the couch, at any given time though flames were still burning on the adjacent sections and, as seen in the pictorial timeline (Figure 4.5), the fire did spread to involve the entire width of the couch. Visually at least, the burning mechanism of the LFR couch C fire more closely resembled sequential sets of smaller pool fires in terms of the evolution of fire diameter over time. Nonetheless, it can be seen in Figure 4.28c that Heskestad's correlation starts to break down between 454s and 495s, when the heat release rate is about 250kW and increases to 380kW. For this fire also, the heat release rate was still significantly under predicted for times after an initial growth phase due the series of factors discussed in Section 4.3 on Flame Geometry.

The combined effects of the fire plume impinging on the ceiling, smoke layer interacting with the top of the fire plume, the long rectangular shape of the fire, decreasing oxygen concentrations in the fire compartment and uncertainties with respect to the actual time-dependent size of the fire contribute to the severe limitations in applicability of Heskestad's correlation for prediction of fire heat release rate in any of the present fires. Added to this, the specific burning characteristics of the thermoplastic polyester fabric and the relationship between the melting of the fabric and burning of the foam may contribute to a higher degree of in-depth combustion than could be accounted for with the present values of effective burning area as a function of time. All these factors point to the fact that this, or any

similar correlation, should be used with extreme caution if values of effective flame height or fire heat release rate are required in compartment fire scenarios such as those presented in this research. More work is needed to investigate if there are any corrections that can be applied to account for any of the complexities in this type of scenario. It is likely that a much more detailed, physics based model for the burning behaviour will be required in order to account for the interacting phenomena of air availability and entrainment, multi-surface burning and flame spread, smoke layer and ceiling interactions that characterize the present couch fires.

The next Section delves into calculations of peak heat release rate from fires fuelled by the three types of furniture using factor-based approaches [111] combined with input values of heat release rate for the furnishing materials, as derived from cone calorimeter testing [110].

4.5.3 Babrauskas Predictions

Calculations of peak heat release were made for each of the present couch fires using both the bench-scale [110] and full-scale correlation methods outlined in Section 3.2.3 [111]. A summary of the values needed as input to these correlations are summarized in Table 4.7 below. Again all of the present furniture tests are included: 3 NFR couch A tests, 2 FR couch B tests, and 3 LFR couch C tests. For clarity, tests are labelled by their numbers as Tx, and the specific couch in a given test fire as Ax, Bx or Cx, dependent on the couch type respectively. In the Table, the corresponding mass factor for each test is taken as the total mass of the couch multiplied by the wooden frame factor. The couches in the present study were constructed with wooden frames, and although the frames charred and did not completely burn, they were not considered to be entirely non-combustible, so the 0.3 wooden frame factor was used instead of the 1.66 that would be applied for a non-combustible frame [110, 111]. Input values of heat release rate as determined using the cone calorimeter are listed as Avg. HRR in Table 4.7. These values are the heat release rates measured for each set of composite couch materials, averaged over the first 180 seconds of burning in the cone calorimeter. The labels ‘a’, ‘b’ and ‘c’ correspond to values obtained from samples of 25mm foam and fabric tested at 35kW/m^2, 50mm foam and fabric tested at 50kW/m^2 and a repeat of the 50mm foam and fabric tested at 50kW/m^2 respectively for the NFR A and FR B materials. In the case of the LFR couch C materials, ‘a’, ‘e’ and ‘d’ correspond to the samples consisting of 25mm thick foam and fabric, 50mm thick foam and fabric and a repeat of the 50mm thick foam and fabric, all tested at 35kW/m^2. The padding, style and fabric factors were selected based on the materials used in the construction of the furniture as stipulated by Babrauskas [110, 111]. In the case of the

FR polyester fabric used in the construction of FR couch B, when the fabric factor of 1 was used to predict the peak heat release rates, values were, as anticipated, significantly over-predicted due to differences in the burning characteristics of the present materials relative to those on which the correlations were originally based. Reduction of this factor to a value 0.42 produces much more comparable results to the other methods and therefore a reduced value of this factor would be needed to account for the FR nature of this fabric.

Furniture Type	Mass Factor	Avg. HRR* (kW/m^2)	Padding Factor	Style Factor	Fabric Factor
T2 NFR couch Ai T5 NFR couch Aii T8 NFR couch Aiii	18.01kg 18.03kg 16.94kg	a:184.42 b:256.97 c:290.64	1	1	1
T4 FR couch Bi T7 FR couch Bii	18.36kg 18.17kg	a:141.61 b:209.63 c:266.89	1	1	0.42
T3 LFR couch Ci T6 LFR couch Cii T9 LFR couch Ciii	15.76kg 16.85kg 15.72kg	a:93.35 d:119.74 e:106.27	1	1	0.4

*Average HRR values are from representative foam and fabric samples across the couches of each type; they do not correspond to a particular couch in the Table

Table 4.7: Summary of Inputs into Babrauskas Correlation Methods (a: 2018 25mm thick foam/fabric sample, $35kW/m^2$; b: 2020 50mm thick foam/fabric, $50kW/m^2$; c: 2020 repeat 50mm thick foam/fabric, $50kW/m^2$; d: 2020 50mm thick foam/fabric, $35kW/m^2$; e: 2020 repeat 50mm thick foam/fabric, $35kW/m^2$)

Using the inputs as summarized in Table 4.7, in the correlations in Equation 2.13 [111], peak heat release rates, referred to as predicted PHRR, were determined for each test and are presented in Tables 4.8, 4.9 and 4.10 for NFR couch A, FR couch B and LFR couch C fires respectively. The designation 'a' through 'e' included in the second column of the Table for each test correspond to the cone calorimeter heat release rates summarized in Table 4.7. For comparison, the values for peak heat release rate calculated using the mass loss rate method for each test, referred to as MLR PHRR, are included in the Tables, along with the percent difference between the predicted peak heat release rates from the Babrauskas correlations and the mass loss rate method.

As seen in Table 4.8, the peak heat release rate is significantly under-predicted using the bench-scale correlation of Equation 2.12, when compared to the mass loss rate method for all tests. On the other hand, the full-scale correlation over-predicts the peak heat release

Furniture Type	Bench-Scale PHRR	Avg. PHRR Bench-Scale	PHRR Full-Scale	MLR PHRR	% Diff to MLR PHRR (bench/full)
T2 NFR Couch Ai	a 1495kW b 1458kW c 1649kW	1534kW	3783kW	2652kW	53%/35%
T5 NFR Couch Aii	a 1496kW b 1459kW c 1650kW	1535kW	3786kW	3345kW	74%/12%
T8 NFR Couch Aiii	a 1406kW b 1372kW c 1551kW	1443kW	3558kW	2813kW	64%/23%

Table 4.8: NFR Couch A Predicted Babrauskas Peak Heat Release Rates (a: 2018 25mm thick foam/fabric sample, 35kW/m^2; b: 2020 50mm thick foam/fabric, 50kW/m^2; c: 2020 repeat 50mm thick foam/fabric, 50kW/m^2)

rate for all tests when compared to the mass loss rate method with differences as high as 35% and 23% for tests 2 and 8 respectively. Furthermore, while there is apparent consistency of values within a given correlation, there is a large discrepancy, roughly 2200kW between predicted values of peak heat release rate for the two methods for this couch. In the case of the bench-scale correlation, values for peak heat release rate estimated for T2 NFR couch A:a are close to those for T2 NFR couch A:b and values from the full-scale predictions are all within roughly 200kW of one another. When these results are compared to one another or examined in conjunction with values of peak heat release rate determined using the mass loss rate method, however, neither of the correlations appears appropriate for the prediction of peak HRR for this type of furniture fire. Even considering the potential range of values of between 1372kW and 1650kW for peak heat release rate using the bench-scale method with different input parameters, values are significantly lower than the average value of 3709kW estimated using the full-scale correlation or 2937 KW using the MLR method for the NFR couch A fire tests.

Looking at Table 4.9 for the FR couch B tests, both bench- and full-scale Babrauskas correlations predict peak heat release rates that are very comparable to the peak heat release rate estimated using the mass loss rate method. Using the bench-scale method for tests 4 and 7 with input based on cone calorimeter testing of a 50mm thick sample under 50kW/m^2 incident heat flux, the highest input value, estimates of peak heat flux of 1541kW and 1525kW, respectively, are very comparable to those found using the mass loss

Furniture Type	Bench-Scale PHRR	Avg. PHRR Bench-Scale	PHRR Full-Scale	MLR PHRR	% Diff to MLR PHRR (bench/full)
T4 FR Couch Bi	a 1169kW b 1212kW c 1541kW	1308kW	1619kW	1557kW	17%/4%
T7 FR Couch B Bii	a 1158kW b 1200kW c 1525kW	1294kW	1602kW	1453kW	12%/10%

Table 4.9: FR Couch B Predicted Babrauskas Peak Heat Release Rates (a: 2018 25mm thick foam/fabric sample, 35kW/m^2; b: 2020 50mm thick foam/fabric, 50kW/m^2; c: 2020 repeat 50mm thick foam/fabric, 50kW/m^2)

rate method. In assessing results from the full-scale correlation, it is important to note that the fabric factor was adjusted downward in value to 0.42 from the original value of 1 recommended for thermoplastic fabrics due to the presence of FR in the fabric in couch B. The full-scale method, with the above adjustment, predicts only slightly larger peak heat release rates compared to the mass loss rate method. In contrast, when the original fabric factor of 1 was used, the predicted peak heat release rates for Tests 4 and 7 were 3856kW and 3817kW, respectively, 2.5 times the peak heat release rate calculated by the mass loss rate method and very close in magnitude to the values estimated for the NFR couch A fires. This highlights an acknowledged potential limitation in these correlation methods in terms of their ability to appropriately account for differences in fire growth between NFR, FR and even newer materials, and provides reason for further investigation into the development of more updated factors that might better account for fire behaviour of modern materials [110]. That an adjustment of 0.42 might be appropriate is this case is supported here by the fact that the overall range of values for peak heat release rate in the FR couch B fires was from 1158kW - 1541kW based on bench-scale correlations, very comparable to to the average value of 1500kW for the MLR method and 1611 kW using the adjusted full-scale correlations.

In reference to Table 4.10, both of the Babrauskas correlation methods under-predict values of peak heat release rate in comparison to values determined using the mass loss rate method, with the bench-scale method providing significantly worse predictions than the full-scale method. Similar to results tabulated for NFR couch A fires, peak heat release rate values predicted by the two correlation methods vary greatly, with values from the full-scale method being 560kW - 600kW higher than those from the bench-scale method

Furniture Type	Bench-Scale PHRR	Avg. PHRR Bench-Scale	PHRR Full-Scale	MLR PHRR	% Diff to MLR PHRR (bench/full)
T3 LFR Couch Ci	a 662kW d 849kW e 754kW	755kW	1324kW	1652kW	75%/22%
T6 LFR Couch Cii	a 708kW d 908kW e 806kW	807kW	1416kW	1660kW	69%/16%
T9 LFR Couch Ciii	a 660kW d 847kW e 752kW	753kW	1320kW	2786kW	115%/71%

Table 4.10: LFR Couch C Predicted Babrauskas Peak Heat Release Rates (a: 2018 25mm thick foam/fabric, 35kW/m^2; d: 2020 50mm thick foam/fabric, 35kW/m^2; e: 2020 repeat 50mm thick foam/fabric, 35kW/m^2)

for all three tests. The overall range of values for peak heat release rate for LFR couch C fires based on the bench-scale correlation range from 660kW to 908kW, in comparison to an average value from the full-scale correlation of 1353kW and much higher 2030kW for the MLR method.

The differences in values observed for LFR couch C fires could again relate to the applicability of the fabric factor. As with the FR polyester in the case of FR couch B, the fabric factor of 0.4 originally recommended for cotton fabrics may not be representative of, thus entirely appropriate for, the newer modern cotton covering fabric used in the LFR C couches here. For example, when a fabric factor of 0.5 is used instead of 0.4, predicted values become very comparable to those estimated from measured mass loss rates for tests 3 and 6 as they are 1655kW and 1769kW, though the value of 1650kW for test 9 still deviates from the apparently high value measured using the MLR method for that test.

It was also observed that the average heat release rate values for the couch C specimens were relatively lower as compared to the values of heat release determined for the other couch material samples and did not appear representative of how a combined fabric and polyurethane foam composite sample would be expected to contribute to overall heat release rate, and also to the characteristics of the fires observed, in the full-scale fire tests. The cotton fabric tended to char on the surface, so in the bench-scale tests, particularly in the early stages, it is thought that the fabric may drive too much of the burning behaviour, such that a thicker sample of foam is actually required to make a small-scale specimen that

is more representative of the full-scale couch. Alternately, the sample may need to be tested under a higher incident heat flux or results may need to be averaged over a longer period of time than 180s after ignition to obtain more representative average bench-scale heat release rate values to use as input parameters in the correlation.

Interestingly, both Babrauskas correlations predict that the LFR couch C would have the lowest overall peak heat release rates of all furniture types. While this is, in part, due to the low values of the averaged heat release rate over 180s after ignition, it is also because the mass factors for these tests are the smallest, only about 15.5kg compared to 18kg for couches NFR A and FR B. The foam used in the LFR couch C construction was a lighter density foam, and the cotton fabric was lighter than the polyester fabric (refer to Table 3.1 in Chapter 3) resulting in lighter overall furniture items. That this might affect used of the correlation to predict heat release rate for the LFR couches is consistent with limitations that were discussed [96, 120] for other predictive methods for furniture as part of the CBUF project [9] - that there can be an over-dependence on the mass of the sample in a generalized correlation, particularly when the estimation involves scaling from bench-scale cone calorimeter values to full-scale behaviour in furniture fires.

To summarize, in this section values of peak heat release rate determined using the mass loss rate method were compared against those determined based on bench- and full-scale correlations. Consistency between flame structure, heat release rate values and heat flux measurements suggested these values would provide reasonable reference values for comparison. In most cases, the bench-scale correlation presented in this section [110] results in under-predictions of the peak heat release rate for the present furniture fires, while the full-scale method [111] over-predicts the peak heat release rate when compared to values calculated using the mass loss rate method. The exception is in the full-scale method for the fires of LFR couch C, which also leads to under-prediction of peak heat release rate when compared to the mass loss rate method.

Differences in these predictive correlations can be attributed to several different causes. The first relates to how well the cone calorimeter inputs truly represent the burning behaviour of a given couch material in the full-scale fire. In addition, the fabric and padding factors in the correlations need to be adjusted for modern furniture materials, and the dependence of the correlations on the mass of the full-scale couch, without more detailed consideration of materials involved or the area of the fire burning over time, needs to be examined in more detail.

Specific to these limited ventilation fires, all of the previous correlations were developed for furniture under well-ventilated burning conditions and therefore do not account for any relationship between the development of the fire and the materials burning, the combustion

processes and the ventilation state in the fire environment. An example of this was seen in Test 9, where the smoke layer and fire plume appeared to oscillate, a phenomenon that was picked up by the load cells and therefore was reflected in the values of peak heat release rate which grew to higher values compared to the other LFR couch C fires. Such environmental interactions are not accounted for in global correlations, making it important to consider the implications of using such correlations to predict peak heat release rate in some compartment fire scenarios. Finally, the predictive correlations in this section do not provide any indication of the burning history of the fire, so although an estimation of the peak heat release rate might be possible, time-resolved heat release rate curves are often much more valuable from perspectives of both understanding fire physics and similarly designing for real fire exposures. Therefore, the strength of these predictive equations lies in the fact that they are easy to use and often applicable to general furniture fires based on broad-spectrum characteristics; however, this is at the expense of ability to account for complex physical interactions that take place as part of the local combustion processes and the ensuing global fire environment.

Babrauskas's correlations set a high standard for predicting full-scale peak heat release rate of furniture fires, considering that this work was done experimentally and before computers were able to handle any larger models that might allow more complex inputs related to fuel configuration, compartment characteristics and fire growth. Here, it provided a strong foundation for continued work. Adapting some aspects from the bench-scale correlations, a different cone extrapolation method, developed for estimation of heat release rate as part of this work, is introduced in the next Section.

4.5.4 Cone Extrapolation Method

In this final section, calculations of peak heat release are made for each of the present couch fires using the cone extrapolation method outlined in Section 3.2.4 [104] and according to Equation 3.7. For this, the area of the fire at peak heat release rate was taken as 1.58m^2, as previously discussed. Values for the effective heats of combustion for couches NFR A, FR B and LFR C, respectively, were taken as 17.5MJ/kg, 11.9MJ/kg and 16.5MJ/kg. Finally, values of effective mass loss rate were determined based on values of the effective heats of gasification of 1250kJ/kg, 1000kJ/kg and 1111 kJ/kg for couches NFR A, FR B and LFR C respectively, combined with three different values of net heat flux, q''_f, of 110kW/m^2, 120kW/m^2 and 130kW/m^2 back to the surface of the couches. Calculated values of effective mass loss rate for each value of net heat flux with corresponding values of peak heat release rate, labelled as PHRR are tabulated for each furniture type in Table 4.11.

Furniture Type	Net Heat Flux (kW/m^2)	Effective Mass Loss Rate ($kg/s\ m^2$)	Predicted PHRR (kW)
NFR A	100	0.088	2430
	120	0.096	2650
	130	0.104	2870
FR B	100	0.110	2570
	120	0.120	2800
	130	0.130	3040
LFR C	100	0.099	2070
	120	0.108	2260
	130	0.117	2450

Table 4.11: Predicted Peak Heat Release Rates Using Cone Extrapolation Method

As seen in the table above, the values of net heat flux as estimated based on values in [115], resulted in both underestimated (NFR couch A) and overestimated (FR couch B and LFR couch C) values of peak heat release rate for the present fires in comparison to values calculated with the mass loss rate method.

In making these comparisons, it should be noted that a limitation in the method as applied here lay in interpretation of the multi-stage mass loss rate per unit area values that characterized the test data from the cone calorimeter for these materials. Using a peak value of mass loss rate appeared to be most appropriate in determining values for heat of gasification of the materials based on comparative values in the literature and supported by the assumption that soon after the foam was subjected to the irradiance by the cone heater/fire, it would vaporize and ignite. Whether this is the equivalent process in the full scale fire is unknown, so without better knowledge of the detailed mechanisms by which the material burns at large-scale, incorrect values of mass loss may be selected and carried through the calculations as well.

In any case, since both measured and estimated values of mass loss were available for the present tests, it was interest to determine which values of net heat flux would result in values of effective mass loss rate and predicted peak heat release rate that matched those measured in the actual fires. For NFR couch A, when the net heat flux was increased to a value of $152kW/m^2$, the effective mass loss rate was $0.122kg/s\ m^2$ (comparable to the mass loss rate per area of the couch: 0.191kg/s mass loss rate at $1.58m^2$ is $0.121kg/s\ m^2$) and predicted peak heat release rate was 3360kW, a value comparable to 3345kW calculated with the mass loss rate method. For FR couch B, the net heat flux was decreased to a

value of 82.5kW/m^2, resulting in an effective mass loss rate of 0.083kg/s m^2 (comparable to the couch mass loss rate per area: 0.130kg/s mass loss rate at 1.58m^2 is 0.083kg/s m^2) and predicted peak heat release rate was 1556kW, again comparable to the value of 1557kW calculated with the mass loss rate. Lastly, for LFR couch C when the net heat flux was set to a value of 72kW/m^2, the effective mass loss rate decreased to 0.065kg/s m^2 (comparable again to the couch mass loss rate per area, 0.101kg/s mass loss rate at 1.58m^2 is 0.064kg/s m^2) and predicted peak heat release rate was 1685kW close to the value of 1660kW calculated with the mass loss rate method. The variance in this value required to match predicted and measured values of peak heat release rate across the different fires highlights the dependence and importance of this value for estimation of heat release rates in full-scale furniture fires. The difficulty in selecting an appropriate input value for this variable is clear from the present calculations, and if there is no benchmark mass loss rate data for a comparable fire situation to the one of interest choice of value becomes a judgement call on the part of the person trying to apply the method. The comparison here indicates that extreme caution should be used when attempting to apply this equation in a fire safety design or set of hazard calculations. These calculations could potentially be refined to some degree by incorporation of the ventilation corrections derived by Tewarson [104], but only if the change of ventilation over time in the large-scale compartment is also known. Due to these concerns, this method appears most applicable for determination of a singular peak value of heat release rate, as the net heat flux over time would be even more difficult to determine in a real fire. Improving the method and determining a way to adjust the calculations in order to predict time-resolved heat release rate curves would certainly be beneficial and would provide important information for more comprehensive hazard assessment or fire safety design.

4.6 Summary

Differences in peak heat release rate, time to reach peak heat release rate, fire areas and spreading behaviour between different couches result from the combined impacts of differences in couch materials, FR treatments, fabric types, smoke layer development, smoke layer interaction with the plume and ventilation conditions in the fires. Across the various methods and aligned with measured values of heat release rate, the highest predicted heat release rates were consistently determined for NFR couch A fires, followed by those on LFR couch C and FR couch B, except in the case of the Babrauskas correlations wherein LFR couch C fires led to the lowest overall predicted peak heat release rate value. Peak heat release rates for NFR couch A fires were roughly 3MW, FR couch B fires were around

1.5MW and LFR couch C fires were about 1.6MW (with the exception of test 9 which was 2.8MW).

Results demonstrate that time-resolved curves of fire heat release rate provide much more information than a single peak value, as the curves provide insight into the early development, growth and decay the fires. Predicted heat release rates based on the Heskestad correlation aligned with values of heat release rate calculated based on measured values of mass loss rate up until a certain time for each test. This point corresponded with when the fire had grown to be the size of the first cushion, the smoke layer was descending and growing thicker within the compartment, oxygen levels were steadily decreasing and the flame height was approaching ceiling height. For all couches, due to the flame spread mechanisms, an effective diameter was a more appropriate input than a measured width across the base of the fire and resulted in more comparable measurements of the peak heat release rate when compared to the mass loss rate method. The exception was in the LFR couch C fire, since at peak heat release rate, the full width of the couch was involved that input predicted relatively better heat release rates. In all cases, regardless of the input for fire diameter used, the correlation significantly under-predicted the fire heat release rate as the fire grew and conditions in the compartment degraded.

Scaling from small-scale cone calorimeter results to predict heat release rates in large-scale fires is very difficult. The extrapolation method from cone calorimeter data outlined in this research can be adjusted to produce comparable results to those obtained based on measured values of mass loss rate. However, the method is not particularly feasible without a-priori information on fuel mass loss rates or fire areas. Difficulty comes in attempting to relate the experimentally obtained parameters across scales; without having any large-scale data, it is very difficult to account for the complex physics occurring in a real fire using only inputs derived from the small-scale tests.

To address the two important questions posed in the beginning of Chapter 2:

- which method is most appropriate for prediction of heat release rate for a given fuel source and fire environment, and
- out of the available methods which incorporate different input parameters, which input parameters are most important to most accurately represent the physics and chemistry present in a given fire environment?

Particularly for a compartment fire environment that is changing significantly with time, as was the case for these fires as they progressed through well-ventilated to ventilation-limited modes of burning, methods which incorporate parameters that are a reflection

of the environment produce results that can be interpreted with more confidence. This would include the mass loss rate method due to the incorporation of changing values as the fire grows and fire environment changes. Heskestad's correlation predicts fire heat release rates quite well in the early stages of the fire if fire growth rate is known to allow estimation of time-varying fire height and diameter. Although there are inherent challenges with acquiring large-scale data, and overcoming difficulties due to smoke filling of the fire compartment, obtaining more reliable large-scale data with respect to flame spread and flame area progression in different fire situations would be extremely beneficial since use of these more detailed inputs will result in more accurate heat release rate calculations over the longer term.

Predicting full-scale fire heat release rate is very challenging, even though there is a strong foundation of work to build upon. It was clear from the present results that conducting a large number of ventilation-limited furniture fires with various types of modern furniture could be extremely valuable in refining input factors into simpler correlations such as those of Babrauskas to render these predictive correlations more accurate for estimation of peak heat release rates that might occur in modern furniture fires. Moreover, using cone calorimeter mass loss rate and heat flux curves to determine the parameters used to predict peak heat release rate values, given a particular magnitude of heat flux to the fuel surface is a viable way to scale a peak heat release rate value from bench-scale outputs to a large-scale prediction. With this method however, it is important to state that knowledge of time-dependent fire growth, and thus burning area, is crucial to combine appropriate inputs for mass loss rate, net heat flux, heat of gasification and heat of combustion for appropriately calculating fire heat release rate.

Chapter 5

Conclusions and Recommendations

To conclude, the two main objectives of this research were:

1. to further understanding of the evolution of a ventilation-limited fire environment in a multi-compartment, multi-storey structure and investigate how this environment impacts the fire growth and development, smoke and oxygen movement, as well as heat release rate and generation combustion products, and;

2. to compare a selection of available methods for the calculation of fire heat release rate to explore the application of these methods in a ventilation-limited furniture fire scenario.

The progression of fires from initially well ventilated situations to ventilation-limited environments was explored through compilation of thermal, radiative, gas concentration and velocity data for three representative furniture fires. The furniture items used in the experiments each represented a furniture standard from the UK, US and Europe, with varying amounts of fire-retardant additives. Differences in the overall fire behaviour, and by extension nature of the environment and heat release rates, were compared across test scenarios and found to result from both ventilation conditions and material combinations in the furniture.

Five calculation methods were used to estimate the heat release rate of the furniture fires in these ventilation-limited environments selected from a pool of existing methods; the t^2 fire growth rate, mass loss rate method [13], Heskestad's flame height correlation [31], Babrauskas's correlations [110, 111] and the cone extrapolation method [104]. These methods were selected as they are widely used by researchers and engineers to calculate

heat release rates for design fires, represent a cross-section of methods based on combined physical and chemical derivations for the input parameters, and cover various ways in which predictive equations have previously been determined, such as theoretical-analytical, experimental-analytical and experimental-correlational methods.

It is clear from the present results that predicting heat release rate and evolution of the environment in full-scale fires established on real furniture items is very challenging. To address the two important questions posed in the beginning of Chapter 2; however, this work has illustrated that use of methods which incorporate parameters that reflect the dynamic and ever-changing environment of a fire will lead to more reliable results particularly for environments that are progressing from well-ventilated to ventilation-limited modes of burning. The mass loss rate method incorporates a variable which change as the fire grows according to the changing environment, namely time variations in mass loss rate. Heskestad's correlation predicts heat release rate well in the early stages of the fire with use of time-varying fire height and diameter inputs. Although there are inherent challenges in acquiring appropriate large-scale data to better understand these characteristics due to difficulties around making measurements in full-scale fires, smoke filling of real fire compartments and determination of flame heights and areas, use of better inputs will result in more accurate heat release rate calculations over the longer term.

The next two sections contain key conclusions on the nature of the ventilation-limited fire environments and heat release rate calculation methods studied in the course of this research. These are followed by a brief outline of the potential impact of the results on tenability and egress to highlight the importance of this type of experimental work, which directly relates to the recommendations for future work.

5.1 The Ventilation-Limited Environment

In the present research, it was found that a crucial step in understanding differences in fire growth, furniture burning characteristics and the developing ventilation-limited fire environment was to conduct a detailed look at specific burning behaviours of each type of furniture through use of video footage taken from four camera angles during each fire.

Oxygen levels within the structure decreased between 3%-9% volume depending on the sensor location (main floor or second floor) and the furniture type. Ventilation-limited compartment environments resulted from the fires on all three couches in the airtight burn house configuration, with doors and windows sealed. In all fires, oxygen was depleted from the living (burn) room first, then the other main floor compartment (main floor SW room),

and finally the second floor compartment. The draw of oxygen from the second floor was further illuminated through velocity profiles measured at the bottom of the staircase, where the counter-flow of hot fire gases and smoke flowing up and cooler ambient air flowing down the staircase increased in velocity as fire heat release rates peaked and minimum oxygen concentrations were reached on the second floor. Carbon monoxide concentrations reached values above 2000ppm-2500ppm in the living (burn) room even at 0.6m above the floor, with FR couches producing generally higher levels of CO than the other furniture materials.

As anticipated, measured temperatures followed trends seen in the fire heat release rate curves with time, in terms of growth to peak and subsequent decay. Values of temperature measured in the upper layer of the living (burn) room corresponded with the relative magnitudes of peak heat release rate for NFR couch A (high) and FR couch B (lower); while LFR couch C fire had the second highest heat release rates, but lower overall upper layer temperatures than the FR couch B fire. The slower progression of the couch C fire, as captured by the video footage and mirrored in the mass loss rate data, may have resulted in more mixing between the fire gases and cooler ambient air, leading globally to apparently lower overall temperatures. Temperature was vertically stratified from highest at the ceiling to coolest at the floor and higher in areas located closer to the fire. In general, temperatures were more uniform in the lower regions of compartments as well as in areas further away from the fire, due to mixing and entrainment as hot gases travelled away from the fire source.

Values of radiative fraction calculated using a point source estimated using the mass loss rate and effective heat of combustion, divided by the measured heat flux of the gauge, vary from the early stages of fire development to the later stages as the smoke layer develops. Over this period, estimated values oscillate but generally become greater and more comparable to documented χ values for large, sooty fires. Careful consideration of impacts combustion efficiency on this estimated value of radiative fraction were not possible with the current data set. Based on measured heat flux by a gauge positioned on one wall of the fire compartment, radiative contributions from the smoke layer and from the fire were estimated. These were different for the different furniture types and consistent with observed and known relationships between heat release rate, smoke production and smoke filling in the compartment. The comparison of radiation and heat flux across fires fuelled by the three furniture types highlighted the importance of incorporating smoke layer contributions into the overall radiative feedback during a compartment fire scenario.

The differences in the fire development between the three furniture types as conditions transitioned from well-ventilated to limited ventilation form not only a unique set of results, but also highlight the importance of forming much better understanding of the similarities and contrasts in air exchange, smoke layer development, smoke movement throughout the

structure, thermal development, radiative contributions and the impacts that the environment has on the heat release rate and fire progression for a variety of furniture types.

5.2 Heat Release Rate Methods

The mass loss rate method and cone extrapolation method with appropriate inputs for heat of gasification and net heat flux produced comparable results for the peak values of the heat release rates. The Babrauskas correlations did not estimate as credible values of peak heat release rate, most likely due to the modern materials involved in these fires being very different to the original materials that were used in development of the correlations, as well as assumptions inherent in use of simplified factors which cannot fully account for the complex physics taking place during burning of the different materials in a ventilation-limited compartment fire. Heskestad's correlation worked up to a point, and then did not produce comparable heat release rates as the fire deviated further away from the conditions by which the correlation was originally derived; namely a non-circular fuel bed, a high degree of in-depth combustion, smoke layer interactions with the fire plume and limited-ventilation.

Methods that incorporate experimentally obtained data in the calculation of heat release rate provide more confidence in predicted results, particularly for time-resolved curves of the heat release rate in the unique and changing environment in the present fires. Unfortunately, the necessary data is not always available. For example, the actual mass loss rate for each furniture type is inherently linked with oxygen depletion; as oxygen concentration decreased to a minimum in the living (burn) room, the peak heat release rate of the fire was observed, though the relation of this value of heat release rate to the same couch burning under well-ventilated conditions remains unknown.

This work highlights several important aspects pertaining to the calculation of heat release rate of furniture fires in ventilation-limited environments:

- It is important to assess existing methods for the calculation of heat release rate of available furniture, as furniture materials continue to change rapidly and therefore input parameters used in some correlations may be too far removed from those appropriate for prediction of heat release rates from modern furniture;
- It is important to ensure, or at least understand, how appropriate a selected method for calculation of heat release rate is for the fire environment of interest;

- Different furniture types, even those with similar generic base materials (polyurethane and polyester fabric) can result in very different fires, so it is important to consider specifics of the furniture materials when evaluating fire progression and heat release rate;
- Bench-scale data can be used to predict full-scale results but such predictions must be done with care, as mass loss rate per area measured in the cone calorimeter may not be directly extrapolated to a full-scale case. Nonetheless, using parameters in a predictive method that mirror changes seen in a full-scale environment, such as mass loss rate and area, is one way to capture characteristics of ventilation-limited full-scale fires relative to well-ventilated bench-scale characteristics, albeit requires information which may not be readily available; and
- Validation of any selected method for prediction of fire heat release rate against other methods with different input parameters is important for carrying out consistency checks and identifying potential limitations in the final estimated values.

As seen from these tests, the environment greatly impacts details of the fire growth and heat release rate as it changes with time. Compartment and furniture geometry further complicate use of prediction methods that were based simplified compartment geometries and physics best understood for a free-burning scenario. It is therefore important to choose an appropriate data set which aligns with the fuel and environmental conditions for successful prediction of fire heat release rates.

5.3 Tenability and Egress Implications

There are three main factors contributing to the overall hazard of a fire scenario; the heat release rate, smoke obscuration and smoke toxicity [97]. The heat release rate has an impact on the temperatures within the compartment in areas local and global to the fire and can be an indicator of fire events such as flashover. Smoke obscuration is spatially and time variant and can affect egress of the occupants [97]. Smoke toxicity governs the impacts from inhalation of harmful fire effluents. As building and furnishing materials change, it is important to keep these three aspects of fire hazard in mind and conduct research that builds upon the current understanding of the potential risks and outcomes of our changing built and living environments.

In terms of safety to the general populous, tenability limits are set to be the time between the discovery of a fire and until untenable conditions are reached [9]. Untenable

conditions can result from any combination of the above three factors, but are normally associated with high levels of CO, low levels of oxygen and high temperatures, all of which are, either in isolation or in conjunction, incompatible with human life. This points to the importance of determining the heat released by the fire, since this can cause burns and make breathing very difficult. The fire size is also important as once it grows too large it can become a barrier rendering egress impossible or it can promote rapid flame spread to other flammable surfaces. Coupled to fire size is the production of of smoke from the fire. Smoke particles (soot) can harm the eyes and cause visual obscuration which leads to disorientation and anxiety during escape. Hot particles and gases in the smoke are also detrimental to breathing as hot gases can harm airways, soot can partially obstruct airflow and increasing levels of toxic products and decreasing levels of oxygen make cardiopulmonary function increasingly difficult under prolonged exposure. As oxygen levels decrease and combustion becomes less efficient, the generation rate of incomplete combustion products increases, and due to the buoyancy of the fire plume and developing smoke layer, these harmful effluents are easily transported throughout a structure. Understanding the levels at which these effluents impact human physiology as well as development of appropriate ways to measure concentration of these toxic products, derive input and improve models, and interpret results in context of occupant safety are important areas of research within the fire safety community.

The low oxygen levels measured at a height of 0.6m above the floor in the present fires, particularly in conjunction with the high CO levels, are concerning from a human safety perspective since these can pose significant threat to the biological processes needed for bodily function and therefore can lead to incapacitation and death. Further, the concerning levels were measured in locations close to the floor, where traditionally there is thought to be relatively clean/fresh air. This preliminary data set therefore provides reason for further detailed investigation into the gaseous species present during ventilation-limited fires coupled to improved understanding of how exposure to multiple toxic gases might impact potential for occupant escape. In a broad perspective, it may also demonstrate a need for re-evaluation of evacuation protocols and education for the general public in some modern fire scenarios. Building on the basis developed through this research, data from additional large fire tests will be integral to enhancing fire risk assessment with positive impact on building and occupant safety.

5.4 Recommendations for Future Work

With the strong foundation of work upon which to build, conducting a number of ventilation-limited furniture fires with various types of modern furniture could be extremely valuable in refining input factors to modify the Babrauskas correlations and rendering them more accurate for use in estimating peak heat release rates in modern furniture fires. Moreover, further investigation should be conducted to determine appropriate methods for scaling of cone calorimeter mass loss and heat release rate data, in conjunction with full-scale data on fire growth and burning area from experimental fires, and cross-checking results through corresponding information on rate of mass loss with time. In this, it should be noted that combining better estimates of fuel bed area with appropriate mass loss rate and heat of combustion input will be crucial for calculating comparable results.

5.4.1 Large-Scale Furniture Tests

The present large scale fire tests identified several sets of measurements as crucial to understanding the progression of global environment in the structure. Along with standard temperature measurements, these include improved video recording with specific camera placement and enhanced measurement of gas species data, smoke flow and heat flux from the smoke layer. Collecting more data with respect to the smoke flow throughout the different areas of the space in conjunction with the gas sensor data will provide valuable information regarding the safety of occupants. To address this, more dense instrumentation of the house is being carried out in readiness for another series of large-scale furniture fires to be conducted at the UW Fire Research Facility this summer. Boxes which contain electrochemical gas sensors for CO_2, CO, O_2, NO_x, HCN, HCl, VO_x, NH_3 and methane have been constructed and have been installed at heights of 1ft, 3ft and 6ft in eight locations throughout the structure to provide more detailed spatial and time-resolved data pertaining to the gaseous environment. Pressure transducers with co-located thermocouples have also been added throughout the space to measure velocity and smoke flow across the majority of opening in the structure. In addition to 9 probes at the bottom of the staircase, 9 have been added to the top of the stair case, 4 added to the opening from the staircase landing to the SW room on the second floor, and 2 have been added to all other door vents and windows at heights of 40% and 60% of the opening heights. Lastly, there are three heat flux gauges installed, two on the adjacent wall to the couch (one inline with the first cushion, and the second inline with the 3rd cushion) to measure heat flux from the fire, and thus estimate fire size, and one installed to better estimate the contribution of the smoke layer to radiation in the burn room as the fire develops.

5.4.2 Image Analysis Program

Several aspects of the image analysis program should be adapted to be more detailed and provide results to a higher degree of accuracy in future research. Firstly, the 8x8 pixel squares used to verify the edge of the fire was chosen as it was large enough to check pixels around the edge of the fire without compromising computational time. It was found that a larger box increased computation time exponentially, but the selected 8x8 pixel size may not be optimal. Further, it was found that more than 65% and less than 35% flaming pixels (GB average less than 10) in a box were good conditions to verify the edge in this program, however these thresholds may need to be adapted for different fires, at noted in the false heights determined early in the LFR couch C fires. Similarly, once the smoke layer interfered with the the fire plume, the program could no longer detect the tips or edges of the fire, leading to inaccuracies in estimates of both flame height and width. A different programming tool, or different colour-dependence in processing may be able to distinguish the intermittency of the flaming areas or detect the possible presence of flame behind the smoke layer. Alternately, an additional algorithm might be integrated into the program to extrapolate the height of the plume when it is momentarily obscured by smoke.

5.4.3 Point Source Radiation Inputs

Point source methods for calculating the radiative heat flux from the fire and smoke layer could be refined through modification of several assumptions made to simplify the calculations in the present work. In this research, a constant distance from the fire to the gauge was chosen, and the center of the fire was assumed to align with the gauge. In reality these distances vary with growth of the fire and descent of the hot smoke layer over time. Since the impact of the changes was not investigated here, it is recommended that these calculations be done again using time varying configuration factors which might better account for the changing angles between the center of the fire and the gauge as the fire spreads across the couch. In addition, more advanced camera placement and processing of images taken with several camera angles could be integrated with temperature data to better chart the fire geometry and depth of the smoke layer for the full duration of the test, even if one camera becomes obscured, as in the case of these tests. For estimates of heat flux using emissive power calculations, a better measurement of the temperature of the flame could be obtained by positioning thermocouples directly in the fire plume, which is also planned for the next large scale experimental series. This will provide real, time varying flame temperature data that can be used with more confidence than the present data in refined radiation heat flux calculations. Due to the convective flow of smoke and

ambient gases in front of the gauge, there is a need to also estimate the temperature very close to the position of the gauge. Attempting to account for the impacts of the convective flow into an analysis of the heat flux to the gauge would again help to make the radiative calculations more accurate.

5.4.4 Furniture Materials

The differences in cone calorimeter results for the composite furniture samples tested between 2018 and 2020 highlight the need for a longitudinal study on the impact of changes of foam and fabric materials on the fire properties over time, both in isolation and in combination. Moreover, it is imperative that more furniture characterization studies be done, to develop more insight into appropriate factors to use to account for fabric and padding, which may strengthen existing methods for the prediction of heat release rates in large scale fires using existing correlations and/or methods that employ input based on bench scale cone calorimeter data.

JOHN WILEY AND SONS LICENSE
TERMS AND CONDITIONS

Jun 03, 2020

This Agreement between Ms. Bronwyn Forrest ("You") and John Wiley and Sons ("John Wiley and Sons") consists of your license details and the terms and conditions provided by John Wiley and Sons and Copyright Clearance Center.

License Number	4841371049456
License date	Jun 03, 2020
Licensed Content Publisher	John Wiley and Sons
Licensed Content Publication	Fire and Materials
Licensed Content Title	Smoke development and movement during ventilation-limited fires in a multi-storey house
Licensed Content Author	Noah Ryder, Peter Senez, Matt DiDomizio, et al
Licensed Content Date	May 28, 2020
Licensed Content Volume	0
Licensed Content Issue	0
Licensed Content Pages	12

Type of use	Dissertation/Thesis
Requestor type	Author of this Wiley article
Format	Electronic
Portion	Figure/table
Number of figures/tables	11
Will you be translating?	No
Title	Smoke development and movement during ventilation-limited fires in a multi-storey house
Institution name	University of Waterloo
Expected presentation date	Jun 2020
Portions	Figures 1-11
	Ms. Bronwyn Forrest
Requestor Location	
	Attn: Ms. Bronwyn Forrest
Publisher Tax ID	EU826007151
Total	0.00 CAD
Terms and Conditions	

TERMS AND CONDITIONS

This copyrighted material is owned by or exclusively licensed to John Wiley & Sons, Inc. or one of its group companies (each a"Wiley Company") or handled on behalf of a society with which a Wiley Company has exclusive publishing rights in relation to a particular work (collectively "WILEY"). By clicking "accept" in connection with completing this licensing transaction, you agree that the following terms and conditions apply to this transaction (along with the billing and payment terms and conditions established by the Copyright Clearance Center Inc., ("CCC's Billing and Payment terms and conditions"), at the time that you opened your RightsLink account (these are available at any time at http://myaccount.copyright.com).

Terms and Conditions

- The materials you have requested permission to reproduce or reuse (the "Wiley Materials") are protected by copyright.

- You are hereby granted a personal, non-exclusive, non-sub licensable (on a stand-alone basis), non-transferable, worldwide, limited license to reproduce the Wiley Materials for the purpose specified in the licensing process. This license, **and any CONTENT (PDF or image file) purchased as part of your order,** is for a one-time use only and limited to any maximum distribution number specified in the license. The first instance of republication or reuse granted by this license must be completed within two years of the date of the grant of this license (although copies prepared before the end date may be distributed thereafter). The Wiley Materials shall not be used in any other manner or for any other purpose, beyond what is granted in the license. Permission is granted subject to an appropriate acknowledgement given to the author, title of the material/book/journal and the publisher. You shall also duplicate the copyright notice that appears in the Wiley publication in your use of the Wiley Material. Permission is also granted on the understanding that nowhere in the text is a previously published source acknowledged for all or part of this Wiley Material. Any third party content is expressly excluded from this permission.

- With respect to the Wiley Materials, all rights are reserved. Except as expressly granted by the terms of the license, no part of the Wiley Materials may be copied, modified, adapted (except for minor reformatting required by the new Publication), translated, reproduced, transferred or distributed, in any form or by any means, and no derivative works may be made based on the Wiley Materials without the prior permission of the respective copyright owner.**For STM Signatory Publishers clearing permission under the terms of the STM Permissions Guidelines only, the terms of the license are extended to include subsequent editions and for editions in other languages, provided such editions are for the work as a whole in situ and does not involve the separate exploitation of the permitted figures or extracts,** You may not alter, remove or suppress in any manner any copyright, trademark or other notices displayed by the Wiley Materials. You may not license, rent, sell, loan, lease, pledge, offer as security, transfer or assign the Wiley Materials on a stand-alone basis, or any of the rights granted to you hereunder to any other person.

- The Wiley Materials and all of the intellectual property rights therein shall at all times remain the exclusive property of John Wiley & Sons Inc, the Wiley Companies, or their respective licensors, and your interest therein is only that of having possession of and the right to reproduce the Wiley Materials pursuant to Section 2 herein during the continuance of this Agreement. You agree that you own no right, title or interest in or to the Wiley Materials or any of the intellectual property rights therein. You shall have no rights hereunder other than the license as provided for above in Section 2. No right,

license or interest to any trademark, trade name, service mark or other branding ("Marks") of WILEY or its licensors is granted hereunder, and you agree that you shall not assert any such right, license or interest with respect thereto

- NEITHER WILEY NOR ITS LICENSORS MAKES ANY WARRANTY OR REPRESENTATION OF ANY KIND TO YOU OR ANY THIRD PARTY, EXPRESS, IMPLIED OR STATUTORY, WITH RESPECT TO THE MATERIALS OR THE ACCURACY OF ANY INFORMATION CONTAINED IN THE MATERIALS, INCLUDING, WITHOUT LIMITATION, ANY IMPLIED WARRANTY OF MERCHANTABILITY, ACCURACY, SATISFACTORY QUALITY, FITNESS FOR A PARTICULAR PURPOSE, USABILITY, INTEGRATION OR NON-INFRINGEMENT AND ALL SUCH WARRANTIES ARE HEREBY EXCLUDED BY WILEY AND ITS LICENSORS AND WAIVED BY YOU.

- WILEY shall have the right to terminate this Agreement immediately upon breach of this Agreement by you.

- You shall indemnify, defend and hold harmless WILEY, its Licensors and their respective directors, officers, agents and employees, from and against any actual or threatened claims, demands, causes of action or proceedings arising from any breach of this Agreement by you.

- IN NO EVENT SHALL WILEY OR ITS LICENSORS BE LIABLE TO YOU OR ANY OTHER PARTY OR ANY OTHER PERSON OR ENTITY FOR ANY SPECIAL, CONSEQUENTIAL, INCIDENTAL, INDIRECT, EXEMPLARY OR PUNITIVE DAMAGES, HOWEVER CAUSED, ARISING OUT OF OR IN CONNECTION WITH THE DOWNLOADING, PROVISIONING, VIEWING OR USE OF THE MATERIALS REGARDLESS OF THE FORM OF ACTION, WHETHER FOR BREACH OF CONTRACT, BREACH OF WARRANTY, TORT, NEGLIGENCE, INFRINGEMENT OR OTHERWISE (INCLUDING, WITHOUT LIMITATION, DAMAGES BASED ON LOSS OF PROFITS, DATA, FILES, USE, BUSINESS OPPORTUNITY OR CLAIMS OF THIRD PARTIES), AND WHETHER OR NOT THE PARTY HAS BEEN ADVISED OF THE POSSIBILITY OF SUCH DAMAGES. THIS LIMITATION SHALL APPLY NOTWITHSTANDING ANY FAILURE OF ESSENTIAL PURPOSE OF ANY LIMITED REMEDY PROVIDED HEREIN.

- Should any provision of this Agreement be held by a court of competent jurisdiction to be illegal, invalid, or unenforceable, that provision shall be deemed amended to achieve as nearly as possible the same economic effect as the original provision, and the legality, validity and enforceability of the remaining provisions of this Agreement shall not be affected or impaired thereby.

- The failure of either party to enforce any term or condition of this Agreement shall not constitute a waiver of either party's right to enforce each and every term and condition of this Agreement. No breach under this agreement shall be deemed waived or excused by either party unless such waiver or consent is in writing signed by the party granting such waiver or consent. The waiver by or consent of a party to a breach of any provision of this Agreement shall not operate or be construed as a waiver of or consent to any other or subsequent breach by such other party.

- This Agreement may not be assigned (including by operation of law or otherwise) by you without WILEY's prior written consent.

- Any fee required for this permission shall be non-refundable after thirty (30) days from receipt by the CCC.

- These terms and conditions together with CCC's Billing and Payment terms and conditions (which are incorporated herein) form the entire agreement between you and WILEY concerning this licensing transaction and (in the absence of fraud) supersedes all prior agreements and representations of the parties, oral or written. This Agreement may not be amended except in writing signed by both parties. This Agreement shall be binding upon and inure to the benefit of the parties' successors, legal representatives, and authorized assigns.

- In the event of any conflict between your obligations established by these terms and conditions and those established by CCC's Billing and Payment terms and conditions, these terms and conditions shall prevail.

- WILEY expressly reserves all rights not specifically granted in the combination of (i) the license details provided by you and accepted in the course of this licensing transaction, (ii) these terms and conditions and (iii) CCC's Billing and Payment terms and conditions.

- This Agreement will be void if the Type of Use, Format, Circulation, or Requestor Type was misrepresented during the licensing process.

- This Agreement shall be governed by and construed in accordance with the laws of the State of New York, USA, without regards to such state's conflict of law rules. Any legal action, suit or proceeding arising out of or relating to these Terms and Conditions or the breach thereof shall be instituted in a court of competent jurisdiction in New York County in the State of New York in the United States of America and each party hereby consents and submits to the personal jurisdiction of such court, waives any objection to venue in such court and consents to service of process by registered or certified mail, return receipt requested, at the last known address of such party.

WILEY OPEN ACCESS TERMS AND CONDITIONS

Wiley Publishes Open Access Articles in fully Open Access Journals and in Subscription journals offering Online Open. Although most of the fully Open Access journals publish open access articles under the terms of the Creative Commons Attribution (CC BY) License only, the subscription journals and a few of the Open Access Journals offer a choice of Creative Commons Licenses. The license type is clearly identified on the article.

The Creative Commons Attribution License

The Creative Commons Attribution License (CC-BY) allows users to copy, distribute and transmit an article, adapt the article and make commercial use of the article. The CC-BY license permits commercial and non-

Creative Commons Attribution Non-Commercial License

The Creative Commons Attribution Non-Commercial (CC-BY-NC)License permits use, distribution and reproduction in any medium, provided the original work is properly cited and is not used for commercial purposes.(see below)

Creative Commons Attribution-Non-Commercial-NoDerivs License

The Creative Commons Attribution Non-Commercial-NoDerivs License (CC-BY-NC-ND) permits use, distribution and reproduction in any medium, provided the original work is properly cited, is not used for commercial purposes and no modifications or adaptations are made. (see below)

Use by commercial "for-profit" organizations

Use of Wiley Open Access articles for commercial, promotional, or marketing purposes requires further explicit permission from Wiley and will be subject to a fee.

Further details can be found on Wiley Online Library
http://olabout.wiley.com/WileyCDA/Section/id-410895.html

Other Terms and Conditions:

v1.10 Last updated September 2015

Questions? customercare@copyright.com or +1-855-239-3415 (toll free in the US) or +1-978-646-2777.

Bronwyn Forrest
15 Forestwood Dr.
Kitchener, ON
N2N 1A9

June 8th, 2020

Chris Jelenewicz
Technical Director
Society of Fire Protection Engineers
9711 Washingtonian Blvd. Ste 380
Gaithersburg, MD
20878

Dear Mr. Jelenewicz

I am a student at the University of Waterloo, and I am preparing my Master's thesis. I understand that you are the copyright holder for two of the configuration factor schematics included in Figure D-7 and Figure 3-5.5 published in the SFPE Handbook of Fire Protection Engineering (3rd Edition).

I would like permission to include these two view factor schematics (specifically "plane element dA 1 to plane parallel rectangle; normal to element passes through corner of rectangle" and "plane element dA 1 to rectangle in plane 90° to plane of element") as part of Figure D-7 and Figure 3-5.5 in my thesis which will be made available open access in the University of Waterloo institutional repository UWSpace. Proper citation will be included with the reproduction of these figures.

If you agree to provide me with permission, please confirm by completing and returning the acknowledgement included on page two, to the address above.

If you do not hold the copyright for this material, or the right to grant this type of permission, I would greatly appreciate any information you can provide to me regarding the rights holder(s), including any contact information.

Thank you for considering this request,

Bronwyn Forrest

Title of thesis	Heat Release Rate in Ventilation-Limited Furniture Fires

Permission is granted to: _Bronwyn Forrest_____,
(Author the above mentioned work)
to reproduce the following in the manner described below.

Title of Article/Book:	SFPE Handbook of Fire Protection Engineering
Figure or Page Numbers:	D-7 (pp. A-46) and 3-5.5 (pp. 3-168)
Journal Name, Year, Volume Number:	Third Edition
Book place, Publisher, Year:	NFPA
Intended use:	In my thesis that will be made available open access in the University of Waterloo institutional repository UWSpace.

As copyright holder or representative of the copyright holder(s), I have authority to grant permission for the use requested above and I grant permission for the use requested above.

Full Name and Address:	Chris Jelenewicz SFPE 9711 Washingtonian Blvd. Suite 380 Gaithersburg, MD 20878
Position/Title:	Technical Director
Date:	7/7/20
Signature:	

References

[1] J. Quintiere, *Chapter 5: Compartment Fire Modelling, in Section 3: Hazard Calculations*. National Fire Protection Association, 3rd ed., 2002.

[2] B. Forrest, E. Weckman, M. DiDomizio, P. Senez, and N. Ryder, "Smoke development and movement during ventilation-limited fires in a multi-storey house," *Fire and Materials*, 2020.

[3] *Appendix D: Configuration Factors*. National Fire Protection Association, 3rd ed., 2002.

[4] "Statistics Canada Insurance Bureau of Canada and the Conference Board of Canada: Fort McMurray 2016 Wildfire Economic Impact," 2017.

[5] "BBC News: Grenfell Tower fire mental health treatment to cost 10 million pounds," 2018.

[6] "Office of the Ontario Fire Marshal. Fire Losses: Causes, Trends, Issues 2014-2016," 2018.

[7] J. A. de Boer, "Fire and furnishing in building and transport, statistical data on the existing situation in europe," *Fire and Furnishing in Buildings and Transport Conference proceedings, 6-8 November, Luxemborg*, pp. 1–14, 1990.

[8] "Fire statistics in canada, selected observations from the national fire information database 2005 to 2014," 2017.

[9] B. Sundstrom, S. Grayson, and P. Van Ness, "Short communication: An overview of the findings of the combustion behaviour of upholstered furniture project*," *Fire and Materials*, vol. 20, pp. 205–211, 1996.

[10] "UL Firefighter Safety Research Institute: Comparison of Modern and Legacy Home Furnishings," 2005.

[11] B. Karlsson and J. Quintiere, *Enclosure Fire Dynamics*. CRC Press LLC, 2000.

[12] S. Grayson, *Heat Release in Fires*. Elsevier Science Publsihers, 1992.

[13] A. Tewarson, "Heat release rate in fires," *Fire and Materials*, vol. 4, no. 4, pp. 185–191, 1980.

[14] C. Hopkin, M. Spearpoint, and D. Hopkin, "A review of design values adopted for heat release rate per unit area," *Fire Technology*, vol. 55, pp. 1599–1618, 2019.

[15] J. Torero, A. Majdalani, C. Abecassis, and C. A., "Revisiting the compartment fire," pp. 28–45, 2014.

[16] M. Janssens, *Heat Release in Fires*. Elsevier Science Publishers, 1992.

[17] G. Heskestad, *Fire Plumes, Flame Height and Air Entrainment*. Qunicy MA, National Fire Protection Association and Society of Fire Protection Engineers, 3rd edition ed., 2002.

[18] P. DiNenno and R. Custer, eds., *Design Calculations: Design of Detection Systems*. Quincy, Mass; Bethesda, Md.: National Fire Protection Association, 2002.

[19] B. Karlsson and J. Quintiere, *Enclosure Fire Dynamics*. CRC Press LLC, 2000.

[20] W. Thornton, "The relation of oxygen to the heat of combustion of organic compounds," *Philosophical Magazie and Journal of Science*, vol. 33, no. 196, 1917.

[21] C. Huggett, "Estimation of the rate of heat release by means of oxygen consumption," *Journal of Fire and Flammability*, vol. 12, 1980.

[22] M. Janssens and W. Parker, *Chapter 3: Oxygen Consumption Calorimetry in, Heat Release in Fires*. Elsevier Science Publsihers, 1992.

[23] N. Thompson and E. Cousins, "The FM Construction Materials Calorimeter," technical report, National Fire Protection Association, 1959.

[24] V. Babrauskas, *Chapter 2: From Bunsen Burner to Heat Release Rate Calorimeter, in: Heat Release in Fires*. Elsevier Science Publsihers, 1992.

[25] E. Zukoski, B. Cetegen, and T. Kubota, "Visible structure of buoyant diffusion flames," *20th Int'l Symposium on Combustion, The Combustion Institute*, pp. 361–366, 1984.

[26] H. Becker and L. D., "Visible length of vertical free turbulent diffusion flames," *Combustion and Flame*, vol. 32, pp. 115–137, 1978.

[27] P. Thomas, "The size of flames from natural fires," *Proceedings of the 9th International Symposium on Combustion*, pp. 844–860, 1963.

[28] F. Steward, "Prediction of the height of turbulent diffusion buoyant flames," *Combustion Science and Technology*, vol. 2, pp. 203–212, 1970.

[29] G. Heskestad, "Luminous heights of turbulent diffusion flames," *Fire Safety Journal*, vol. 5, pp. 103–108, 1983.

[30] E. Zukoski, T. Kubota, and B. Cetegen, "Entrainment in fire plumes," *Fire Safety Journal*, vol. 3, pp. 107–121, 1980.

[31] G. Heskestad, "on q* and the dynamics of turbulent diffusion flames," *Fire Safety Journal*, vol. 30, pp. 215–227, 1998.

[32] D. Drysdale, *An Introduction into Fire Dynamics*. John Wiley and Sons, Ltd., 3rd edition ed., 2011.

[33] G. Heskestad, "Engineering relations for fire plumes," *Fire Safety Journal*, vol. 7, pp. 25–32, 1984.

[34] A. Modak, "Thermal radiation from pool fires," *Combustion and Flame*, vol. 29, pp. 177–192, 1977.

[35] J. de Ris, "A scientific approach to flame radiation and material flammability," *Fire Safety Science, Proceedings of the 2nd Int'l Symposium*, pp. 29–46, 1988.

[36] J. de Ris, "Fire radiation- a review," *Seventeenth Int'l Symposium on Combustion*, pp. 1003–1015, 1979.

[37] D. Drysdale, *An Introduction into Fire Dynamics*. John Wiley and Sons, Ltd., 3rd edition ed., 2011.

[38] K. Mudan, "Geometric view factors for thermal radaition hazard assessment," *Fire Safety Journal*, vol. 12, pp. 89–96, 1987.

[39] G. Markstein, "Relationship between smoke point and radiant emission from buoyant turbulent and laminar diffusion flames," *Twentieth Int'l Symposium on Combustion.*

[40] J. Gore, M. Klassen, A. Hamins, and T. Kashiwagi, "Fuel property effects on burning rate and radiative transfer from liquid pool flames," *Fire Safety Science, Proceedings of the 3rd Int'l Symposium*, pp. 395–404, 1992.

[41] D. Burgess and M. Hertzberg, *Radiation from Pool Flames, in Heat Transfer in Flames.* John Wiley, New York, 1974.

[42] H. Koseki and T. Yumoto, "Air entrainment and thermal radiation from heptane pool fires," *Fire Technology*, pp. 33–47, 1988.

[43] R. Buch, A. Hamins, K. Konishi, D. Mattingly, and T. Kashiwagi, "Radiative emission fraction of pool fires burning silicone fluids," *Combustion and Flame*, vol. 108, pp. 118–126, 1997.

[44] G. Santo and F. Tamanini, "Influence of oxygen depletion on the radiative properties of pmma flames," pp. 619–631, 1981.

[45] NIST, "Fire dynamics," 2018.

[46] B. Karlsson and J. Quintiere, *Enclosure Fire Dynamics.* CRC Press LLC, 2000.

[47] J. Fang and J. Breese, "Fire development in residential basement rooms," technical report, National Bureau of Standards, 1980.

[48] S. Michaletz and E. Johnson, "How forest fires kill trees: A review of the fundamental biophysical processes," *Scandinavian Journal of Forest Research*, vol. 22, 2007.

[49] H. Emmons, *Chapter 3: Vent Flows, in Section 2: Fire Dynamics.* National Fire Protection Association, 3rd ed., 2002.

[50] R. Alpert, "Calculation of response time of ceiling-mounted fire detectors," *Fire Technology*, vol. 8, pp. 181–195, 1972.

[51] Y. Utiskul, *Theoretical and Experimental Study on Fully-Developed Compartment Fire.* PhD thesis, 2006.

[52] R. Blevins, *Chapter 4: Dimensional Analysis in, Applied Fluid Dynamics Handbook.* Van Nostrand Reinhold Company, 1984.

[53] Y. Utiskul, J. Quintere, A. Rangwala, B. Ringwelski, K. Watatsuki, and T. Naruse, "Compartment fire phenomena under limited ventilation," *Fire Safety Journal*, vol. 40, pp. 367–390, 2005.

[54] H. Takeda and Z. Akita, "Critical phenomena in compartment fires with liquid fuels," 1981.

[55] Q. He, O. Ezekoye, C. Li, and S. Lu, "Ventilation-limited extinction of fires in ceiling vented compartments," *International Journal of Heat and Mass Transfer*, vol. 91, pp. 570–583, 2015.

[56] "International standard for fire testsfull-scale room test for surface products," standard, International Organization for Standardization (ISO), Switzerland, 1993.

[57] G. Andrews, J. Ledger, and H. Phylaktou, "Enclosed pool fires in low ventilation enclosures: Flame temperatures and global heat loss using gas analysis," *Fire Safety Science - Proceedings of the Sixth International Symposium*, pp. 591–602.

[58] E. Yii, C. Fleischmann, and A. Buchanan, "Experimental study of fire compartment with door opening and roof opening," *Fire and Materials*, vol. 29, pp. 315–334, 2005.

[59] O. Aljumaiah, G. Andrews, H. Phylaktou, B. Mustafa, H. Al-Qattan, and V. Shah, "Air-starved wood crib compartment fire heat release rate and toxic gas yeilds," *Fire Safety Science, Proceedings of 10th International Symposium*, pp. 1263–1276, 2011.

[60] A. Nasr, S. Suard, H. El-Rabii, J. Garo, L. Gay, and L. Rigollet, "Heat feedback to the fuel surface of a pool fire in an enclosure," *Fire Safety Journal*, vol. 60, pp. 56–63, 2013.

[61] W. Pitts, "The global equivalence ratio concept and the formation mechanisms of carbon monoxide in enclosure fires," *Progress in Energy and Combustion Science*, vol. 21, pp. 197–237, 1995.

[62] C. Beyler, *Development and burning behaviour of a layer of products of incomplete combustion generated by a buoyant diffusion flame*. PhD thesis, Harvard University, Boston, United States, 1983.

[63] B. Forell and D. Hoser, "The relationship between ventilation conditions and co source term in fully developed compartment fires," pp. 825–835, 2007.

[64] D. Gottuck, R. Roby, and C. Beyler, "A study of carbon monoxide and smoke yields from compartment fires with external burning," pp. 1729–1735, 1992.

[65] S. Ukleja, M. Delichatsios, M. Delichatsios, and J. Zhang, "Smoke concentrations inside and outside of a corridor-like enclosure," *Fire Safety Journal*, vol. 60, pp. 37–45, 2013.

[66] S. Ukleja, M. Delichatsios, J. Zhang, and M. Suzanne, "Carbon monoxide production during underventilated fires in corridors," pp. 316–330, 2014.

[67] P. Blomqvist and A. Lonnermark, "Characterization of the combustion products in large-scale fire tests: comparison of three experimental configurations," *Fire and Materials*, vol. 25, pp. 71–81, 2001.

[68] W. Fitzgerald, "Quantification of fires: 1. Energy kinetics of burning in a dynamic room size calorimeter," *Fire and Flammability*, vol. 9, pp. 510–525, 1978.

[69] W. Fitzgerald and M. Kanakia, "Calorimetric evaluation of the role of fire retardants in selected polymers," 1978.

[70] W. Le Saux, H. Pretrel, C. Lucchesi, and P. Guillou, "Experimental study of the fire mass loss rate in confined and mechanically ventilation multi-room scenarios," *Fire Safety Science*, vol. 9, pp. 943–954, 2009.

[71] A. Coppalle, J. Garo, G. Mitanchez, P. Jourda, and F. Gaviot-Blanc, "Underventilated compartment fires: A full scale test with wood pallets," *Fire Safety Science, Proceedings of the 10th International Symposium*, pp. 1501–1512, 2011.

[72] H. Pretrel, P. Querre, and M. Forestier, "Experimental study of burning rate behaviour in confined and ventilated fire compartments," *Proceedings of the 8th Intl Fire Safety Science Symposium*, pp. 1217–1228, 2005.

[73] H. Pretrel and J. Such, "Effect of ventilation procedures on the behaviour of a fire compartment scenario," *Nuclear Engineering and Design*, vol. 235, pp. 2155–2169, 2005.

[74] M. Peatross and C. Beyler, "Ventilation effects on compartment fire characterization," *Fire Safety Science, Proceedings of the 5th International Symposium*, pp. 403–414.

[75] J. Backovsky and N. Alvares, "Profiles in forced ventilation enclosure fires," *Proceedings of the 2nd Int'l Symposium of Fire Safety Science*, pp. 315–324, 1988.

[76] W. Chow, S. Han, H. Dong, Y. Gao, and G. Zou, "Full-scale burning tests on heat release rates of furniture," *International Journal on Engineering Performance-Based Fire Codes*, vol. 6, pp. 168–180, 2004.

[77] H. Pretrel and L. Audouin, "Doorway flows induced by the combined effects of natural and forced ventilation in a three compartment assembly," *Fire Safety Science, Proceedings of the 10th International Symposium*, pp. 1015–1028, 2011.

[78] R. Bryant, "A comparison of gas velocity measurements in full-scale enclosure fire," *Fire Safety Journal*, vol. 44, pp. 793–800, 2009.

[79] W. Parker and B. Lee, "A small-scale enclosure for characterizing the fire buildup potential of a room," 1975.

[80] J. Lassus, L. Courty, E. Studer, J. Garo, P. Jourda, and P. Aine, "Experimental approach to estimate species concentrations in a compartment fire," *FIRE SAFETY SCIENCE-PROCEEDINGS OF THE ELEVENTH INTERNATIONAL SYMPOSIUM*, pp. 346–360, 2011.

[81] A. Heskestad and P. Hovde, "Empirical prediction of smoke production in the iso room corner fire test by use of iso cone calorimeter fire test data," *Fire and Materials*, vol. 23, pp. 193–199, 1999.

[82] M. Dietenberger, *Chapter 14: Upholstered Furniture: Detailed Model, in: Heat Release Rate in Fires*. Elsevier Science Publsihers, 1992.

[83] S. Levchik and E. Weil, "Review: Thermal decomposition, combustion and fire-retardancy of polyurethanes - a review of the recent literature," *society of Chemical Industry, Polymers International*, vol. 53, pp. 1585–1610, 2004.

[84] N. Grassie and G. Perdomo Mendoza, "Thermal degradation of polyether-urethanes: part 4. effect of ammonium polyphosphate on the thermal degradation of polyether-urethanes prepared from methylene bis(4-phenylisocyanate) and low molecular weight poly(ethylene glycols)," *Polymer Degradation and Stability*, vol. 11, pp. 145–166, 1985.

[85] N. Grassie and G. Perdomo Mendoza, "Thermal degradation of polyurethane: part 5. polyether-urethanes prepared from methylene bis(4-phenylisocyanate) and high molecular weight poly(ethylene glycols) and the effect of ammonium polyphosphate.," *Polymer Degradation and Stability*, vol. 11, pp. 359–379, 1985.

[86] J. Liggat, C. Denecker, C. Dick, S. Martin, C. Snape, M. Mohammed, G. Seely, B. Eling, C. Lindsay, and P. Chaffanjon *Polymer Material Science Engineering*, vol. 84, p. 186, 2000.

[87] K. Troev, V. Atanasov, R. Tsevi, G. Grancharov, and A. Tsekova, "Chemical degradation of polyurethanes. degradation of microporous polyurethane elastomer by dimethyl phosphonate," *Polymer Degradation and Stability*, vol. 67, pp. 159–165, 2000.

[88] E. Weil, M. Ravey, and G. D., *Proceedings of the Conference on Recent Advances in Flame Retardancy of polymeric Materials*. BBC Inc., 1996.

[89] J. Lefebvre, B. Bastin, R. Paleja, and R. Delobel, "Flexible polyurethane foams: Flammability," *Journal of Fire Sciences*, vol. 21, pp. 343–366, 2003.

[90] B. Levin, M. Paabo, E. Braun, and R. Harris, *Proceedings of the Conference on Recent Advances in Flame Retardancy of Polymeric Materials*. BBC Inc., 1991.

[91] R. Vanspeybroeck, P. Van Hees, and P. Vandevelde, "Combustion behaviour of fabric and polyurethane flexible foam mock-up combinations under cone calorimetry test conditions," *Fire and Materials*, vol. 17, pp. 167–172, 1993.

[92] D. Price, Y. Liu, R. Hull, J. Milnes, B. Kandola, and R. Horrocks, "Burning behaviour of fabric/ polyurethane foam combinations in the cone calorimeter," *Society of Chemical Industry, Polymer International*, vol. 49, pp. 1153–1157, 2000.

[93] C. Fleischmann and C. Fleischmann, "The impact of using wool fleece as an upholstered furniture fabric."

[94] R. Davis, T. Ohlemiller, and K. Steckler, "Materials and fire performance testing of barrier fabrics in mattresses and upholstered furniture."

[95] D. Olabode, J. Rigg, E. Weckman, B. Epling, and T. D., "Preliminary cone and furniture-scale calorimeter tests on non-fr and fr laminated polyurethane foams."

[96] A. Coles, "Flammability of upholstered furniture using the cone calorimeter," Master's thesis, University of Cantebury, New Zealand, 2000.

[97] V. Babrauskas, R. Harris, R. Gann, B. Levin, B. Lee, R. Peacock, M. Paabo, W. Twilley, F. Yoklavich, and H. Clark, "Fire hazard comparison of fire-retarded and non-fire-retarded products," technical report, National Bureau of Standards, 1988.

[98] "Reaction-to-fire tests heat release, smoke production and mass loss rate part 1: Heat release rate (cone calorimeter method) and smoke production rate (dynamic measurement)," standard, International Standards Organization, 2015.

[99] "Standard test method for heat and visible smoke release rates for materials and products using an oxygen consumption calorimeter," standard, American Society for Testing and Materials.

[100] M. Schartel and T. Hull, "Development of fire-retarded materials - interpretation of cone calorimeter data," *Fire and Materials*, vol. 31, pp. 327–354, 2007.

[101] M. Checchin, C. Cecchini, B. Cellarosi, and F. Sam, "Use of cone calorimeter for evaluating fire performances of polyurethane foams," *Polymer Degradation and Stability*, vol. 64, pp. 573–576, 1998.

[102] V. Babrauskas, D. Baroudi, J. Myllymaki, and M. Kokkala, "The cone calorimeter used for predictions of the full-scale burning behaviour of upholstered furniture," *Fire and Materials*, vol. 21, pp. 95–105, 1997.

[103] T. Ohlemiller, "An examination of the correlation between cone calorimeter data and full-scale furniture mock-up fires," 1995.

[104] A. Tewarson and R. Pion, "Flammability of plastics part one: Burning instensity," *Combustion and Flame*, vol. 26, pp. 85–103, 1976.

[105] "Fire safety of upholstered furniture- the final report on the cbuf research programme," technical report, European Commission Measurement Testing Report, 1995.

[106] S. Nazare, W. Pitts, M. Zammarano, J. Shields, E. Knowlton, and B. De Leon, "Assessing fire-blocking effectiveness of barrier fabrics in the cone calorimeter," technical report, National Institute of Science and Technology, 2019.

[107] R. Crewe, J. Staggs, and H. Phylaktou, "The temperature-dependent cone calorimeter: An appoximate alternative to furnace testing," *Journal of Fire Sciences*, vol. 29, pp. 131–151, 2011.

[108] V. Babrauskas, *Chapter 5: Full-Scale Heat Release Rate Measurements, in: Heat Release Rate in Fires*. Elsevier Science Publsihers, 1992.

[109] "Standard guide for obtaining data for fire growth models," standard, American Society for Testing and Materials, West Conshohocken, PA, Unites States, 2020.

[110] S. Ames, V. Babrauskas, and W. Parker, *Chapter 15: Upholstered Furniture Prediction by Correlation, in: Heat Release Rate in Fires.* Elsevier Science Publsihers, 1992.

[111] V. Babrauskas and W. Walton, "A simplified characterization of upholstered furniture heat release rates," *Fire Safety Journal*, vol. 11, pp. 181–192, 1986.

[112] Y. Shintani, T. Nagaoka, Y. Deguchi, and K. Harada, "An application method of free burning hrr data to room fire scenarios," *Fire Safety Science, Proceedings of the 11th Int'l Symposium*, 2014.

[113] P. DiNenno and R. Custer, eds., *Hazard Calculations: Calorimetry.* Quincy, Mass; Bethesda, Md.: National Fire Protection Association, 2002.

[114] H. Hottel, "Certain laws governing diffusive burning of liquids," *Fire Research Abstracts and Reviews*, vol. 1, pp. 41–44, 1959.

[115] K. Mudan, "Thermal radiation hazards from hydrocarbon pool fires," *Progress in Energy and Combustion Science*, vol. 10, pp. 59–80, 1984.

[116] M. Gawlowski, D. Gcka, C. Kuhr, I. Vela, and A. Schnbucher, "The probabilistic thermal radiation model osramo ii for hydrocarbon pool fires," *Proceedings of the Combustion Institute*, vol. 31, 2006.

[117] I. Vela, C. Kuhr, and A. Schnbucher, "Cfd simulation of large hydrocarbon pool fires," *Proceedings of the Combustion Institute*, vol. 31, 2006.

[118] W. Jones, "A model for the transport of fire, smoke, and toxic gases , (fast), nbsir 84-2934, national bureau of standards," Gaithersburg, MD, 1984.

[119] "Upholstered furniture: Burning behaviour - full scale test," standard, International Standards Organization, 1991.

[120] P. Enright, *Heat Release and the Combustion Behaviour of Upholstered Furniture.* PhD thesis, University of Cantebury, New Zealand, 1999.

[121] N. Girgis, "Full scale compartment fire experiments on upholstered furniture," Master's thesis, University of Cantebury, Christchurch NZ, 2000.

[122] M. J.A. and H. S.M., "Full scale room fire experiments conducted at the university of maryland," technical report, Test Report to National Institute of Standards and Technology, Department of Fire Protection Engineering, 1996.

[123] A. Putorti, "Full scale room burn pattern study," technical report, Fire Safety Engineering Divisions, National Institute of Standards and Technology, 1997.

[124] A. Grand, H. Kaplan, J. Beiel, W. Switzer, and G. Hartzell, "An evaluation of toxic hazards from full-scale furnished room fire studies," *Fire Safety Science and Engineering, ASTM STP 882, Harmathy Ed, American Society for Testing Materials, Philadelphia*, pp. 330–353, 1985.

[125] A. Cowlard, T. Steinhaus, C. Abecassis-Empis, and J. Torero, *The Dalmarnock Fire Tests: Experiments of Modelling*. School of Engineering and Electronics, University of Edinburgh, 2007.

[126] T. Morikawa, E. Yanai, and T. Nishina, "Toxicity evaluation of fire effluent gases from experimental fires in a building," *Journal of Fire Sciences*, vol. 5, pp. 248–271, 1987.

[127] T. Morikawa and E. Yanai, "Toxic gases from house fires involving natural and synthetic polymers under various conditions," *Fire Safety Journal*, vol. 20, pp. 257–274, 1993.

[128] E. Guillaume, F. Didieux, A. Thiry, and A. Bellivier, "Real-scale fire tests of one bedroom apartments with regard to tenability assessment," *Fire Safety Journal*, vol. 70, pp. 81–97, 2014.

[129] S. McKenna, R. Birtles, K. Dickens, R. Walker, M. Spearpoint, A. Stec, and R. Hull, "Flame retardants in uk furniture increase smoke toxicity more than they reduce fire growth rate," *Chemosphere*, vol. 196, pp. 429–439, 2018.

[130] M. Blais, K. Carpenter, and K. Fernandez, "Comparative room burn study of furnished rooms from the united kingdom, france and the united states," *Fire Technology*, 2019.

[131] A. Wolfe, C. Mealy, and D. Gottuk, "Fire dynamics and forensic analysis of limited ventilation compartment fires, volume 1: Experimental," technical report, Report for the U.S. Department of Justice, 2009.

[132] "Requirement, test procedure and apparatus for testing the smolder resistance of materials used in upholstered furniture," standard, Bureau of Electronic and Appliance Repair Home Furnishings and Thermal Insulation, State of California Department of Consumer Affairs, Sacramento CA, 2013.

[133] S. Verstockt, S. Van Hoecke, N. Tilley, B. Merci, B. Sette, P. Lambert, H. C.F.J., and R. Van De Walle, "Firecube: A multi-view localization framework for 3d fire analysis," *Fire Safety Journal*, vol. 46, pp. 262–275, 2011.

[134] T. Beji, S. Verstockt, R. Van de Walle, and B. Merci, "Global analysis of multi-compartment full scale fire tests," *Fire Safety Journal*, vol. 76, pp. 9–18, 2015.

[135] S. Verstockt, T. Beji, P. De Potter, V. H. S., B. Sette, B. Merci, and R. Van de Walle, "Video driven fire spread forecasting (f) using multi-modal lwir and visual flame and smoke data," *Pattern Recognition Letters*, vol. 34, pp. 62–69, 2013.

[136] B. Stratton, "Determining flame height and flame pulsation frequency and estimating heat release rate from 3d flame reconstruction," Master's thesis, 2005.

[137] P. Senez, P. Mulherin, and E. Weckman, "Repeatability of underventilated compartment fire testing with complex fuel packages," *15th Int'l Conference Proceedings on Fire and Materials*, vol. 1, pp. 349–353, 2017.

[138] "Methods of test for assessment of the ignitability of upholstered seating by smouldering and flaming ignition sources," standard, British Standards, 2006.

[139] M. DiDomizio, N. Ryder, and E. Weckman, "Electronic gas sensors in fire testing," *Proceedings of the 14th Int'l Conference and Exhibition on Fire Science Engineering, Interflam. Windsor UK*, vol. 2, pp. 969–980, 2016.

[140] A. Bwalya, G. Lougheed, A. Kashef, and H. Saber, "Survey results of combustible contents and floor areas in canadian multi-family dwellings," *Fire Technology*, vol. 47, pp. 1121–1140, 2010.

[141] F. T. Technology, "Conecalc5 software," 2009.

[142] J. Schindelin, I. Arganda-Carreras, and E. Frise, "Fiji: an open-source platform for biological-image analysis," *Nature Methods*, vol. 9, pp. 676–682, 2012.

[143] VideoLAN, "Vlc media player, version 2.2.6." https://www.videolan.org/vlc/index.html.

[144] R. Siegel and J. Howell, *Thermal Radiation Heat Transfer*. Hemisphere Publishing Corporation, 1981.

[145] L. Blevins and W. Pitts, "Modeling of bare and aspirated thermocouples in compartment fires," *Fire Safety Journal*, vol. 33, pp. 239–259, 1999.

[146] L. Zhao and N. Dembsey, "Measurement uncertainty analysis for calorimetry," *Fire and Materials*, vol. 32, pp. 1–26, 2008.

[147] T. Fritz and P. Hunsberger, "Testing of mattress composites in the cone calorimeter," *Fire and Materials*, vol. 21, pp. 17–22, 1997.

[148] A. Little, "Deterioration of textile materials," *Studies in Conservation*, vol. 9, pp. 67–78, 1964.

[149] L. G. Bwalya A., Gibbs E. and K. A., "Heat release rates of modern residential furnishings during combustion in a room calorimeter," *Fire and Materials*, vol. 39, pp. 685–716, 2015.

[150] J. M. Gann R.G., Averill J.D. and P. R.D., "Smoke component yields from room-scale fire tests," technical report, National Institute of Standards and Technology, Department of Fire Protection Engineering, 2003.

[151] H. Nelson, "FPETOOL: Fire protection engineering tools for hazard estimation," internal report, National Institute of Standards and technology, NIST, Gaithersburg, MD, 1990.

[152] B. Bastin, R. Paleja, and J. Lefebvre, "Fire behaviour of polyurethane foams," *Journal of Cellular Plastics*, vol. 39, pp. 323–339, 2003.

[153] B. McCaffrey. Qunicy MA, National Fire Protection Association and Society of Fire Protection Engineers, 2nd edition ed., 1995.

[154] A. Tewarson, J. Lee, and P. R.F., "The influence of oxygen concentration on fuel parameters for fire modeling," pp. 563–570, 1981.

[155] G. Mulholland, M. Janssens, S. Yusa, W. Twilley, and V. Babrauskas, "The effect of oxygen concentration on co and smoke produced by flames," pp. 585–594, 1991.

[156] P. Blomqvist, L. Rosell, and M. Simonson, "Emissions from fires part 2: Simulated room fires," *Fire Technology*, vol. 40, pp. 59–73, 2004.

[157] "Standard method of test for heat release rates for upholstered furniture components or composites and mattresses using oxygen consumption calorimeter," standard, National Fire Protection Association, Qunicy, M.A., 1990.

[158] R. Schifilliti, *Use of Fire Plume Theory in the Design and Analysis of Fire Detector and Sprinkler Response*. PhD thesis, Worcester Polytechnic Institute, Worcester, United States, 1986.

[159] "Office of the Ontario Fire Marshal. Ontario Fire Incident Summary 2007-2016," 2016.

[160] D. Purser, "Toxic product yields and hazard assessment for fully enclosed design fires," *Society of Chemical Industry, Polymer International*, pp. 1232–1255, 2000.

[161] "Life-threatening components of fire guidelines for the estimation of time to compromised tenability in fires," standard, International Standards Organization, 2012.

[162] K. McGrattan and R. McDermott, "FDS and Smokeview." https://www.nist.gov/services-resources/software/fds-and-smokeview.

[163] Oasys, "Crowd simulation software, Mass Motion, by Oasys." https://www.oasys-software.com/products/pedestrian-simulation/massmotion/.

[164] M. Van Dyke, *An Album of Fluid Motion*. The Parabolic Press, Stanford California, 1982.

[165] P. R. . B. V., "Analysis of large-scale fire test data," *Fire Safety Journal*, vol. 17, pp. 387–414, 1991.

[166] R. Schaal, "A users guide for the CFI calculator and fire dynamics equations," 2005-2008.

[167] R. Alpert and E. Ward, "Evaluation of unsprinklered fire hazards," *Fire Safety Journal*, vol. 7, pp. 127–143, 1984.

APPENDICES

Appendix A

Repeat Test Timelines, Chronologies and Plots

This Appendix includes the data and plots for the remaining tests not included in the main body. These tests are the two NFR couch A tests 2 and 8, the other FR couch B test 7, and the two LFR couch C tests 3 and 9. The plots are shown in the order of the NFR couch A, FR couch B followed by LFR couch C.

A.1 Test Chronologies and Picture Timelines

The letter captions below each of the images captured from the V2 camera (facing the couch in the living room) for each pictorial timeline correspond to the following fire events from a)-g) respectively; 1st cushion fully involved, smoke at the top of the window, heat release rate approximately 500kW, peak heat release rate, minimum oxygen measured in the living (burn) room, minimum measured in the main floor SW adjacent compartment and minimum oxygen measured on the second floor. Note that some tests due to smoke obscuration do not have a corresponding image of the fire at that event.

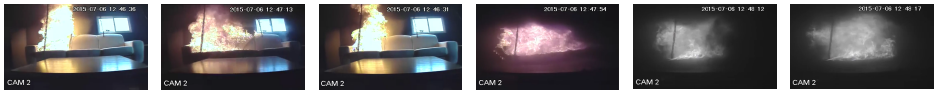

(a) (b) (c) (d) (e) (f)

Figure A.1: Pictorial Timeline of NFR Couch A, Test 2

1st cushion fully involved (a)	Smoke at top of window (b)	Approx. time to 500kW (c)	Peak HRR (d)	Minimum Oxygen in BR (e) 1F (f), 2F (g)
270s 760kW	257s 460kW	230s	348s 2652kW	8% at 366s 7% at 371s 7% at 712s

Table A.1: Chronology of Events for NFR Couch A, Test 2

1st cushion fully involved (a)	Smoke at top of window (b)	Approx. time to 500kW (c)	Peak HRR (d)	Minimum Oxygen in BR (e) 1F (f), 2F (g)
208s 965kW	245s 2150kW	195s	290s 2813kW	3% at 306s 10% at 291s 12% at 336s

Table A.2: Chronology of Events for NFR Couch A, Test 8

(a) (b) (c) (d) (e) (f) (g)

Figure A.2: Pictorial Timeline of Events for NFR Couch A, Test 8

1st cushion fully involved (a)	Smoke at top of window (b)	Approx. time to 500kW (c)	Peak HRR (d)	Minimum Oxygen in BR (e) 1F (f), 2F (g)
292s 230kW	273s 230kW	320s	421s 1453kW	7% at 421s 10% at 396s 12% at 431s

Table A.3: Chronology of Events for FR Couch B, Test 7

(a) (b) (c) (d) (e) (f) (g)

Figure A.3: Pictorial Timeline of Events for FR Couch B, Test 7

1st cushion fully involved (a)	Smoke at top of window (b)	Approx. time to 500kW (c)	Peak HRR (d)	Minimum Oxygen in BR (e) 1F (f), 2F (g)
402s 130kW	605s 550kW	580s	686s 1652kW	3% at 612s 6% at 682s 12% at 722s

Table A.4: Chronology of Events for LFR Couch c, Test 3

(a) (b) (c) (d) (e) (f) (g)

Figure A.4: Pictorial Timeline for LFR Couch C, Test 3

1st cushion fully involved (a)	Smoke at top of window (b)	Approx. time to 500kW (c)	Peak HRR (d)	Minimum Oxygen in BR (e) 1F (f), 2F (g)
350s, 190kW	546s 810kW	512s	630s 2786kW	9% at 607s 8% at 562s 8% at 727s

Table A.5: Chronology of Events for LFR Couch C, Test 9

(a) (b) (c) (d) (e) (f) (g)

Figure A.5: Pictorial Timeline for LFR Couch C, Test 9

A.2 Fire Geometry

Measured widths and calculated diameters as well as the calculated heights from Heskestad's correlation and measured flame heights from the image analysis program with vertical line markers of fire events are presented here for the ancillary tests.

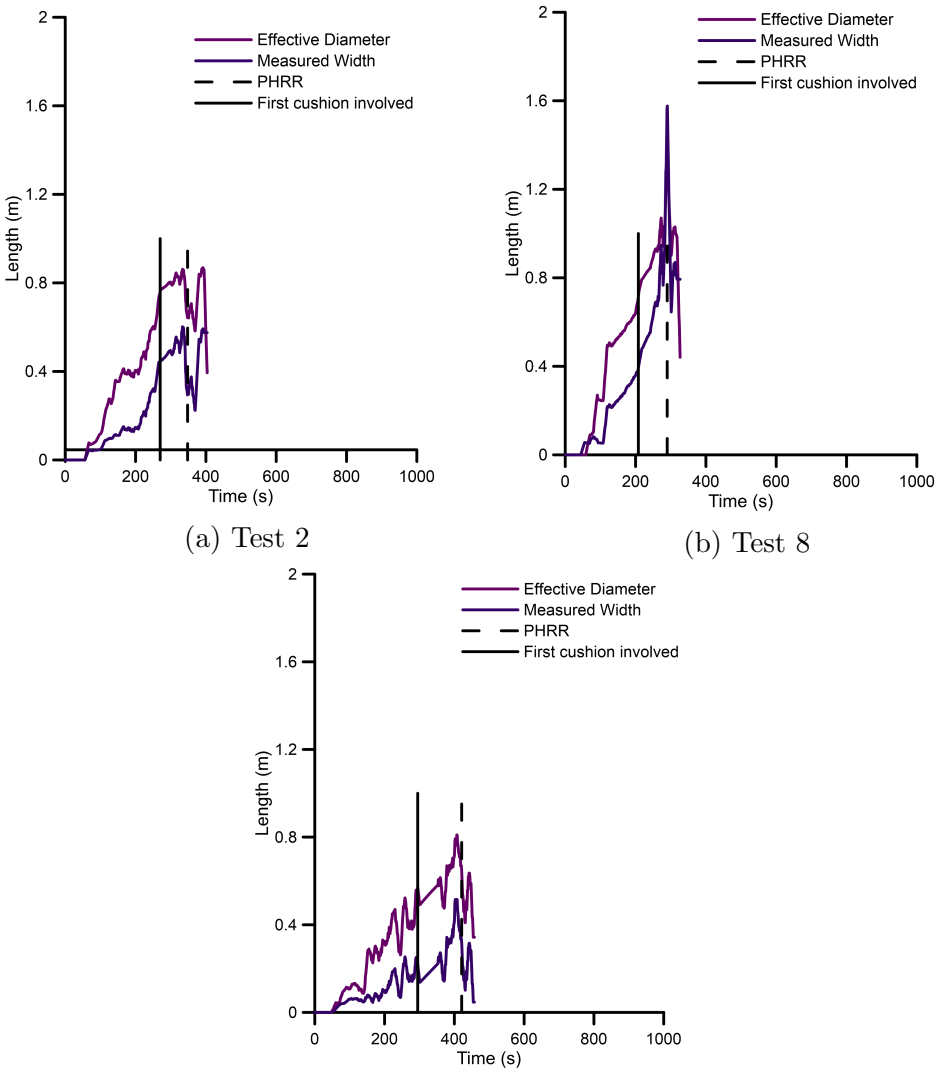

(a) Test 2

(b) Test 8

(c) Test 7

Figure A.6: Ancillary Tests Measured Flame Widths and Effective Diameters

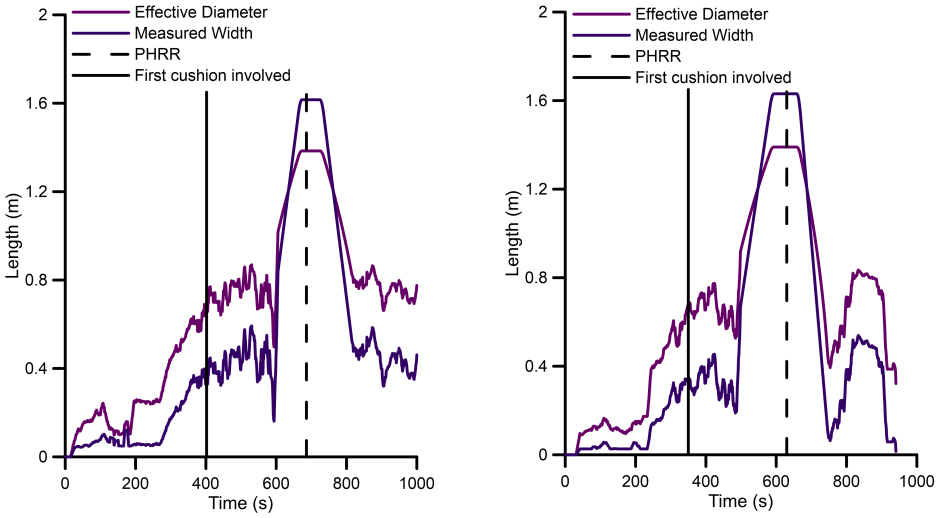

(a) Test 3

(b) Test 9

Figure A.7: Ancillary Tests Measured Flame Widths and Effective Diameters

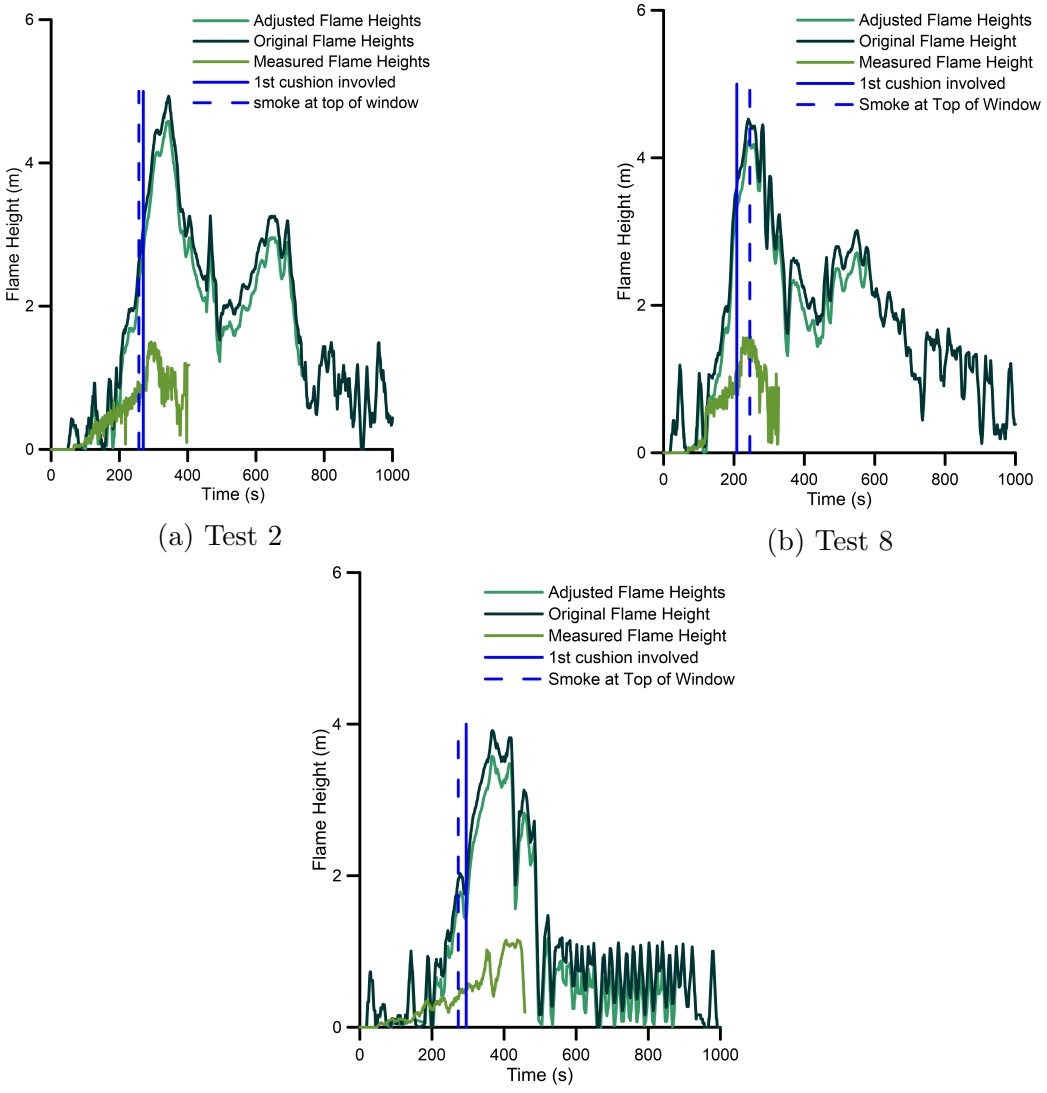

(a) Test 2

(b) Test 8

(c) Test 7

Figure A.8: NFR A and FR B Calculated and Measured Flame Heights

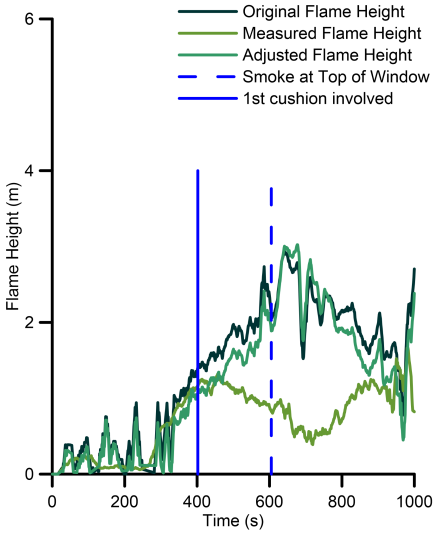

(a) Test 3

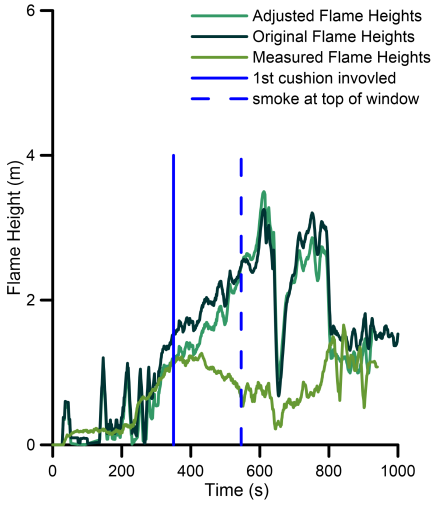

(b) Test 9

Figure A.9: LFR C Calculated and Measured Flame Heights

A.3 Oxygen and Heat Release Rate

The following plots show the relationship between the heat release rate and measured oxygen in the various areas of the structure. The same trends discussed in Chapter 4 can be seen consistently across the repeat tests.

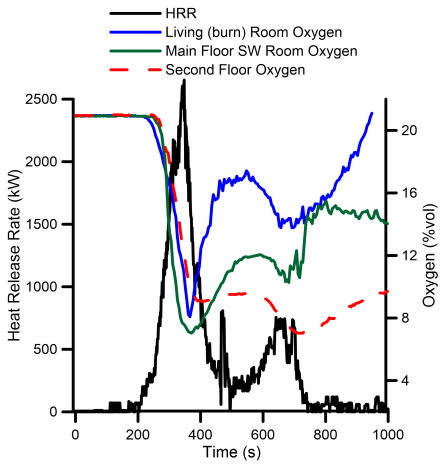

(a) Test 2

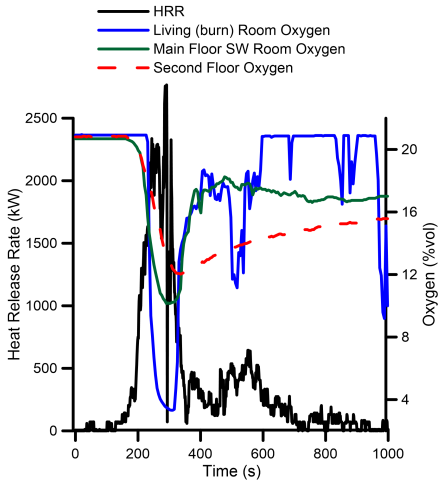

(b) Test 8

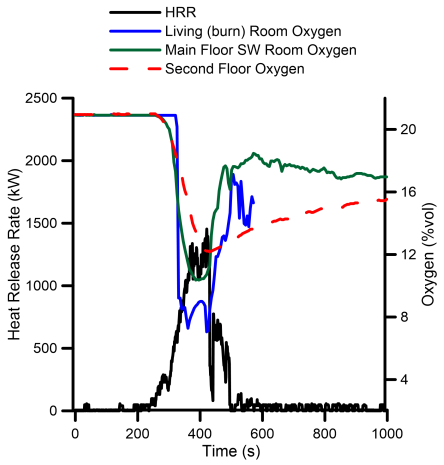

(c) Test 7

Figure A.10: NFR A and FR B O_2 Heat Release Rate

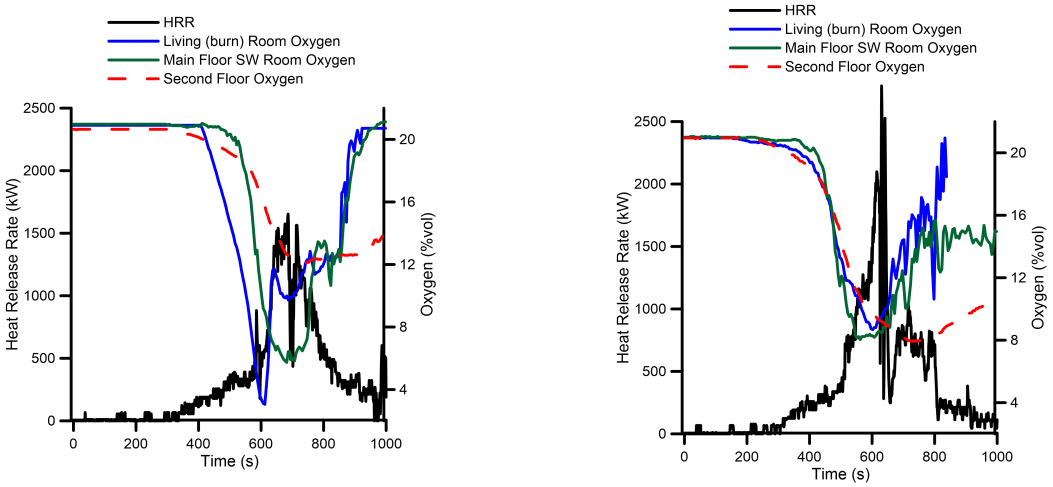

(a) Test 3

(b) Test 9

Figure A.11: LFR C O_2 and Heat Release Rate

A.4 Carbon Monoxide and Heat Release Rate

The following plots show the relationship between the heat release rate and measured carbon monoxide in the various areas of the structure. The same trends discussed in Chapter 4 can be seen consistently across the repeat tests.

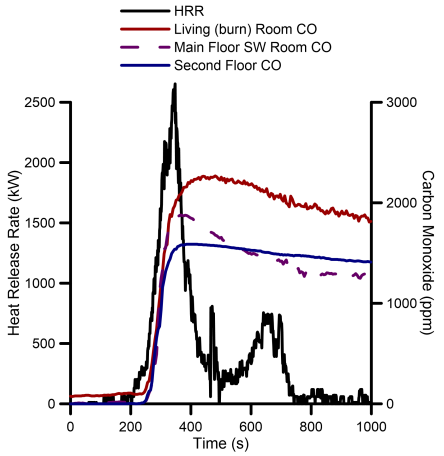

(a) Test 2

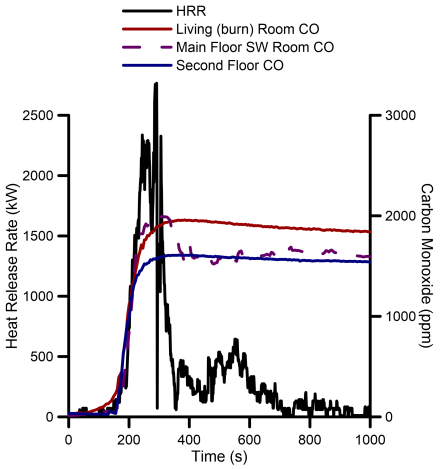

(b) Test 8

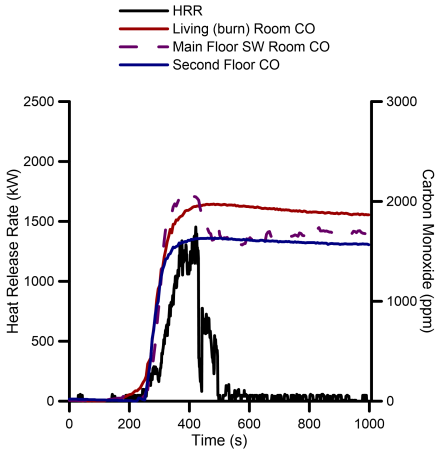

(c) Test 7

Figure A.12: NFR A and FR B CO and Heat Release Rate

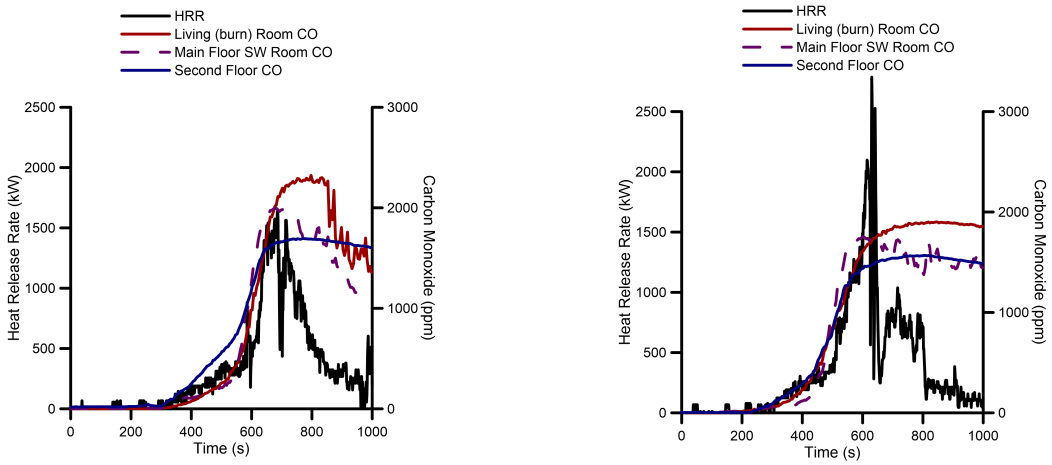

(a) Test 3

(b) Test 9

Figure A.13: LFR C CO and Heat Release Rate

A.5 Temperature Plots

The following plots show the thermal development as measured by the thermocouples in the various areas of the structure. The same trends discussed in Chapter 4 can be seen consistently across the repeat tests.

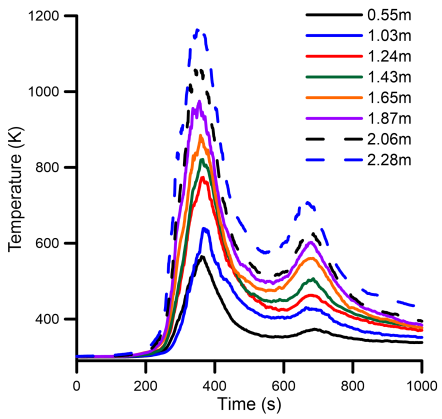

(a) Burn Room Center

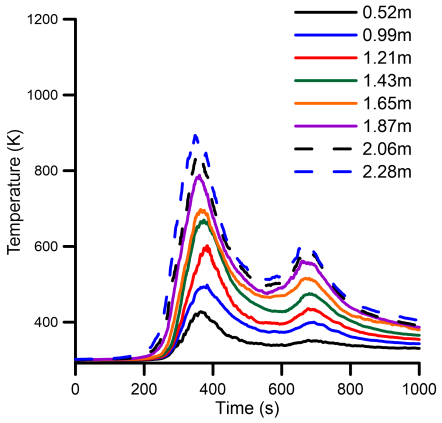

(b) Burn Room Corridor Side

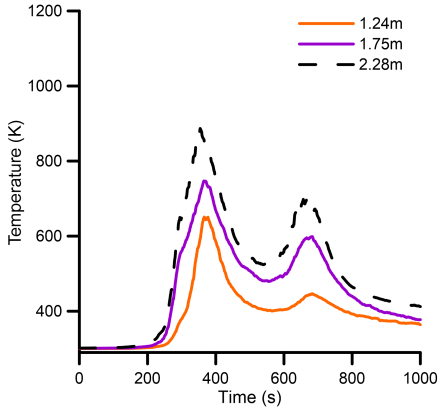

(c) Burn Room SW Corner

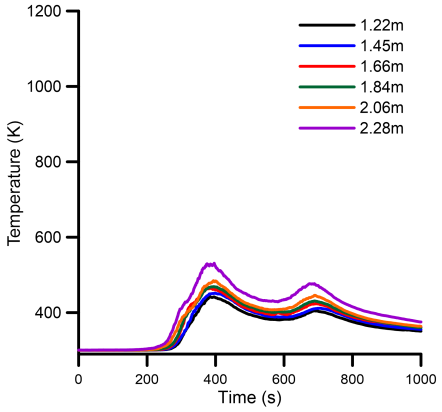

(d) Main Floor SW Room

Figure A.14: Test 2 NFR Couch A Main Floor Temperatures

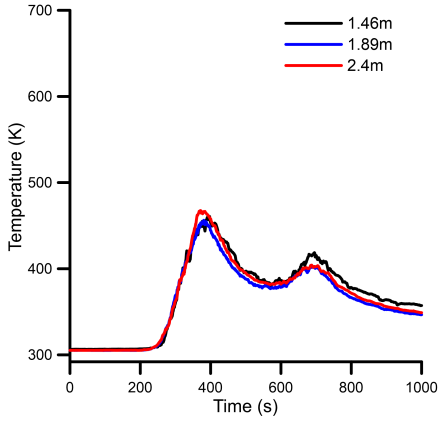

(a) Top of Staircase

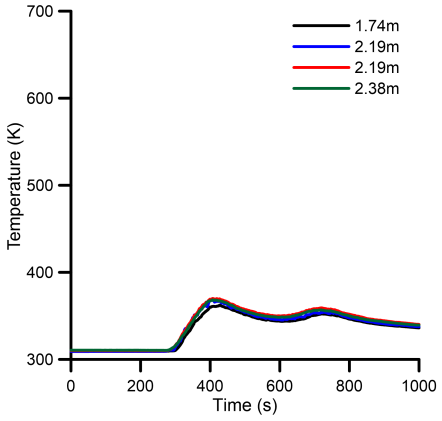

(b) Second Floor SE Room

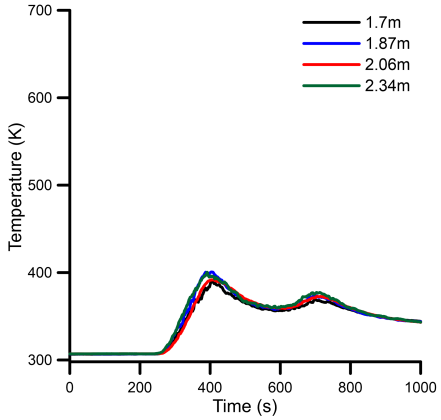

(c) Second Floor SW Room

Figure A.15: Test 2 NFR Couch A Staircase and Second Floor Temperatures

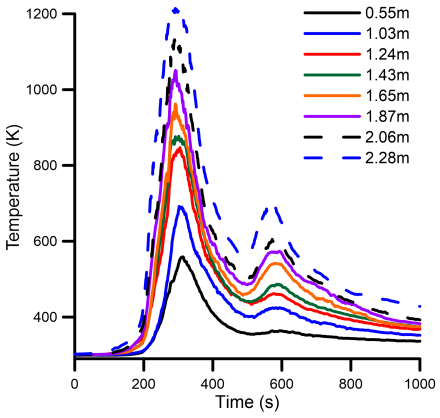

(a) Burn Room Center

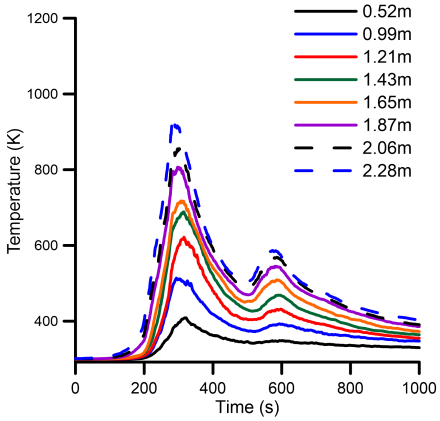

(b) Burn Room Corridor Side

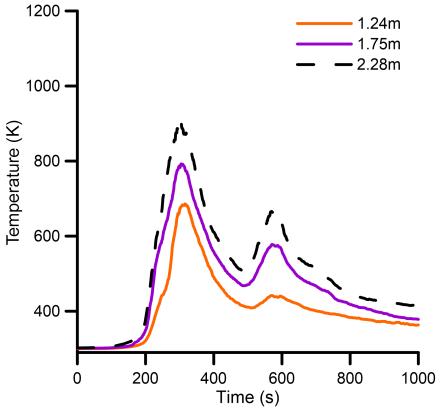

(c) Burn Room SW Corner

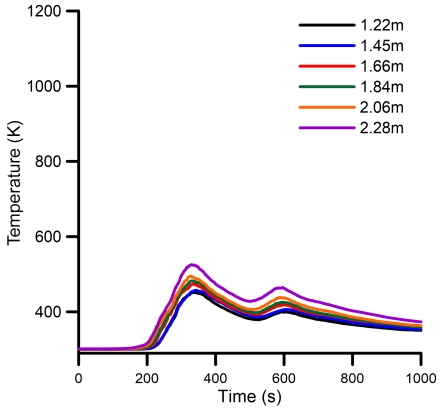

(d) Main Floor SW Room

Figure A.16: Test 8 NFR Couch A Main Floor Temperatures

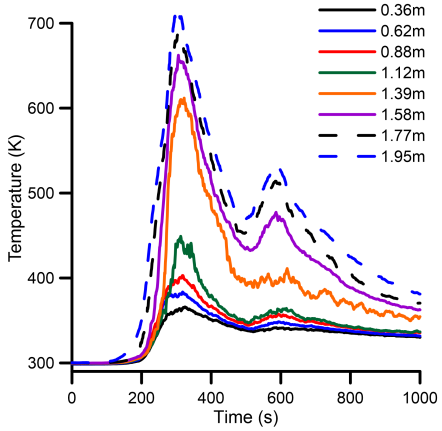

(a) Bottom of Staircase

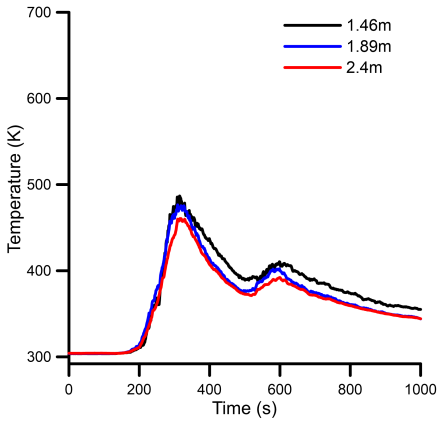

(b) Top of Staircase

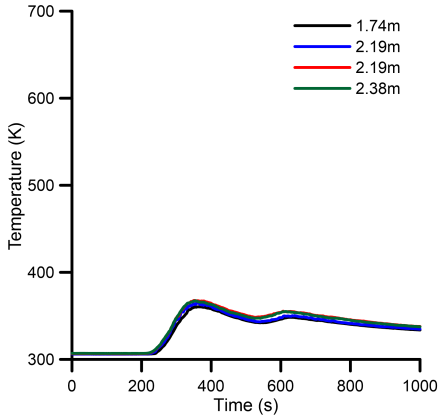

(c) Second Floor SE Room

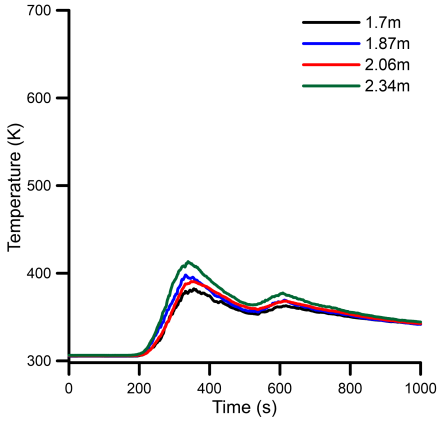

(d) Second Floor SW Room

Figure A.17: Test 8 NFR Couch A Staircase and Second Floor Temperatures

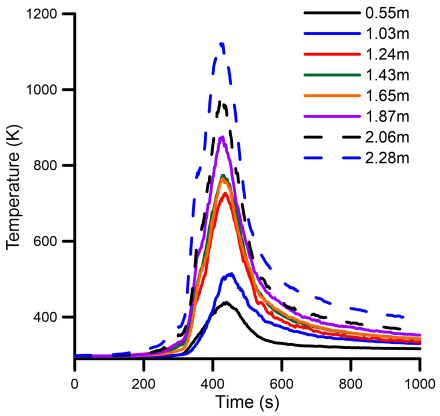

(a) Burn Room Center

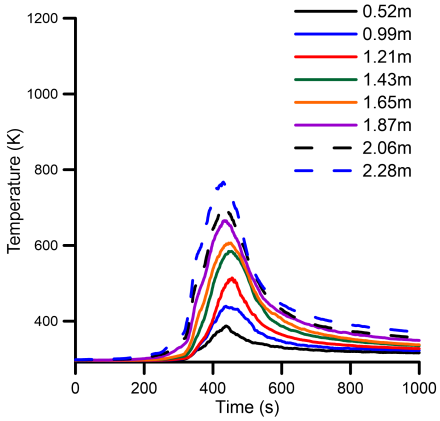

(b) Burn Room Corridor Side

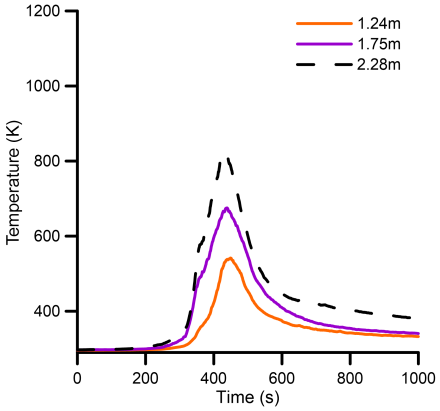

(c) Burn Room SW Corner

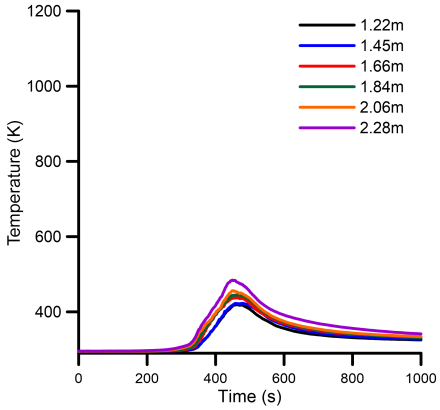

(d) Main Floor SW Room

Figure A.18: Test 7 FR Couch B Main Floor Temperatures

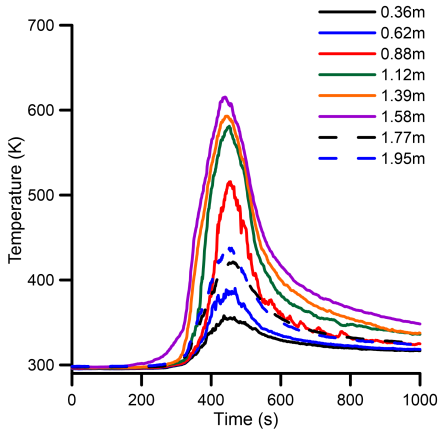

(a) Bottom of Staircase

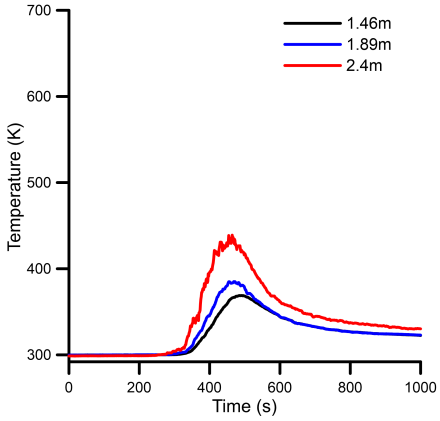

(b) Top of Staircase

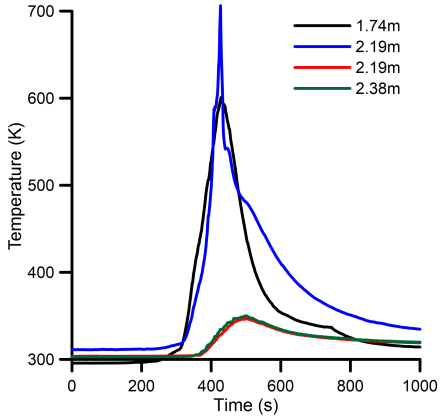

(c) Second Floor SE Room

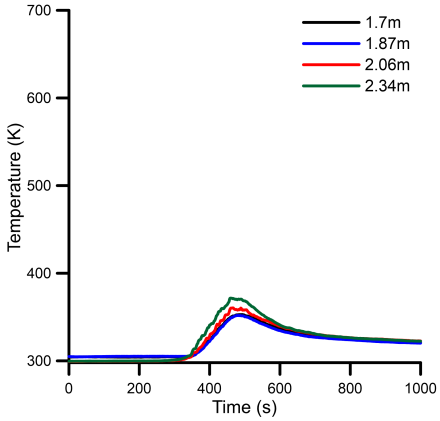

(d) Second Floor SW Room

Figure A.19: Test 7 FR Couch B Staircase and Second Floor Temperatures

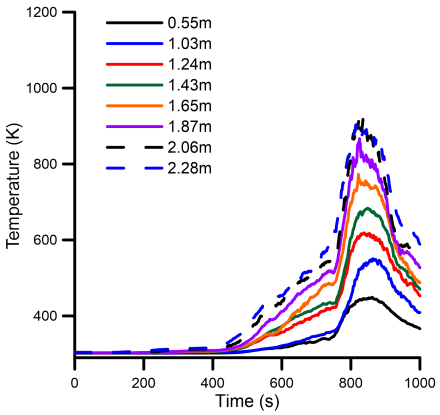

(a) Burn Room Center

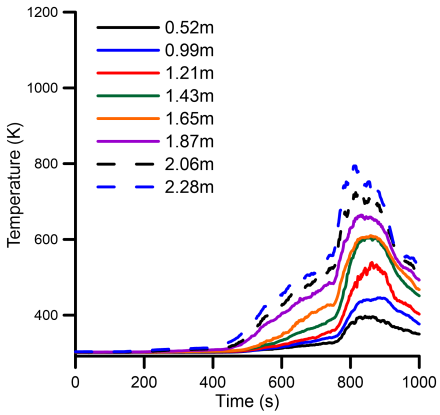

(b) Burn Room Corridor Side

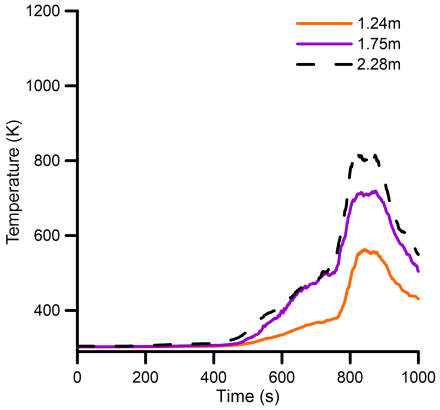

(c) Burn Room SW Corner

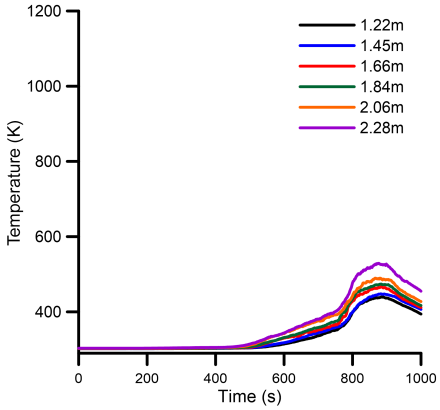

(d) Main Floor SW Room

Figure A.20: Test 3 LFR Couch C Main Floor Temperatures

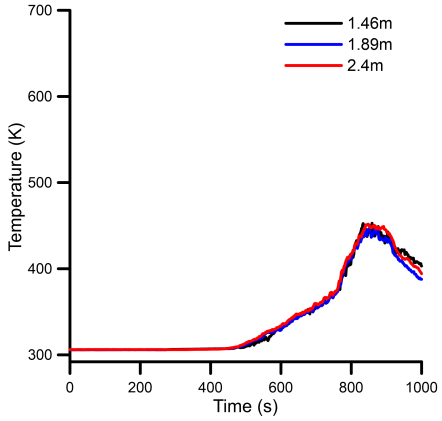

(a) Top of Staircase

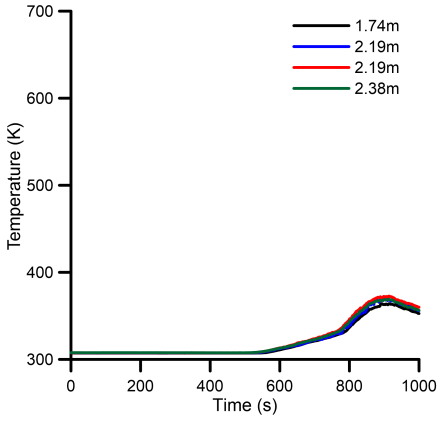

(b) Second Floor SE Room

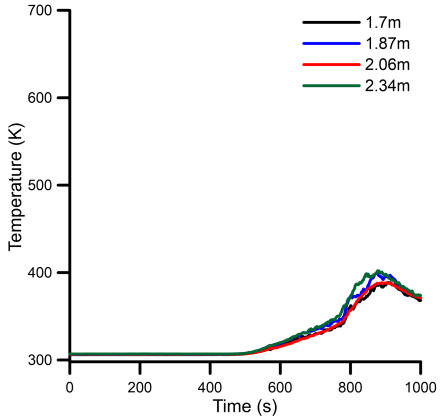

(c) Second Floor SW Room

Figure A.21: Test 3 LFR Couch C Staircase and Second Floor Temperatures

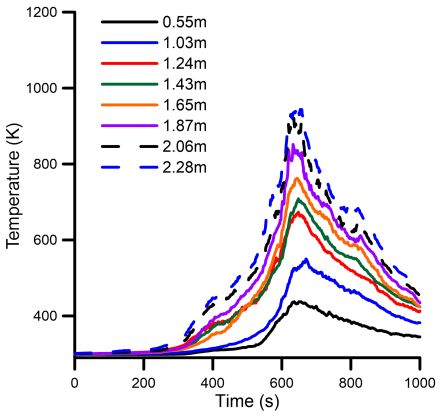

(a) Burn Room Center

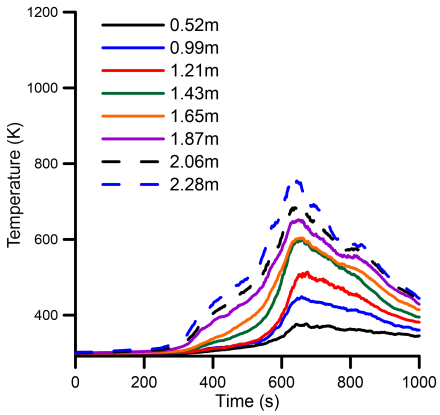

(b) Burn Room Corridor Side

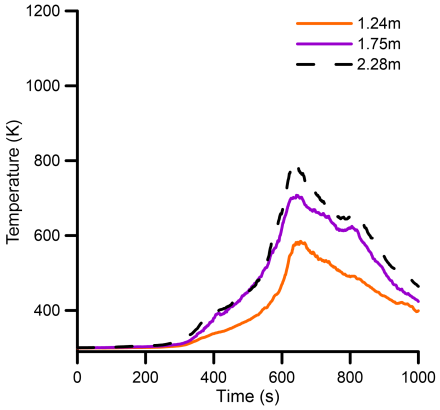

(c) Burn Room SW Corner

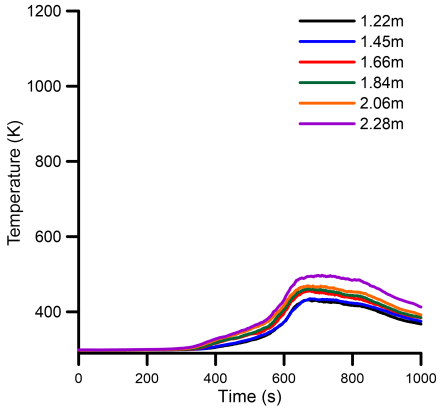

(d) Main Floor SW Room

Figure A.22: Test 9 LFR Couch C Main Floor Temperatures

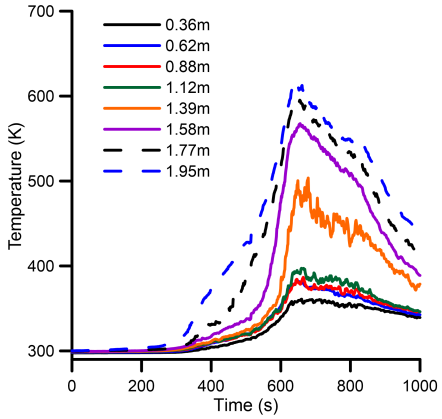

(a) Bottom of Staircase

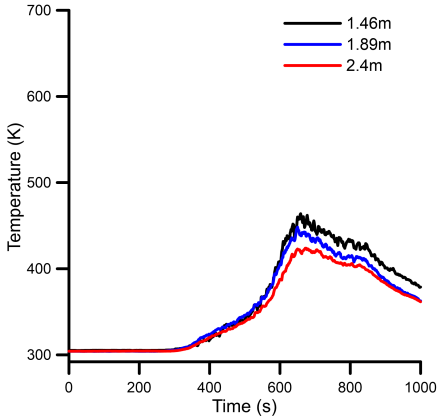

(b) Top of Staircase

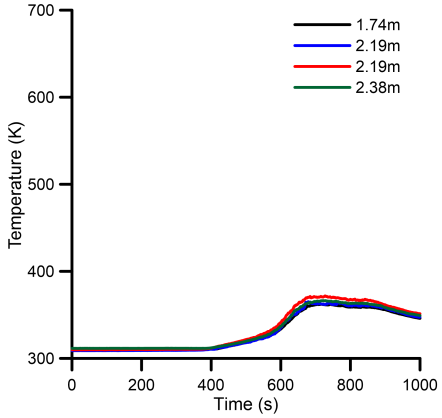

(c) Second Floor SE Room

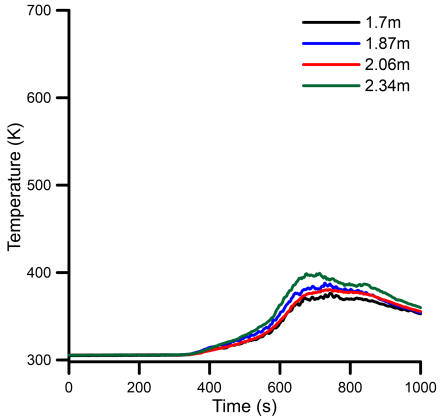

(d) Second Floor SW Room

Figure A.23: Test 9 LFR Couch C Staircase and Second Floor Temperatures

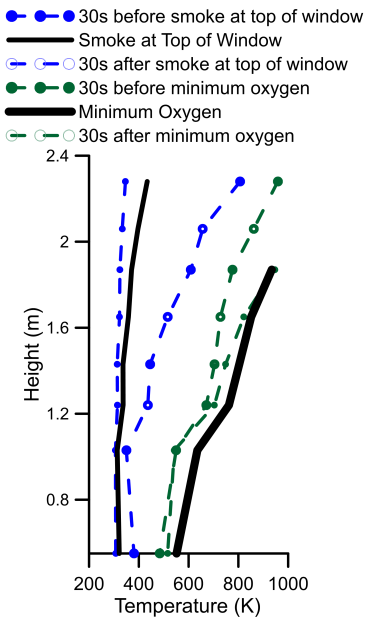

(a) Test 2 NFR A

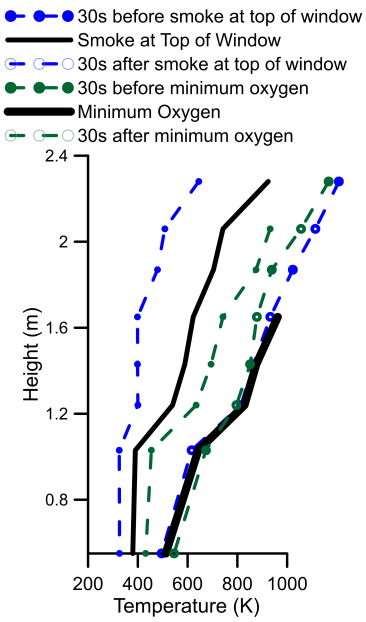

(b) Test 8 NFR A

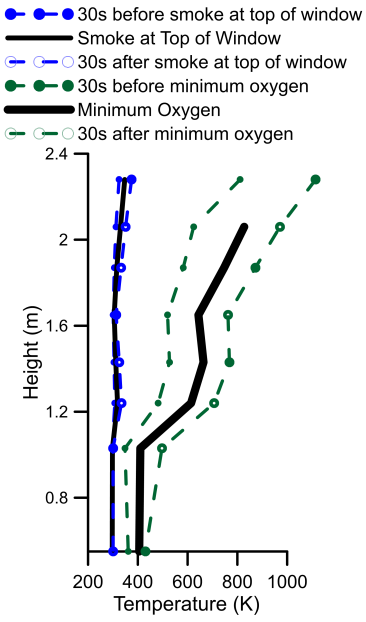

(c) Test 7 FR B

Figure A.24: Temperature Stratification Profiles Living (Burn) Room Center

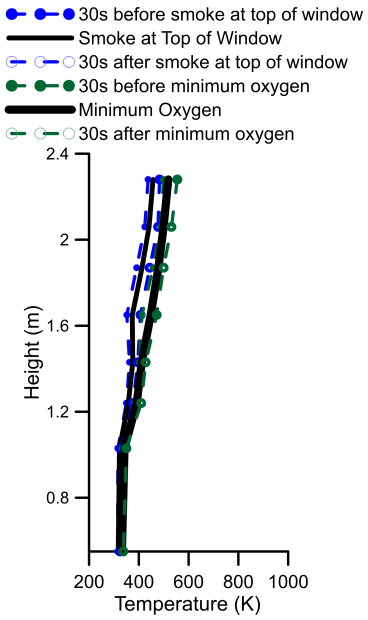

(a) Test 3 LFR C

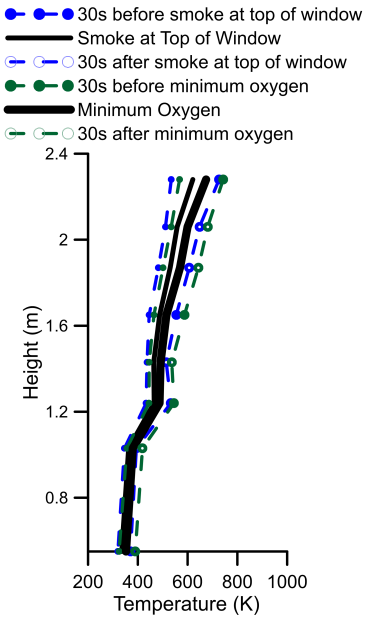

(b) Test 9 LFR C

Figure A.25: Temperature Stratification Profiles Living (Burn) Room Center

A.6 Heat Flux and Radiative Contributions

Maximum heat flux as measured by the gauge as well as maximum fire temperatures are included in Table A.6 below. Following the Table are the point source and emissive power calculations of heat flux for the fire and smoke layer are included in the plots below in conjunction with the actual heat flux measured by the gauge in the compartment for the ancillary tests.

Furniture Type	Maximum $\dot{q}''_{measured}$	Maximum Flame Temperature
T2 NFR Couch Ai	12.3kW/m^2	1081K
T8 NFR Couch Aiii	13.9kW/m^2	1124K
T7 FR Couch Bii	5.6kW/m^2	819K
T3 LFR Couch Ci	12kW/m^2	1031K
T9 LFR Couch Ciii	10.9kW/m^2	1064K

Table A.6: Maximum Heat Flux and Flame Temperatures Measured

In the case of test 3, the actual heat flux is considered to be around 9kW/m^2, not the measured 12kW/m^2 included in the Table above. In this test the fire spread along the ceiling and down the wall of the gauge, so the high heat flux measured relative to the other LFR couch C fires is suspected to be artificially high due to this rollover effect of flames across the face of the gauge. The radiative fraction was adjusted to be 0.62 so maximum heat flux calculated with the point source method aligned with the emissive power calculation. Time-resolved scatter plots of the radiative fractions are included as well, however without the oxygen over-plotted as the representative tests were presented in the main body.

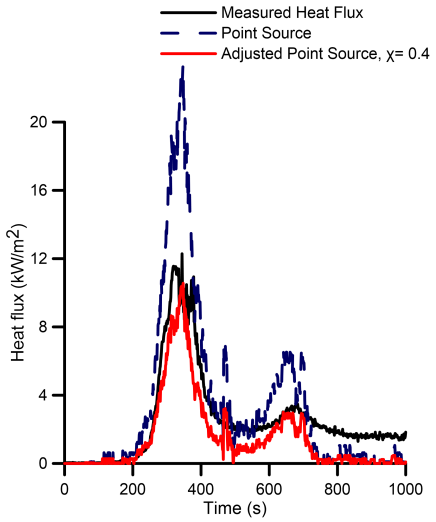

(a) Point Source

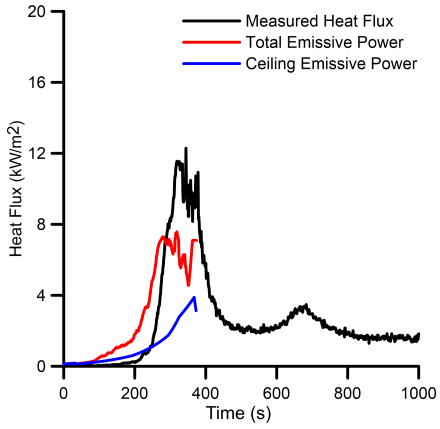

(b) Emissive Power

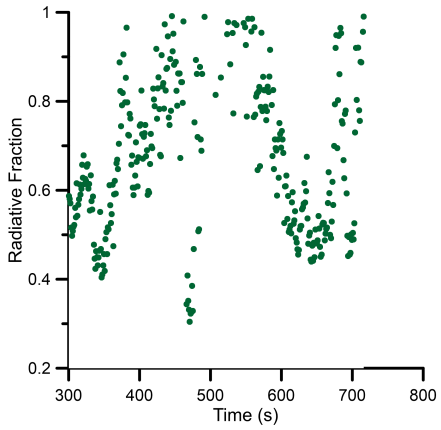

(c) Radiative Fraction

Figure A.26: Heat Flux Measured by Gauge, Point Source, Emissive Power and Radiative Fraction, NFR Couch A, Test 2

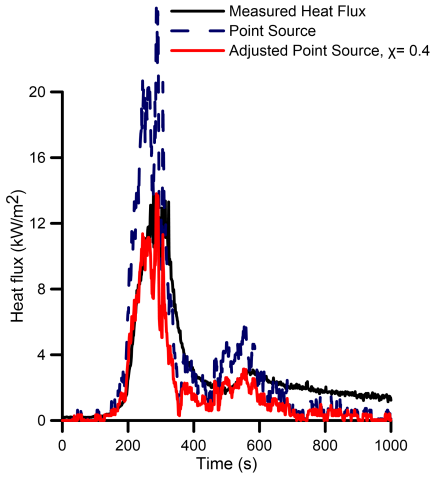

(a) Point Source

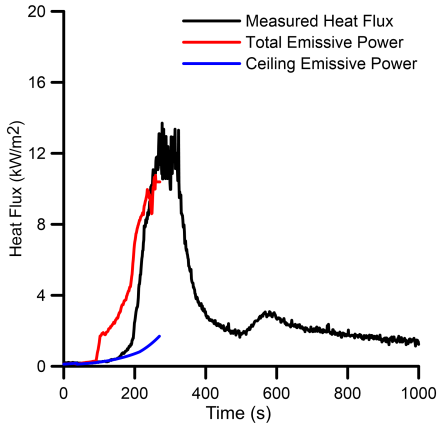

(b) Emissive Power

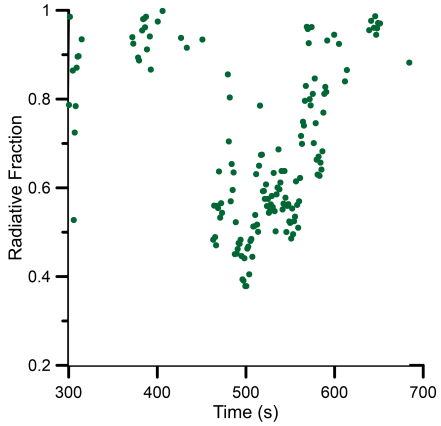

(c) Radiative Fraction

Figure A.27: Heat Flux Measured by Gauge, Point Source, Emissive Power and Radiative Fraction, NFR Couch A, Test 8

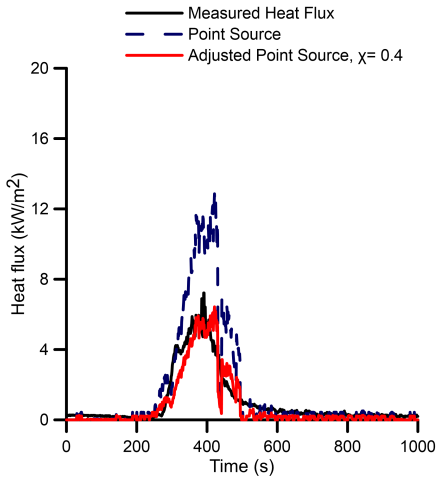

(a) Point Source

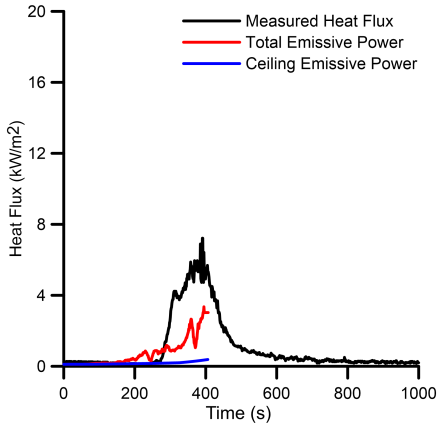

(b) Emissive Power

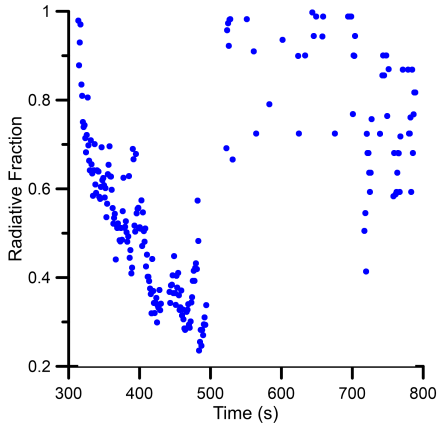

(c) Radiative Fraction

Figure A.28: Heat Flux Measured by Gauge, Point Source, Emissive Power and Radiative Fraction, FR Couch B, Test 7

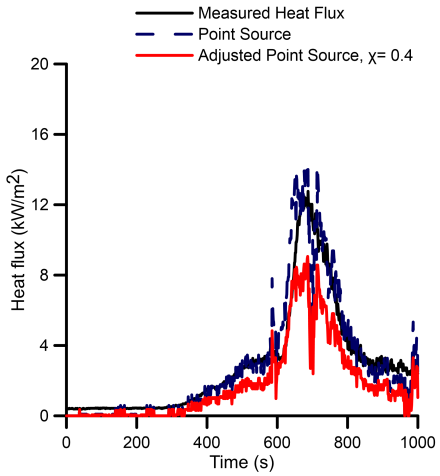

(a) Point Source

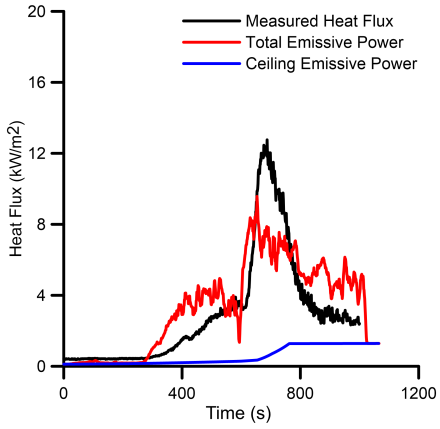

(b) Emissive Power

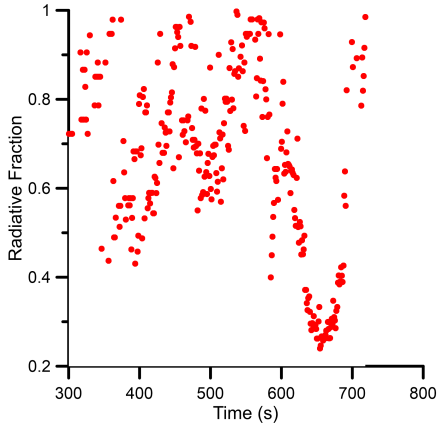

(c) Radiative Fraction

Figure A.29: Heat Flux Measured by Gauge, Point Source, Emissive Power and Radiative Fraction, LFR Couch C, Test 3

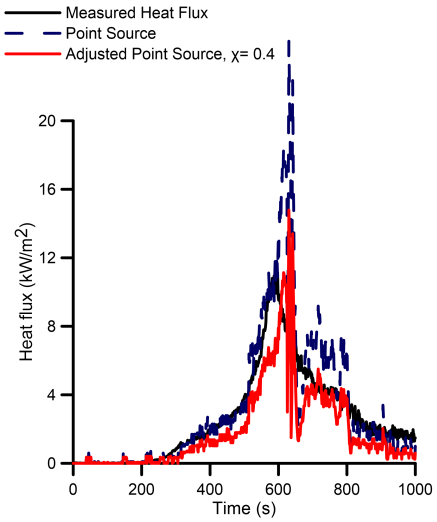

(a) Point Source

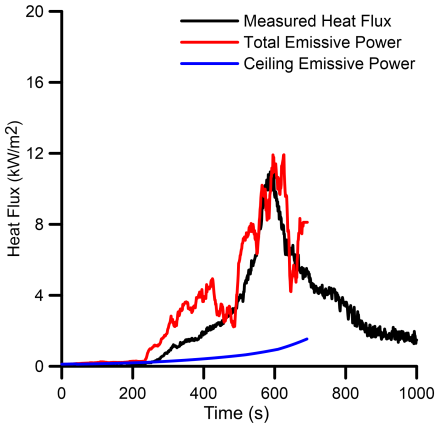

(b) Emissive Power

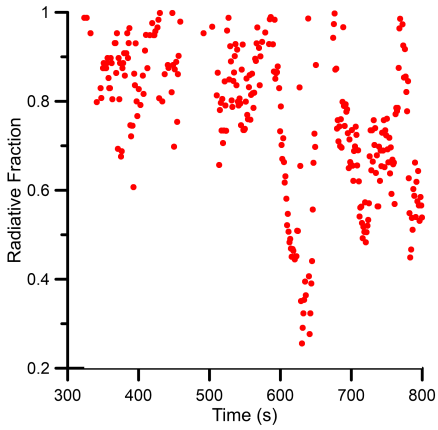

(c) Radiative Fraction

Figure A.30: Heat Flux Measured by Gauge, Point Source, Emissive Power and Radiative Fraction, LFR Couch C, Test 9

A.7 Velocity, Oxygen, Temperature Plots and Velocity Profiles

The thermocouples and velocity probes were not installed for the first three tests, as such, the velocity data included below are for the repeat tests of 8, 7 and 9 for couches A, B and C respectively. Peak temperature is taken from the top thermocouple, positioned 2.28m above the floor in the center of the living (burn) room (T2) represented by the dashed line. Minimum oxygen in the main floor SW compartment and second floor are represented by the solid and dash-dot lines respectively. The velocity measurements are taken from the top velocity probe at the bottom of the stair case 1.95m above the floor, the middle from the probe positioned 1.4m above the floor and the bottom probe 0.36m above the floor. Positive values indicate flow into the living (burn) room from the second floor, and the negative values indicate flow out of the living (burn) room into the second floor. The velocity profiles feature the same three events as the ones in the main body; first cushion fully involved, peak heat release rate and minimum oxygen measured on the second floor as indicators of early, peak and later-stages in the fire. The same trends discussed in Chapter 4 can be seen in the plots of the repeat tests as well.

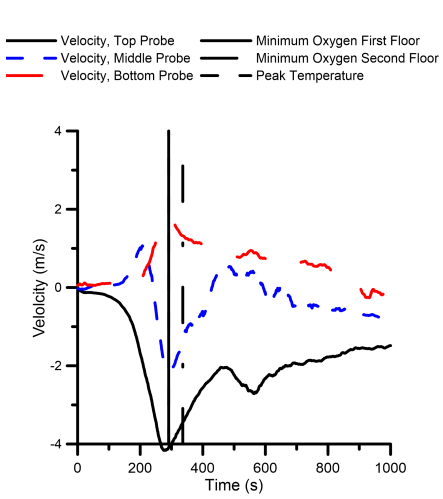

(a) Velocity, Temperature and O_2

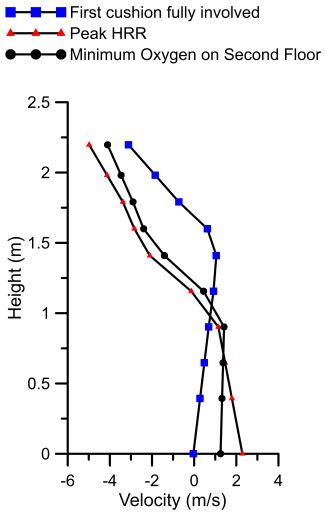

(b) Velocity Profile

Figure A.31: Velocity Profiles and Velocity Plots with Peak Temperature and Minimum Oxygen Measured on the First and Second Floors for Test 8, NFR Couch A

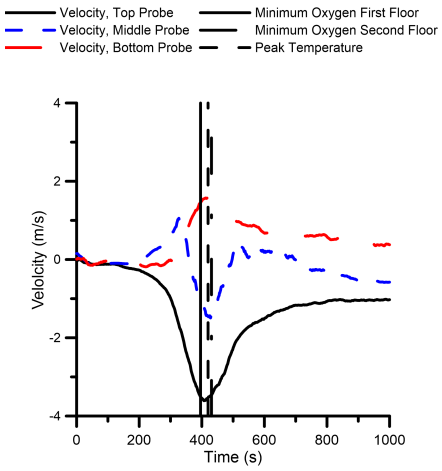

(a) Velocity, Temperature and O_2

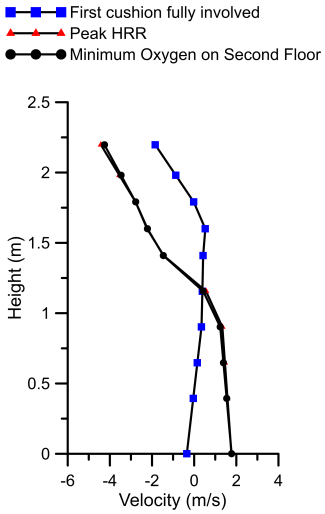

(b) Velocity Profile

Figure A.32: Velocity Profiles and Velocity Plots with Peak Temperature and Minimum Oxygen Measured on the First and Second Floors for Test 7, FR Couch B

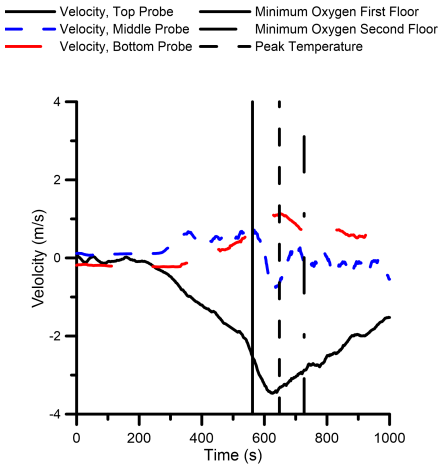

(a) Velocity, Temperature and O_2

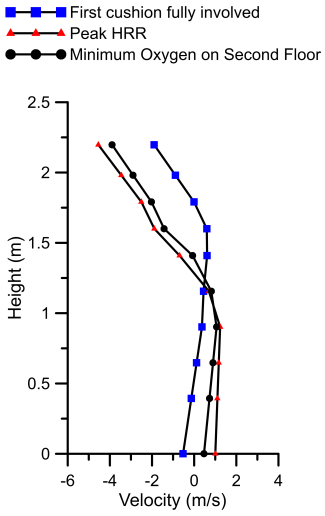

(b) Velocity Profile

Figure A.33: Velocity Profiles and Velocity Plots with Peak Temperature and Minimum Oxygen Measured on the First and Second Floors for Test 9, LFR Couch C

A.8 Heskestad Correlation and Mass Loss Rate Heat Release Rates

The calculated heat release rate using Heskestad's correlation with both width and effective diameter inputs for the repeat tests are shown below. Similar to the tests discussed in the main body, the correlation breaks down when the fire gets too large and rectangular and the smoke layer starts to develop and impinge on the top of the fire plume.

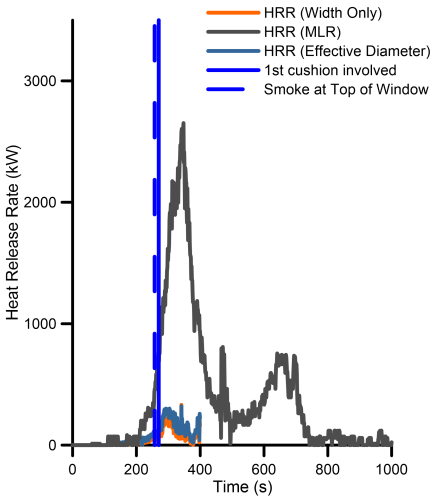

(a) Test 2

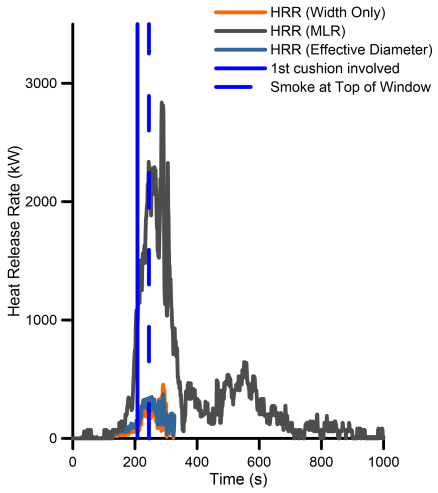

(b) Test 8

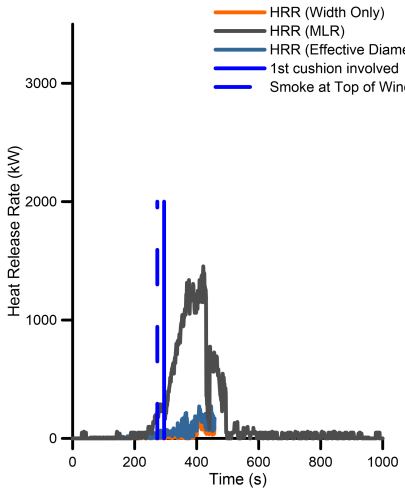

(c) Test 7

Figure A.34: NFR A and FR B Ancillary Tests Heskestad and MLR HRR

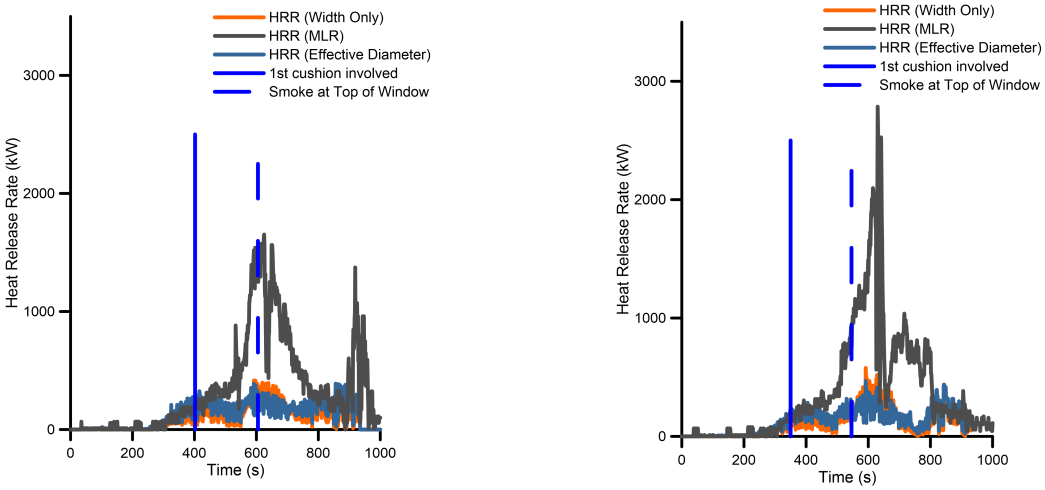

(a) Test 3

(b) Test 9

Figure A.35: LFR Couch C Ancillary Tests Heskestad and MLR HRR

Appendix B

Data Acquisition

B.1 Ignition Time and Time Shifts

The NIST DAQ and DVR have internal clocks but the clocks were not synced to one another, additionally the ardunios did not have a timestamp so ignition time had to be calculated for each system using a combination of recorded stopwatch times on the master test sheets, pictures from a camera which was synced to a GPS timestamp as well as a combination of watching video footage for the time of ignition and backing out when that would have occurred on each system.

For example, the ignition time on the DAQ was calculated by the following equations:

$$T_{\text{event}} - y = z \tag{B.1}$$

Where T event is the recorded time of ignition (or another event of interest) on the master test sheet which was a running stopwatch time after the start of test (time of day), and y is the time lapse for the instrument to be turned on as recorded on the master test sheet after start of test. The variable z is the difference in time from when the DAQ was turned on to the event of interest. This second formula then adds that difference onto the first timestamp on the DAQ output file.

$$MT + z = CT \tag{B.2}$$

Where MT is the master time on the DAQ output file, or the first timestamp marking

when it was turned on and started the recording, z is the difference found in the above equation, and CT is the calculated time of ignition (or other event of interest) for the DAQ.

Sample Calculation: DAQ Ignition Time

MT of DAQ = 12:27:39 (44859 seconds) start time of test on the DAQ. T of ignition = 22:19 (1339 seconds) stopwatch time, how long after start of test ignition occurred as recorded on the test sheet. y = 19:00 (1140 seconds) stopwatch time, how long after start of test DAQ was turned on. So z was equal to 199s. So 199 was added to MT, and the calculated time of ignition on the DAQ for this particular test was 12:30:58.

The ignition time of the crib could be observed from the security camera footage (camera two). The difference in ignition times between the camera DVR time and the DAQ time was calculated for each test and was used to determine when the cameras would see certain events recorded from the DAQ instruments. Below, Table B.1 summarizes the ignition times of the crib calculated for the DAQ, and observed ignition times as seen on the camera footage.

Test	Calculated DAQ Crib Ignition	Observed Crib Ignition on Camera	Delta t (min)
1	17:32:40	17:43:51	11:11
2	12:30:58	12:52:06	11:08
3	17:15:43	17:28:53	13:10
4	10:51:19	10:51:57	00:38
5	16:36:57	16:37:51	00:54
6	14:04:15	14:04:54	00:39
7	11:28:02	11:28:36	00:34
8	16:26:24	16:27:02	00:38
9	11:28:45	11:29:31	00:46

Table B.1: DAQ and Camera Crib Ignition Times

Once the ignition time on the DAQ was calculated, the number of samples to ignition on the arduinos could be calculated in a similar fashion. Step one was to calculate the number of arduino samples until the start of DAQ trace, then take the difference in time between the starting of the DAQ and the starting of the arduino, and divide by 5. Step two was to calculate the number of DAQ samples from the start of the DAQ trace to ignition, and divide by 1.1. Step three was to calculate the time from the start of the ardunio to ignition then, the time taken from the start of the DAQ to ignition was added

to the time between the start of the arduino and start of the DAQ traces (from step two and one). This last number was simply divided by 5 to get the number of arduino samples to ignition. These calculations were then cross-checked with camera photos and security camera footage. Some tests needed additional shifts/ corrections to the arduino data because the CO and O_2 data did not follow the trends seen in the other tests of the same furniture types. Also, for test 6, there was no arduino data collected due to an error in the data acquisition. The table, B.2 below summarizes the the number of arduino samples to ignition, and the corrections as well as additional shifts if needed. The asterisks beside the numbers represent the number of samples that were chosen as the number of samples to ignition.

Test	Arduino Samples to Ignition	Correction	Additional Shift
1	543	550	N/A
2	262	268*	N/A
3	291*	322	N/A
4	153	161*	N/A
5	283	294*	N/A
7	156	165	180*
8	159	167	199*
9	190	199	232*

Table B.2: Arduino Samples to Ignition and Corrections

As stated above, some of the tests had issues with the calculated and corrected times to ignition of the gas data not lining up correctly with the heat release rate data (tests 7, 8 and 9). The plots below are the plots with the calculated time to ignition, without any additional shift to the data. As you can see, the data does not line up well with the other trends seen across other repeat tests of the same furniture.

Possible explanations as to why these tests needed an additional shift could be due to the surfaces of the sensors becoming dirty and therefore creating an additional delay in the reaction and subsequent voltage output, and/or the arduino boards could also have been over-heating, making the circuitry delay.

Additionally, due to the nature of the image processing program, the fire had to be well-enough established on the couches for the program to have a sufficient baseline. As such, the video footage that was used for the image processing program (spliced into frames and run through Fiji) was shorter than the full video footage from crib ignition to end of

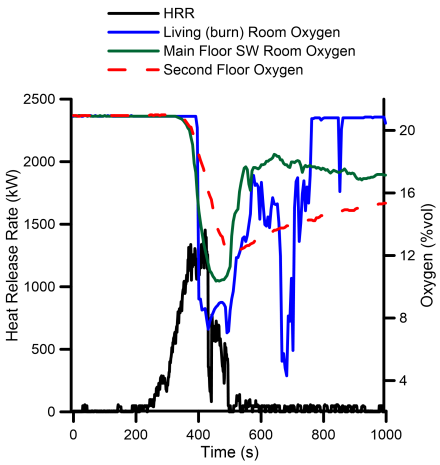

(a) Original Oxygen and HRR Curve, FR Couch B, Test 7

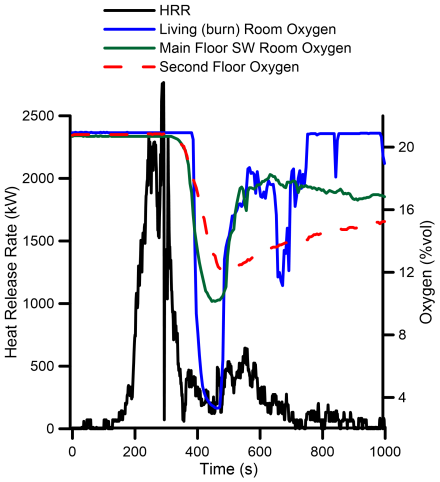

(b) Original Oxygen and HRR Curve, NFR Couch A, Test 8

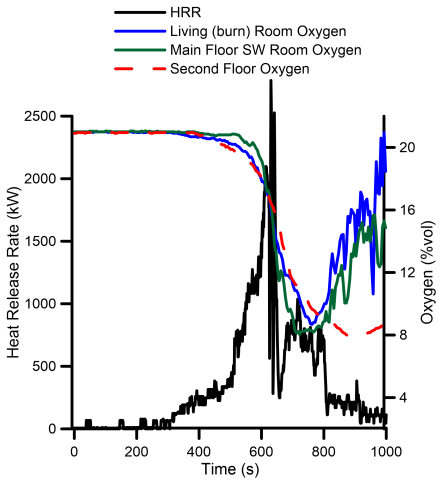

(c) Original Oxygen and HRR Curve, LFR Couch C, Test 9

Figure B.1: Original Oxygen Data without Additional Shift with HRR Curves for Tests 7, 8 and 9.

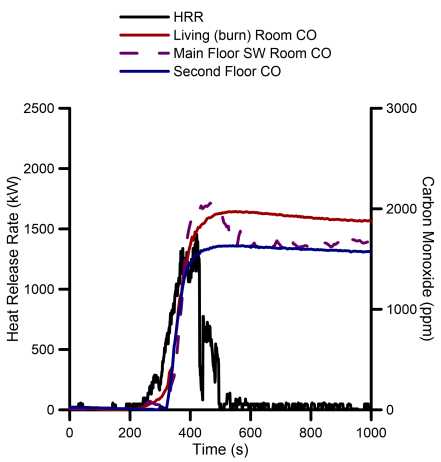

(a) Original CO and HRR Curve, FR Couch B, Test 7

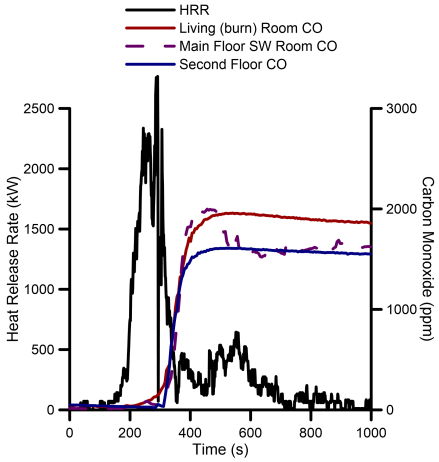

(b) Original CO and HRR Curve, NFR Couch A, Test 8

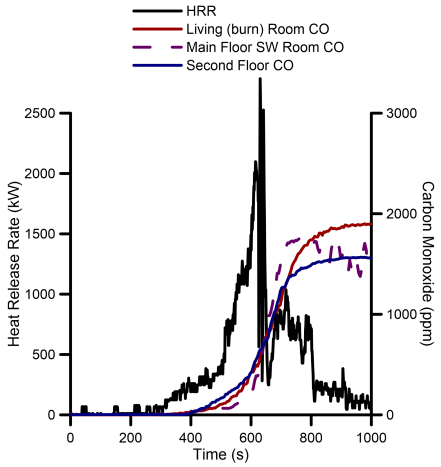

(c) Original CO and HRR Curve, LFR Couch C, Test 9

Figure B.2: Original Carbon Monoxide Data without Additional Shift with HRR Curves for Tests 7, 8 and 9.

test, and rather started closer to couch ignition. Therefore, there was a certain amount of time that the image processing videos were ahead of the DAQ traces (when using crib ignition as t=0). To line up a heat release rate curve (taken from the mass loss rate as recorded by the DAQ) a certain number of data points, as summarized in table B.3 below, were added to the start of the width and height traces so that t=0 corresponded with the start time of the DAQ/CAM crib ignition time. This time correction was made for the flame area inputs used in the Heskestad correlation and point source radiation calculations. Table B.3 below summarizes the difference in time between the camera/DAQ start of tests (crib ignition) and the start of the videos cut and used for the image processing program. Note in this table that CAM crib ignition time is equal to the DAQ crib ignition time; they are both t=0, so once the difference between the two CAM times were calculated, the same number of data points were added to any fire dimension or area trace.

Test	CAM Crib Ignition Time	SOT Video for Image Processing	Delta t (seconds)
2	12:42:06	12:42:41	35
3	17:28:53	17:29:20	27
4	10:51:57	10:52:25	28
5	16:37:51	16:38:19	28
6	14:04:54	14:05:30	36
7	11:28:36	11:29:12	36
8	16:27:02	16:27:41	39
9	11:29:31	11:30:14	43

Table B.3: Difference in time between Crib IGN on CAM and SOT image processing Videos

B.2 Calibration Curves

B.2.1 Weigh Scales and Heat Flux Gauge

The weigh scales were calibrated before the start of each test by collecting several data points using known calibration masses. By finding the slope and y-intercepts, linear calibration curves were generated for each test. The equation to convert from voltage output to kilograms is shown in the equation below:

$$Mass(kg) = A * voltage + B \tag{B.3}$$

Test	A	B
2	7490.1882	-29.5937
3	7464.1474	-29.5506
4	7475.5301	-29.5433
5	7489.5124	-29.621
6	7502.5428	-29.62
7	7533.7992	-29.7738
8	7514.5	-29.849
9	7540.6718	-29.8158

Table B.4: Calibration Values for Weigh Scales

The manufacturer of the heat flux gauge supplied the linear calibration curve to convert from voltage to heat flux (kW/m^2) shown below:

$$HF(kW/m^2) = a * V \tag{B.4}$$

Where a = 9510.

B.2.2 Electrochemical Sensors

The calibration curves for the electrochemical sensors were based on the formula below:

$$concentration = A * voltage + (B + C) \tag{B.5}$$

Values of A and B+C for each location and each test are included in the tables below.

Location	A	B+C
BR O_2	0.0491	-1.0468
1F O_2	0.0443	-4.3453
2F O_2	0.0467	-10.0588
BR CO	3.1002	-597.322
1F CO	2.7151	-608.182
2F CO	2.90765	-1195.04

Table B.5: Calibration Curves for Test 2

Location	A	B+C
BR O_2	0.0321	-0.6684
1F O_2	0.04914	-7.4789
2F O_2	0.0321	-0.6684
BR CO	3.1002	-393.725
1F CO	2.7151	-428.986
2F CO	2.90765	-1055.48

Table B.6: Calibration Curves for Test 3

Location	A	B+C
BR O_2	0.032	-0.6684
1F O_2	0.0491	-6.7424
2F O_2	0.0467	-9.59185
BR CO	3.1002	-260.725
1F CO	2.7151	-308.986
2F CO	2.90765	-885.48

Table B.7: Calibration Curves for Test 4

Location	A	B+C
BR O_2	0.0443	-2.086
1F O_2	0.0491	-6.7424
2F O_2	0.0467	-9.6385
BR CO	3.1002	-536.335
1F CO	2.7151	-331.242
2F CO	2.90765	-1035.12

Table B.8: Calibration Curves for Test 5

Location	A	B+C
BR O_2	0.0491	-12.8308
1F O_2	0.0443	-4.3453
2F O_2	0.0467	-9.4517
BR CO	3.17	-1078.87
1F CO	2.8	-418.125
2F CO	2.99	-1154.34

Table B.9: Calibration Curves for Test 7

Location	A	B+C
BR O_2	0.0289	1.0645
1F O_2	0.0443	-4.5668
2F O_2	0.0467	-9.6
BR CO	3.1002	-1026.17
1F CO	2.7151	-401.835
2F CO	2.90765	-1100.04

Table B.10: Calibration Curves for Test 8

Location	A	B+C
BR O_2	0.0443	-2.6166
1F O_2	0.0491	-7.1352
2F O_2	0.0467	-9.872
BR CO	3.1002	-936.26
1F CO	2.7151	-350.248
2F CO	2.94	-1055.48

Table B.11: Calibration Curves for Test 9

Appendix C

Image Processing Program

Included in this Appendix are a series of inverted images of the fires at different points in time to show the ability of the program to discern between flames, ambient air and smoke.

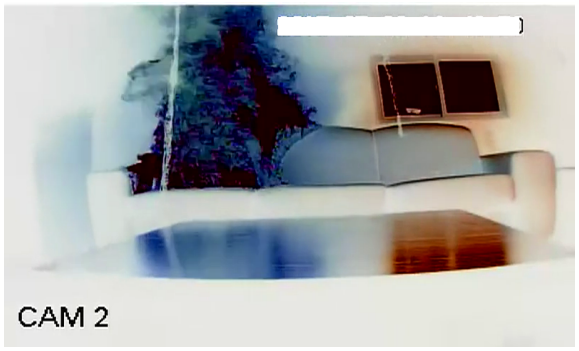

Test 2

Test 3

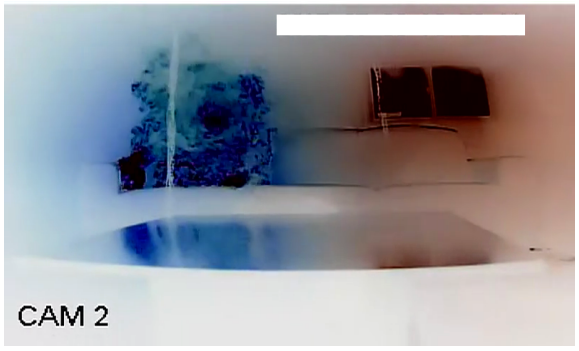

Test 4

Test 5

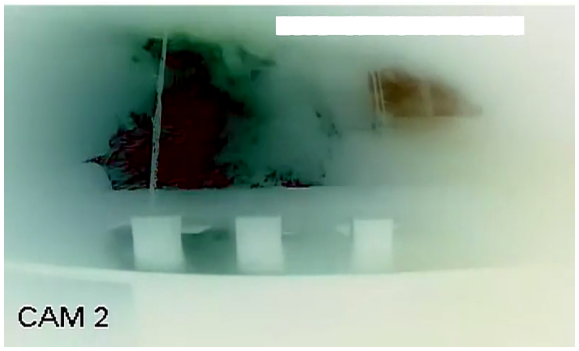

Test 7

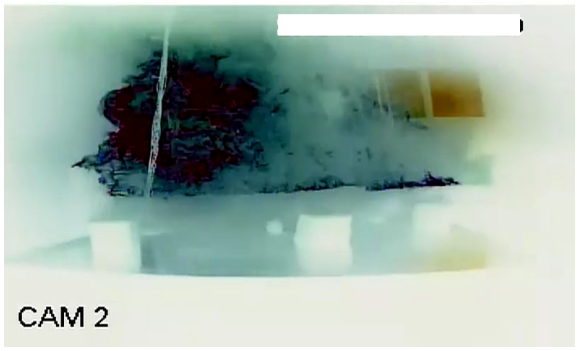

Test 8

Test 9

Figure C.1: Examples of Various Converted Frames from Original Footage after the Video Processing at Different Stages of the Fire Development

C.1 Image Processing Program Code

Below is the raw Fiji code developed for the video analysis.

```
//!!!Input below before running code

minFrame = 1;//input minimum frame number
maxFrame = 24511;//input maximum frame number
xIgn = 275;//input x-value of ignition point
base = 290; //Top right corner of table, this gives a baseline value to
search for flame that is consistent opposed to a variable couch baseline.
couch_base = 249; //Highest point of slanted couch surface
```

```
maxL = 208; //this gives a x-value for the corner edge of the couch so the
program knows when to stop searching for x2 values (to the left).
maxR = 641; //this gives an x-value for the far right corner edge of the couch
so the program knows when the fire reaches that end = the full width of couch.

xRect = 381; yRect = 21; w = 347; h = 24;

makeRectangle(xRect, yRect, w, h);
run("Clear");
run("Select None");


run("Invert");//invert colours to make it easier for user to select flame

a = getTitle();//get name of file

frame = substring(a, 0, 5);
frameNum = parseFloat(frame);

frmRng = maxFrame - minFrame;


x2 = 0;
x1 = 0;
Yx2 = 0;
//Finding x1 and x2
found = false;

for(x = maxR; x >= maxL && !found; x--)
{
stop = false;
y = base;

while(y > couch_base && !stop)
{
avgGB = 0;
storeValue = getPixel(x, y);
red = (storeValue>>16)&0xff;
```

```
green = (storeValue>>8)&0xff;
blue = (storeValue>>0)&0xff;

avgGB = (green + blue)/2.0;
countFireL = 0;
countFireR = 0;
if(x2 != 0 && y <= (Yx2 - 5))
stop = true;////Don't look for x1 at a height greater than the height of x2

if(avgGB <= 10)
{
SQSIZE = 8;
SQWIDTH = x - maxL - 2;
if(SQWIDTH > 8)
SQWIDTH = 8;
if(SQWIDTH < 0)
SQWIDTH = 0;

//countFireL to check the square to the left of x1 or x2
for(Ya = y - SQSIZE; Ya < y; Ya++)
{
for(Xa = (x - 2 - SQSIZE); Xa < (x - 2); Xa++)
{
if(Xa >= maxL)
{
storeValue = getPixel(Xa, Ya);
redTemp = (storeValue>>16)&0xff;
greenTemp = (storeValue>>8)&0xff;
blueTemp = (storeValue>>0)&0xff;

tempAvg = (greenTemp + blueTemp)/2.0;
if (tempAvg <= 10)
countFireL++;
}
}
}
//countFireR to check the square to the right of x1 or x2
for(Ya = y - SQSIZE; Ya < y; Ya++)
```

```
{
for(Xa = (x + 2 + SQSIZE); Xa > (x + 2); Xa--)
{
storeValue = getPixel(Xa, Ya);
redTemp = (storeValue>>16)&0xff;
greenTemp = (storeValue>>8)&0xff;
blueTemp = (storeValue>>0)&0xff;

tempAvg = (greenTemp + blueTemp)/2.0;
if (tempAvg <= 10)
countFireR++;
}
}

if (x2 == 0 && countFireL > 0.65*SQSIZE*SQSIZE &&
\\
((x < maxR - 9 && countFireR < 0.35*SQSIZE*SQSIZE) || x >= maxR - 9))
{
stop = true;
x2 = x;
Yx2 = y;
}

else if(x2 != 0 && countFireR > 0.65*SQSIZE*SQSIZE && countFireL
\\
<= 0.35*SQSIZE*SQWIDTH)
{
x1 = x;
found = true;
stop = true;
}
}
//Was determined through some trial and error that 8 was the optimal size to check.

//Min. of couch surface and x2 height. Could be stop limit up looking for x1
//For x1 --> a) if fire found and box to the left is mostly empty OR
//b) if fire found for 5-10 x-values AND x2 is known then box check
/After x2, use previous y-value for every new x, no fire near the previous y,store x1
```

```
y--;
}
}

if (x1 == 0)
x1 = maxL;

if (x2 == 0)
x2 = x1 = xIgn;

///////Start Finding y-values here
Xc = (x1 + x2)/2;

lowest = couch_base;

if(Yx2 != 0)
lowest = maxOf(Yx2, couch_base);

maxY = lowest;
centerY = lowest;
yAbs = lowest; xAbs = 0;
absMaxDelta = lowest;

for(x = x1; x <= x2; x++)
{
y = 0;
stop = false;

Yh = lowest;

maxDelta = 0;
yDel = 0;

while(y <= lowest && !stop) //Record the y-values of x1 and x2
{
avgGB = 0;
storeValue = getPixel(x, y);
red = (storeValue>>16)&0xff;
```

```
green = (storeValue>>8)&0xff;
blue = (storeValue>>0)&0xff;

avgGB = (green + blue)/2.0;
countFireT = 0;
countFireB = 0;


///Delta method for y-values
if(x > maxL + 15 && frameNum > (0.6*frmRng + minFrame) &&
\\
(x < xRect || y > yRect + h + 7))
{
sum = 0;
for(Xb = x - 1; Xb <= x + 1; Xb++)
{
for(Yb = y - 5; Yb < y; Yb++)
{
storeValue = getPixel(Xb, Yb);
redTemp = (storeValue>>16)&0xff;
greenTemp = (storeValue>>8)&0xff;
blueTemp = (storeValue>>0)&0xff;

sum = sum + ((greenTemp + blueTemp)/2.0);
}
}
avgT = sum/15.0;

sum = 0;
for(Xb = x - 1; Xb <= x + 1; Xb++)
{
for(Yb = y ; Yb < y + 5; Yb++)
{
storeValue = getPixel(Xb, Yb);
redTemp = (storeValue>>16)&0xff;
greenTemp = (storeValue>>8)&0xff;
blueTemp = (storeValue>>0)&0xff;
```

```
sum = sum + ((greenTemp + blueTemp)/2.0);
}
}
avgB = sum/15.0;

delta = avgT - avgB;
if(avgT > avgB && y > 10 && delta > maxDelta)
{
maxDelta = delta;//maxDelta is the largest delta within a column
yDel = y;
}
}
////////////End Delta Method


if(avgGB <= 10)
{
SQHEIGHT = 5;
SQWIDTH = 3;

//Create variable Square dimensions for near endpoints
endDist = minOf(x - 1, x2 - x);

if(y < 6)
SQHEIGHT = y - 1;
else if((lowest - y) < 6)
SQHEIGHT = lowest - y;

if(endDist <= 3)
SQWIDTH = 1;//I don't think this is necessary anymore

if(SQHEIGHT == 0 || SQWIDTH == 0)
stop = true;

//Checking rectangle below the point
for(Ya = y + 1 + SQHEIGHT; Ya > (y + 1); Ya--)
{
cancel = 0;
```

```
if(x < Xc)
cancel = 1;

for(Xa = (x + (cancel - 1)*SQWIDTH); Xa < (x + (cancel)*SQWIDTH); Xa++)
{
storeValue = getPixel(Xa, Ya);
redTemp = (storeValue>>16)&0xff;
greenTemp = (storeValue>>8)&0xff;
blueTemp = (storeValue>>0)&0xff;

tempAvg = (greenTemp + blueTemp)/2.0;
if (tempAvg <= 10)
countFireB++;
}
}

//Checking rectangle above the point
for(Ya = y - 1 - SQHEIGHT; Ya < (y - 1); Ya++)
{
cancel = 0;
if(x > Xc)//flipped the sign here for box on opposite side
cancel = 1;

for(Xa = (x + (cancel - 1)*SQWIDTH); Xa < (x + (cancel)*SQWIDTH); Xa++)
{
storeValue = getPixel(Xa, Ya);
redTemp = (storeValue>>16)&0xff;
greenTemp = (storeValue>>8)&0xff;
blueTemp = (storeValue>>0)&0xff;

tempAvg = (greenTemp + blueTemp)/2.0;
if (tempAvg <= 10)
countFireT++;
}
}

if(countFireB > 0.65*SQWIDTH*SQHEIGHT && countFireT < 0.35*SQWIDTH*SQHEIGHT)
{
```

```
Yh = y;
stop = true;
}

if(Yh < maxY)
maxY = Yh;
if(abs(x - Xc) <= 5 && Yh < centerY)
centerY = Yh;
}

y++;
}

if(maxDelta > 0 && maxDelta < absMaxDelta)
{
absMaxDelta = maxDelta;
yAbs = yDel;
xAbs = x;
}
}
//print("xAbs = " + xAbs + ", absMaxDelta = " + absMaxDelta + ", yAbs = " + yAbs);

if(maxY < centerY && (centerY - maxY) <= 10)
maxY = centerY;

if(frameNum > (0.6*frmRng + minFrame) && yAbs < maxY && abs(yAbs - maxY) < 50)
maxY = yAbs;

maxHeight = lowest - maxY;

print(frameNum + ", " + x2-x1 + ", " + maxHeight);
//print(xAbs + ", " + maxY + ", " + yAbs);

//print("x1 = " + x1 + ", x2= " + x2);
```